

CO-GASIFICATION OF COAL AND BIOMASS: IMPACT ON CONDENSATE AND SYNGAS PRODUCTION

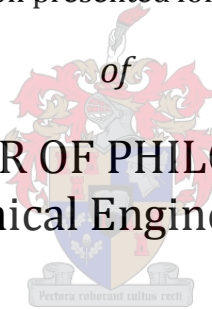
by

Akinwale Olufemi Aboyade

Dissertation presented for the Degree

of

DOCTOR OF PHILOSOPHY
(Chemical Engineering)



in the Faculty of Engineering
at Stellenbosch University

Supervisor

Prof. Johann Görgens

Co-Supervisor

Prof. Edson Meyer

March 2012

Declaration

By submitting this dissertation electronically, I declare that the entirety of the work contained therein is my own, original work, that I am the sole author thereof (save to the extent explicitly otherwise stated), that reproduction and publication thereof by Stellenbosch University will not infringe any third party rights and that I have not previously in its entirety or in part submitted it for obtaining any qualification.

.....

Signature

March 2012

Date

Copyright © 2012 Stellenbosch University

All rights reserved

Abstract

Gasification provides a proven alternative to the dependence on petroleum for the production of high value products such as liquid fuels and chemicals. Syngas, the main product from gasification can be converted to fuels and chemicals via a number of possible synthesis processes. Coal and natural gas are currently the main feedstock used for syngas production. In South Africa (SA), Sasol operates the largest commercial coal-to-liquids conversion process in the world, based on updraft fixed bed gasification of low grade coal to syngas. Co-utilizing alternative and more sustainable feedstock (such as biomass and wastes) with coal in existing coal-based plants offers a realistic approach to reducing the costs and risks associated with setting up dedicated biomass conversion plants.

An experimental and modelling investigation was performed to assess the impacts of co-gasifying two of the most commonly available agricultural wastes in SA (sugarcane bagasse and corn residue) with typical low grade SA coals, on the main products of updraft fixed bed gasification, i.e. liquid condensates and syngas. Condensates are produced in the pyrolysis section of the updraft gasifier, whereas syngas is a result of residual char conversion. An experimental set-up that simulates the pyrolysis section of the gasifier was employed to investigate the yield and composition of devolatilized products at industrially relevant conditions of 26 bars and 400-600°C. The results show that about 15 wt% of coal and 70 wt% of biomass are devolatilized during the pyrolysis process. The biomass derived condensates were determined to comprise of significantly higher quantities of oxygenates such as organic acids, phenols, ketones, and alcohols, whereas coal derived hydrocarbon condensates were dominated by polycyclic aromatic hydrocarbons, creosotes and phenols. Results of investigation into the influence of coal-biomass feedstock mix ratio on yields of products from pyrolysis show limited evidence of non-additive or synergistic behaviour on the overall distribution of solid, liquid and gas yields. On the other hand, in terms of the distribution of specific liquid phase hydrocarbons, there was significant evidence in favour of non-additive pyrolysis behaviour, as indicated

by the non-additive yield distribution of specific chemicals. Synergistic trends could also be observed in the thermogravimetric (TGA) study of pyrolysis under kinetically controlled non-isothermal conditions. Model free and model fitting kinetic analysis of the TGA data revealed activation energies ranging between 94-212 kJ mol⁻¹ for the biomass fuels and 147-377 kJ mol⁻¹ for coal. Synergistic interactions may be linked to the increased presence of hydrogen in biomass fuels which partially saturates free radicals formed during earlier stages of devolatilization, thereby preventing secondary recombination reactions that would have produced chars, allowing for the increased formation of volatile species instead.

Analysis of char obtained from the co-pyrolysis experiments revealed that the fixed carbon and volatile content of the blended chars is proportional to the percentage of biomass and coal in the mixture. CO₂ reactivity experiments on the chars showed that the addition of biomass to coal did not impose any kinetic limitation on the gasification of blended chars. The blended chars decomposed at approximately the same rate as when coal was gasified alone, even at higher biomass concentrations in the original feedstock blend. Based on these observations, a semi-empirical equilibrium based simulation of syngas production for co-gasification of coal-biomass blends at various mix ratios was developed using ASPEN Plus. The model showed that H₂/CO ratio was relatively unaffected by biomass addition to the coal fuel mix, whereas syngas heating value and thermal efficiency were negatively affected. Subsequent evaluation of the production cost of syngas at biomass inputs ranging between 0-20 wt% of coal reflected the significant additional cost of pre-treating biomass (3.3% of total capital investment). This resulted in co-gasification derived syngas production costs of ZAR146/tonne (ZAR12.6/GJ) at 80:20 coal-biomass feedstock ratio, compared to a baseline (coal only) cost of ZAR130/tonne (ZAR10.7/GJ). Sensitivity analysis that varied biomass costs from ZAR0 – ZAR470 revealed that syngas production costs from co-gasification remained significantly higher than baseline costs, even at low to zero prices of the biomass feedstock. This remained the case even after taking account of a carbon tax of up to ZAR117/tCO₂. However, for range of carbon tax values suggested by the SA treasury (ZAR70 tCO₂ to

ZAR200 tCO₂), the avoided carbon tax due to co-feeding biomass can offset between 40-96% of the specific retrofitting cost at 80:20 coal-biomass feedstock mass ratio.

In summary, this dissertation has showed that in addition to the widely recognized problems of ash fouling and sintering, co-feeding of biomass in existing coal based updraft gasification plants poses some challenges in terms of impacts on condensates and syngas quality, and production costs. Further research is required to investigate the potential in ameliorating some of these impacts by developing new high value product streams (such as acetic acid) from the significant fraction of condensates derived from biomass.

Opsomming

Vergassing bied 'n beproefde alternatief vir die afhanklikheid van petroleum vir die produksie van hoë waarde produkte soos vloeibare brandstof en chemikalieë. Sintese gas, die belangrikste produk van vergassing, kan omskakel word na brandstof en chemikalieë deur 'n aantal moontlike sintese prosesse. Steenkool en aardgas is tans die belangrikste grondstowwe wat gebruik word vir sintese gas produksie. In Suid-Afrika (SA) bedryf Sasol die grootste kommersiële steenkool-tot-vloeistof omskakelingsproses in die wêreld, gebaseer op stygstroom vastebed vergassing van laegraadse steenkool na sintese gas. Die gebruik van alternatiewe en meer volhoubare grondstowwe (soos biomassa en afval) saam met steenkool in die bestaande steenkool-gebaseerde aanlegte bied 'n realistiese benadering tot die vermindering van die koste en risiko's wat verband hou met die oprigting van toegewyde biomassa omskakelingsaanlegte.

'n Eksperimentele en modelleringsondersoek is uitgevoer om die impak van gesamentlike vergassing van twee van die mees algemeen beskikbare landbou-afvalprodukte in Suid-Afrika (suikerriet bagasse en mieliereste) met tipiese laegraadse SA steenkool op die vernaamste produkte van stygstroom vastebed vergassing, dws vloeistof kondensate en sintese gas, te evalueer. Kondensate word geproduseer in die piroliese gedeelte van die stygstroomvergasser, terwyl sintese gas 'n resultaat is van die omskakeling van oorblywende houtskool. 'n Eksperimentele opstelling wat die piroliese gedeelte van die vergasser simuleer is gebruik om die opbrengs en die samestelling van produkte waarvan die vlugtige komponente verwyder is by industrie relevante toestande van 26 bar en 400-600°C te ondersoek. Die resultate toon dat ongeveer 15% (massabasis) van die steenkool en 70% (massabasis) van die biomassa verlore gaan aan vlugtige komponente tydens die piroliese proses. Daar is vasgestel dat die kondensate afkomstig van biomassa uit aansienlik hoër hoeveelhede suurstofryke verbindings soos organiese sure, fenole, ketone, en alkohole bestaan, terwyl koolwaterstofkondensate afkomstig uit steenkool oorwegend bestaan uit polisikliese aromatise verbindings, kreosote en

fenole. Die resultate van die ondersoek na die invloed van die verhouding van steenkool tot biomassa grondstof op piroliese opbrengste toon beperkte bewyse van nie-toevoegende of sinergistiese gedrag op die algehele verspreiding van soliede, vloeistof en gas opbrengste. Aan die ander kant, in terme van die verspreiding van spesifieke vloeibare fase koolwaterstowwe, was daar beduidende bewyse ten gunste van 'n sinergistiese piroliese gedrag. Sinergistiese tendense is ook waargeneem in die termogravimetriese (TGA) studie van piroliese onder kineties beheerde nie-isotermiese toestande. Modelvrye en modelpassende kinetiese analise van die TGA data het aan die lig gebring dat aktiveringsenergieë wissel tussen $94\text{-}212\text{ kJ mol}^{-1}$ vir biomassa brandstof en $147\text{-}377\text{ kJ mol}^{-1}$ vir steenkool.

Ontleding van die houtskool verkry uit die gesamentlike piroliese eksperimente het aan die lig gebring dat die onmiddellike kenmerke van die gemengde houtskool die geweegde gemiddelde van die individuele waardes vir steenkool en biomassa benader. CO_2 reaktiwiteitseksperimente op die houtskool het getoon dat die byvoeging van biomassa by steenkool nie enige kinetiese beperking op die vergassing van gemengde houtskool plaas nie. Die gemengde houtskool ontbind teen ongeveer dieselfde tempo as wanneer steenkool alleen vergas is, selfs teen hoër biomassa konsentrasies in die oorspronklike grondstofmengsel. Op grond van hierdie waarnemings is 'n semi-empiriese ewewig-gebaseerde simulatie van sintese gas produksie vir gesamentlike vergassing van steenkool-biomassa-mengsels vir verskeie mengverhoudings ontwikkel met behulp van Aspen Plus. Die model het getoon dat die H_2/CO verhouding relatief min geraak is deur biomassa by die steenkool brandstofmengsel te voeg, terwyl sintese gas se verhittingswaarde en termiese doeltreffendheid negatief geraak is. Daaropvolgende evaluering van die produksiekoste van sintese gas vir biomassa insette wat wissel tussen 0-20% (massabasis) van die hoeveelheid steenkool het die aansienlike addisionele koste van die vooraf behandeling van biomassa (3.3% van die totale kapitale belegging) gereflekteer. Dit het gelei tot 'n produksiekoste van ZAR146/ton (ZAR12.6/GJ) vir sintese gas afkomstig uit gesamentlike-vergassing van 'n 80:20 steenkool-biomassa grondstof mengsel, in vergelyking met 'n basislyn (steenkool) koste van ZAR130/ton

(ZAR10.7/GJ). Sensitiwiteitsanalise wat biomassa koste van ZAR0 - ZAR470 gevarieër het, het aan die lig gebring dat sintese gas produksiekoste van gesamentlike vergassing aansienlik hoër bly as die basislyn koste, selfs teen 'n lae of nul prys van biomassa grondstof. Dit bly die geval selfs nadat koolstof belasting van tot ZAR117/tCO₂ in ag geneem is.

In opsomming het hierdie verhandeling getoon dat, bykomend tot die wyd-erkende probleme van as besoedeling en sintering, die gesamentlike gebruik van biomassa in bestaande steenkool stygstroom vergassingsaanlegte groot uitdagings inhou in terme van die impak op die kwaliteit van kondensate en sintese gas, asook produksiekoste. Verdere navorsing is nodig om die potensiaal te ondersoek vir die verbetering van sommige van hierdie impakte deur die ontwikkeling van nuwe hoë waarde produkstrome (soos asynsuur) uit die beduidende breukdeel van kondensate wat verkry word uit biomassa.

Dedication

This work is dedicated to the memory of two of the most remarkable people that I've ever known, my brother Sola Aboyade, and my dad Akintola Aboyade.

Gone, but *never* forgotten.

Acknowledgement

This dissertation is represents the culmination of over three and a half years of work across two countries, and four institutions. In all of these places, there have been so many people who have helped shaped the outcome, and who I will forever bear gratitude. First and foremost, I would like to express my deepest and most profound gratitude to my mother Mrs Mary Aboyade for *everything*. Secondly, I thank my promoter, Prof. Johann Görgens of the Department of Process Engineering, Stellenbosch University and my co-promoter, Prof. Edson Meyer of Fort Hare Institute of Technology, South Africa for their guidance and support during this study. In addition, my unparalleled gratitude goes to Prof. Johannes Knoetze, Dr. Marion Carrier, and Dr. Samson Mampwheli for their significant academic contributions and advice throughout the study. My appreciation further goes to the National Research Foundation of South Africa, Sasol Technology, and the Fort Hare Institute of Technology for financial assistance required to complete this study. Appreciation also goes to the staff of the Departments of Process Engineering as well as Forest and Wood Science, Stellenbosch University for technical, analytical and administrative assistance. A special mention must be made of the people in the wood science workshop for their assistance with lignocellulosic characterization, and to the guys in the analytical labs for the help with the lignocellulosic analysis of my samples.

Gratitude also goes to the Coal and Syngas research group at Sasol Technology for welcoming me into their group and providing assistance during my stay. In particular, I would like to extend my gratitude to Dr. Johann van Dyk for his guidance; Christiaan van Tonder, Ben Ashton, Etienne Schuin, Sarel Du Plessis, Rudi Coetzer, and last but certainly not least, 'Chief' Elias Nana for technical assistance during pressurized pyrolysis experiments. My gratitude also goes to Zinhle Mbatha and Dr. Joshua Oni for various other forms of assistance and encouragement during my time at Sasolburg. A special mention goes to Paul Smith and Jaco Nel for his guidance on the ASPEN modelling aspect of this study. I also appreciate the help of

the staff at the Institute of Technical Chemistry, Forschungszentrum Karlsruhe (Now Karlsruhe institute of Technology), Germany for their warm and welcoming attitudes and support during my stay there. Specific mention goes to Dr. Raphl Stahl and Dr Christoph Kornmayer who helped supervised my work there. I also appreciate the help of Dr Esbeth van Dyk of CSIR, Stellenbosch with translating the abstract to Afrikaans.

I would like to acknowledge friends I've made during the course of my studies for various forms of support they've extended to me over these last years; Benjamin Yuda, Stephen Danje, Callistus, Thomas Hugo, Lilian Busingye, Dr. Michael Daramola, Dr. Bamikole Amigun, Joice Ndlovu, Pastor Funlola Olojede, Ayo Oladokun, Drs. Francis and Nike Lewu, Dr. Tom Ashafa, Agboola Teeru, and Dr. Abimbola Badmus. My siblings, Opeyemi and Oluwole Aboyade, have also been of immense help and support whenever needed. I also thank my son, Ayomide Aboyade for being the bundle of joy that he is. He is still too young to realize it, but the way his eyes light up when I come home gives me all the motivation I need to succeed in life. Finally, I would like to acknowledge the immeasurable and invaluable support of my dear wife, Dr. Oluwaseyi Aboyade. There are no words to describe her influence my life, but it is clear that none of this would be possible without her. Thank you Seyi, you are my world.

Table of contents

Declaration	ii
Abstract.....	iii
Opsomming	vi
Dedication.....	ix
Acknowledgement.....	x
Table of contents.....	xii
List of Figures	xvii
List of Tables.....	xix
1 Motivation for the study and research objective	1
1.1 Introduction.....	1
1.2 Objectives	4
1.3 Thesis Outline	5
1.4 References.....	6
2 Literature Background.....	8
2.1 Overview of gasification	8
2.1.1 Gasifier reactor types.....	8
2.1.2 Syngas utilization.....	11
2.1.3 The Sasol CTL process	12
2.2 Up-draft gasification.....	14
2.3 Pyrolysis in the context of gasification	16
2.3.1 Coal pyrolysis	17
2.3.2 Plant biomass pyrolysis	22
2.3.3 Pyrolysis mechanism.....	26

2.4	Char Gasification.....	29
2.5	Co-gasifying coal and biomass feedstock blends	32
2.5.1	Co-pyrolysis	33
2.5.2	Co-gasification	35
2.5.3	Modelling and kinetics.....	37
2.6	Concluding remarks	38
2.7	References.....	39
3	Model free kinetics of the pyrolysis of agricultural waste	47
3.1	Introduction.....	48
3.2	Material and methods.....	49
3.2.1	Samples.....	49
3.2.2	Experimental method	49
3.2.3	Numerical analysis.....	49
3.3	Results and Discussions.....	50
3.3.1	Description of thermoanalytical curves.....	50
3.3.2	Global kinetic analysis	51
3.3.3	Kinetic analysis of pseudocomponents.....	52
3.3.4	Validation of kinetic analysis approach.....	53
3.4	Conclusions.....	55
3.5	References.....	56
4	Model free kinetics of the co-pyrolysis of coal blends with corn and sugarcane residues.....	57
4.1	Introduction.....	57
4.2	Material and methods.....	59
4.2.1	Samples.....	59
4.2.2	Experimental method	61
4.2.3	Kinetic analysis.....	62

4.3	Results	64
4.3.1	Characteristics of TGA curves.....	64
4.3.2	Kinetic analysis.....	69
4.3.3	Validation of kinetic approach.....	73
4.4	Discussions	76
4.5	Conclusions.....	80
4.6	References.....	80
5	Model fitting kinetics of the co-pyrolysis of coal blends with corn and sugarcane residues.....	84
5.1	Introduction.....	84
5.2	Material and methods.....	87
5.2.1	Kinetic analysis.....	88
5.3	Results and Discussions.....	90
5.3.1	Single fuels.....	90
5.3.2	Blends.....	101
5.4	Conclusions.....	106
5.5	References.....	107
6	Characterization of devolatilized products from the pyrolysis and co-pyrolysis of coal and agricultural residues.....	112
6.1	Introduction.....	112
6.2	Experimental.....	114
6.3	Feedstock.....	114
6.4	Pyrolysis products generation	115
6.5	Volatile product analysis	116
6.5.1	Gas	116
6.5.2	Liquids	117
6.6	Results	117

6.6.1	Kinetic and transport dynamics.....	118
6.6.2	Pyrolysis products distribution	120
6.6.3	Compositional analysis of volatile products	123
6.7	Discussions	128
6.8	Conclusions.....	131
6.9	Nomenclature	132
6.10	References.....	132
7	Characterization of devolatilized products from co-pyrolysis of coal-biomass blends	138
7.1	Introduction.....	138
7.2	Experimental.....	139
7.3	Experimental design	139
7.3.1	Influence of coal-biomass mix ratio	141
7.4	Results and Discussions.....	142
7.5	Influence of mix ratio.....	143
7.5.1	Products yields/distribution.....	143
7.5.2	Compositional analysis of volatile products	145
7.6	Influence of process variables	150
7.6.1	Product distribution	150
7.6.2	Compositional analysis of volatile products	154
7.7	Comments on synergistic behaviour	161
7.8	Conclusions.....	164
7.9	References.....	165
8	Gasification process modelling and economics	168
8.1	Introduction.....	168
8.2	Material and Methods.....	170
8.2.1	Char characterisation.....	170

8.2.2	Char reactivity measurements	170
8.2.3	ASPEN modelling.....	171
8.3	Results and Discussion.....	174
8.3.1	Char properties and reactivity	174
8.3.2	Gasification modelling.....	179
8.3.3	Process Economics.....	184
8.4	Other industrial implications of simulation results.....	191
8.5	Conclusion.....	193
8.6	References.....	194
9	Conclusions and recommendations.....	197
9.1	Main conclusions.....	197
9.1.1	Pyrolysis kinetics.....	198
9.1.2	Pyrolysis product distribution	200
9.1.3	Gasification modelling and process economics	201
9.2	Recommendations	202
9.3	References.....	203
	Appendix A – Data relating to chapters 6 & 7.....	205
	Appendix B – ASPEN model input file.....	215

List of Figures

Figure 1-1: Main thermochemical pathways for liquid fuel and chemicals production.....	2
Figure 2-1: Commercial gasification systems classified according to a) feedstock b) technology	10
Figure 2-2: Syngas market distribution	11
Figure 2-3: Schematic of dry bottom updraft gasifier	13
Figure 2-4: Coalification series	17
Figure 2-5: Cellulose degradation mechanism	24
Figure 2-6: Co-gasification process routes	32
Figure 3-1: TG and DTG curves of CC and SB at 10°C min ⁻¹ heating rate.....	49
Figure 3-2: Apparent E , $\ln(A^*f(\alpha))$ dependence on conversion for CC and SB. E is depicted by thick lines, $\ln(A^*f(\alpha))$ is depicted by thin lines and the calculated correlation coefficients are represented by the dashed lines.....	50
Figure 3-3: Deconvolution of DTG curves for CC and SB at 20 °C min ⁻¹	50
Figure 3-4: DTG of SB and CC pseudocomponents obtained by deconvolution of global curves at 10, 20, 30 and 40°Cmin ⁻¹ heating rates	51
Figure 3-5: Apparent E , $\ln(A^*f(\alpha))$ dependence on conversion for the pseudocomponents. E is depicted by thick lines, $\ln(A^*f(\alpha))$ is depicted by thin lines and the calculated correlation coefficients are represented by the dashed lines.....	52
Figure 3-6: Reproduction of experimental DTG curves for heating rates 10-40°C min ⁻¹ based on parameters from global kinetic analysis (Shaped markers depict experimental curves while simulated curves are depicted by solid lines).....	52
Figure 3-7: Comparison of experimental and predicted DTG curves for 50°C min ⁻¹ heating rate based on parameters from global kinetic analysis (Shaped markers depict experimental curves while predicted curves are depicted by solid lines).....	54
Figure 3-8: Reproduction of experimental curves for SB (20°Cmin ⁻¹) and CC (40°Cmin ⁻¹) based on kinetic analysis of pseudocomponents (Shaped	

markers depict experimental curves while predicted curves are depicted by lines).....55

Figure 3-9: Comparison of predicted and experimental curves for SB and CC at 50°Cmin⁻¹ heating rate based on kinetic analysis of pseudocomponents (Shaped markers depict experimental curves while predicted curves are depicted by lines).....55

Figure 4-1: TG and DTG curves of individual fuel pyrolysis at 10°C min⁻¹.....62

Figure 4-2: DTG curves of various mix ratios of Coal-BG and Coal-CC blends obtained at 10°C min⁻¹.....66

Figure 4-3: Influence of mix ratio on volatile yields.....67

Figure 4-4: Comparing experimental and calculated (weighted average) TG and DTG curves of coal-biomass blends at 90:10 mix ratio68

Figure 4-5: Isoconversional kinetic parameters of individual fuels. Also shown are average apparent E values and deviation (%)70

Figure 4-6: Isoconversional kinetic parameters for Coal-BG blends at 10, 20, and 40 wt% biomass mix ratio. Also shown are average apparent E values and deviation (%)71

Figure 4-7: Isoconversional kinetic parameters for Coal-CC blends at 10, 20, and 40 wt% biomass mix ratio. Also shown are average apparent E values and deviation (%)72

Figure 4-8: Experimental and simulated reaction rate curves at 5, 10, 30 and 50°C min⁻¹.....74

Figure 4-9: Experimental and simulated reaction rate curves for various mix ratios of Coal-BG and Coal-CC blends at 10°C min⁻¹.....75

Figure 4-10: Experimental and predicted reaction rate curves at 150°Cmin⁻¹ based on kinetics obtained at 5-50°C min⁻¹76

Figure 5-1: DTG curves of individual fuel pyrolysis at 10°C min⁻¹91

Figure 5-2: Simulated reaction rate curves for BG and CC based on nth order model for 3- pseudocomponent (plots a and b) and 4-pseudocomponent (plots c and d) fitting.....95

Figure 5-3: Simulated reaction rate curves for coal obtained from 3 (a), 4 (b) 5 (c) pseudocomponent fitting96

Figure 5-4: DTG and TG curves of various mix ratios of Coal-BG and Coal-CC blends obtained at 50°C min ⁻¹	102
Figure 5-5: Simulated DTG curves of coal-BG (a) and coal-CC (b) blends based on 6 pseudocomponent model fitting for 90:10 coal-biomass mix ratio.....	104
Figure 5-6: Simulated DTG curves for Coal-BG (a) and Coal-CC (b) blends based on kinetic parameters obtained from pyrolysis of individual fuels for 90:10 coal-biomass mix ratio	105
Figure 6-1: Schematic of fixed bed pyrolysis experimental setup.....	114
Figure 6-2: Lumped product distribution	119
Figure 6-3: Distribution of liquid fractions on air dried and daf basis	121
Figure 6-4: Evolution of CO, CO ₂ , CH ₄ , and H ₂ yields as pyrolysis proceeds	122
Figure 6-5: Overall yields of CO, CO ₂ , CH ₄ , and H ₂ of total feedstock.....	123
Figure 6-6: Distribution of main functional groups identified in the combined condensates.....	124
Figure 7-1: Influence of mix ratio on overall product distribution and the distribution of liquid phase fractions.....	145
Figure 7-2: Influence of mix ratio on yields of gas species	145
Figure 7-3: Normal probability plot for total liquid yields	150
Figure 7-4: Influence of temperature and pressure on total liquid yields at 5 wt% and 25 wt% biomass blends	151
Figure 7-5: Influence of temperature and pressure on tar yields at 5 wt% and 25 wt% biomass blends	153
Figure 7-6: Influence of temperature and pressure on gas species production from 25 wt% BG blends.....	155
Figure 7-7: Influence of final temperature and pressure on gas species production from 25 wt% CC blends.....	156
Figure 7-8: Influence of temperature and pressure on key aspects of liquids composition from 25 wt% BG blends.....	158
Figure 7-9: Influence of temperature and pressure on key aspects of liquids composition from 25 wt% CC blends	159
8-1: ASPEN PLUS model flowsheet.....	173
Figure 8-2: comparing proximate analysis of raw fuels and their chars (obtained at 600°C and 26 bars)	176

Figure 8-3: Influence of blending on proximate analysis results of coal-BG and coal-CC chars.....	179
Figure 8-4: Conversion-time plots for Coal-BG and Coal-CC char blends.....	178
Figure 8-5: Instantaneous gasification rates versus conversion for single fuels as well as Coal-BG and Coal-CC char blends.....	179
Figure 8-6: Simulated mass and energy flows for gasification of 100% coal feedstock.....	181
Figure 8-7: Influence of Coal-CC blend ratio on raw syngas composition and H ₂ /CO ratio	182
Figure 8-8: Distribution of capital costs for co-gasification (based on 20% biomass input).....	188
Figure 8-9: Influence of carbon tax on distribution of specific production cost.	191
Figure 8-10: Sensitivity of syngas cost and cost distribution to biomass cost ...	192

List of Tables

Table 2-1: Characteristic timescales of major transport processes during biomass pyrolysis	29
Table 3-1: Proximate and ultimate characteristics of corn cobs (CC) and sugar cane bagasse (SB) from this study and from other authors	49
Table 3-2: Devolatilization parameters for CC and SB at different heating rates.	50
Table 3-3: Relative contributions of pseudocomponents obtained from deconvolution	50
Table 3-4: Quality of fit values obtained from comparing simulated and experimental DTG curves using both global and pseudocomponent analysis	52
Table 4-1: Proximate, ultimate and biochemical (biomass only) characteristics of feedstock samples	61
Table 4-2: Deviation between experimental and calculated curves for individual fuels.....	75
Table 5-1: Proximate, ultimate and biochemical (biomass only) characteristics of feedstock samples	87
Table 5-2: Kinetic parameters for single fuels based obtained from nth order model fitting based on multiple heating rate data (5, 10 20, 30, 40 and 50°C min ⁻¹).....	93
Table 5-3: Quality of fit or percentage deviation for simulated curves based on assumption of various numbers of pseudocomponents	94
Table 5-4: Kinetic parameters obtained from 6-pseudocomponent, nth order model fitting of coal biomass blends based on multiple heating rate DTG data (5, 10 and 50°C min ⁻¹)	103
Table 5-5: Quality of fit values for simulated DTG curves of blends obtained via nth order model fitting.....	105
Table 5-6: Quality of fit values for DTG predictions recreated from simulated coal and biomass curves	105
Table 6-1: Size distribution of feedstock	114

Table 6-2: Characteristic time-scales of major physical and chemical processes during devolatilization of wood and coal.....	117
Table 6-3: Key characteristics of the combined and separate liquid phases.....	126
Table 7-1: Experimental plan (values in parenthesis represents coded factors in factorial design)	139
Table 7-2: ANOVA results and measures of model adequacy for both coal-BG and coal-CC blends	141
Table 7-3: Influence of mix ratio on composition and some other key characteristics of liquid phase hydrocarbons	148
Table 8-1: Proximate and ultimate parameters of pyrolysis chars.....	171
Table 8-2: Properties of Kentucky No. 9 coal	174
Table 8-3: Comparing actual gasifier outputs with model predictions	175
Table 8-4: Influence of coal-biomass mix ratio on gasifier performance of a 44 ton/hr (input) installation.....	184
Table 8-5: Capital cost estimate for fixed coal gasification system for a 44.5 t/hr capacity plant	186
Table 8-6: Cost estimate for biomass processing scaled to 20% coal substitution	187
Table 8-7: Specific syngas production costs based on fixed retrofitting costs (at 20% coal substitution by mass)	189
Table 8-8: Specific production costs based on pro-rata retrofitting costs	190

List of Abbreviations

ANOVA	Analaysis of variance
ASTM	American Society for Testing and Materials
BG	Bagasse
BGL	British Gas-Lurgi
CC	Corn cobs
CEN	European Committee for Standardization
CHP	Combined heat and power
CS	Corn stover
CTL	Coal-to-Liquid
DAEM	Distributed activation energy model
DAF	Dry and ash free
DSC	Differential scanning calorimetry
DTG	Differential thermogravimetry
FBDB	Fixed bed dry bottom
FT	Fischer Tropsch
FTIR	Fourier Transform Infrared
GC-MS	Gas chromatography – Mass spectrometer
HHV	Higher heating value
HPLC	High performance liquid chromatography
LOF	Lack of fit
MW _{th}	Megawatts (thermal)
NETL	National Energy Technology Laboratory
PAH	Polycyclic aromatic hydrocarbons
QOF	Quality of fit
SA	South Africa
TGA	Thermogravimetric analysis
UV	Ultra violet

1 Motivation for the study and research objective

1.1 Introduction

The thermochemical conversion of solid carbonaceous fuels such as coal, biomass and municipal waste has customarily been directed towards the production of heat and power, predominantly via combustion [1–4]. In large and industrial scale processes, coal is the main feedstock employed while biomass finds use in mostly small to medium scale applications [4]. There is however, current considerable interest in expanding the use of coal and biomass from such traditional uses, to the production of higher value transport fuels and chemicals which presently are largely obtained from petroleum and natural gas [2,5–9]. Interests in alternative sources for these products were initially driven by uncertainties surrounding the long term supply of oil and gas in the international market, concerns about which were first observed during the oil crises in the 1970s [1].

Before the discovery and wide use of crude oil in the 1950s coal was the principal source for a wide range of hydrocarbon derived chemicals. The main technologies employed in its conversion were carbonisation (slow pyrolysis) and direct liquefaction [2,4]. Carbonisation was used to produce mainly coke - a key resource for the iron and steel industry. The process also yields pyrolysis tars which via distillation and cracking formed the basis for the production of many chemicals [3,10]. Direct liquefaction (or hydrogenation) employs hydrogen donor solvents to aid the decomposition of coal's molecular structure at high temperature and pressure and in the presence of catalysts, into a product called synthetic crude oil, which can be further processed by conventional refining methods to liquid fuels and chemicals [1,3]. Today, the main technologies available for thermally converting solid feedstock into liquid fuels and chemicals are shown in Fig. 1-1. The first two routes, direct liquefaction and pyrolysis are technically feasible but still have question marks over their economic feasibility especially when compared to conventional oil and gas based technologies [3].

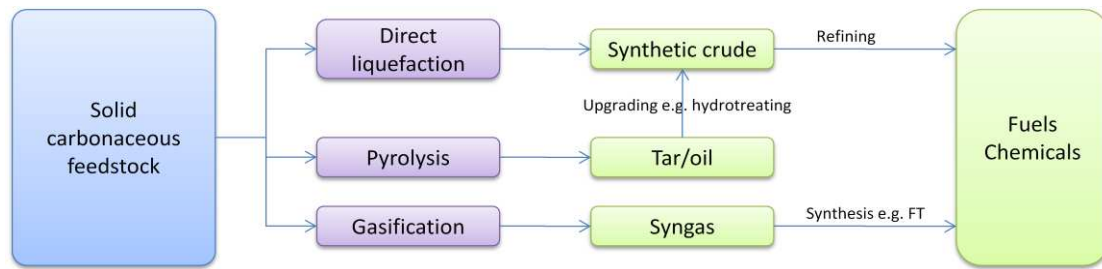


Figure 1-1: Main thermochemical pathways for liquid fuel and chemicals production

The third option shown in Fig. 1-1 – indirect liquefaction – has been in commercial use since the 1960's and involves the initial conversion of the solid feedstock into a combustible gas mixture (called syngas) consisting mainly of H_2 and CO via gasification, and the subsequent liquefaction of the syngas via a number of possible chemical synthesis processes. The most successful commercial example of the gasification/synthesis approach are Sasol's coal-to-liquid (CTL) conversion process based in Sasolburg and Secunda, South Africa (SA) [1,11]. Sasol was established in 1950 by the SA government with the main aim of converting low grade coal into liquid fuels and chemicals as an alternative to petroleum [12]. Sasol 1 was built in Sasolburg and started operation in 1955 followed a few decades later by Sasol 2 and 3 at the Secunda site. As at 2006, Sasol produced about 150 000 barrels per day of fuels and chemicals via its CTL process [12].

While coal has retained its dominance as a solid fuel source in the energy and chemicals industry [4], recent climate change concerns have led to global calls for mitigation of GHG emissions which has in turn led to calls for the replacement of non-renewable fuels like coal with more sustainable and less carbon intensive fuels (on net basis) such as biomass and waste [13]. Co-utilization of coal and biomass/wastes in existing coal based thermal conversion plants have been recognised as a promising approach to realizing those goals, while avoiding the considerable cost and risks associated with setting up dedicated biomass conversion plants [4,14]. These risks are partly due to the relatively unproven conversion of biomass at industrial scales, and partly due to the difficulties involved in maintaining reliable biomass supply chains to satisfy industrial scale needs [15]. These points are particularly relevant to South Africa, given the scale of the dependence on coal (90%

of energy supply and 30% of liquid fuel supply [16,17]), and the comparative lack of an established bioenergy supply infrastructure [8]. Co-gasification can allow biomass feedstock to benefit from the economies of scale which large scale coal gasification already enjoys and could therefore be useful in bridging the gap between established large scale processes for coal and the relatively unproven biomass based technologies.

The Sasol CTL process is based on updraft fixed bed dry bottom (FBDB) gasification technology. Gasification is a process that describes the conversion of usually solid fuels to a predominantly gaseous fuel via 4 main steps including drying, pyrolysis, combustion and gasification. After initial drying, the biomass is devolatilized in the pyrolysis section into gas, liquid hydrocarbons, and a solid char product. The char is converted in gasification zone to syngas in a primarily endothermic process. The energy for all the steps is provided by the reactions of the combustion zone. In updraft gasification, the pyrolysis or devolatilization step is particularly important because liquid condensates produced during this step – comprising tars, oils, and water – are released in significant quantities along with syngas [5,18]. These condensates are produced in the devolatilization reaction zone of updraft gasifiers and are normally considered an unwanted by-product of gasification that has to be minimised [19–21]. In the Sasol process, however, they have chosen to utilize the hydrocarbon fraction of these liquids via conventional refining processes to produce commercially valuable chemicals such as naphtha, creosotes, and phenols [5,22]. Volatile matter content in biomass is known to be significantly higher than in coal, and with considerably different composition. Therefore, the devolatilization step is vital when considering the potential for biomass to be used as feedstock in existing coal based updraft gasification processes [23,24].

Based the aforementioned, substantial attention was devoted in this work to investigating the pyrolysis behaviour of selected coal and biomass samples, and their blends. Gasification performance was evaluated by means of an equilibrium based simulation of syngas yield and composition. Processes downstream of crude syngas

production, such as gas cleaning and conditioning, were considered outside the scope of the study. The coal sample used was a blend of various typical South African hard coals that can be described as low grade, high ash and inertinite rich coal [17]. This type of coal is commonly reserved for domestic use – primarily by Eskom¹ and Sasol – while the higher grade coals such as anthracite are mainly exported [17,25]. Biomass samples used comprised of corn and sugar cane biomass residues, two of the most abundant sources of agricultural waste in South Africa [8,26].

1.2 Objectives

Against the background provided in the previous section therefore, the main purpose of this study was to investigate the impact of adding biomass to coal on condensate and crude syngas production, and to assess the techno-economic feasibility of co-gasification of coal and biomass in SA. In pursuing these goals, the following objectives were set:

- Comparison of the thermal characteristics (proximate and ultimate analysis) of low grade South African coal and agriculture residues (from sugar cane and corn)
- Analysis of the non-isothermal pyrolysis kinetics of the selected coal and biomass samples and their blends via model free and model fitting techniques, based on thermogravimetric experiments
- Experimental assessment of yields and composition of volatile pyrolysis products (gas and condensates) from coal, biomass, and coal-biomass blends, under conditions that simulate the environment within a Sasol FBDB type gasifier.
- In the study of both the kinetics and product distribution of pyrolysis, a key objective was to investigate the existence and extent of synergistic interactions between coal and biomass
- Equilibrium modelling of pressurized fixed bed gasification performance based on empirical pyrolysis data as previously

¹ Eskom is the national power utility in South Africa

determined, to determine the impact of co-gasification on syngas quality and yields

- Preliminary evaluation of the financial impact of selected coal and biomass co-gasification on the production cost of syngas

1.3 Thesis Outline

The dissertation is organized as follows: Chapter 2 discusses the state of the art of syngas production via gasification and reviews the literature on the pyrolysis and gasification of coal, biomass and their blends. In Chapters 3 to 5, global devolatilization kinetics of the samples were investigated via non-isothermal thermogravimetry. Chapter 3 gives the results of the kinetic study of corn cob and sugarcane bagasse using the model free kinetic approach. Comparison of the kinetics of biomasses to coal via model fitting and model free analysis techniques was presented in Chapters 4 and 5 respectively. Blends of coal and biomass were also investigated in these chapters with the purpose of detecting potential synergistic behaviour during pyrolysis.

In Chapter 6, the yield and composition of pyrolysis products from coal were compared with those obtained from sugarcane bagasse, corn cobs and corn stover. A fixed bed batch reactor was employed for simulating the devolatilization zone in updraft gasifiers under the following operating conditions; heating rate of $10^{\circ}\text{C min}^{-1}$, 26 bars pressure, and final temperature of 600°C . Particular attention was paid to liquid phase products which were separated into aqueous and non-aqueous fractions before being chemically characterized by GC-MS.

Chapter 7 reports on the investigation of the yields of volatiles from various mix ratios of coal-biomass blends, with a view to detecting possible synergistic behaviour. The influence of operating parameters such as pressure and temperature has also been investigated. The experimental plan was based on a 2^3 factorial design with mix ratio, pressure and temperature as the three factors. Observed

devolatilization behaviour was discussed in the context of the relative importance of kinetic and transport phenomena on the pyrolysis process.

In Chapter 8, reports of the characterization of chars obtained from pyrolysis experiments described in Chapters 6 and 7 were presented. Results of the equilibrium modelling and economics of co-gasification were also outlined. Chapter 9 summarizes the contributions of this research and suggests some useful recommendations for future research work.

1.4 References

- [1] G. Couch, Coal to liquids, IEA Clean Coal Centre, 2008.
- [2] D.L. Klass, Thermal Conversion: Pyrolysis and Liquefaction, in: Biomass for Renewable Energy, Fuels, and Chemicals, Academic Press, San Diego, 1998: pp. 225-269.
- [3] B.G. Miller, Coal Energy Systems, 1st ed., Academic Press, 2004.
- [4] R. Davidson, A. Doig, J. Ekmann, R. Fernando, N. Harding, R. Moreea-Taha, et al., Cofiring coal with other fuels, IEA Clean Coal Centre, 2007.
- [5] H. Boerrigter, A. Van Der Drift, J.H. Hazewinkel, G. Kupers, BIOSYNGAS; Multifunctional intermediary for the production of renewable electricity, gaseous energy carriers, transportation fuels, and chemicals from biomass, Energy Research Centre of the Netherlands (ECN), 2004.
- [6] C. Song, H.S. Schobert, J.M. Andersen, Premium carbon products and organic chemicals from coal, IEA Clean Coal Centre, 2005.
- [7] A.V. Bridgwater, G. Grassi, eds., Biomass Pyrolysis Liquids Upgrading and Utilization, Hardcover, Springer, 1991.
- [8] L.R. Lynd, H. Von Blottnitz, B. Tait, J. de Boer, I.S. Pretorius, K. Rumbold, et al., Converting plant biomass to fuels and commodity chemicals in South Africa: a third chapter?, South African Journal of Science. 99 (2003) 499-507.
- [9] S. Yaman, Pyrolysis of biomass to produce fuels and chemical feedstocks, Energy Conversion and Management. 45 (2004) 651-671.
- [10] F. Fischer, The conversion of coal into oils, Authorized English Translation, Ernst Benn, London, 1925.
- [11] NETL, Worldwide Gasification Database, (2007).
- [12] J.C. van Dyk, M.J. Keyser, M. Coertzen, Syngas production from South African coal sources using Sasol-Lurgi gasifiers, International Journal of Coal Geology. 65 (2006) 243-253.
- [13] C. Turner, Y. Uchiyama, S. Vuori, N. Wamukonya, X. Zhang, R. Sims, et al., Energy supply. In Climate Change 2007: Mitigation. Contribution of Working Group III to the Fourth Assessment Report of the Intergovernmental Panel on Climate Change [B. Metz, O.R. Davidson, P.R. Bosch, R. Dave, L.A. Meyer (eds)], (2007).

- [14] W.. Livingston, A review of the recent experience in Britain with the co-firing of biomass with coal in large pulverised coal-fired boilers, in: Copenhagen, 2005.
- [15] A. Maciejewska, H. Veringa, J. Sanders, S.D. Peteves, Co-firing of biomass with coal: constraints and role of biomass pre-treatment, Petten, The Netherlands: Institute for Energy. (2006).
- [16] SA National Treasury, Reducing Greenhouse Gas Emissions: The Carbon Tax Option, National Treasury, South Africa, 2010.
- [17] A. Eberhard, The future of South African coal: market, investment, and policy challenges, Freeman Spogli Institute for International Studies, Stanford University, Stanford, 2011.
- [18] C. Higman, M. van der Burgt, Gasification Processes, in: Gasification (Second Edition), Gulf Professional Publishing, Burlington, 2008: pp. 91-191.
- [19] C. Brage, Q. Yu, G. Chen, K. Sjöström, Tar evolution profiles obtained from gasification of biomass and coal, Biomass and Bioenergy. 18 (2000) 87-91.
- [20] J. Leppälahti, T. Koljonen, Nitrogen evolution from coal, peat and wood during gasification: Literature review, Fuel Processing Technology. 43 (1995) 1-45.
- [21] E. Kurkela, P. Ståhlberg, Air gasification of peat, wood and brown coal in a pressurized fluidized-bed reactor. I. Carbon conversion, gas yields and tar formation, Fuel Processing Technology. 31 (1992) 1-21.
- [22] S. Mangena, Effective Utilisation of Coal in Sasol – A SasolFBDB Gasification Technology Perspective, in: SACPS International Conference “Coal Powering the Future,” Secunda, South Africa, 2009.
- [23] J.M. Jones, M. Kubacki, K. Kubica, A.B. Ross, A. Williams, Devolatilisation characteristics of coal and biomass blends, Journal of Analytical and Applied Pyrolysis. 74 (2005) 502-511.
- [24] T. Sonobe, N. Worasuwannarak, S. Pipatmanomai, Synergies in co-pyrolysis of Thai lignite and corncob, Fuel Processing Technology. 89 (2008) 1371-1378.
- [25] Chamber of Mines of South Africa, Fact and Figures:2010, Chamber of Mines of South Africa, Pretoria, 2010.
- [26] Department of Minerals and Energy, White Paper on the Renewable Energy Policy of the Republic of South Africa, Department of Minerals and Energy, 2003.

2 Literature Background

The aim of this chapter is to provide the reader with a brief overview of the most important theory and state of the art technology relevant to syngas production from the co-gasification of coal and biomass in updraft fixed bed reactors.

2.1 Overview of gasification

The indirect conversion of solid feedstock to fuels and chemicals proceeds with syngas production via gasification as the main intermediate step [1]. Although gasification is now considered an advanced fuel conversion process [2], the technology has actually existed since the 19th century [1,3,4]. Early gasification technologies depended heavily on decomposition in the absence of oxygen (pyrolysis), but today's dominant technologies are based on partial oxidation and reforming using pure oxygen, steam, or air as oxidising agents [3,5]. The term partial oxidation refers to the fact that less than stoichiometric amounts of oxygen needed for complete combustion are utilized in the process [5].

2.1.1 Gasifier reactor types

Three main reactor types are used in gasification processes today: fixed bed, fluidized bed and entrained flow gasification.

2.1.1.1 Fluidized bed gasification

Fluidised bed technology is an attractive process for gasification because of its scalability [6]. However temperatures that can be achieved in fluidized beds are limited to between 800-1000°C which makes it generally unsuitable for the conversion of high rank coal where higher temperatures (>1300°C) are required due to the lower reactivity [7]. Even for biomass where reactivity is higher, the carbon conversion in fluidized beds is usually no more than 90-98%. The unconverted feedstock accounts for a significant loss in efficiency [7].

2.1.1.2 Entrained flow gasification

The operational limitations posed by fluidized bed gasifiers do not apply to entrained flow reactors [1,2]. They operate with feed and oxidant in co-current flow and very

short residence time. The feed is ground to a size of 100 μm or less to promote mass transfer and allow transport in the gas. The syngas produced is usually of high quality with negligible condensate composition [7,8]. Entrained-flow gasifiers are not limited to any particular type of fuel, although feedstock with a high moisture or ash content may drive the oxygen consumption to uneconomic levels [9].

2.1.1.3 Fixed-bed gasification

Fixed-bed gasifiers are characterized by a bed in which the feedstock moves slowly downward under gravity as it comes into contact with a blast of the incoming oxidising agent [3,4,9]. Fixed-beds are classified according to the direction of this blast relative to the direction the feedstock. Where the blast is in the same direction as the feedstock (i.e. downwards), it is called a co-current or downdraft gasifiers. In updraft gasifiers the blast is counter-current to the fuel [3]. Compared to the other reactor types, fixed-beds are of simpler construction and operation. They also give high carbon conversion, long solid residence times, and low ash carry-over [10]. Downdraft gasifiers have the lower tar production of the two, but are less thermally efficient present significant scale-up issues. As a result no large-scale downdraft plant (larger than 0.5 t/h) is currently in operation [10]. On the other hand, the updraft process is more thermally efficient than the downdraft process and more readily scalable [4,10].

Examples of industrial scale updraft gasifiers include, the British Gas-Lurgi gasifiers at Schwarze Pumpe in Germany, the Sasol FBDB gasifiers in South Africa and the Harboøre CHP plant in Denmark. The main drawback in updraft gasifiers is the high amount of pyrolysis tar content in gas produced (about 38 g/kg [8]). In the Harboøre CHP plant, the water-tar by-product is processed in a separate unit for district heating, while at Schwarze Pumpe, collected tars are fired in an entrained flow gasifier. Sasol opted to use the tar by-product from their gasifiers to produce chemicals via hydrotreating and other processes similar to what obtains at conventional refineries [7].

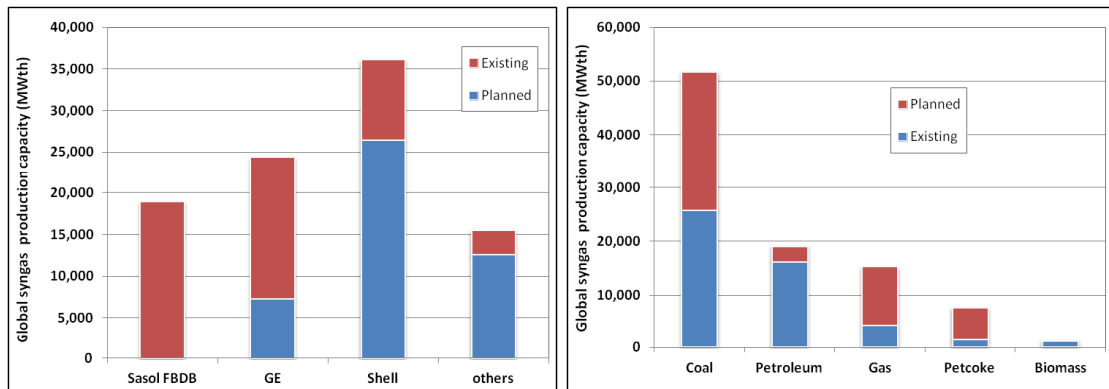


Figure 2-1: Commercial gasification systems classified according to a) technology b) feedstock [11]

As at 1995, 89% of the coal gasified worldwide was processed in fixed bed reactors, while entrained beds accounted for 10%, and 1% by the fluidized bed process [12]. In recent times gasification trends have seen a move away from fixed beds to fluidized beds and entrained flow reactors [11]. Fig. 2-1 shows present and forecasted commercial gasification installations, classified according to feedstock and reactor type. It reveals that most of planned gasification systems will employ the Texaco and Shell technologies, both of which are based on the entrained flow process. It also shows that the vast majority of existing and planned non-petroleum based gasification systems are based on coal feedstock in contrast to biomass (Fig. 2-1). Most of the biomass based gasification plants operate at much smaller scales than coal or petroleum courses because of concerns related to feedstock availability and supply [2,13]. The largest biomass/waste based gasification system is the Schwarze Pumpe plant with a syngas production capacity of 410 MW_{th}, compared to coal and petroleum plants which reach capacities of up to 7 000 MW_{th} and 11 000 MW_{th} respectively [11]. Economies of scale apply to gasification processes which makes the comparative lack of biomass supply in industrial scale economically uncompetitive [2,14]. The relatively few biomass based systems are used in predominantly power based applications [11]. Co-utilization of biomass in coal-based systems could therefore be considered an effective strategy for increasing biomass use in syngas production, particularly for use in liquid fuels and chemical production.

2.1.2 Syngas utilization

The crude gas produced from gasification, is a mixture of combustible (CO, H₂, and CH₄) and non-combustibles (CO₂, H₂O) gases, in addition nitrogen and sulphur compounds. When the mixture has a high proportion of non-combustible elements, it is called producer gas or product gas [15]. Producer gases have low energy value and are not appropriate for high value uses such as synthesis of liquid transport fuels, chemicals or combined heat and power (CHP) applications. For syngas to be suitable for these kinds of applications, it must go through an intensive and expensive cleaning process comprising a multi-level system of scrubbers, filters and separators with each stage targeted at removing particular contaminants to maximise CO and H₂ content [15]. Light hydrocarbons in syngas, like methane can be converted to CO and H₂ by any of a number of different commercially available reforming processes [16,17]. Syngas is probably the most important intermediate product in the chemical industry [15]. A good proportion of syngas produced today is used in the production of ammonia and other chemicals [18], but it also has significant applications in the energy industry as fuel for heat, power and transport. Fig. 2-2 shows the global syngas market distribution in 2007.

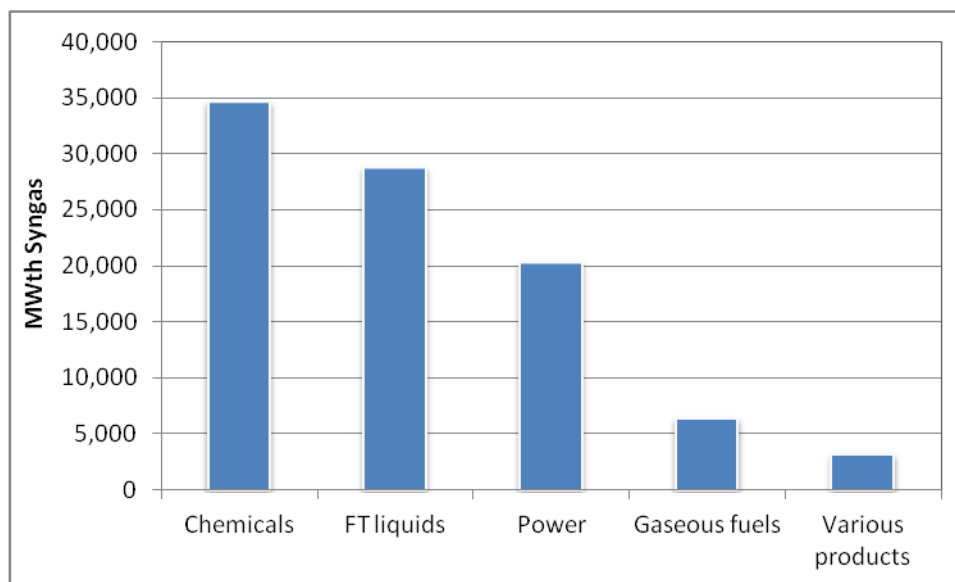


Figure 2-2: Syngas market distribution [11]

The main technological process routes used to process syngas in the context of liquid fuels and chemicals production all involve the catalytic combination of H₂ and CO to

form distillable liquid products. Fisher-Tropsch (FT) synthesis is used to produce mainly diesel, as well as some gasoline and a range of chemicals. A second route is methanol synthesis to produce mainly petrol/gasoline, although the direct use of methanol and DME is being increasingly considered as a third approach [1,19]. Hydrogen production via water gas shift reactions is another common application of syngas.

The largest and most successful application of the gasification/synthesis route is the Sasol process in South Africa where coal is gasified in fixed-bed gasifiers and the produced syngas is converted via FT synthesis to liquid fuels and chemical products [20]. A brief overview of the process follows in the next section.

2.1.3 The Sasol CTL process

The Sasol CTL process is based on the updraft fixed-bed dry bottom gasifier originally patented by Lurgi in 1927 [9,20]. The reactor is a double walled pressure vessel accepting coal feedstock from an overhead lock-hopper under at about 30 bars pressure (Fig. 2-3). An incoming blast of steam and oxygen enters the reactor from the bottom, cooling the ash just leaving the combustion zone to about 300-400°C whilst being heated up itself [9]. The oxygen in the preheated blast reacts with char in the combustion zone to form CO₂. The exothermic nature of combustion makes this the hottest part of the reactor with temperatures approaching 1200°C [9,20]. The CO₂ and steam flow upwards, reacting endothermically with char in the gasification zone to form CO, H₂ and CH₄, using heat energy generated from combustion. These gases continue upwards devolatilizing, preheating and drying the incoming coal feed and in the process losing heat such that it leaves the reactor at about 550°C [9].

The crude gas produced, after separation from liquid pyrolysis co-products, comprises combustible (CO, H₂, and CH₄) and non-combustibles (CO₂, H₂O) gases, in addition other substances such as nitrogen and sulphur compounds. The gas then goes through an intensive cleaning process comprising a multi-level system of scrubbers, filters and separators with each stage targeted at removing particular

contaminants [15] to maximise CO and H₂ content. In Sasol this is done via Rectisol units jointly developed by Lurgi and German Linde [21]. The Rectisol purification process uses methanol at sub zero temperatures and under pressure to remove sulphur containing compounds, CO₂ and other gaseous impurities [21,22]. The process comprises three steps: a) pre-wash that removes hydrocarbons, oxygenates and organic sulphur compounds; b) a main wash that absorbs 95% of the CO₂ and most of COS and CS₂; c) and a fine wash that removes the remaining impurities, leaving a pure syngas with less than 0.1ppm sulphur and 98% of COS removed [22]. Light hydrocarbons in syngas, like methane can be converted to CO and H₂ by reforming [16,17]. After purification, syngas is converted via FT synthesis to synthetic crude consisting of long chained hydrocarbons which is in turn converted via refining to synthetic diesel, and by chemical work-up to other value adding products such waxes and paraffins as well as ammonia.

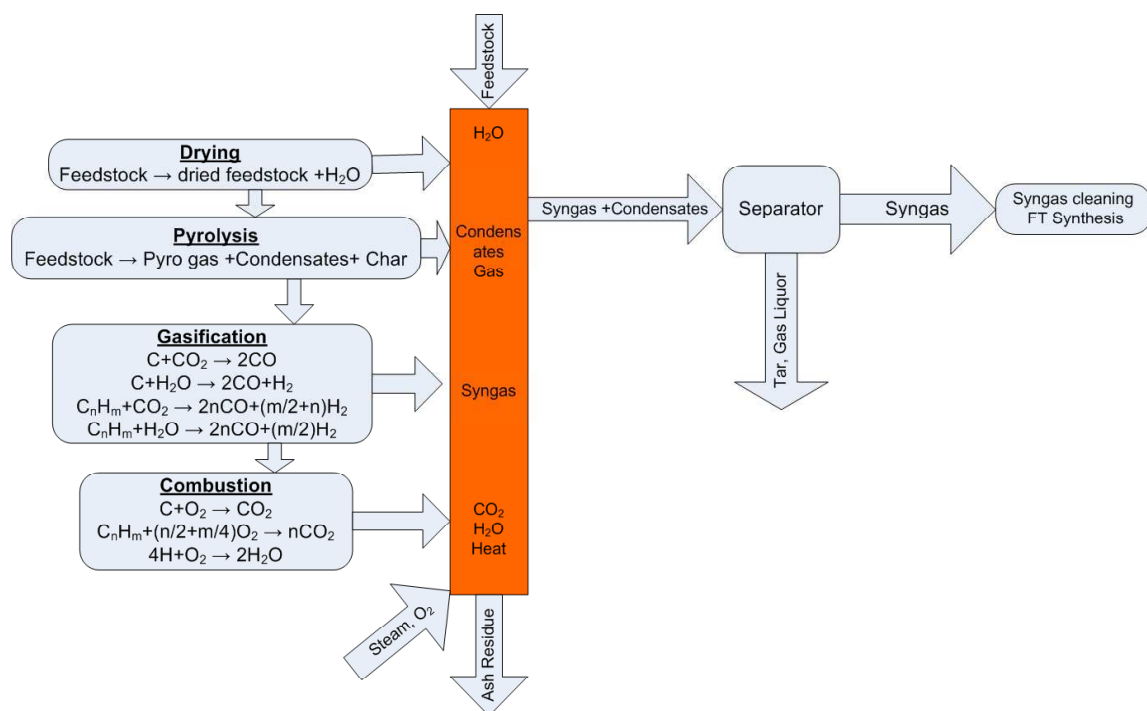


Figure 2-3: Schematic of dry bottom updraft gasifier [19]

In just about every other commercial gasification process, syngas is the main desired product and any liquid condensate/tar obtained is considered an undesirable by-product and considerable efforts are made to reduce its production [23–26]. In fact the co-production of relatively high yields of pyrolysis condensates in low

temperature gasifiers is considered one of their biggest drawbacks [7,27]. A major distinguishing factor of the Sasol process however, is that these condensates have actually been found to be of significant commercial value [7,20] and in 1980s a tar refinery was built and integrated into the CTL process to take advantage [28].

Raw gas exiting the gasifier is quenched initially with recycled gas liquor and subsequently by a system of coolers operating at successively lower temperature ranging from 180°C to 35°C [22,29]. The condensates collected from the various coolers are separated into tars and oils according to their densities. The lighter fraction, or gas liquor, comprising mostly water, ammonia and phenolics, is directed to a phenol extraction process called Phenosolvan. Here the liquor is selectively extracted with butyl acetate to produce a phenol composite containing 40% phenol, 30% cresols, and 7% xylenols [22]. The dephenolated condensate is selectively steam stripped of ammonia (which is then converted into ammonium sulphate for use as fertilizers) while the remaining fluid is desulphurized before being discharged to a biotreater for subsequent disposal as waste water [9,22]. The heavier condensates comprising naphthalene and other high molecular weight hydrocarbons are combined with hydrocarbon residue from the Rectisol unit and are distilled and then hydrogenated in a fixed bed reactor operating at 315-370°C and at 50 bars. The distillation is carried out at atmospheric pressure and produces creosote, road tar and pitch [30]. The hydrogenated product is cleaned by alkali and acid washing before it is itself distilled to produce heavy naphtha fractions as well as benzene, toluene, xylene and a variety of other solvents [22,30]. At the Sasol 2 and 3 plants, the creosote fraction obtained from tar distillation is further hydrogenated to produce a mixture of hydrogenated naphtha and distillate which are used as fuel blending components for FT fuels [22,29].

2.2 Up-draft gasification

The yield and quality of updraft gasification products are driven by the two main processes occurring within the gasifier reactor - devolatilization and char gasification. Investigating these processes is crucial to evaluating the impact of combining coal

and biomass feedstock in a Sasol type CTL process. Different approaches have been taken to study gasification at laboratory scale depending on the research objectives and equipment availability. The most straightforward methodology is to use a reactor capable of gasification (i.e able to withstand high temperatures and control air/fuel ratios). Many researchers have used such gasifiers (bench-scale to PDU to pilot plant scale) to evaluate the overall process dynamics of the gasification process. Many investigated the effect of operating parameters such as air/fuel ratio [31], temperature [31–33], pressure [32], feedstock type [34–36], catalysts [37–39], and particle size [34,40,41], etc, on various aspects of gasification performance such as syngas yield and quality, energy efficiency, and fuel reactivities.

The multi step nature of updraft gasification sometimes makes it possible to separately investigate the individual devolatilization and char gasification steps. This approach is in fact, frequently desirable during gasification research particularly as these two steps have different products streams and more importantly proceed at different rates [42]. Studying devolatilization and char gasification separately can be done either by changing operating parameters to favour pyrolysis in a reactor otherwise designed for gasification [10], or by using an experimental set-up with separate reactors for each step to be studied. An example of the latter is Zhu et al. [43], who used a set-up with separate reactors for pyrolysis and gasification connected in series. A third way is to use completely different set-ups for investigating the particular step of interest. This is a more popular approach because it reduces the need for a dedicated (and usually more expensive) experimental gasifier. A regular application of this method is to use a pyrolysis reactor that simulates the pyrolysis zone of the gasifier of interest to study devolatilization or to produce char (in which case a simple furnace suffices [44]). Char obtained from such processes can be subsequently gasified in a separate step, either in another small-scale reactor [44,45], or as is increasingly common, in a thermogravimetric analyser [43,46–48]. This is the approach taken in this thesis and as such a more detailed discussion of these two steps – pyrolysis and char gasification is presented in the following sections.

2.3 Pyrolysis in the context of gasification

The pyrolysis step is particularly important in updraft gasification because liquid condensates produced are released in significant quantities, compared to other gasifier types [7,9]. Devolatilization also determines the nature of the char product that feed the subsequent gasification step [40,49]. Considerable attention is therefore paid in this review to pyrolysis, its products, and mechanism, with respect to coal and biomass feedstock.

Pyrolysis describes the thermal decomposition of a material in the absence – or limited presence – of an oxidising agent. The pyrolysis or devolatilization of either biomass or coal produces gas, liquid condensates and solid char products. The devolatilization or pyrolysis conditions experienced in a particular gasifier system depend on the type of reactor employed. Fast pyrolysis occurs in fluidized and entrained flow gasifiers [50] while fixed bed gasifiers experience slower pyrolysis heating rates. The slowest heating rates (approx. $12^{\circ}\text{C min}^{-1}$ to $100^{\circ}\text{C min}^{-1}$ [10]) are found in updraft fixed beds [10,49], such as the Sasol FBDB gasifier described in section 2.1.3. This review will thus focus on slow pyrolysis processes.

Slow pyrolysis, is a standalone technology in its own and was initially utilized in the production of charcoal (from biomass feedstock [51]) or coke (from coal [52]) using kilns, mounds or pits [53]. The process also produced tars which formed the foundation of an extensive chemical industry prior to the development of the petrochemical industry. In more recent times, slow pyrolysis is carried out in fixed bed batch reactors for bench scale experiments [52] and in continuously feed reactors such as the screw pyrolyzer, rotary kiln and agitated drum kilns for larger scale applications [53,54].

2.3.1 Coal pyrolysis

2.3.1.1 Feedstock description

Coal pyrolysis is a complex process and the exact mechanism of decomposition is not yet fully understood [55,56]. The complicated nature of coal degradation is informed by the complex chemical composition of the material itself. Coal is a combustible sedimentary rock formed from the very slow decomposition of organic remains from prehistoric times [55,57]. These remains were acted upon by microorganisms to form peat deposits. During this accumulation of peat, factors such as the type of plant community, climate controls, ecological conditions and the pH conditions played a very important role in the transformation of the organic material into the ultimate formation of coal [58]. This process of peat swamp transformation (degradation) under conditions of high pressure and temperatures takes place with time and is called coalification.

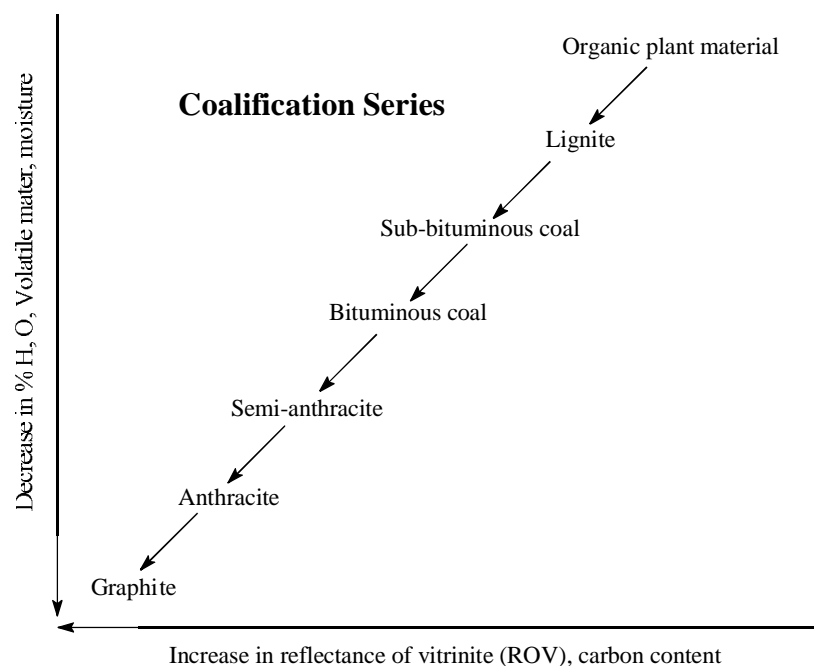


Figure 2-4: Coalification series (Adapted from [57, 58])

Coal is often categorized according to three separate, fundamental parameters [57]:

Rank: The level to which a coal has reached in this continuous coalification series (Fig. 2-4) is termed its rank. The first stage (rank) in coal formation is of brown coal (lignite), and then comes the sub-bituminous and bituminous coals; the last stage is the anthracite and graphite.

Grade: This describes the mineral impurities present in coal and correlates to the ash yield.

Type: This relates to the microscopic component of coal described by the term “macerals”. Three maceral groups are recognized in the coal industry - vitrinite, liptinite and inertinite [57]. Liptinites are richer in hydrogen and produce the highest yield of volatile matter when heated, followed by vitrinite. Vitrinites are formed from cell wall materials and the cell fillings of the woody tissue of plants (trunks, branches, twigs, roots, and leaf tissue). Inertinites are richer in oxygen than the other two groups and are relatively low in volatiles [55,57].

South Africa’s recoverable coal reserves of about 55,000 million tonnes consist mainly of bituminous, inertinite, semi-anthracite, anthracite hard coals [57], with ash content ranging from 7% to 30% [57,58].

2.3.1.2 Principles, products and yields

The start of devolatilization sees coal undergo depolymerization leading to the production of a meta-stable intermediate product. Depolymerisation may be due to the scission of methylene (-CH₂-) bridges and/or ether (-O-) between aromatic clusters [56] and is associated with the release of volatiles some of which are free radicals which are subsequently stabilised either through a re-arrangement of atoms or by collision with other species [60]. Depending on vapour pressure, the resultant stabilised structure evolve either as volatiles (light oil, or heavy tar) or remain as part of char residue.

Char is formed directly as a result of cracking of the coal and also via repolymerisation reactions of the intermediate hydrocarbons. Gas production occurs throughout the duration of pyrolysis as a by product from primary char formation and also via secondary reactions. The aromatic structure of the parent coal persists

in its char residue. The aromatic rings in coal char tend to align with each other to form a layered structure approaching the structure of graphite except for the presence of hydrogen and other heteroatoms [61]. One of the main characteristics of char is its porous structure, the exact nature of which depends on the original coal. Liquid pyrolysis products consists of combinations of high molecular weight compounds such as pitch, creosotes and naphtha, as well as lighter fraction (or gas liquor) containing aqueous and water insoluble hydrocarbons, and water [62]. Evans and Milne grouped pyrolysis liquid compounds as follows [63,64]:

- Primary products: cellulose-derived products (levoglucosan, hydroxyacetaldehyde, furfurals and lignin-derived methoxyphenols).
- Secondary products: phenolics and olefins
- Alkyl tertiary products: methyl derivatives of aromatics (methyl acenaphthylene, methylnaphthalene and toluene).
- Condensed tertiary products: polycyclic aromatic hydrocarbon (PAH) series without substituents (benzene, indene, naphthalene, acenaphthylene, anthracene, phenanthrene, and pyrene)

Gas products are mainly CO, CO₂, H₂, CH₄ and smaller fractions of C₂ and C₃ hydrocarbons [52,62].

2.3.1.3 Influence of operating parameters

The yields of the various products of pyrolysis are influenced by a number of parameters, related to the operating environment and feedstock type. Considering these parameters in isolation is really an oversimplification, but can serve as a convenient device understanding the process better.

Effect of feedstock type:

Coal rank and maceral composition affects the devolatilization characteristics of coal [65]. For bituminous coals, the main volatile product of pyrolysis is tar. The proportion of gases in the volatile products increases at the expense of tar, as the

rank of the coal is reduced from bituminous to sub-bituminous coals and lignites [56]. With regards to macerals, liptinites tend to give the highest volatile yields while inertinites produce the lowest [66]. It follows therefore that coals with high inertinite content, such as much of what occurs in South Africa, tend to have higher char yields during pyrolysis.

Effect of temperature:

Temperature is the most important operational parameter during pyrolysis. For most coals, pyrolysis at slow heating rates starts at 300-400°C after an initial drying period [40,52,55,56,67,68]. Weight loss in this range is due to the release of gases and light hydrocarbons from primary reactions. Tar and gas evolution continues until 500-550°C when the rate of weight loss is drastically reduced. At temperatures higher than 600°C, secondary reactions dominate via a variety of cracking and repolymerization reactions leading to the increased carbonisation of char residues and the increasing production of H₂ at the expense of carbon oxides and hydrocarbons [52].

Effect of heating regime:

When samples are heated rapidly, the speed of the temperature rise overtakes the sequence of pyrolytic events observed during the stages of slow pyrolysis outlined above [52]. At rates above 100–200°C s⁻¹, therefore, the sequence of pyrolytic events is shifted up the temperature scale while the maximum devolatilization rate increases. For example, at 1,000°C s⁻¹, the temperature interval for tar release is found between 600 and 700°C, whereas when coal samples are heated more slowly, say at 1°C s⁻¹, tar release reaches completion between 550 and 600°C [52].

Effect of pressure:

Volatile and tar release tends to decrease with increase in pressure. The observed decrease in the volatile yield is due to increases in the mass transfer limitations for volatiles escaping from within the coal particle to its surface [56]. Pressure increases

the residence time of volatiles within the reaction environment encouraging secondary reactions, which lead to increased cracking and repolymerisation reactions. This results in an overall decrease in total volatile production, as well as the increased conversion of liquid phase intermediates to gas and secondary char. On the flip side, pyrolysis under vacuum produces an increase in volatiles yields as the reduced external pressure facilitates the removal of volatiles from the site of formation within the particles [52]. This effect holds true at both low and high heating rates, and in various type of reactors [69]. This effect depends on the nature of the pressurising gas. Inert atmospheres strongly favour the behaviour described, while in reactive atmospheres (as occurs in hydrolysis or direct liquefaction) the opposite effect is observed [56,66,67].

Effect of reactor type:

In fixed-beds where coal particles are stacked together, devolatilization characteristics is influenced by both intra-particle and extra-particle transport phenomena. Temperature and concentration gradients within the particle influences the rate of release of volatiles to the surface of the solid particle. Evolving tar vapors are likely to deposit on these pyrolyzing solid surfaces, re-polymerize to a char or partially crack to release lighter volatiles. If temperatures are sufficiently high, the volatiles react with bed solids, producing more char, lighter volatiles [52]. Fluidized and entrained flow reactors use much smaller particle sizes with lower mass and heat transport resistance. The design of the process is also such that much shorter residence times occur. The effect of these two attributes is such that devolatilization proceeds much faster than in fixed bed processes, while secondary reactions are limited

2.3.2 Plant biomass pyrolysis

Like for coal, products from the devolatilization of biomass are char and a range of volatiles products, some condensing to form liquids and the rest gases. The relative distribution and composition of these products depend strongly on characteristics of feedstock and the pyrolysis operating conditions.

2.3.2.1 Feedstock description

Biomass, whether woody or herbaceous, is mainly composed of cellulose, hemicellulose and lignin and to a much lesser extent extractives and inorganics. Cellulose forms the cell walls of most biomass along with hemicellulose whereas the middle lamella is mainly lignin. Cellulose is usually the major component of plant tissue (30-50 wt%), followed by hemicelluloses (20-40 wt%) and then lignin (15-25 wt%) [70–72].

Cellulose accounts for much of the cell walls of plants and is a crystalline macromolecule composed of up to 14,000 D-glucopyranoside units linearly linked by weak glycoside bonds [74]. This structure of cellulose is usually the same for all kinds of biomass, varying only with the degree of polymerisation [74]. A combination of various kinetic and molecular characterization studies on isolated cellulose has revealed the following generally accepted reaction scheme for its degradation.

Hemicellulose is also a polysaccharide, but unlike cellulose, is soluble in dilute alkali, is much more heterogeneous and its composition varies significantly for different biomass types [6,72,73]. Hemicellulose represents anywhere between 20-40% of biomass depending on the feedstock and is least thermally stable component [76].

Lignin is a random linked, amorphous, high molecular weight, highly stable biopolymer containing methoxyl substituted phenolic structures from three highly cross-linked phenylpropane monomers; coniferyl, sinapyl, and coumaryl alcohols [63,74,77,78]. Similar to the carbohydrates, it degrades by polymerization to alcohols and phenols [74].

Minerals remain in the char as inert ash, although some studies show that they may also have some catalytic effects on the degradation process [53]. Alkali metals in ash are known to inhibit the formation of levoglucosan in favour of furan derivatives [63] as well as accelerate dehydration and charring reactions [63,79].

2.3.2.2 Principles, product and yields

It is widely accepted that the overall thermal degradation behaviour of biomass is a summation of the decomposition behaviour of the three main lignocellulosic components [53,74].

Cellulose degradation starts with an initial drastic reduction of the degree of polymerization (from 1000-2000 to about 200 [63]) to form “activated cellulose” at temperatures around 250°C, coupled with the elimination of water [74]. This is followed by two main competing pathways shown in Fig. 2-5 [3,80–82]. The first pathway involving inter- and intra-molecular dehydration to produce anhydrocellulose and water is favoured at temperatures lower than 300°C. As pyrolysis proceeds, the anhydrocellulose decomposes further leading to the formation of chars via cross linking and aromatization reactions. This is accompanied by the release and carbon oxides through carbonylation and carboxylation and the continued release of water [74,82–87]. Mok and Antal [83] proposed that anhydrocellulose degrades also by two competing paths. The first proceeds endothermically to produce a further volatile intermediate which then decomposes exothermically to produce CO, CO₂, CH₄ and other permanent gases. The second route leads to char formation which proceeds exothermically. Eventually the glycosyl groups completely degrades leaving a more stable carbonaceous residue, or char [88]. Higher temperatures (>300°C) favour the second main pathway for cellulose decomposition (Fig. 2-5). This involves the formation of tarry levoglucosan via depolymerization i.e. the scission of glucosidic linkage in the cellulose molecule, followed by intra-molecular reorganization of the depolymerised units [3,74,81–85]. Secondary reactions of levoglucosan are mainly responsible for tarry phase products. Initially two reactions compete, evaporation to form vapour phase tar and other condensable volatiles in one case, and decomposition to produce secondary char and gases in the other [74,83]. If allowed to leave the reaction zone the vapour phase tar escapes to form condensed liquids such as phenols, furan derivatives, aldehydes, and acids. Where the volatiles are kept in contact with the remaining solid fuel, the volatiles either degrade to form gases and water, or recondense to form chars [3,83].

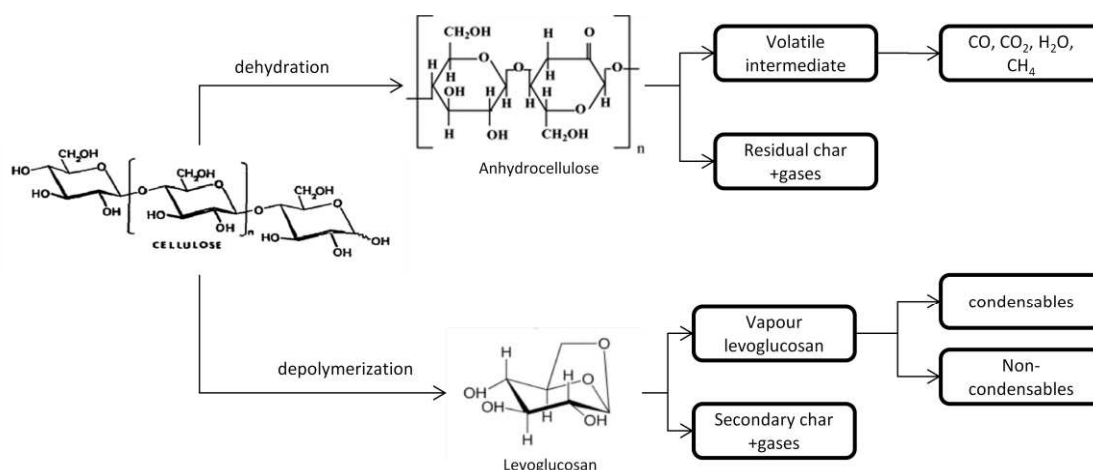


Figure 2-5: Cellulose degradation mechanism [72,81]

Under conventional pyrolysis conditions (400-550°C, slow heating rate), cellulose yields anywhere from 9-15 wt% char. Pyrolysis char is of two types; primary char which is left as residue during dehydration and which usually retains the shape of the original sample and secondary char obtained from the decomposition of levoglucosan [83]. The production of condensables (liquids) increases as pyrolysis proceeds reaching to a maximum when temperature is about 400-550°C. Thereafter the yields starts to fall as a result of secondary and tertiary reactions of levoglucosan- and anhydrocellulose-derived volatiles to form successively lower molecular weight species i.e. light hydrocarbons and non condensable gas like CO , CO_2 , H_2 and CH_4 [3,63,79]. In general, the composition of pyrolytic liquids from cellulose includes compounds such as levoglucosan, acetic acid, formic acid and hydroxyacetaldehyde as the main products [42]. Because cellulose is often the dominating constituent in biomass, it is the most studied and understood of all the biopolymers. As a result its pyrolysis characteristics are sometimes considered representative of the overall behaviour of biomass [3,89,90]. However, there still is some interest in understanding the individual pyrolysis behaviour of the other two components – hemicellulose and lignin.

Hemicellulose starts decomposing at earlier temperatures (200-250°C [78,91]), and thus plays an important role in the initiation of pyrolysis. Shafizadeh [91], Ponder and Richard [75], and Shen and Bridgewater [76] all investigated the pyrolysis

characteristics of various forms of hemicellulose using different process configurations. The products composition of hemicellulose is similar to cellulose, with roughly the same distribution and quality of tars, char and gas production [42,76].

Like for the carbohydrates, lignin devolatilization also proceeds via structural depolymerization [63,93], although with significantly differing product distribution. Evans and Milne [63], in their study of the evolution profile of pine pyrolysis products revealed a lignin derived product as the first to form, followed by hemicellulose, then cellulose derived compounds, and then again lignin derived compounds. This in combination with results from TGA studies shows that lignin decomposes throughout the duration of biomass pyrolysis [92–94]. Lignin tars typically consist of guaiacols, catechols, phenols and acids and produces higher char fractions (up to 60%) than the polysaccharides [63].

In summary, the devolatilization of biomass is based on the degradation behaviour of its individual lignocellulosic components. These components contribute varying amounts to the final distribution of solid, liquid and gaseous products of biomass pyrolysis. Cellulose and hemicellulose contributes the most towards tar and gas production while lignin contributes more towards char yields. Main liquid constituents are typically a mixture of 30% water, 30% phenolics, 20% aldehydes and ketones, 15% alcohols and 10% miscellaneous compounds [42]. Main gas products are CO, CO₂, CH₄, and to a smaller extent H₂ and C₂ hydrocarbons [53,95,96].

2.3.2.3 Influence of operating parameters

As was the case for coal, the pyrolysis behaviour of the biomass components discussed above depend to a large extent on the particular type of feedstock as well as on various operating parameters. One important difference between coal and biomass is the fact that more oxygenated pyrolysis tars evolve from biomass samples and these are thermally more sensitive and break down into gaseous products at lower temperatures, compared to coal tars [52]. In general however, operating

parameters have similar effect on biomass as they do on coal; temperature and heating rate has a generally positive effect on gaseous phase yields. Increase in pressure and residence time generally leads to increase in gas and char yields but has a negative effect on tar production. Increasing temperature favours products of secondary reactions such as CO, H₂, and light tars. This is why tar produced from thermochemical processes with relatively low pyrolysis temperatures (updraft gasifiers, fixed-bed pyrolysis reactors) usually has a composition typical of primary tars in contrast with tars from fluidized beds and downdraft gasifiers [42].

2.3.3 Pyrolysis mechanism

Pyrolysis is a complex process consisting of mass and heat transfer events coupled with several concurrent and competing reactions including dehydration, cracking, fission, decarboxylation, decarbonylation, isomerization, dehydrogenation, aromatization, charring and condensation [3,52,63,74,79]. These reactions produce reactive solid, liquid and gaseous intermediates, which interact with each other in secondary reactions at widely differing reaction rates to produce new intermediates and final products. In the case of such complex reaction schemes, final product distributions depend critically on the time-temperature-pressure distribution, as well as the nature of the feedstock and reaction environment [52].

Comprehensive mechanisms and models of either coal or biomass pyrolysis generally include chemical (kinetics) and physical (mass and energy transfer) aspects. Chemical kinetics govern the rate of reactions whilst physical models inform on the flow of energy and mass (reactants and products). The sheer number, complexity and heterogeneity, of reactions involved in these processes are such that models that completely describes devolatilization have still not been developed [55,56,97]. Instead, proposed models are basically simplifications providing a largely qualitative simulation of the process [96]. An overview of the most common approaches to kinetic and transport modelling are presented in the following sections.

2.3.3.1 Kinetics

Different approaches to the kinetic modelling of biomass and coal pyrolysis can be found in literature. Most of them make use of the Arrhenius dependence on temperature (eqn 1), and consequently the parameters; activation energy, pre-exponential factor and reaction order.

$$\frac{d\alpha}{dt} = A \exp\left[-\frac{E}{RT}\right] f(\alpha) \quad (1)$$

Where α is the conversion (or reacted fraction) of the sample, A and E are the Arrhenius parameters - pre-exponential factor and activation energy respectively, and $f(\alpha)$ is the linear or power law based reaction model. Global devolatilization models represent the total weight loss due to decomposition of the material by a single reaction, usually of 1st order [56,60]. Mechanisms formulated based on these kind of models are frequently analysed via thermogravimetry under kinetic control (i.e. with the effects of transport phenomena minimized). The effects of secondary reactions are also usually limited in such studies by the use of an inert purge gas to reduce the residence time of vapour phase products [90].

There are also multi-component devolatilization models which can be applied to predict the rate of weight loss usually under the assumption of multiple parallel reactions representing pseudocomponents that make up the material being studied [96]:

$$\frac{d\alpha}{dt} = \sum \gamma_i A_i \exp\left[-\frac{E_i}{RT}\right] f(\alpha_i) \quad (2)$$

where γ_i is the contribution of pseudocomponent i to the total mass loss. For coal, the multi-component approach is also commonly evaluated by means of the distributed activation energy model (DAEM), which assumes pyrolysis occurs through an infinite series of parallel, independent reactions. In this model, a continuous distribution of activation energies is described by a Gaussian function [98]. DAEMs are also used in biomass kinetic studies although to a much lesser extent [96].

Another approach to the determination of global kinetic parameters is the isoconversional approach which removes the need for assumption of a reaction order or the function $f(\alpha)$. The method produces activation energy as a function of conversion, or $E(\alpha)$. Although originally intended for single reaction processes, the method is now widely applied for complex reactions, and any variation in the activation energy with respect to conversion is thought to represent the multi-step nature of the process being studied [99]. This method involves computing the logarithms of both sides of equation (1) to get:

$$\ln\left(\frac{d\alpha}{dt}\right) = \ln[A \cdot f(\alpha)] - \frac{E}{RT} \quad (3)$$

A plot of $\ln\left(\frac{d\alpha}{dt}\right)$ against $1/T$ at the same degree of conversion from weight loss data obtained at various heating rates will result in a series of lines, each with slope equal to $-E_\alpha/R$ corresponding to each value of conversion, α . Thus the dependence of E on α is obtained. While the isoconversional method is becoming increasingly popular, it is yet to take hold in the study of biomass kinetics [100].

2.3.3.2 Transport processes

The kinetic models above employ conditions decoupled from the effect of physical or transport processes. However, in actual reactors, solid fuel conversion takes place as a result of the interaction of physical (transport phenomena) and chemical (reaction kinetics) processes [96].

Transport phenomena (mass, momentum and energy) are of interest both at the single particle (intra-particle) and reactor modelling (extra-particle) levels [96,101]. They involve a complex series of steps including “heat conduction, heat loss/gain due to chemical reactions, convective thermal transport due to the outward flow of volatiles, internal convective heat transfer between the volatiles and the solid matrix, accumulation of volatiles within the solid and subsequent pressure build-up within its porous structure, and desorption of fuel moisture content due to external

heat” [101]. The variation of properties such as porosity, permeability, thermal conductivity, thermal capacity and mass diffusivity with conversion also play a part [96,101,102]. The typical timescales of the main physical processes involved during biomass pyrolysis are given in Table 2.1.

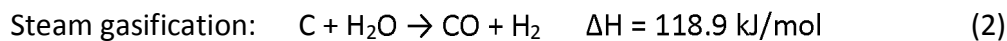
Table 2-1: Characteristic timescales (s) of major transport processes during biomass pyrolysis [101]

Phenomenon	Equation	Time scale at T= 627°C
Diffusion mass transfer	$t_{ch} = L^2/D_{eff}$	120
Mass transfer by intra-particle volatile flow	$t_{ch} = \mu L^2/PK_0$	10
Internal convective heat transfer	$t_{ch} = Ld(\rho c)/h$	0.1
Conduction heat transfer	$t_{ch} = L^2(\rho c)/k$	>200

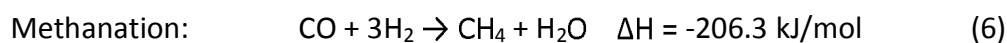
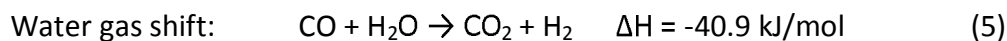
where D_{eff} =effective mass diffusivity; μ =viscosity, P =volatiles over pressure; K_0 =permeability in the longitudinal direction; ρc =volumetric thermal capacity of the solid; k =thermal conductivity; h =internal heat transfer coefficient; d =diameter of typical pore

2.4 Char Gasification

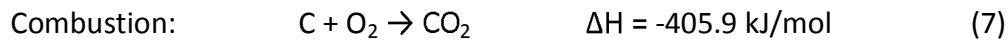
Char gasification reactions proceeds along similar lines for coal and biomass as follows:



Gas phase reactions occur concurrently shaping the eventual composition of gas escaping the reactor;



Stated enthalpies are given for standard conditions, i.e. $\Delta H \rightarrow \Delta H_0$. Some of the reactions are very endothermic, deriving energy from the combustion reaction below;



The extent of char conversion during these reactions is governed by physical and chemical processes which are in turn dependent on operating conditions and the characteristics of the char.

2.4.1.1 Char characteristics

The main char characteristics that affect its gasification performance are its structure and reactivity. The physical structure of chars pertains mainly to its pore structure. Pore sizes are classified into three main groups according to size; micropores (<2 nanometres), mesopores (2-50 nanometres) and macropores (>50 nanometres) [61]. These pores provide access for mass transfer of reactive gases to internal carbon active sites in char, and for escape of product gas from within the char particle to the surrounding atmosphere. Other factors related to char structure that affect the concentration of active sites are the oxygen, hydrogen and mineral content [42,103]. Chars from lower rank coals (e.g. lignite) tend to have higher mineral, and hydrogen content, as well as a higher proportion of meso- and macropores than bituminous coal chars [61,103]. As a result, these chars are known to be more reactive due to the increased concentration of reactive site and efficient mass transport [61]. Biomass in turn comprises even higher concentration of reactive sites for the above mentioned reasons (apart from mineral content). In addition, biomass pores are highly directional, particularly in the case of wood, compared to coal chars [104]. However, the absence of regularity in biomass structure makes it less amenable to kind of the correlation possible between coal rank and type and reactivity [42].

Char structure depends not only on the nature of the parent material but also on the conditions under which the chars are made. Long exposure to high temperatures (>1000°C) increases the carbon content as a result of volatiles release and leads to reduced porosity due to improved alignment of planar regions or layer within the char, reducing access to internal reactive sites [61,104]. Fast heating rates lead to an increase in macropores, while high pressures lead to compaction and lower internal

surface area. Increased porosity and surface area leads to an increase in availability of reactive site which in turn increases the reactivity of the char [103].

2.4.1.2 Reaction mechanism

Global char reactivity (or gasification rate) is usually defined as the heterogeneous conversion rate per remaining mass [42,61,104]:

$$R = -\frac{1}{M} \frac{\partial M}{\partial t} = \frac{dX}{dt} \times \frac{1}{1-X}$$

where M is the ash free mass of the sample, dM/dt is the conversion rate and X is the degree of conversion;

$$X = -\frac{M - M_0}{M_0 - M_\infty}$$

where M_0 and M_∞ are the initial and final values of the sample mass, respectively.

The gasification reactions (reactions 1-7) also give an indication of the stoichiometry and thermodynamics of the process. The two main factors that affect the equilibrium position of these reactions are the temperature and pressure of the gasification process [3,61]. Increasing temperatures causes equilibrium to shift in favour of product formation for the Boudouard and steam gasification reactions, in contrast to hydrogasification and the gas phase reactions where reactants are favoured [3]. Apart from the water gas shift reaction, pressure has an influence on the equilibrium position of gasification reactions. Products formation is favoured during methanation and hydrogasification at high pressures, whilst reactants are favoured for reactions (1) and (2) [61].

2.5 Co-gasifying coal and biomass feedstock blends

There are two main integration routes considered for coal and biomass co-gasification; parallel co-gasification and direct co-gasification [13,19,27]. Parallel co-gasification involves the use of separate systems for some or all of the biomass

gasification steps before integrating with the coal process (i.e. routes 1- 4 in Fig. 2-6). Route 1a is the most common approach taken for parallel co-gasification, in commercial demonstration projects [13].

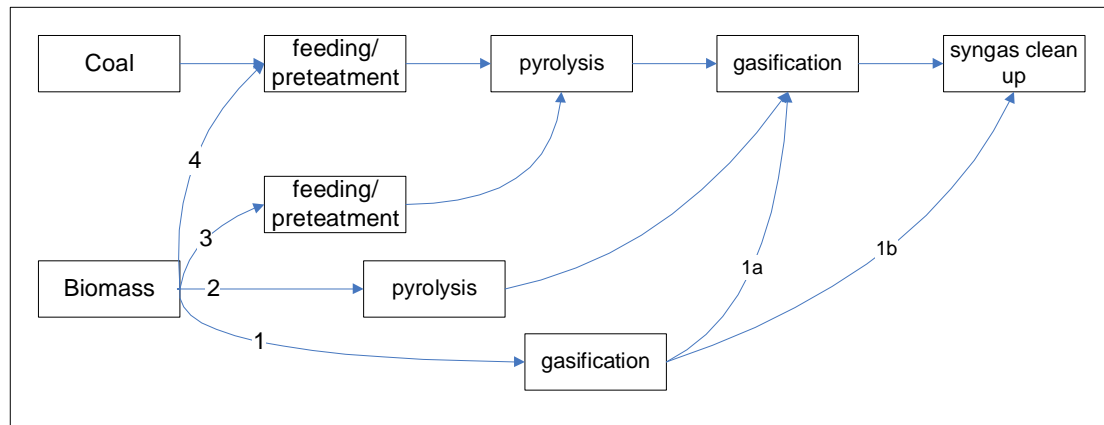


Figure 2-6: Co-gasification process routes (Adapted from [19])

Direct co-gasification is usually employed in operations that require higher quality syngas e.g. IGCC and gasification/synthesis projects. Some examples as detailed by Koukouzas et al. [13] are:

- The Eclogas IGCC power plant in Puertollano Spain; uses a 50:50 blend of coal and petroleum coke
- The Nuon power plant in Buggenum, Holland, utilizes an entrained-flow gasifier with dry powder feeding system for co-gasifying biomass and coal
- Co-gasification of coal and solid wastes at the SVZ GCC/Methanol Plant at Schwarze Pumpe GmbH in Germany and in Kentucky (USA). Both plants utilize the oxygen-blown, fixed-bed, slagging gasifier technology of British Gas Lurgi (BGL).

As explained in section 2.2, it is often desirable to separate the pyrolysis and gasification steps during gasification research. This approach naturally applies to co-gasification research as well, particular in the Sasol type CTL process where products of devolatilization are also of immense economic importance. To this end, some of

the recent efforts and key issues in co-pyrolysis and co-gasification research are presented in following sections.

2.5.1 Co-pyrolysis

Many authors have studied the effect of mixing coal and biomass feedstock on the yields of one or more of char, condensates and gas products [32,105–110]. Only a few of these studies are conducted in the larger context of gasification as described in the last section; e.g. Di Blasi et al. [10] in their attempt to evaluate the role of the pyrolysis stage on fixed-bed gasification dynamics and syngas quality, employed a bench-scale fixed-bed gasifier, modifying the operation (550-850°C, inert atmosphere) to allow only pyrolysis. In the majority of cases, pyrolysis experiments are performed as a standalone technology with the production of pyrolytic oil as the main objective. For this reason, most pyrolysis studies tend to use fluidized bed, and flash pyrolysis conditions which more directly favour the production of liquids. As discussed previously in section 2.2, pyrolysis conditions such as reactor type and heating rate have a strong influence on the nature of products produced. Nevertheless a brief overview of the literature on co-pyrolysis is given.

One of the main research issues in co-pyrolysis research is question of synergy. Do the different fuels interact with each other during the process to affect product distribution? Working with a fluidized and fast-heating fixed-bed reactor, Collot et al. [32] reported no obvious synergistic effects on tar yields from either reactor during the pyrolysis of coal and wood/forestry residue at 850°C and 1000°C and at pressures up to 25 bars. Many other studies [32,105,107,111] show little evidence of interaction during coal/biomass co-pyrolysis, i.e. the samples behave as if they were processed individually, thus exhibiting non-additive behaviour when mixed. This is partly unsurprising as no synergies are observed even between more closely bonded constituents such as maceral concentrates in coal [32,65,66,112] and lignocellulosic components in biomass [32,74]. However some other authors have detected non-additive behaviour [113–116].

The effect of experimental conditions such as temperature [106,108,110], pressure [32,106], presence of catalysts [106,108], residence time [106], etc have also been studied. The general conclusion from these works is that changing operation conditions generally have the same effect on fuels mixtures as they do when fuels are processed individually. Some of these studies applied fast pyrolysis conditions [32,105,111,107,108,117] as found in fluidized and entrained flow reactors and others were based on slow pyrolysis [111,107,113,106,110,109] which usually occurs in fixed/moving bed reactors [10]. Other studies went further to detail the impact of co-processing on evolution of specific gas species [111,107,114,108,110] as well as on char properties like reactivity, heating value [109] and surface characteristics. Only one study by Jones et al. [113] could be found which mentioned the effect of co-pyrolysis on the composition of the condensates fraction. Co-pyrolysis studies using different fuel mixtures such as coal-plastics/polymers [118], coal-petroleum residue [119,120], and biomass-plastics/tire/waste [121–125] can also be found in literature.

In summary, majority of co-pyrolysis studied suggest that the devolatilization yields of coal and biomass blends can be safely described by a summation of the individual behaviour of the blends' components, although some interactions can occur in the vapour phase when residence times are long enough. The sometimes conflicting results in these studies can be attributed to the wide variety of feedstock and operating conditions employed, in combination with the inherent complexity of the pyrolysis process itself.

2.5.2 Co-gasification

Main issues in co-gasification research relate to product yields and composition, synergy, gasifier stability (near steady state syngas flow), and effect of varying experimental conditions.

Change in product yield and quality

It is generally agreed that addition of biomass to coal during pyrolysis caused an increase in tar and hydrocarbon content of produced gas [33,37,38,126,127]. Pan et

al. [33] showed increase in gas yield (1.5 to 3.2Nm³/kg for 100:0 and 20:80 blends of low-grade black coal and pine chips) and heating value (as a result of increase in combustible gas species) with increase in biomass fraction. A contrasting trend in heating value of syngas was observed by Li et al. [128] with increase in biomass fraction also using a fluidized bed gasifier. Using a fluidized bed reactor operating at 800-1050°C and at atmospheric pressure, Andre et al. [124] and many others [31,33,37,38,129] deduced that increasing the biomass fraction caused a decrease in H₂ production and an increase in the production tars and light hydrocarbon which can however be reduced by increasing gasification temperatures, using a catalyst, or increasing oxygen input. Pinto et al. [37,38] also noticed a reduction in H₂ and increase in CO content when either pine waste or polyethylene was added to low grade coal. Alzate et al. [130] noticed the opposite trend in H₂ production when pellets made up of varying fractions of coal and wood were steam gasified in a fluidized bed reactor.

Evidence of synergy

The evidence on synergy between coal and biomass during co-pyrolysis is inconclusive. Collot et al. [32] and Mclendon et al. [35] studied co-gasification on coal and wood under varying conditions a pressurized fluidized bed reactor found no tangible evidence of synergistic effects on product yields similar results were also obtained in atmospheric fluidized beds [34,43,127]. Zhu et al. [43] gasified char obtained from co-pyrolysis of bituminous coal and biomass and also observed no synergy in terms of char reactivity. In contrast, Sjoström et al. [127] indicated the possible presence of some synergy in their co-gasification study using a pressurized fluidized bed reactor operating at about 900°C and 40 bars. They pointed out that less tar and light condensate yields was observed than would be expected assuming a simple additive behaviour when mixing coal and birch wood. The behaviour was ascribed to the possible catalytic effect of biomass ash on the decomposition of coal and difference in reactivities of biomass and coal which allows for the biomass volatiles to react with free radicals obtained from coal as soon as they are formed subsequently preventing the formation of secondary char. Lapuerta et al. [34]

reported synergies in the heating content of producer gas obtained from the co-gasification of low grade coal and biomass using circulating fluidized bed reactor operating at atmospheric pressure.

Effect of operating conditions

Pinto et al. [31] using an atmospheric fluidized bed gasifier showed that experimental conditions have the same effects on gasification on a mixture of low grade coal and pine wood as would be expected on the individual gasification of either coal or biomass [36,41,131]. For instance, increasing temperature was found to generally favour the production of H₂ and the cracking of tars, in both the gasification of single fuels and mixtures at the expense of methane and other hydrocarbons. Andre et al. [31] reported a decrease in hydrocarbon content in syngas with increasing temperature and a corresponding decrease in heating value using a fluidized bed gasifier to process blends made up of coal and olive oil industry waste. Pinto et al. [37,38] reported that the addition of catalysts can also lead to tar abatement. Using a fluidized bed reactor they found nickel based catalysts to have the best tar reduction properties.

Brown et al. [132] studied the catalytic effect of biomass ash on the CO₂ gasification of coal char in more detail using a thermogravimetric analyser. They found that mixing alkali metal rich ash from switch grass with coal in a 90:10 blend increased coal char gasification reactivity almost 8-fold at 895°C and at atmospheric pressure. Co-gasification of coal with biomass was found to in general counterbalance some of the negative effects of gasifying low-grade, high ash, high sulphur coal, particularly by reducing pollutant gas emissions such as sulphur oxides [133].

In summary, the literature shows that mixing has some beneficial effects on gasification but also some adverse effects as well. In the main, co-gasification characteristics are similar to those of the individual fuels that make up the blends. The vast majority of these studies were based on fluidized bed conditions [32,34,35,43,127] as opposed to fixed beds [129]. No studies could be found which

investigated the effect of fixed bed co-gasification on the chemical composition of tars.

2.5.3 Modelling and kinetics

Modelling of coal-biomass blends during thermochemical conversion is a relatively new research area as well. The main interest here is also to determine the possibility of synergy in terms of reaction rates and transport processes. The mechanisms employed are the same with those detailed above for individual studies on coal or biomass. Consequently kinetic approaches used are basically those described in section 2.3.3. For devolatilization, some studies use single reaction global models [109], calculating while others employ multi-reaction models based on curve fitting, isoconversional [97], or DAEM techniques [134]. Some of these studies use kinetic parameters of individual blend components [134,135] while others derive global parameters for the blend as a whole [109]. It is interesting to note that both methods give similar fits to experimental data, as this confirming the absence of synergistic effects during co-processing. Co-gasification models are also based on a similar premise, that the blends behaviour is a simple addition of the individual characteristics of the coal and biomass components [13,14,31,130].

2.6 Concluding remarks

In conclusion, this literature review reveals the following salient points:

- Co-processing of coal and biomass/waste for fuels and/or chemical production via thermochemical conversion has been receiving a lot of research attention recently as part of the global push towards the adoption of renewable energy and waste recovery
- The bulk of that attention is focused more on fluidized bed and entrained flow type gasifiers as opposed to fixed bed processes because of problems related to the latter's scalability (downdraft reactors) and high tar concentration in product gas (updraft reactors)

- Despite this drawback, some key industrial gasification processes still use this technology, the most notable being Sasol of South Africa and Schwarze Pumpe in Germany, both based on Lurgi's pressurized fixed bed technology.
- Co-utilizing biomass with coal in these kinds of systems implies research on the updraft fixed bed gasifier, of which very little is currently available for above stated reasons.

This chapter reveals a gap in published literature dealing with the characterization of pyrolysis condensates and syngas obtained from co-gasification of coal and biomass in pressurized fixed bed processes. The objectives of this study, as presented in section 1.2, will address these gaps by investigating the kinetics and product distribution of pyrolysis and co-pyrolysis of selected coal and biomass types. Particular attention will be paid to identifying the key components present in the condensates of coal, biomass and coal-biomass blends derived from pressurized conditions, with a view to identifying potential synergistic interactions. The study will also include an investigation of the impacts of feedstock co-utilization on syngas quality and production costs.

2.7 References

- [1] G. Couch, Coal to liquids, IEA Clean Coal Centre, 2008.
- [2] B. Ricketts, R. Hotchkiss, B. Livingston, M. Hall, Technology Status Review of waste/Biomass Co-Gasification with Coal, in: 5th European Gasification Conference, Netherlands, IChemE, Netherlands, 2002: pp. 8–10.
- [3] D.L. Klass, Thermal Conversion: Gasification, in: Biomass for Renewable Energy, Fuels, and Chemicals, Academic Press, San Diego, 1998: pp. 271-330.
- [4] A. Kristiansen, Understanding coal gasification, IEA, 1996.
- [5] C. Higman, M. van der Burgt, Introduction, in: Gasification (Second Edition), Gulf Professional Publishing, Burlington, 2008: pp. 1-9.
- [6] W. de Jong, Nitrogen compounds in pressurised fluidised bedgasification of biomass and fossil fuels, PhD, Technische Universiteit Delft, 2005.
- [7] H. Boerrigter, A. Van Der Drift, J.H. Hazewinkel, G. Kupers, BIOSYNGAS; Multifunctional intermediary for the production of renewable electricity, gaseous energy carriers, transportation fuels, and chemicals from biomass, Energy Research Centre of the Netherlands (ECN), 2004.
- [8] R. Parekh, Handbook of gasification and gas treatment systems, United States Department of Energy (DOE), McLean, VA, 1982.

- [9] C. Higman, M. van der Burgt, Gasification Processes, in: Gasification (Second Edition), Gulf Professional Publishing, Burlington, 2008: pp. 91-191.
- [10] C. Di Blasi, G. Signorelli, G. Portoricco, Countercurrent Fixed-Bed Gasification of Biomass at Laboratory Scale, *Industrial & Engineering Chemistry Research*. 38 (1999) 2571-2581.
- [11] NETL, Worldwide Gasification Database, (2007).
- [12] P.T. Radulovic, M.U. Ghani, L.D. Smoot, An improved model for fixed bed coal combustion and gasification, *Fuel*. 74 (1995) 582-594.
- [13] N. Koukouzas, A. Katsiadakis, E. Karlopoulos, E. Kakaras, Co-gasification of solid waste and lignite—A case study for Western Macedonia, *Waste Management*. 28 (2008) 1263-1275.
- [14] A. Valero, S. Usón, Oxy-co-gasification of coal and biomass in an integrated gasification combined cycle (IGCC) power plant, *Energy*. 31 (2006) 1643-1655.
- [15] A. van der Drift, H. Boerrigter, Synthesis gas from biomass: for fuels and chemicals, ECN, 2006.
- [16] A. Faaij, Modern Biomass Conversion Technologies, Mitigation and Adaptation Strategies for Global Change. 11 (2006) 335-367.
- [17] C. Hamelinck, Outlook for Advanced Biofuels. Utrecht, The Netherlands:, PhD, Facultiet Scheikunde van de Universiteit Utrecht, 2004.
- [18] A. Van Der Drift, R. van Ree, H. Boerrigter, K. Hemmes, Bio-syngas: key intermediate for large scale production of green fuels and chemicals, Acknowledgement/Preface. (2004) 88.
- [19] J.P. Ciferno, J.J. Marano, Benchmarking biomass gasification technologies for fuels, chemicals and hydrogen production, US Dept of Energy. (2002).
- [20] J.C. van Dyk, M.J. Keyser, M. Coertzen, Syngas production from South African coal sources using Sasol-Lurgi gasifiers, *International Journal of Coal Geology*. 65 (2006) 243-253.
- [21] G. Hochgesand, Rectisol and purisol, *Industrial & Engineering Chemistry*. 62 (1970) 37-43.
- [22] A. de Klerk, Fisher-Tropsch Refining, PhD Thesis, University of Pretoria, 2008.
- [23] Y.G. Pan, X. Roca, E. Velo, L. Puigjaner, Removal of tar by secondary air in fluidised bed gasification of residual biomass and coal, *Fuel*. 78 (1999) 1703-1709.
- [24] E.G. Baker, L.K. Mudge, Catalytic tar conversion in coal gasification systems, *Industrial & Engineering Chemistry Research*. 26 (1987) 1390-1395.
- [25] L. Devi, K.J. Ptasinski, F.J.J. Janssen, A review of the primary measures for tar elimination in biomass gasification processes, *Biomass and Bioenergy*. 24 (2003) 125-140.
- [26] P. Basu, Tar Production and Destruction, in: *Biomass Gasification Design Handbook*, Academic Press, Boston, 2010: pp. 97-116.
- [27] R. Davidson, A. Doig, J. Ekmann, R. Fernando, N. Harding, R. Moreea-Taha, et al., Cofiring coal with other fuels, IEA Clean Coal Centre, 2007.
- [28] D. Leckel, Catalytic Hydroprocessing of Coal-Derived Gasification Residues to Fuel Blending Stocks: Effect of Reaction Variables and Catalyst on Hydrodeoxygenation (HDO), Hydrodenitrogenation (HDN), and, *Energy and Fuels*. 20 (2006) 1761-1766.

- [29] D. Lamprecht, R. Nel, D. Leckel, Production of On-Specification Fuels in Coal-to-Liquid (CTL) Fischer-Tropsch Plants Based on Fixed-Bed Dry Bottom Coal Gasification, *Energy & Fuels*. 24 (2010) 1479-1486.
- [30] D. Leckel, Diesel Production from Fischer-Tropsch: The Past, the Present, and New Concepts, *Energy & Fuels*. 23 (2009) 2342-2358.
- [31] F. Pinto, C. Franco, R.N. Andre, C. Tavares, M. Dias, I. Gulyurtlu, et al., Effect of experimental conditions on co-gasification of coal, biomass and plastics wastes with air/steam mixtures in a fluidized bed system, *Fuel*. 82 (2003) 1967-1976.
- [32] A.G. Collot, Y. Zhuo, D.R. Dugwell, R. Kandiyoti, Co-pyrolysis and co-gasification of coal and biomass in bench-scale fixed-bed and fluidised bed reactors, *Fuel*. 78 (1999) 667-679.
- [33] Y.G. Pan, E. Velo, X. Roca, J.J. Manya, L. Puigjaner, Fluidized-bed co-gasification of residual biomass/poor coal blends for fuel gas production, *Fuel*. 79 (2000) 1317-1326.
- [34] M. Lapuerta, J.J. Hernández, A. Pazo, J. López, Gasification and co-gasification of biomass wastes: Effect of the biomass origin and the gasifier operating conditions, *Fuel Processing Technology*. 89 (2008) 828-837.
- [35] T.R. McLendon, A.P. Lui, R.L. Pineault, S.K. Beer, S.W. Richardson, High-pressure co-gasification of coal and biomass in a fluidized bed, *Biomass and Bioenergy*. 26 (2004) 377-388.
- [36] J. Herguido, J. Corella, J. Gonzalez-Saiz, Steam gasification of lignocellulosic residues in a fluidized bed at a small pilot scale. Effect of the type of feedstock, *Industrial & Engineering Chemistry Research*. 31 (1992) 1274-1282.
- [37] F. Pinto, H. Lopes, R.N. André, I. Gulyurtlu, I. Cabrita, Effect of catalysts in the quality of syngas and by-products obtained by co-gasification of coal and wastes. 1. Tars and nitrogen compounds abatement, *Fuel*. 86 (2007) 2052-2063.
- [38] F. Pinto, R.N. André, C. Franco, H. Lopes, I. Gulyurtlu, I. Cabrita, Co-gasification of coal and wastes in a pilot-scale installation 1: Effect of catalysts in syngas treatment to achieve tar abatement, *Fuel*. (2009).
- [39] P. Lv, Z. Yuan, L. Ma, C. Wu, Y. Chen, J. Zhu, Hydrogen-rich gas production from biomass air and oxygen/steam gasification in a downdraft gasifier, *Renewable Energy*. 32 (2007) 2173-2185.
- [40] H. Chen, Z. Luo, H. Yang, F. Ju, S. Zhang, Pressurized Pyrolysis and Gasification of Chinese Typical Coal Samples, *Energy & Fuels*. 22 (2008) 1136-1141.
- [41] J. Gil, M.P. Aznar, M.A. Caballero, E. Frances, J. Corella, Biomass Gasification in Fluidized Bed at Pilot Scale with Steam-Oxygen Mixtures. Product Distribution for Very Different Operating Conditions, *Energy & Fuels*. 11 (1997) 1109-1118.
- [42] C. Di Blasi, Combustion and gasification rates of lignocellulosic chars, *Progress in Energy and Combustion Science*. 35 (2009) 121-140.
- [43] W. Zhu, W. Song, W. Lin, Catalytic gasification of char from co-pyrolysis of coal and biomass, *Fuel Processing Technology*. 89 (2008) 890-896.
- [44] W.F. DeGroot, F. Shafizadeh, Kinetics of gasification of Douglas Fir and Cottonwood chars by carbon dioxide, *Fuel*. 63 (1984) 210-216.
- [45] K. Sipilä, Reactivity of biomass chars in fluid-bed steam gasification, Technical Research Centre of Finland, Laboratory of Fuel Processing and Lubrication Technology, Espoo, Finland. (1989).

- [46] M. Barrio, I.E. Hustad, CO₂ gasification of birch char and the effect of CO inhibition on the calculation of chemical kinetics, *Progress in Thermochemical Biomass Conversion*. (2001) 47.
- [47] E. Cetin, B. Moghtaderi, R. Gupta, T.F. Wall, Influence of pyrolysis conditions on the structure and gasification reactivity of biomass chars, *Fuel*. 83 (2004) 2139-2150.
- [48] H. Yang, H. Chen, F. Ju, R. Yan, S. Zhang, Influence of Pressure on Coal Pyrolysis and Char Gasification, *Energy & Fuels*. 21 (2007) 3165-3170.
- [49] C. Di Blasi, G. Signorelli, C. Di Russo, G. Rea, Product Distribution from Pyrolysis of Wood and Agricultural Residues, *Industrial & Engineering Chemistry Research*. 38 (1999) 2216-2224.
- [50] A. Zabaniotou, O. Ioannidou, E. Antonakou, A.A. Lappas, Experimental study of pyrolysis for potential energy, hydrogen and carbon material production from lignocellulosic biomass, *International Journal of Hydrogen Energy*. 33 (2008) 2433-2444.
- [51] A.V. Bridgwater, S.A. Bridge, Review of biomass pyrolysis technologies, in: *Biomass Pyrolysis Liquids Upgrading and Utilization*, Hardcover, Springer, 1991: pp. 11-92.
- [52] R. Kandiyoti, A.A. Herod, K.D. Bartle, Pyrolysis: Thermal Breakdown of Solid Fuels in a Gaseous Environment, in: *Solid Fuels and Heavy Hydrocarbon Liquids*, Elsevier Science Ltd, Oxford, 2006: pp. 36-90.
- [53] P.A. Brownsort, Biomass pyrolysis processes: review of scope, control and variability, UK Biochar Research Centre, 2009.
- [54] J. Lehmann, S. Joseph, Biochar for environmental management, Earthscan, 2009.
- [55] D.B. Anthony, J.B. Howard, Coal devolatilization and hydrogasification, *AIChE Journal*. 22 (1976) 625-656.
- [56] A. Radjenović, Pyrolysis of Coal, *Kemija u Industriji*. 55 (2006).
- [57] B.G. Miller, Introduction to Coal, in: *Coal Energy Systems*, Academic Press, Burlington, 2005: pp. 1-27.
- [58] P.S. Baruya, S. Benson, J. Broadbent, A.M. Carpenter, L.B. Clarke, M. Daniel, et al., *Coal Resources*, IEA Clean Coal Centre, 2003.
- [59] H. Jüntgen, Review of the kinetics of pyrolysis and hydrolysis in relation to the chemical constitution of coal, *Fuel*. 63 (1984) 731-737.
- [60] J.H. Slaghuis, Coal gasification, Sasol Technology, Sasolburg, SA, 1993.
- [61] C. Song, H.S. Schobert, J.M. Andriessen, Premium carbon products and organic chemicals from coal, IEA Clean Coal Centre, 2005.
- [62] R.J. Evans, T.A. Milne, Molecular characterization of the pyrolysis of biomass, *Energy and Fuels*. 1 (1987) 123-137.
- [63] A. Dufour, P. Girods, E. Masson, S. Normand, Y. Rogaume, A. Zoulalian, Comparison of two methods of measuring wood pyrolysis tar, *Journal of Chromatography A*. 1164 (2007) 240-247.
- [64] J. Duxbury, Prediction of coal pyrolysis yields from BS volatile matter and petrographic analyses, *Fuel*. 76 (1997) 1337-1343.
- [65] C.-Z. Li, K.D. Bartle, R. Kandiyoti, Characterization of tars from variable heating rate pyrolysis of maceral concentrates, *Fuel*. 72 (1993) 3-11.

- [66] P. Arendt, K.-H. van Heek, Comparative investigations of coal pyrolysis under inert gas and H₂ at low and high heating rates and pressures up to 10 MPa, *Fuel*. 60 (1981) 779-787.
- [67] J.R. Gibbins, Z.S. Gonenc, R. Kandiyoti, Pyrolysis and hydrolysis of coal: comparison of product distributions from a wire-mesh and a hot-rod reactor, *Fuel*. 70 (1991) 621-626.
- [68] D. Zeng, Effects of pressure on coal pyrolysis at high heating rates and char combustion E, PhD Thesis, Brigham Young University, 2005.
- [69] C.A. Koufopoulos, A. Lucchesi, G. Maschio, Kinetic modelling of the pyrolysis of biomass and biomass components, *The Canadian Journal of Chemical Engineering*. 67 (1989) 75-84.
- [70] O. Ioannidou, A. Zabaniotou, E.V. Antonakou, K.M. Papazisi, A.A. Lappas, C. Athanassiou, Investigating the potential for energy, fuel, materials and chemicals production from corn residues (cobs and stalks) by non-catalytic and catalytic pyrolysis in two reactor configurations, *Renewable and Sustainable Energy Reviews*. 13 (2009) 750-762.
- [71] C. Branca, A. Albano, C. Di Blasi, Critical evaluation of global mechanisms of wood devolatilization, *Thermochimica Acta*. 429 (2005) 133-141.
- [72] F. Shafizadeh, Introduction to pyrolysis of biomass, *Journal of Analytical and Applied Pyrolysis*. 3 (1982) 283-305.
- [73] G.R. Ponder, G.N. Richards, Thermal synthesis and pyrolysis of a xylan, *Carbohydrate Research*. 218 (1991) 143-155.
- [74] D.K. Shen, S. Gu, A.V. Bridgwater, Study on the pyrolytic behaviour of xylan-based hemicellulose using TG-FTIR and Py-GC-FTIR, *Journal of Analytical and Applied Pyrolysis*. 87 (2010) 199-206.
- [75] E. Dorrestijn, P. Mulder, The radical-induced decomposition of 2-methoxyphenol, *Journal of the Chemical Society, Perkin Transactions 2*. 1999 (1999) 777-780.
- [76] H. Haykiri-Acma, S. Yaman, S. Kucukbayrak, Comparison of the thermal reactivities of isolated lignin and holocellulose during pyrolysis, *Fuel Processing Technology*. In Press, Corrected Proof (2010).
- [77] C. Zaror, D. Pyle, The pyrolysis of biomass: A general review, *Sadhana*. 5 (1982) 269-285.
- [78] W.S.-L. Mok, M.J. Antal, Effects of pressure on biomass pyrolysis. I. Cellulose pyrolysis products, *Thermochimica Acta*. 68 (1983) 155-164.
- [79] S. Li, J. Lyons-Hart, J. Banyasz, K. Shafer, Real-time evolved gas analysis by FTIR method: an experimental study of cellulose pyrolysis, *Fuel*. 80 (2001) 1809-1817.
- [80] F. Shafizadeh, A.G.W. Bradbury, Thermal degradation of cellulose in air and nitrogen at low temperatures, *Journal of Applied Polymer Science*. 23 (1979) 1431-1442.
- [81] W.S.-L. Mok, M.J. Antal, Effects of pressure on biomass pyrolysis. II. Heats of reaction of cellulose pyrolysis, *Thermochimica Acta*. 68 (1983) 165-186.
- [82] D.F. Arseneau, Competitive reactions in the thermal decomposition of cellulose, *Canadian Journal of Chemistry*. 49 (1971) 632-638.
- [83] F. Shafizadeh, Y.L. Fu, Pyrolysis of cellulose, *Carbohydrate Research*. 29 (1973) 113-122.

- [84] G. Varhegyi, M.J. Antal, E. Jakab, P. Szabó, Kinetic modeling of biomass pyrolysis, *Journal of Analytical and Applied Pyrolysis*. 42 (1997) 73-87.
- [85] Q. Liu, C. Lv, Y. Yang, F. He, L. Ling, Study on the pyrolysis of wood-derived rayon fiber by thermogravimetry-mass spectrometry, *Journal of Molecular Structure*. 733 (2005) 193-202.
- [86] Q. Liu, C. Lv, Y. Yang, F. He, L. Ling, Study on the pyrolysis of wood-derived rayon fiber by thermogravimetry-mass spectrometry, *Journal of Molecular Structure*. 733 (2005) 193-202.
- [87] M.J. Antal, M. Gronli, The Art, Science, and Technology of Charcoal Production†, *Industrial & Engineering Chemistry Research*. 42 (2003) 1619-1640.
- [88] M.J. Antal, G. Varhegyi, Cellulose pyrolysis kinetics: the current state of knowledge, *Industrial and Engineering Chemistry Research*. 34 (1995) 703-717.
- [89] F. Shafizadeh, G.D. McGinnis, C.W. Philpot, Thermal degradation of xylan and related model compounds, *Carbohydrate Research*. 25 (1972) 23-33.
- [90] D. Ferdous, A.K. Dalai, S.K. Bej, R.W. Thring, Pyrolysis of lignins: Experimental and kinetics studies, *Energy Fuels*. 16 (2002) 1405–1412.
- [91] E. Biagini, F. Barontini, L. Tognotti, Devolatilization of Biomass Fuels and Biomass Components Studied by TG/FTIR Technique, *Industrial & Engineering Chemistry Research*. 45 (2006) 4486-4493.
- [92] T. Hosoya, H. Kawamoto, S. Saka, Pyrolysis gasification reactivities of primary tar and char fractions from cellulose and lignin as studied with a closed ampoule reactor, *Journal of Analytical and Applied Pyrolysis*. 83 (2008) 71-77.
- [93] D.L. Klass, Thermal Conversion: Pyrolysis and Liquefaction, in: *Biomass for Renewable Energy, Fuels, and Chemicals*, Academic Press, San Diego, 1998: pp. 225-269.
- [94] C. Di Blasi, Modeling chemical and physical processes of wood and biomass pyrolysis, *Progress in Energy and Combustion Science*. 34 (2008) 47-90.
- [95] M. Garcí-a-Pèrez, A. Chaala, J. Yang, C. Roy, Co-pyrolysis of sugarcane bagasse with petroleum residue. Part I: thermogravimetric analysis, *Fuel*. 80 (2001) 1245-1258.
- [96] K. Muira, A New and Simple Method to Estimate $f(E)$ and $ko(E)$ in the Distributed Activation Energy Model from Three Sets of Experimental Data, *Energy & Fuels*. 9 (1995) 302-307.
- [97] S. Vyazovkin, Model-free kinetics, *Journal of Thermal Analysis and Calorimetry*. 83 (2006) 45-51.
- [98] E. Biagini, A. Fantei, L. Tognotti, Effect of the heating rate on the devolatilization of biomass residues, *Thermochimica Acta*. 472 (2008) 55-63.
- [99] B. Moghtaderi, The state-of-the-art in pyrolysis modelling of lignocellulosic solid fuels, *Fire and Materials*. 30 (2005) 1–34.
- [100] C. Di Blasi, Kinetic and heat transfer control in the slow and flash pyrolysis of solids, *Ind. Eng. Chem. Res*. 35 (1996) 37–46.
- [101] N.M. Laurendeau, Heterogeneous kinetics of coal char gasification and combustion, *Progress in Energy and Combustion Science*. 4 (1978) 221-270.
- [102] C. Di Blasi, Kinetic modeling of biomassgasification and combustion, *Thermalnet*, n.d.

- [103] H. Rudiger, U. Greul, H. Spliethoff, K.R.G. Hein, Co-pyrolysis of Coal/Biomass and Coal/Sewage Sludge Mixtures in an Entrained Flow Reactor, APAS Clean Coal Technology Program. Volume 3, by European Commission, 1999.
- [104] I. Rafiqul, B. Lugang, Y. Yan, T. Li, Study on co-liquefaction of coal and bagasse by factorial experiment design method, *Fuel Processing Technology*. 68 (2000) 3-12.
- [105] B. Moghtaderi, C. Meesri, T.F. Wall, Pyrolytic characteristics of blended coal and woody biomass, *Fuel*. 83 (2004) 745-750.
- [106] S. Rodjeen, L. Mekasut, P. Kuchontara, P. Piumsomboon, Parametric studies on catalytic pyrolysis of coal-biomass mixture in a circulating fluidized bed, *Korean Journal of Chemical Engineering*. 23 (2006) 216-223.
- [107] P.R. Bonelli, E.L. Buonomo, A.L. Cukierman, Pyrolysis of Sugarcane Bagasse and Co-pyrolysis with an Argentinean Subbituminous Coal, *Energy Sources-Part A Recovery Utilization and Environmental Effects*. 29 (2007) 731-740.
- [108] T. Sonobe, N. Worasuwanarak, S. Pipatmanomai, Synergies in co-pyrolysis of Thai lignite and corncob, *Fuel Processing Technology*. 89 (2008) 1371-1378.
- [109] C. Meesri, B. Moghtaderi, Lack of synergetic effects in the pyrolytic characteristics of woody biomass/coal blends under low and high heating rate regimes, *Biomass and Bioenergy*. 23 (2002) 55-66.
- [110] A. Megaritis, R.C. Messenböck, I.N. Chatzakis, D.R. Dugwell, R. Kandiyoti, High-pressure pyrolysis and CO₂-gasification of coal maceral concentrates: conversions and char combustion reactivities, *Fuel*. 78 (1999) 871-882.
- [111] D.K. Park, S.D. Kim, S.H. Lee, J.G. Lee, Co-pyrolysis characteristics of sawdust and coal blend in TGA and a fixed bed reactor, *Bioresource Technology*. Article in Press (n.d.).
- [112] H. Haykiri-Acma, S. Yaman, Interaction between biomass and different rank coals during co-pyrolysis, *Renewable Energy*. 35 (2010) 288-292.
- [113] H. Haykiri-Acma, S. Yaman, Synergy in devolatilization characteristics of lignite and hazelnut shell during co-pyrolysis, *Fuel*. 86 (2007) 373-380.
- [114] H.-X. Wu, H.-B. Li, Z.-L. Zhao, Thermogravimetric analysis and pyrolytic kinetic study on coal/biomass blends, *Ranliao Huaxue Xuebao/Journal of Fuel Chemistry and Technology*. 37 (2009) 538-545.
- [115] M. Yilgin, N. Deveci Duranay, D. Pehlivan, Co-pyrolysis of lignite and sugar beet pulp, *Energy Conversion and Management*. 51 (2010) 1060-1064.
- [116] P. STRAKA, K. Vlastimil, HYDROGEN PRODUCTION BY TWO-STAGE CO-PYROLYSIS OF BITUMINOUS COAL-POLYMERS MIXTURES, *Acta Geodynamica Et Geomaterialia*. (2008) 77.
- [117] I. Suelves, R. Moliner, M.J. Lázaro., Synergetic effects in the co-pyrolysis of coal and petroleum residues: influences of coal mineral matter and petroleum residue mass ratio, *Journal of Analytical and Applied Pyrolysis*. 55 (2000) 29-41.
- [118] I. Suelves, M.J. Lázaro, R. Moliner, Synergetic effects in the co-pyrolysis of samca coal and a model aliphatic compound studied by analytical pyrolysis, *Journal of Analytical and Applied Pyrolysis*. 65 (2002) 197-206.
- [119] H. Darmstadt, M. Garcia-Perez, A. Chaala, N.Z. Cao, C. Roy, Co-pyrolysis under vacuum of sugar cane bagasse and petroleum residue properties of the char and activated char products, *Carbon*. 39 (2001) 815-825.

- [120] J.L. Ye, Q. Cao, Y.S. Zhao, Co-pyrolysis of Polypropylene and Biomass, *Energy Sources, Part A: Recovery, Utilization, and Environmental Effects*. 30 (2008) 1689.
- [121] Q. Cao, L. Jin, W. Bao, Y. Lv, Investigations into the characteristics of oils produced from co-pyrolysis of biomass and tire, *Fuel Processing Technology*. 90 (2009) 337–342.
- [122] F. Paradela, F. Pinto, I. Gulyurtlu, I. Cabrita, N. Lapa, Study of the co-pyrolysis of biomass and plastic wastes, *Clean Technologies and Environmental Policy*. 11 (2009) 115–122.
- [123] Q. Ren, C. Zhao, X. Wu, C. Liang, X. Chen, J. Shen, et al., TG-FTIR study on co-pyrolysis of municipal solid waste with biomass, *Bioresource Technology*. 100 (2009) 4054-4057.
- [124] R.N. Andre, F. Pinto, C. Franco, M. Dias, I. Gulyurtlu, M.A.A. Matos, et al., Fluidised bed co-gasification of coal and olive oil industry wastes, *Fuel*. 84 (2005) 1635-1644.
- [125] K. Sjöström, G. Chen, Q. Yu, C. Brage, C. Rosén, Promoted reactivity of char in co-gasification of biomass and coal: synergies in the thermochemical process, *Fuel*. 78 (1999) 1189-1194.
- [126] K. Li, R. Zhang, J. Bi, Experimental study on syngas production by co-gasification of coal and biomass in a fluidized bed, *International Journal of Hydrogen Energy*. 35 (2010) 2722-2726.
- [127] K. Kumabe, T. Hanaoka, S. Fujimoto, T. Minowa, K. Sakanishi, Co-gasification of woody biomass and coal with air and steam, *Fuel*. 86 (March) 684-689.
- [128] C.A. Alzate, F. Chejne, C.F. Valdés, A. Berrio, J.D.L. Cruz, C.A. Londoño, CO-gasification of pelletized wood residues, *Fuel*. 88 (2009) 437-445.
- [129] Y.J. Kim, S.H. Lee, S.D. Kim, Coal gasification characteristics in a downer reactor, *Fuel*. 80 (2001) 1915-1922.
- [130] R.C. Brown, Q. Liu, G. Norton, Catalytic effects observed during the co-gasification of coal and switchgrass, *Biomass and Bioenergy*. 18 (2000) 499-506.
- [131] F. Pinto, H. Lopes, R.N. André, I. Gulyurtlu, I. Cabrita, Effect of catalysts in the quality of syngas and by-products obtained by co-gasification of coal and wastes. 2: Heavy metals, sulphur and halogen compounds abatement, *Fuel*. 87 (2008) 1050-1062.
- [132] E. Biagini, F. Lippi, L. Petarca, L. Tognotti, Devolatilization rate of biomasses and coal–biomass blends: an experimental investigation, *Fuel*. 81 (2002) 1041-1050.
- [133] A.K. Sadhukhan, P. Gupta, T. Goyal, R.K. Saha, Modelling of pyrolysis of coal-biomass blends using thermogravimetric analysis, *Bioresource Technology*. 99 (2008) 8022-8026.

3 Model free kinetics of the pyrolysis of agricultural waste

Published in Thermochimica Acta as:

Title: “Non-isothermal kinetic analysis of the devolatilization of corn cobs and sugar cane bagasse in an inert atmosphere”

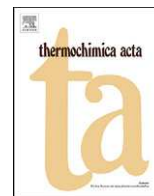
Authors: Akinwale O. Aboyade^{a,b}, Marion Carrier^a, Edson L. Meyer^b, Ralph Stahl^c, Johannes H Knoetze^a, Johann F. Görgens^a

^aDepartment of Process Engineering, Stellenbosch University, Stellenbosch, South Africa

^bFort Hare Institute of Technology, University of Fort Hare, Alice, South Africa

^cInstitute of Technical Chemistry-Division of Chemical and Physical Processing, Forschungszentrum Karlsruhe, Germany

Reproduced in this thesis with copyright approval from Elsevier Limited



Non-isothermal kinetic analysis of the devolatilization of corn cobs and sugar cane bagasse in an inert atmosphere

Akinwale O. Aboyade^{a,b}, Thomas J. Hugo^a, Marion Carrier^a, Edson L. Meyer^b, Ralph Stahl^c, Johannes H. Knoetze^a, Johann F. Görgens^{a,*}

^a Department of Process Engineering, Stellenbosch University, Stellenbosch, South Africa

^b Fort Hare Institute of Technology, University of Fort Hare, Alice, South Africa

^c Institute of Technical Chemistry-Division of Chemical and Physical Processing, Forschungszentrum Karlsruhe, Germany

ARTICLE INFO

Article history:

Received 10 August 2010

Received in revised form 21 January 2011

Accepted 26 January 2011

Available online 5 March 2011

Keywords:

Biomass

Devolatilization

Pyrolysis

Thermogravimetric analysis (TGA)

Non-isothermal

Kinetic analysis

Corn cobs

Sugar cane bagasse

ABSTRACT

Corn cobs and sugar cane bagasse are two of the most important agricultural residues in South Africa in terms of availability and potential for use as a bioenergy resource. The thermal devolatilization of samples of these two fuels in an inert atmosphere was studied by non-isothermal thermogravimetric analysis in the heating rate range of 10–50 °C min⁻¹. Friedman's isoconversional method was applied using the AKTS Thermokinetics software to obtain the dependence of activation energy on conversion. The same method was also applied to the kinetic analysis of lignocellulosic pseudocomponents derived from the mathematical deconvolution of the original DTG curves. The results showed that apparent activation energy in the 0.1–0.8 conversion interval ranged from 170–225 kJ mol⁻¹ to 75–130 kJ mol⁻¹ for sugar cane bagasse and corn cobs respectively. The range of apparent activation energy obtained for the pseudocomponents representing hemicelluloses, cellulose and lignin derived from sugar cane bagasse were given as 200–300 kJ mol⁻¹, 163–245 kJ mol⁻¹, and 80–180 kJ mol⁻¹, while for corn cobs the values were 85–110 kJ mol⁻¹, 80–140 kJ mol⁻¹, and 10–60 kJ mol⁻¹ respectively. The derived thermokinetic parameters from both global and pseudocomponent analyses satisfactorily reproduced the experimental curves used for the analysis and could also successfully predict reaction progress at a heating rate outside what was used in the analysis. The fits obtained between simulated and experimental results were comparable to what has been reported in the literature based on conventional model-fitting techniques.

© 2011 Elsevier B.V. All rights reserved.

1. Introduction

Various procedures for evaluating kinetic parameters from data derived from non-isothermal thermogravimetric analysis (TGA) have been developed, and the vast majority of them can be classified as either 'model-free' or 'model-fitting'. Until recently, the model-fitting approach has found wider application in biomass thermochemical conversion studies, although it is widely recognised that the method suffers from two main deficiencies, particularly in cases where data from only a single heating rate is applied: i) it can often yield different values of kinetic parameters describing the same thermogravimetric curve, leading to an ambiguity in terms of interpretation of the results; ii) it generally tends to yield one set of kinetic parameters for the whole range of conversion, therefore not taking into account the complexity of mechanisms involved during pyrolysis of plant biomasses. Applying model fitting to datasets from multiple heating rates addresses

the first concern [1] but not the second [2]. On the other hand, model-free methods shown to be effective in overcoming the aforementioned problems associated with model fitting [2–4]. As the name implies, model-free techniques do not require assumption of reaction models, and yield kinetic parameters as a function of either conversion (isoconversional analysis) or temperature (non-parametric kinetics) [3].

The isoconversional approach is the more commonly adopted of the two main model-free methods and is increasingly being adopted in biomass thermochemical conversion research. In 2001, García-Pérez et al. [5] employed Friedman's isoconversional approach to the study of the pyrolysis kinetics of sugar cane bagasse. More recently, Biagini et al. [6,7], Cai et al. [8–10], Leroy et al. [11], Gašparovič et al. [12], Xiao et al. [13], Tonbul [14], and Santos et al. [15], have all employed various isoconversional methods in the analysis of the non-isothermal decomposition of biomass and/or its components. Only a few of these studies [11,12] attempted to validate their model-free derived kinetic parameters by simulating or predicting the non-isothermal experimental data. According to Varhegyi [1] the lack of comparison of analytical results with experimen-

* Corresponding author. Tel.: +27 21 808 3503; fax: +27 21 808 2059.
E-mail address: jgorgens@sun.ac.za (J.F. Görgens).

Table 1
Proximate and ultimate characteristics of corn cobs (CC) and sugar cane bagasse (SB) from this study and from other authors.

	CC Present study	SB Present study	CC Ioannidou et al. [30]	CC Sonobe et al. [49]	SB Drummond and Drummond [43]	SB Munir et al. [45]
Proximate analysis (wt.% dry basis)						
Moisture	6.5	6.8	7.6			
Volatiles	80.2	76.9	84.3	82.2	86.5	81.5
Fixed Carbon ^a	16.7	17.8	7.63	16.9	11.9	13.3
Ash	3.1	5.3	8.06	0.9	1.6	5.2
HHV (MJ/kg)	17.2	17.5	18.3 (LHV)			17.7
Ultimate analysis (wt.% dry and ash free basis)						
C	49.0	50.3	43.8	45.5	46.3	46.2
H	6.0	6.3	6.2	6.2	6.3	6.3
O ^a	44.7	43.1	50	37.9	47.2	45.7
N	0.3	0.3		1.3	0.2	1.8
S	0.08	0.07		0.0		

^a Calculated by difference.

tal data calls into question the reliability of derived kinetic parameters.

The present work aims at obtaining information on the devolatilization behaviour and kinetics of corn cobs and sugar cane bagasse. These two feedstocks represent the bulk of agricultural residue in South Africa that is potentially available for bioenergy production [16,17]. It has been estimated that up to 3.3 and 6.7 million tonnes of sugar cane bagasse and corn residue are generated in South Africa per annum, representing an energy equivalence of 118 and 58 PJ/yr, respectively [16]. Friedman's isoconversional method has been employed to obtain the variation of kinetic parameters over the entire range of conversion for the samples. Furthermore, a unique approach was employed to derive kinetic parameters of the constituent lignocellulosic pseudocomponents. Global TGA data of the samples were deconvoluted and the separated peaks representing hemicelluloses, cellulose and lignin were subjected to the same Friedman's analysis. Predictions based on the derived kinetic parameters were compared with experimental data in order to obtain an indication of the reliability of the kinetic approach employed.

2. Material and methods

2.1. Samples

Dried corn cobs (CC) were collected from a farm in the Free State province in South Africa, soon after grain harvesting in 2008. Sugar cane bagasse (SB) used in this work was provided by the South African Sugar Milling Research Institute (SMRI). First, dried samples of both materials were chopped to a particle size <1 mm; afterwards representative fractions were milled using a cryogenic grinder and sieved with a fraction of 125–350 μm retained for the experimental runs. The proximate and ultimate characteristics of CC and SB from this study as well as from previous studies by other authors are presented in Table 1.

2.2. Experimental method

The higher heating value (HHV) of the samples was measured using a plain jacket calorimeter (Parr Instruments, USA, Model 1341). Ultimate analysis was done using a Vario EL elemental analyzer (Elementar Analysensysteme, Hanau, Germany). A Netzsch STA 409 balance was used for thermogravimetric analysis. Low sample masses and particle sizes (approximately 20–50 mg, and <350 μm) were used in order to reduce the occurrence of secondary vapour–solid interactions, and the effects of mass and intra-particle heat transfer [18]. For each experimental run, samples were held at

room temperature for 15 min, heated to 105 °C and held again for 30 min. At this stage, the sample mass would have stabilized at a constant dry weight and was then heated to 700 °C at the following heating rates; 10 °C min⁻¹, 20 °C min⁻¹, 30 °C min⁻¹, 40 °C min⁻¹, and 50 °C min⁻¹. These low heating rates are characteristic of fixed bed processes [19,20]. The nitrogen flow during pyrolysis was set to be 55 mL min⁻¹ (protective gas into the balance) plus 15 mL min⁻¹ directly into the oven chamber. For combustion of the formed char, the temperature was maintained at 700 °C for a further 30 min and the nitrogen flow into the balance was kept constant at 55 mL min⁻¹ and 15 mL min⁻¹ of oxygen were fed into the oven (instead of 15 mL min⁻¹ nitrogen). Variation of the sample residual mass with respect to time and temperature change (TG data), and its derivative with respect to time (DTG data), were continuously collected using the Netzsch Proteus software.

2.3. Kinetic analysis

Kinetic evaluation in this study focuses on the temperature range where devolatilization mainly occurs, i.e. 115–500 °C (corresponding to stages 2 and 3 of Fig. 1). Curves derived from 10–40 °C min⁻¹ heating rate experiments were used in the analysis. The kinetic analysis of the thermal decomposition of biomass is usually based on the rate equation for solid state decomposition processes [3,21]

$$\frac{d\alpha}{dt} = A \exp\left[-\frac{E}{RT}\right] f(\alpha) \quad (1)$$

where α is the reacted fraction of the sample or conversion, $f(\alpha)$ is the reaction model, A and E are the Arrhenius–pre-exponential factor and activation energy, respectively. The isoconversional approach does not require the choosing of a reaction model and is thus 'model-free'. It allows the estimation of E as a function of conversion, α independent of the reaction model, $f(\alpha)$. The most common application of the isoconversional analysis was developed by Friedman [22] and is used in this work. The method involves computing the logarithms of the Arrhenius rate equation to get:

$$\ln\left(\frac{d\alpha}{dt}\right) = \ln\left(\beta \frac{d\alpha}{dT}\right) = \ln[A \cdot f(\alpha)] - \frac{E}{RT} \quad (2)$$

A plot of $\ln(d\alpha/dt)$ against $1/T_i$ at the same degree of conversion from data taken at various heating rates will result in a series of lines, each with slope equal to $-E/R$ corresponding to each value of conversion, α , at different heating rates β . Thus the dependence of E and $\ln(A \cdot f(\alpha))$ on α can be obtained.

A multi-component analysis approach is also frequently adopted as part of the kinetic study of biomass degradation [1,23–25]. In this approach, biomass is generally assumed to be

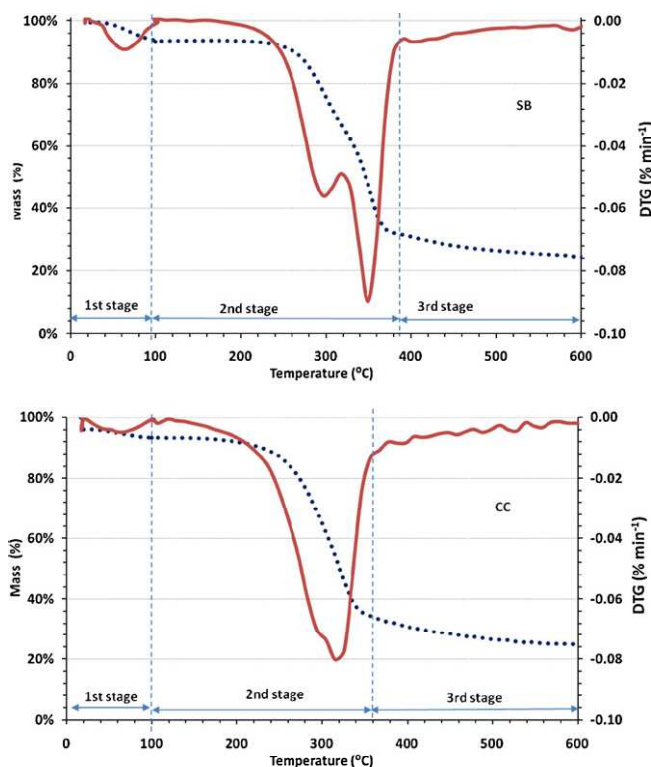


Fig. 1. TG and DTG curves of CC and SB at $10^{\circ}\text{Cmin}^{-1}$ heating rate with TG (●●●) and DTG (—) curves.

composed of pseudocomponents reacting in parallel or in series [1]. Assuming parallel, multi-component reactions, Eq. (1) becomes;

$$\frac{d\alpha}{dt} = \sum \gamma_i A_i \exp\left[-\frac{E_i}{RT}\right] f(\alpha_i) \quad (3)$$

where γ_i is the contribution of pseudocomponent i to the total mass loss. Normally, such multi-component analysis of biomass devolatilization kinetics is conducted via the model-fitting approach [1,23,26]. However, in this study the Friedman's method has been applied to the evaluation of the kinetics of individual pseudocomponents present in the biomass. Global DTG curves for each heating rate considered were first deconvoluted into three peaks corresponding to the pseudocomponents—hemicelluloses, cellulose and lignin. Deconvolution was done based on the application of Gaussian and/or Fraser-Suzuki (asymmetric) type signals [27]. The fitting of calculated signal to the experimental data is performed using Marquardt's non-linear optimization [27].

Simulation of experimental curves was obtained from the following expression [2,4];

$$t_{\alpha} = \frac{1/\beta \int_0^{T_{\alpha}} \exp(-E_{\alpha}/RT) dT}{\exp(-E_{\alpha}/RT_0)} \quad (4)$$

where t refers to the time, R refers to the gas constant, β refers to the heating rate and T_0 refers to initial temperature. The integral in Eq. (4) is solved based on values of E_{α} and T_{α} which are obtained directly from tables derived from Eq. (2). The obtained quality of fit (QOF) between simulated and experimental curves was evaluated via the expression:

$$\text{QOF}(\%) = 100 \times \sum_{i=1}^{N_k} \frac{\sqrt{\{(d\alpha/dt)_{\text{exp}} - (d\alpha/dt)_{\text{calc}}\}^2 / N_k}}{\text{Max}|d\alpha/dt|_{\text{exp}}} \quad (5)$$

where N_k is the number of experimental points employed. The AKTS-Thermokinetics software was used for all kinetic analysis in this study [27]. The software allows the baseline optimization of

Table 2
Devolatilization parameters for CC and SB at different heating rates.

Sample	Heating rate ($^{\circ}\text{Cmin}^{-1}$)	T_h ($^{\circ}\text{C}$)	T_c ($^{\circ}\text{C}$)	T_f ($^{\circ}\text{C}$)	$\%R_{\text{ash}}$ (at 680°C)
CC	10	283	318	330	20.3
	20	305	330	365	20.8
	30	308	337	375	20.0
	40	312	339	387	19.5
SB	10	295	350	376	24.1
	20	307	362	391	19.5
	30	312	370	400	18.7
	40	320	374	412	21.6

T_f : the final temperature of cellulose degradation.

T_h, T_c : the peak temperature corresponding to a maximum weight loss for hemicelluloses and cellulose, respectively.

$\%R_{\text{ash}}$: the final residue.

data curves simultaneously with the estimation of kinetic parameters [27,28].

3. Results and discussions

3.1. Description of thermoanalytical curves

Fig. 1 shows mass loss (TG) and derivative mass loss (DTG) curves for SB and CC at $10^{\circ}\text{Cmin}^{-1}$ under inert atmosphere. In general, three distinct weight loss stages could be identified, in agreement with previous findings [29–31]. The first stage, corresponding to the reduction in mass at temperatures lower than 100°C can be attributed to the demineralization of the samples, 6.5–11.8 wt.% and 5.0–7.1 wt.% respectively for CC and SB. In the second stage, the temperature range 100 – 200°C , we see negligible weight loss (<1.5% for CC, and <1% for SB), which was followed by the start of devolatilization characterized by rapid weight loss, at 200°C for CC and at 230°C for SB. The insignificant weight loss prior to the start of devolatilization has been attributed to the removal of bound moisture and the start of polysaccharide hydrolysis [29,32].

Lignocellulosic biomasses are comprised of hemicelluloses, cellulose and lignin as the major components [33]. The second stage of weight loss depicted in Fig. 1 corresponds mainly to the degradation of these components [34]. Hemicelluloses typically decompose in the range of 160 – 360°C , while cellulose degrades at the higher temperature range of 240 – 390°C [23]. The loss of lignin typically occurs at a slower rate over a much wide temperature range of 180 – 900°C [18,23,35]. On the DTG curves the temperatures at which maximum rate of weight loss occurred are described by the position of the peaks in the curve. The DTG curve of SB during the devolatilization stage shows two distinct peaks which are represented by a noticeable change in slope of the TG curve. The DTG peaks are much closer to each other for CC than for SB and the maximum of hemicelluloses and cellulose peaks occurring at lower temperatures. Antal and Varhegyi [18] ascribed the cause of the merged DTG peaks to the catalytic behaviour of mineral matter present in biomass, which may explain why SB with an ash content of 5.3% exhibits a more distinct peak compared to CC which has 3.1% ash content.

The third stage, starting from the base of the DTG peak assigned to cellulose (Fig. 1), has a much lower rate of weight loss (12% for CC and 10% for SB) than the second stage (58% for CC and 60% for SB). According to Roque-Diaz et al. [29], for SB, this stage of biomass decomposition corresponds partly to the end of cellulose decomposition, and partly to the beginning of secondary decomposition of heavier volatiles and the formation of char. The decomposition of lignin has also been reported to continue into this stage [31].

Table 2 shows the effect of heating rate on peak temperatures and fraction of mass remaining at the end of conversion. The posi-

Table 3
Relative contributions of pseudocomponents obtained from deconvolution.

Heating rate ($^{\circ}\text{C min}^{-1}$)	γ_i -CC (%)			γ_i -SB (%)		
	Hemicelluloses	Cellulose	Lignin	Hemicelluloses	Cellulose	Lignin
10	54.5	28.4	17.1	20.5	38.3	41.2
20	44.3	39.5	16.2	23.9	48.8	27.3
30	46.7	31.9	21.4	27.1	42.7	30.2
40	52.6	25.9	21.5	25.6	43.1	31.3
Average	49.5	31.4	19.1	24.3	43.2	32.5

tion of peaks ascribed to hemicelluloses and cellulose in SB shifted from 295°C to 321°C and from 350°C to 376°C respectively. For CC, the peaks in the DTG curve are so close that they tended to overlap, especially at higher heating rates. According to Haykiri-Acma et al. [36] and Di Blasi [37] the overlapping of DTG peaks was probably due to sufficiently low heating rates allowing enough time for each individual component in the biomass to decompose at its own typical peak temperature, while at high heating rates decomposition is almost simultaneous and as such adjacent peaks representing hemicelluloses and cellulose are merged to form broader peaks.

3.2. Global kinetic analysis

Apparent E and $\ln(A \cdot f(\alpha))$ values for both SB and CC calculated via Friedman's method are presented in Fig. 2. The plots also show correlation coefficients for the parameter estimation over the entire conversion range. The correlation coefficients relate to the linearity (R^2) of the lines joining isoconversional points on the Friedman's plots, i.e. plots of $\ln(d\alpha/dt)_i$ against $1/T_i$ described earlier. It highlights the limitations arising from experimental data variations in the beginning and towards the end of thermogravimetric pyrolytic conversion [6]. For this reason, further discussions will focus on the 0.1–0.9 (0.8 for CC) conversion range.

The overall trend of apparent activation energy (E) dependence on α was relatively similar for both CC and SB in the sense that E more or less increased in the 0.1–0.6 conversion ranges for both materials, followed by a reduction at higher conversion levels. At

the start of CC devolatilization, E increased from just less than 100 kJ mol^{-1} to peak at 150 kJ mol^{-1} (at $\alpha=0.2$). This was followed by a further increase until a new peak of 160 kJ mol^{-1} was reached at about $\alpha=0.6$. Another peak in the apparent activation energy curve can be observed at about $\alpha=0.9$ although the low correlation coefficient at this point implies the values might be more unreliable. The apparent E curve for SB was smoother, starting with an initial peak of about 200 kJ mol^{-1} at $\alpha=0.05$, increasing to the highest point of 225 kJ mol^{-1} at about $\alpha=0.5$. Thereafter, E decreased reaching 150 kJ mol^{-1} at $\alpha=0.9$. The range of overall E values obtained here for SB agreed well with those arrived at by Garcìa-Pèrez et al. [5] using the same isoconversional method, i.e. $150\text{--}200 \text{ kJ mol}^{-1}$ in the conversion range, 0.05–0.75. No isoconversional based literature was available to compare CC results with, although Cao et al. [38] and Zabanitoutou et al. [39] obtained $68\text{--}176 \text{ kJ mol}^{-1}$ and $65\text{--}75 \text{ kJ mol}^{-1}$ respectively, using a curve fitting approach based on single first order reaction model.

The E values presented in the results are not the actual activation energy of any particular single reaction step, but is rather an aggregate (or apparent) value reflecting the contributions of numerous competing and parallel reaction steps to the overall reaction rate. These contributions, for a complex process such as biomass devolatilization, are known to vary with respect to temper-

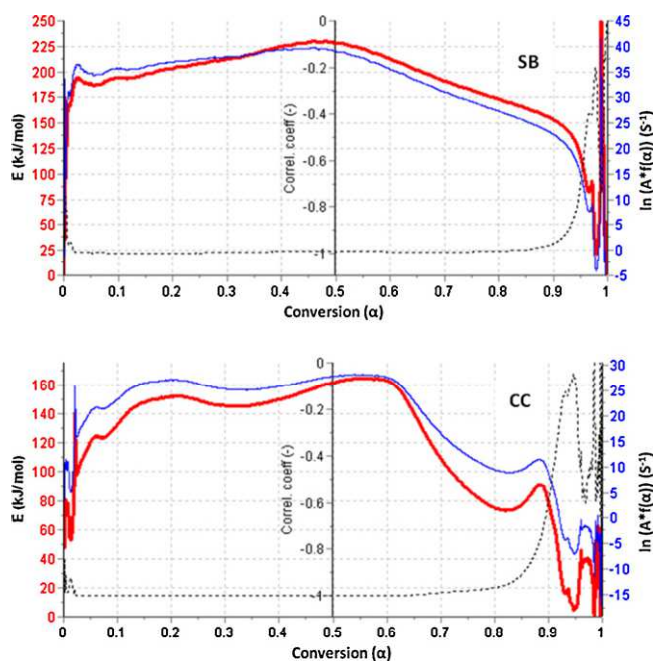


Fig. 2. Apparent E , $\ln(A \cdot f(\alpha))$ dependence on conversion for CC and SB with E (—), $\ln(A \cdot f(\alpha))$ (—) and the calculated correlation coefficients (.....).

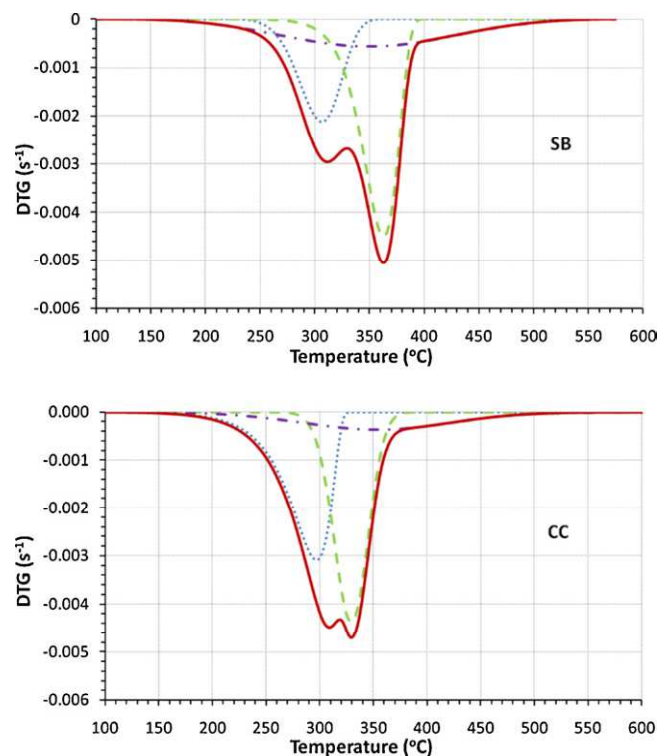


Fig. 3. Deconvolution of DTG curves for CC and SB at $20^{\circ}\text{C min}^{-1}$ with hemicelluloses (▲▲▲), cellulose (■ ■ ■), lignin (● ● ●) and the sum of the curves (—).

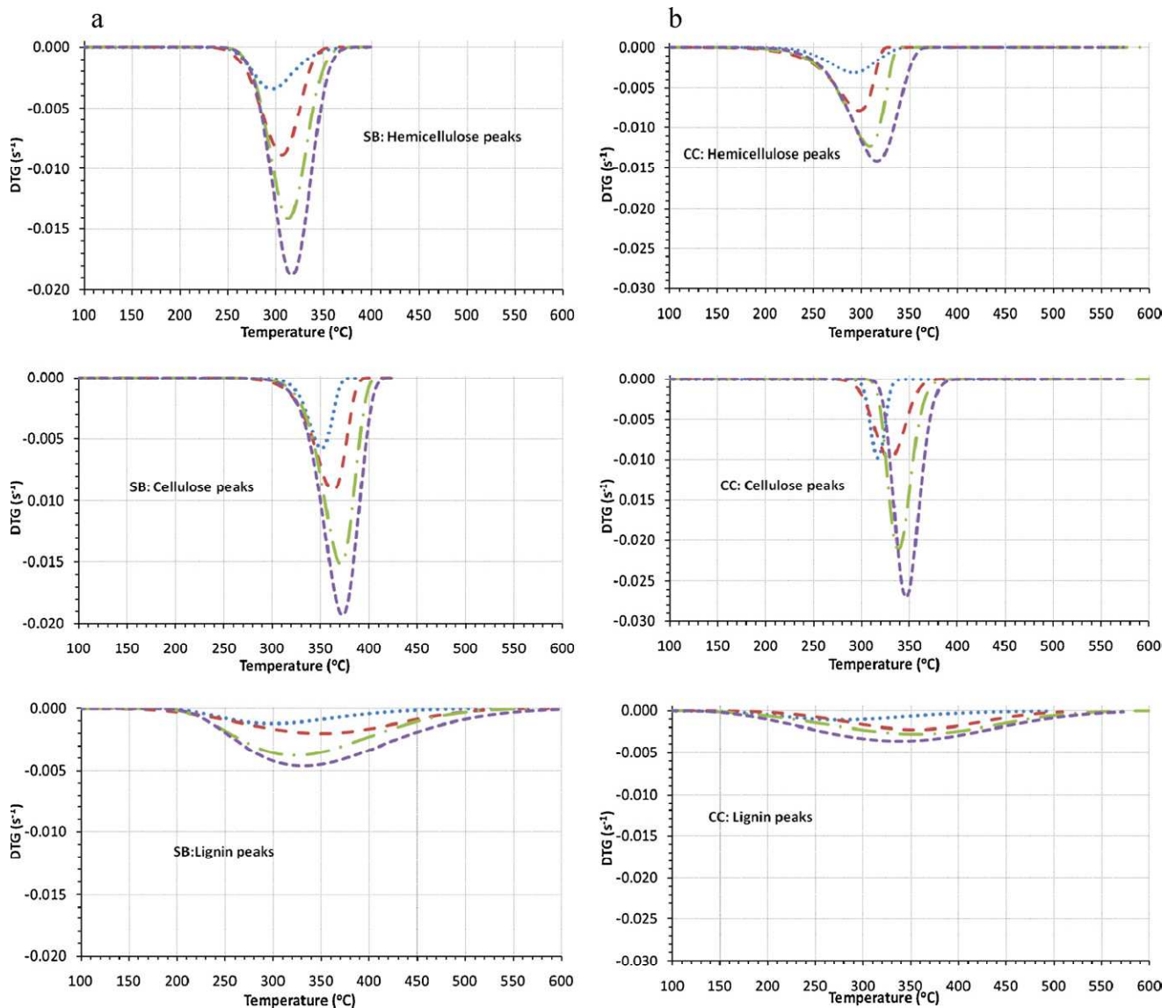


Fig. 4. DTG of SB and CC pseudocomponents obtained by deconvolution of global curves with $10^{\circ}\text{C min}^{-1}$ (—), $20^{\circ}\text{C min}^{-1}$ (—), $30^{\circ}\text{C min}^{-1}$ (—●—) and $40^{\circ}\text{C min}^{-1}$ (—).

ature and extent of reaction [2], and frequently overlap one another. This factor limits the theoretical utility of such global kinetic parameters in describing specific decomposition reactions mechanisms since no particular reactions can be identified [2,40]. Nevertheless some general tendencies in the global reaction mechanism can still be drawn. For instance, the results could allow a qualitative comparison of the reactivity of both fuels, since higher apparent E values are generally due to the decomposition of the less reactive components in biomass [6]. Based on this, it can be deduced that CC is more reactive than SB. The catalytic effect of ash was not read-

ily discernable, since the higher ash content in SB should result in lower activation energy, which was not observed. This suggests that factors other than ash are more prominent. The overall trend of $E(\alpha)$ for SB and CC in Fig. 2 also indicates that the less reactive constituents decompose at earlier stages of conversion followed in the later stages ($\alpha > 0.6$) by the more reactive components corresponding to lower E values. The decreasing trend of $E(\alpha)$ at higher conversion agrees with reported results from some previous studies [11] based on similar biomass materials but contradicts a few others [6,8]. This again highlights the unreliability of the theoretical

Table 4

Quality of fit (QOF) values obtained from comparing simulated and experimental DTG curves using both global and pseudocomponent analysis.

Heating rate ($^{\circ}\text{C min}^{-1}$)	Global analysis (QOF of DTG curves, %)		Pseudocomponent analysis (QOF of DTG curves, %)	
	CC	SB	CC	SB
10	2.1	1.9	6.8	1.8
20	3.8	1.4	6.7	1.7
30	2.1	1.7	3.3	3.1
40	1.8	0.5	2.9	1.9
50	6.9	2.3	9.6	5.3

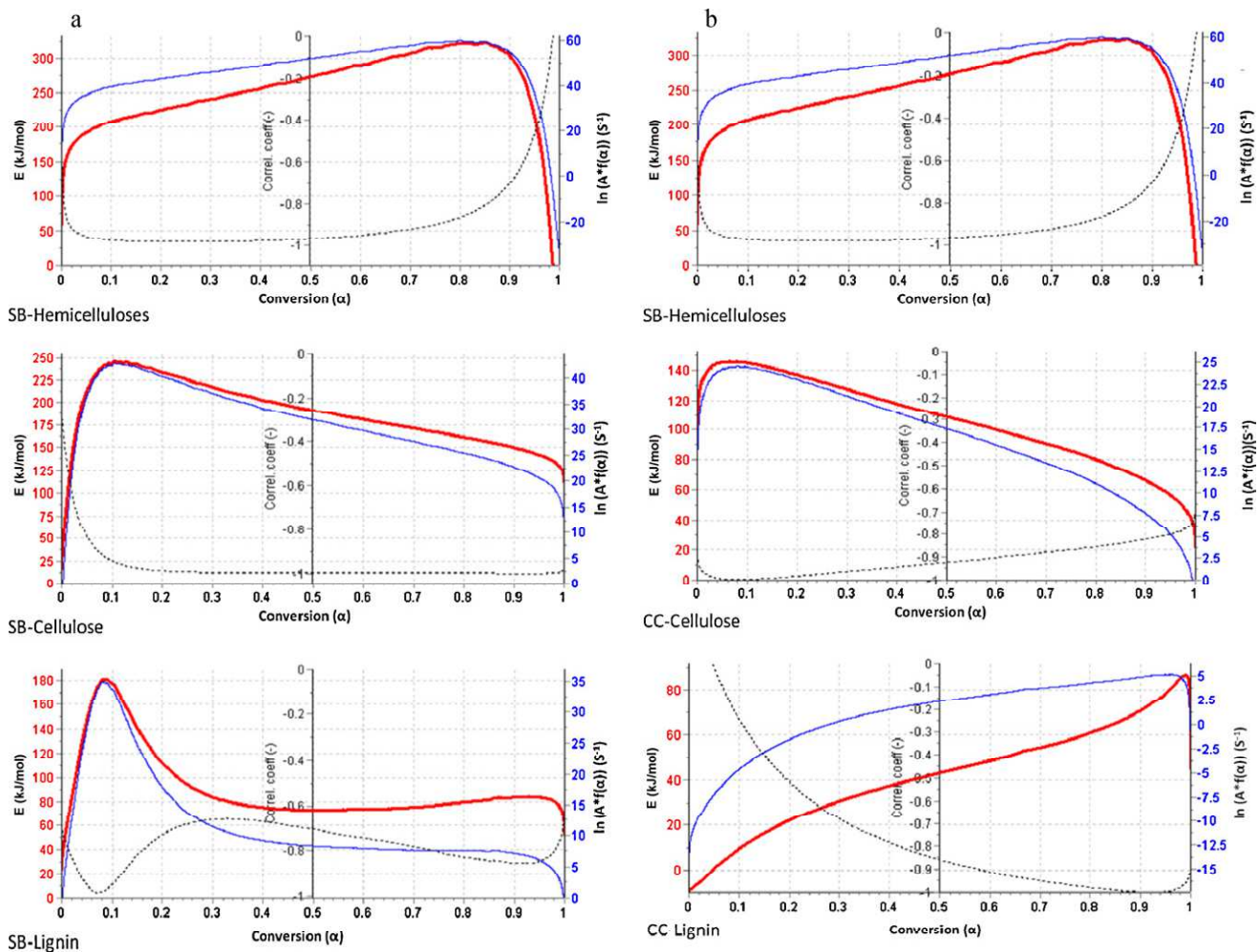


Fig. 5. Apparent E and $\ln(A \cdot f(\alpha))$ dependences on conversion for the pseudocomponents with E (—), $\ln(A \cdot f(\alpha))$ (—) and the calculated correlation coefficients (.....).

or mechanistic interpretation of the kinetic trends obtained from complex materials.

3.3. Kinetic analysis of pseudocomponents

It is widely recognised that the devolatilization behaviour of lignocellulosic biomass is heavily dependent on the behaviour of their constituent components namely hemicelluloses, cellulose and lignin [24,40,41]. Considering that similar experimental conditions (i.e. heating rate, temperature, pressure and particle size) were employed, the difference in the devolatilization and apparent kinetic trends between the two fuels can be attributed to the differences between the relative composition and nature of these components. Analysis of pseudocomponents representing these constituents was accomplished by first deconvoluting the DTG curves of the samples as described in the methodology section. The results of the deconvolution are displayed in Fig. 3 and the derived percentage contribution of the separated peaks to the total curve area is provided in Table 3. The percentage contribution of the pseudocomponents shown in Table 3 are broadly in the range of chemical composition values reported in literature for SB; 20–32% hemicelluloses, 31–40% cellulose, 18–27% lignin, and 6–25% extractives [42–45]. For CC, reported values range between 32% and 40.6% for SB hemicelluloses, 34–51% for cellulose, 3–19% for lignin, and 4.9–12.6% for extractives [30,46–49] differ significantly from our results particularly with reference to lignin which

seems to be overestimated at the expense of cellulose. Deviations from the reported values for both samples could be explained by the presence of alcohol–benzene–water-soluble extractives which could represent up to 25 wt.% of the original untreated material [42]. The devolatilization of extractives generally occurs in the same range of temperature as hemicelluloses and parts of lignin. This effect also highlights why the deconvoluted peaks cannot, strictly speaking, be assigned to specific components. Hence the use of the term ‘pseudocomponents’ in literature [1], where reaction steps represented by the peaks are thought to be dominated by one component or the other. For these peaks to be realistically considered as true representations of lignocellulosic components, a calibration using TGA results of each of the extracted components may be necessary in the manner shown by Carrier et al. [50].

The high deviation within the reported composition values themselves partly point to the heterogeneous nature of biomass, but may also be attributed to the different methodologies employed in determining composition. Whereas the chemical composition of cellulose is known to vary little between biomass materials, the types and properties of hemicelluloses and lignin often differ widely [41], further highlighting the heterogeneous nature of various lignocellulosic biomasses. In addition, the amount and composition of ash contained within biomass are known to influence devolatilization, as mentioned earlier. All of the aforementioned is reflected in the variance observed in Table 1 between proximate

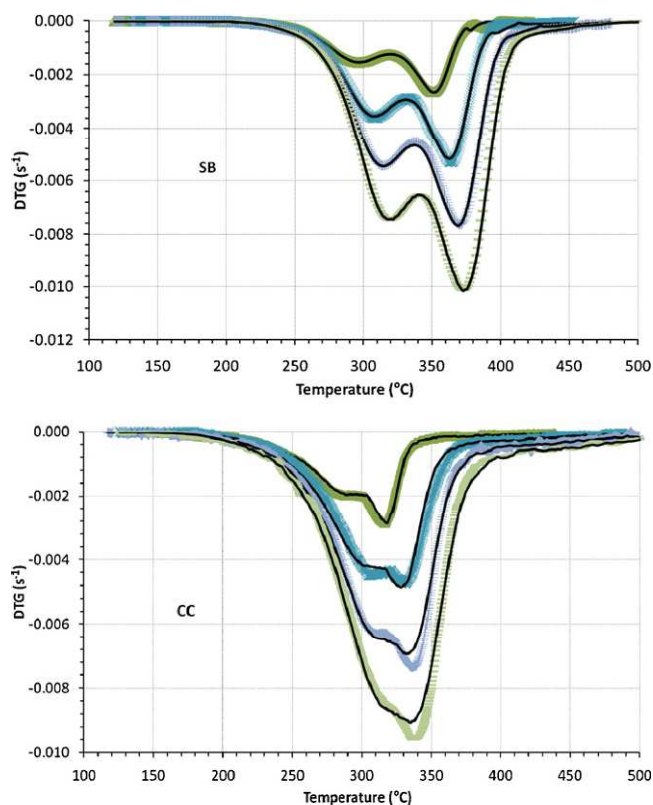


Fig. 6. Reproduction of experimental DTG curves for heating rates 10–40 °C min⁻¹ based on parameters from global kinetic analysis with 10 °C min⁻¹ (▲), 20 °C min⁻¹ (X), 30 °C min⁻¹ (+), 40 °C min⁻¹ (■) and simulated curves (—).

and ultimate parameters derived for this study and those from previous authors.

To obtain the kinetics of each pseudocomponent, peaks representing them were extracted from each heating rate and are shown grouped together in Fig. 4. From these peaks, apparent E and $\ln(A \cdot f(\alpha))$ dependence on α for each pseudocomponent were derived via the same isoconversional analysis employed for global single component analysis and are shown in Fig. 5. The $E(\alpha)$ trends for both materials confirm that the decomposition of the pseudocomponents also proceeds via a multi-step process comprising numerous complex reactions.

The concerns mentioned during the discussion of global kinetic analysis above, about the apparent nature of E , apply even more to pseudocomponents analysis because of the extra mathematical manipulations involved. Therefore even more care must be taken in deriving theoretical interpretations from the results, especially when the poor correlation coefficients shown in Fig. 5 are also considered. In general, it can be observed that the apparent E obtained for each pseudocomponent is largely consistent with literature where often lower activation energy values are reported for lignin (18–65 kJ mol⁻¹) than for cellulose (195–286 kJ mol⁻¹) or hemicelluloses (80–116 kJ mol⁻¹) [24,25]. The fact that these reported values were obtained via a different analytical approach (model-fitting) gives an indication of the reliability of our approach. Another indicator of our method's versatility can be obtained by validating simulations produced from the results with experimental data as shown in the next section.

3.4. Validation of kinetic analysis approach

Ultimately, the main usefulness of kinetic analysis of polymers such as biomass is more practical than theoretical. According to Vyazovkin [3] and Varhegyi [1], kinetic analysis should also include

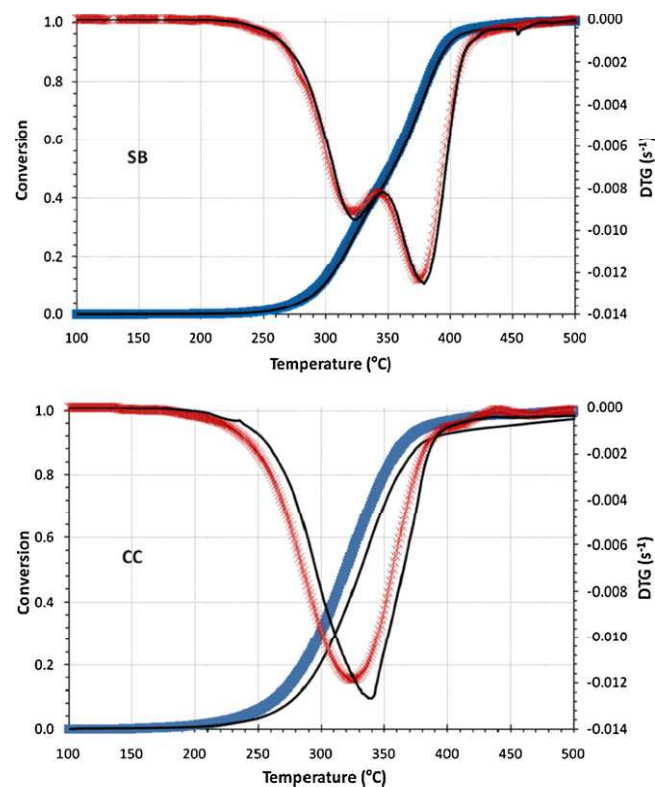


Fig. 7. Comparison of experimental and predicted DTG curves for 50 °C min⁻¹ heating rate based on parameters from global kinetic analysis with TG-experimental (■), DTG-experimental (X) and predicted curves (—).

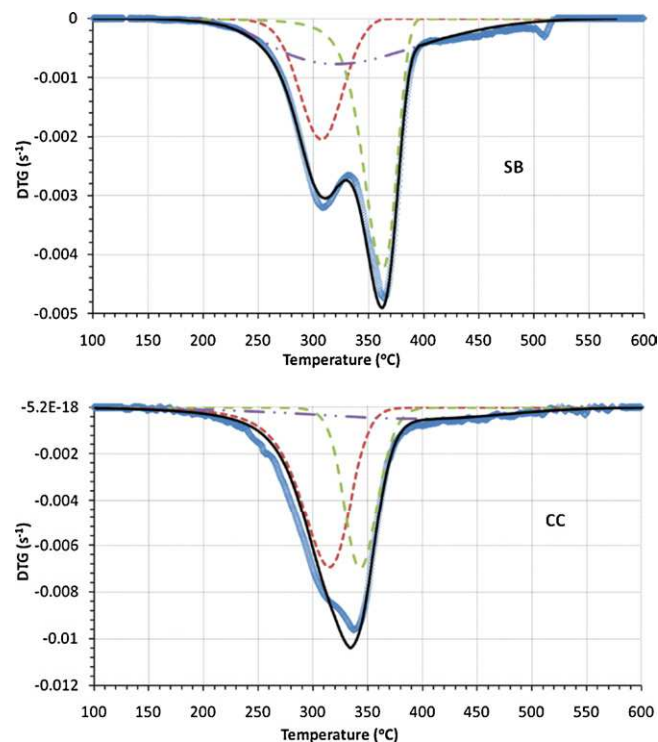


Fig. 8. Reproduction of experimental curves for SB (20 °C min⁻¹) and CC (40 °C min⁻¹) based on kinetic analysis of pseudocomponents with hemicelluloses (■), cellulose (■) and lignin (—), total predicted (—) and experimental curves (○).

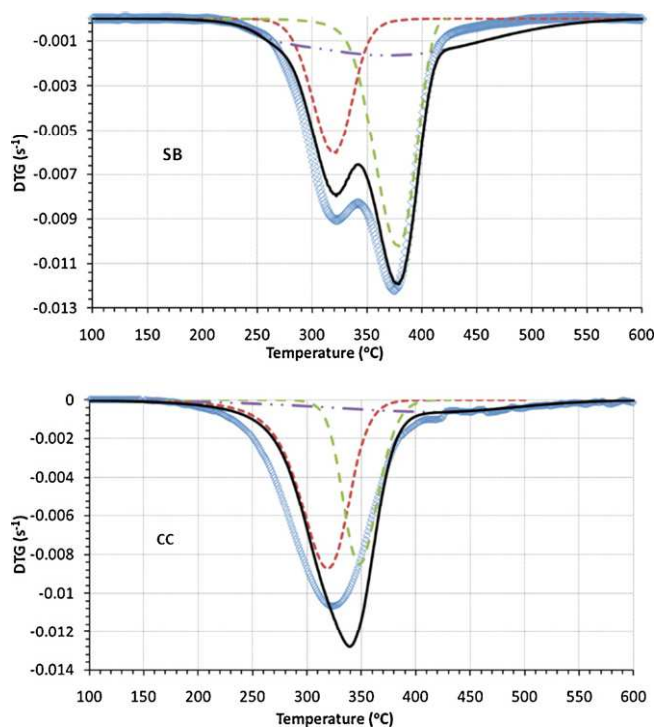


Fig. 9. Comparison of predicted and experimental curves for SB and CC at $50\text{ }^{\circ}\text{C min}^{-1}$ heating rate based on kinetic analysis of pseudocomponents with hemicelluloses (—■—), cellulose (—■—), lignin (—■—), total predicted (—■—) and experimental curves (○).

the practical ability to simulate and predict degradation rates which help in the design and sizing of thermochemical process reactors. For the current paper, the validation was achieved by simulating the heating rate curves employed in the analysis, and by predicting the reaction rate progress at a different heating rate, $50\text{ }^{\circ}\text{C min}^{-1}$, not used in the analysis.

In traditional kinetic analysis, it is normally expected that all three parameters that form the kinetic triplets – activation energy (E), pre-exponential factors (A) and decomposition function ($f(\alpha)$) – are needed in order to predict TG or DTG curves using Eq. (1). However, Vyazovkin [4] showed that it was not necessary to derive these parameters when isoconversional analysis is applied. In the first place their theoretical relevance as a tool for interpreting reaction mechanism has been questioned [2]. Furthermore their practical relevance in terms of simulating or predicting reaction progress or reaction rate data are rendered redundant (during isoconversional analysis) as reaction curve predictions can be readily obtained from Eq. (4). Fig. 6 shows a reproduction of the DTG curves (10, 20, 30 and $40\text{ }^{\circ}\text{C min}^{-1}$) used in the kinetic analysis from the results obtained from global kinetic analysis. The quality ranging of fits obtained using Eq. (5) between the simulated and experimental DTG curves for both CC and SB are shown in Table 4. The fit values displayed in Table 4 using the global, single component analytical approach compared well with those obtained via conventional model fitting approaches employed in previous reports. Branca et al. [24] who employed multi-heating rate, multi-component model fitting on wood devolatilization obtained fits from 3% to 26% using a 1, 2, and 3 independent parallel reactions model. Gronli et al. [25] obtained better fits ranging from 0.6% to 2.2% using a 5 parallel reactions model. This clearly shows that model-free methods produce comparably reliable predictions to multiple heating rate model-fitting methods.

Another indication of the reliability of the kinetic analysis method is the ability to predict reaction progress for heating rates

outside the range used in the analysis. Fig. 7 shows good agreement between the predicted and experimental TG and DTG curves for CC and SB at $50\text{ }^{\circ}\text{C min}^{-1}$. The fit values obtained are comparable to those obtained at heating rates within the range used for kinetic analysis.

Simulation and prediction from pseudocomponent analysis were achieved using Eqs. (3) and (4). First, Eq. (4) was applied to each pseudocomponent, and then the global curve was calculated as the weighted sum of the simulated curves assigned to the pseudocomponents according to Eq. (3). Fig. 8 shows the reproduction of curves employed in the analysis while Fig. 9 shows the predicted reaction rate at $50\text{ }^{\circ}\text{C min}^{-1}$. In both cases, simulated or predicted curves were compared with experimental data and the QOFs obtained are presented in Table 4. The results show a better fit between simulated and experimental curves for SB than for CC. Compared to results from the global kinetic approach, generally lower fits were obtained from the analysis of pseudocomponents, probably as a result of errors from mathematical manipulations of the data during the deconvolution. However, fits obtained from the pseudocomponent analysis are still comparable and in some cases better than those derived from conventional model-fitting as mentioned above.

4. Conclusions

The thermokinetics of the devolatilization of two of the most prominent agricultural residues in South Africa, corn cobs and sugar cane bagasse, have been investigated in this paper by thermogravimetric analysis. Friedman's isoconversional analysis was applied to global and deconvoluted DTG curves to obtain the dependence of the kinetic parameters on conversion for the samples and their constituent pseudocomponents.

To our knowledge, this study represents the only attempt to use this approach. Some differences in the devolatilization characteristics (devolatilization rates, peak temperatures and kinetics parameters) were observed between the two fuels and their pseudocomponents, with sugar cane bagasse having generally higher activation energy values than corn cobs. Considering that similar experimental conditions (i.e. heating rate, temperature, pressure and particle size) were employed, this could be attributed to the differences between the relative composition and nature of these components. However, these observed differences between the two agricultural wastes studied were relatively small, and may suggest that there are no kinetic barriers to the thermal co-processing of these fuels, where other factors such as heat and transport phenomena are not limiting.

Furthermore, it was pointed out that while some useful theoretical interpretations of the kinetic parameters are possible, the main utility of these kinetic parameters is their applicability to the prediction of experimental decomposition data. Results from both global and pseudocomponent analysis were therefore used to simulate experimental curves and reasonably high fits between simulated and experimental data were obtained, comparable to those obtained from model-fitting studies. This implies that the results can be reliably used in the design and optimization of the devolatilization section of reactors used in thermochemical processes where low heating rates occur, such as slow pyrolysis/carbonisation and updraft fixed bed gasification.

Acknowledgements

This research was conducted in part with funds from the South African National Research Foundation, the South African National Energy Research Institute, Fort Hare Institute of Technology (South Africa), and Karlsruhe Institute of Technology's (Germany) basic funding.

References

- [1] G. Varhegyi, Aims and methods in non-isothermal reaction kinetics, *Journal of Analytical and Applied Pyrolysis* 79 (2007) 278–288.
- [2] S. Vyazovkin, Model-free kinetics, *Journal of Thermal Analysis and Calorimetry* 83 (2006) 45–51.
- [3] S. Vyazovkin, Computational aspects of kinetic analysis Part C: the ICTAC Kinetics Project – the light at the end of the tunnel? *Thermochimica Acta* 355 (2000) 155–163.
- [4] S. Vyazovkin, A unified approach to kinetic processing of nonisothermal data, *International Journal of Chemical Kinetics* 28 (1996) 95–101.
- [5] M. García-Pérez, A. Chaala, J. Yang, C. Roy, Co-pyrolysis of sugarcane bagasse with petroleum residue. Part I: thermogravimetric analysis, *Fuel* 80 (2001) 1245–1258.
- [6] E. Biagini, A. Fantei, L. Tognotti, Effect of the heating rate on the devolatilization of biomass residues, *Thermochimica Acta* 472 (2008) 55–63.
- [7] E. Biagini, L. Guerrini, C. Nicoletta, Development of a variable energy model for biomass 361 devolatilization, in: *Chemical Engineering Transactions*, 2009, pp. 1–6.
- [8] J.M. Cai, L.S. Bi, Kinetic analysis of wheat straw pyrolysis using isoconversional methods, *Journal of Thermal Analysis and Calorimetry* 98 (2009) 325–330.
- [9] J. Cai, S. Chen, R. Liu, Weibull mixture model for isoconversional kinetic analysis of biomass oxidative pyrolysis, *Journal of the Energy Institute* 82 (2009) 238–241.
- [10] J. Cai, R. Liu, C. Sun, Logistic regression model for isoconversional kinetic analysis of cellulose pyrolysis, *Energy & Fuels* 22 (2008) 867–870.
- [11] V. Leroy, D. Cancellieri, E. Leoni, J. Rossi, Kinetic study of forest fuels by TGA: model-free kinetic approach for the prediction of phenomena, *Thermochimica Acta* 497 (2010) 1–6.
- [12] L. Gašparovič, Z. Koreňová, L. Jelemský, Kinetic study of wood chips decomposition by TGA, *Chemical Papers* 64 (2009) 174–181.
- [13] H. Xiao, X. Ma, Z. Lai, Isoconversional kinetic analysis of co-combustion of sewage sludge with straw and coal, *Applied Energy* 86 (2009) 1741–1745.
- [14] Y. Tonbul, Pyrolysis of pistachio shell as a biomass, *Journal of Thermal Analysis and Calorimetry* 91 (2007) 641–647.
- [15] A.G. Santos, A.S. Araujo, V.P. Caldeira, V.J. Fernandes Jr., L.D. Souza, A.K. Barros, Model-free kinetics applied to volatilization of Brazilian sunflower oil, and its respective biodiesel, *Thermochimica Acta* 506 (2010) 57–61.
- [16] L. Lynd, H. Von Blottnitz, B. Tait, J. de Boer, I. Pretorius, K. Rumbold, et al., Converting plant biomass to fuels and commodity chemicals in South Africa: a third chapter? *South African Journal of Science* 99 (2003) 499–507.
- [17] Department of Minerals and Energy, White Paper on the Renewable Energy Policy of the Republic of South Africa, Department of Minerals and Energy, 2003.
- [18] M.J. Antal, G. Varhegyi, Cellulose pyrolysis kinetics: the current state of knowledge, *Industrial & Engineering Chemistry Research* 34 (1995) 703–717.
- [19] C. Di Blasi, G. Signorelli, C. Di Russo, G. Rea, Product distribution from pyrolysis of wood and agricultural residues, *Industrial & Engineering Chemistry Research* 38 (1999) 2216–2224.
- [20] C. Di Blasi, G. Signorelli, G. Portoricco, Countercurrent fixed-bed gasification of biomass at laboratory scale, *Industrial & Engineering Chemistry Research* 38 (1999) 2571–2581.
- [21] M.E. Brown, *Introduction to Thermal Analysis: Techniques and Applications*, Kluwer Academic Publishers, 2001.
- [22] H.L. Friedman, Kinetics of Thermal Degradation of Char-Forming Plastics from Thermogravimetry. Application to a Phenolic Plastic, Wiley Subscription Services, Inc., A Wiley Company New York, 1964.
- [23] G. Varhegyi, M.J. Antal, T. Szekeley, P. Szabo, Kinetics of the thermal decomposition of cellulose, hemicellulose, and sugarcane bagasse, *Energy & Fuels* 3 (1989) 329–335.
- [24] C. Branca, A. Albano, C. Di Blasi, Critical evaluation of global mechanisms of wood devolatilization, *Thermochimica Acta* 429 (2005) 133–141.
- [25] M.G. Gronli, G. Varhegyi, C. Di Blasi, Thermogravimetric analysis and devolatilization kinetics of wood, *Industrial & Engineering Chemistry Research* 41 (2002) 4201–4208.
- [26] J.A. Caballero, J.A. Conesa, Mathematical considerations for nonisothermal kinetics in thermal decomposition, *Journal of Analytical and Applied Pyrolysis* 73 (2005) 85–100.
- [27] AKTS, AKTS Advanced Thermal Analysis Software, <http://www.akts.com/> (2010).
- [28] A. Ilyas, K. Hawboldt, F. Khan, Advanced kinetics for calorimetric techniques and thermal stability screening of sulfide minerals, *Thermochimica Acta* 501 (2010) 35–45.
- [29] P. Roque-Diaz, C. University, L.C.V. Villas, Zh. Shemet, V.A. Lavrenko, V.A. Khristich, Studies on thermal decomposition and combustion mechanism of bagasse under non-isothermal conditions, *Thermochimica Acta* 93 (1985) 349–352.
- [30] O. Ioannidou, A. Zabaniotou, E.V. Antonakou, K.M. Papazisi, A.A. Lappas, C. Athanassiou, Investigating the potential for energy fuel materials and chemicals production from corn residues (cobs and stalks) by non-catalytic and catalytic pyrolysis in two reactor configurations, *Renewable and Sustainable Energy Reviews* 13 (2009) 750–762.
- [31] A. Kumar, L. Wang, Y.A. Dzenis, D.D. Jones, M.A. Hanna, Thermogravimetric characterization of corn stover as gasification and pyrolysis feedstock, *Biomass and Bioenergy* 32 (2008) 460–467.
- [32] K.G. Mansaray, A.E. Ghaly, Determination of kinetic parameters of rice husks in oxygen using thermogravimetric analysis, *Biomass and Bioenergy* 17 (1999) 19–31.
- [33] F. Shafizadeh, Introduction to pyrolysis of biomass, *Journal of Analytical and Applied Pyrolysis* 3 (1982) 283–305.
- [34] E. Biagini, F. Barontini, L. Tognotti, Devolatilization of biomass fuels and biomass components studied by TG/FTIR technique, *Industrial & Engineering Chemistry Research* 45 (2006) 4486–4493.
- [35] P. Luangkiattikhun, C. Tangsathitkulchai, M. Tangsathitkulchai, Non-isothermal thermogravimetric analysis of oil-palm solid wastes, *Bioresource Technology* 99 (2008) 986–997.
- [36] H. Haykiri-Acma, S. Yaman, S. Kucukbayrak, Effect of heating rate on the pyrolysis yields of rapeseed, *Renewable Energy* 31 (2006) 803–810.
- [37] C. Di Blasi, Modeling chemical and physical processes of wood and biomass pyrolysis, *Progress in Energy and Combustion Science* 34 (2008) 47–90.
- [38] Q. Cao, K. Xie, W. Bao, S. Shen, Pyrolytic behaviour of waste corn cob, *Bioresource Technology* 94 (2004) 83–89.
- [39] A. Zabaniotou, O. Ioannidou, E. Antonakou, A.A. Lappas, Experimental study of pyrolysis for potential energy, hydrogen and carbon material production from lignocellulosic biomass, *International Journal of Hydrogen Energy* 33 (2008) 2433–2444.
- [40] B.A. Howell, Utility of kinetic analysis in the determination of reaction mechanism, *Journal of Thermal Analysis and Calorimetry* 85 (2006) 165–167.
- [41] F. Shafizadeh, Introduction to pyrolysis of biomass, *Journal of Analytical and Applied Pyrolysis* (1982).
- [42] P. Das, A. Ganesh, P. Wangikar, Influence of pretreatment for deashing of sugarcane bagasse on pyrolysis products, *Biomass and Bioenergy* 27 (2004) 445–457.
- [43] A.F. Drummond, I.W. Drummond, Pyrolysis of sugar cane bagasse in a wire-mesh reactor, *Industrial & Engineering Chemistry Research* 35 (1996) 1263–1268.
- [44] E.S. Lipinsky, Perspectives on preparation of cellulose for hydrolysis, in: *Hydrolysis of Cellulose: Mechanisms of Enzymatic and Acid Catalysis*, American Chemical Society, 1979, 1–23.
- [45] S. Munir, S. Daood, W. Nimmo, A. Cunliffe, B. Gibbs, Thermal analysis and devolatilization kinetics of cotton stalk, sugar cane bagasse and shea meal under nitrogen and air atmospheres, *Bioresource Technology* 100 (2009) 1413–1418.
- [46] C.A. Koufopoulos, A. Lucchesi, G. Maschio, Kinetic modelling of the pyrolysis of biomass and biomass components, *The Canadian Journal of Chemical Engineering* 67 (1989) 75–84.
- [47] B. Rivas, A.B. Moldes, J.M. Domínguez, J.C. Parajó, Lactic acid production from corn cobs by simultaneous saccharification and fermentation: a mathematical interpretation, *Enzyme and Microbial Technology* 34 (2004) 627–634.
- [48] N. Pece, N. Perotti, O. Molina, Bacterial protein production from corn cob pretreated with NaOH at room temperature, *World Journal of Microbiology and Biotechnology* 10 (1994) 593–594.
- [49] T. Sonobe, N. Worasuwannarak, S. Pipatmanomai, Synergies in co-pyrolysis of Thai lignite and corncob, *Fuel Processing Technology* 89 (2008) 1371–1378.
- [50] M. Carrier, A. Loppinet-Serani, D. Denux, J. Lasnier, F. Ham-Pichavant, F. Cansell, et al., Thermogravimetric analysis as a new method to determine the lignocellulosic composition of biomass, *Biomass and Bioenergy* 35 (2011) 298–307.

Page left blank intentionally

3 Model free kinetics of the co-pyrolysis of coal blends with corn and sugarcane residues

Submitted to Fuel Processing Technology in July 2011 using the following details:

Title: “Thermogravimetric study of the pyrolysis characteristics and kinetics of coal blends with corn and sugarcane residues”

Authors: Akinwale O. Aboyade^{a,b}, Johann F. Görgens^a, Marion Carrier^a, Edson L. Meyer^b, Johannes H Knoetze^a,

^aDepartment of Process Engineering, Stellenbosch University, Stellenbosch, South Africa

^bFort Hare Institute of Technology, University of Fort Hare, Alice, South Africa

This chapter investigates the non-isothermal thermokinetics of the co-pyrolysis of sugarcane bagasse and corn residue blended with low grade coal, using the model-free kinetic approach. The biomass samples used were obtained from different locations to those used in the previous chapter. The individual devolatilization behaviour of each of the fuels obtained separately was compared with the behaviour of the biomass blends with coal at various mix ratios. Synergistic behaviour that point to the existence of chemical interactions during pyrolysis between the coal and biomass fractions of the blends was also identified.

3.1 Introduction

The co-utilization of coal-biomass blends as feedstock in already existing industrial-scale coal conversion plants is a promising technological option for taking advantage of available biomass resources. Examples of existing processes for coal conversion into energy products include combustion, direct liquefaction (carbonisation/pyrolysis) and indirect liquefaction (gasification). Coal converted via these technological routes currently account for 26% of the world’s primary energy supply and 46% of global electricity production [1]. Coal is also playing an increasingly important role in the production of liquid fuels and chemicals [2], and is the fastest growing energy resource in the world with reserves expected to last for up to 200 years compared to about 65 years and 40 years for natural gas and crude oil respectively [3]. Co-processing biomass with coal for energy and chemicals production will reduce fossil-derived CO₂ emissions from coal, and can also limit the

discharge of local air pollutants such as SO_x and NO_x [4,5]. Further advantages of co-processing biomass with coal include avoiding the costs of dedicated biomass based installations, and avoiding concerns related to biomass feedstock supply limitations for industrial scale processes, while still satisfying economies of scale requirements. More importantly, this will also help to address concerns about potential competition between energy crop demands and food requirements on land use [6].

Since pyrolysis/devolatilization is a fundamental step in all main thermochemical conversion routes, the adaptation of coal based processes to biomass co-feeding necessitates an understanding of the devolatilization kinetics of the biomass-coal blends. Various procedures for evaluating kinetic parameters from data derived from non-isothermal thermogravimetric analysis (TGA) have been developed, and the vast majority of them can be classified as either 'model-free' or 'model-fitting' [7]. Until recently, the model-fitting approach has found wider application in biomass thermochemical conversion studies. However, it is widely recognised that the method suffers from two main deficiencies, particularly in cases where data from only a single heating rate is applied [7,8]: i) it can often yield different values of the kinetic parameters describing the same thermogravimetric curve, leading to an ambiguity in terms of interpretation of the results; ii) it generally tends to yield one set of kinetic parameters for the whole range of conversion, therefore not taking into account the complexity of mechanisms involved during pyrolysis of plant biomasses. The model-free methods however addresses these concerns [7,9,10]. As the name implies, the model-free approach does not require assumption of specific reaction models, and yields unique kinetic parameters as a function of either conversion (isoconversional analysis) or temperature (non parametric kinetics [9]). Of the two main model-free methods the isoconversional approach is more frequently adopted, and is increasingly being used in biomass thermochemical conversion research. In 2001, Garcia-Perez et al. [11] employed Friedman's isoconversional approach to the study of the pyrolysis kinetics of sugar cane bagasse. More recently, Biagini et al. [12], Cai et al. [13], Leroy et al. [14], Santos et al. [15],

and Aboyade et al. [16] employed various isoconversional methods in the analysis of the non-isothermal decomposition of biomass and/or its components.

Numerous recent studies on the TGA pyrolysis of coal [17-19] and coal-biomass blends [20-25] are available and most were based on different variations of model fitting techniques. Co-pyrolysis studies tend to focus on whether the reacting fuels interact with each other during pyrolysis, to produce synergistic behaviour. Older reports have usually concluded that no interactions between the biomass and coal exist during co-pyrolysis of coal-biomass blends [20-23]. However more recent efforts by Ulloa et al. [24] and Hayciri Acma [25] have challenged this view, showing that there are indeed significant interactions between the coal and biomass fractions during pyrolysis.

The present work considers the devolatilization behaviour and kinetics of coal blends with corn and sugar cane biomass residues, two of the most abundant sources of waste derived biomass in South Africa [26,27]. An atmospheric TGA was employed, but as Hillier and Fletcher [18] showed, pyrolysis kinetic parameters obtained under atmospheric conditions are also applicable to pressurized conditions of up to 40 bars. The changes in pyrolysis kinetic parameters during the pyrolysis process were analysed to identify possible synergistic behaviour. Predictions based on the derived kinetic parameters were compared with experimental data in order to obtain an indication of the reliability of the kinetic approach employed.

3.2 Material and methods

3.2.1 Samples

The coal sample used was a blend of various typical South African hard coals that can be described as low grade, with high ash and inertinite content. The biomass types used in the study were sugarcane bagasse (BG) and corn residues separated into cobs (CC) and corn stover (CS), all obtained from farms in the Free State Province of South Africa. CS was received already shredded, while CC arrived in whole pieces.

Both types of corn residues were received already dried with moisture content less than 7%. CS particles smaller than 0.25 mm were sieved because they were determined to consist mostly of sand. BG samples were received wet with 35-40% moisture content and was air dried for 48 hours until a moisture content of less than 10% was achieved. Representative sub-samples for experiments were obtained for all samples according to CEN/TS 14780/2005 [28].

C, H, and N content in the samples were determined according to ASTM D5373 [29]. Sulphur was determined according to ASTM D4239 [30]. Higher heating value was determined using BS EN 14918:2009 [31], while proximate analysis was conducted according to ASTM E1131 [32].

The chemical components of biomass raw materials were analysed by the standard method developed by NREL analysis procedure LAP 002, 003, 017, and 019 (http://www.nrel.gov/biomass/analytical_procedures.html). In brief, 5 g of milled and sieved samples was extracted with water for 24 hours in a Soxhlet apparatus. Then water extractive free sample was then extracted with 95% ethanol for 24 hours. Extractive-free biomass was hydrolysed with 72% sulphuric acid (% w/w) (0.3 g material and 3 ml H₂SO₄) in a heating water bath set at 30°C for 60 minutes. The sample was then diluted with 84 ml of de-ionised water to make the final concentration 4% w/w H₂SO₄ and the mixture was autoclaved at 121°C for 60 minutes. The resulted mixture was filtered in a porous crucible. The filtrate (liquid fraction) was taken for monomeric sugars analysis by HPLC and for acid soluble lignin analysis by spectrophotometer. The solid fraction was dried at 105 ± 2° C for 12 hours and then was put into the furnace set at 575°C. The left material was cooled in desiccators and weighed to determine the amount of insoluble lignin. Soluble lignin was in the liquid fraction was measured by UV-spectrophotometer at a wavelength of 280 nm. Samples from raw material were analyzed for sugar content (cellobiose, glucan, xylose and arabinose) by high performance anionic exchange chromatography on a Dionex Ultimate® 3000 system equipped with a CarboPac PA1 column (4x250 mm) operated at 25°C with a mobile phase of 30 mM sodium

hydroxide and a flow rate of 1 ml min^{-1} . The results of the ultimate and proximate analysis for the samples used as well as the biochemical characteristics of the biomasses are presented in Table 4-1.

Table 3-1: Proximate, Ultimate and biochemical (biomass only) characteristics of feedstock samples

Properties	BG	CC	CS	Coal
Ultimate analysis (wt % dried basis)				
C	43.1±0.5	45.7±0.5	34.2±0.4	45.4±0.5
H	5.7±0.1	6.0±0.1	4.8±0.1	3.0±0.1
N	0.3±0.1	0.2±0.1	0.6±0.1	1.1±0.1
S	0.3±0.1	0.32±0.02	0.2±0.1	1.0±0.1
O*	40.3±0.4	46.2±0.5	35.7±0.4	10.9±0.2
HHV (MJ/kg)	16.6±0.2	18.0±0.2	13.2±0.1	17.4±0.2
Proximate analysis (wt %)				
Moisture	6.7±0.1	7.0±0.1	6.9±0.1	4.0±0.1
Ash (db)	10.3±0.1	1.6±0.1	24.5±0.1	38.6±0.2
Volatiles (daf)	91.7±0.3	84.3±0.3	84.1±0.3	31.7±0.1
Fixed carbon (daf)	8.3±0.1	15.7±0.1	15.9±0.1	68.3±0.3
Lignocellulosic composition (daf wt%)				
Cellulose	44.2±0.6	35.9±0.8		
Hemicellulose	23.8±0.4	38.1±0.8		
Lignin	22.4±0.3	16.7±0.2		
Extractives and others	9.7±0.5	9.5±0.8		

3.2.2 Experimental method

A Mettler Toledo TGA/DCS 1 analyzer was employed for TGA experiments. Nitrogen was used as the purge gas, and was set to a flow rate of 150 mL min^{-1} to ensure an inert atmosphere and to prevent secondary reactions by volatiles produced during pyrolysis. For each experimental run, samples were heated to 105°C and held at that temperature for 15 minutes to ensure drying. Thereafter the samples were heated at selected heating rates to a final pyrolysis temperature of 900°C and held at that temperature for another 15 mins to allow for stabilization of mass. The purge gas was then changed to oxygen for carbon burn-off in order to determine the ash content. A graphical representation of the temperature program just described is shown in Fig.4-1.

Based on preliminary runs conducted and the literature, sample masses of between 5-25 mg and particle size of less than 212 μm were used to ensure that the effects of external and intra-particle heat transfer were limited in both coal and biomass samples [31,32]. Coal-biomass blends were prepared and according to the following mix ratios (by mass); 90:10, 80:20, and 60:40. Vigorous mixing was achieved by passing each sample blend 4 times through a Retsch PT 100 rotary sample divider. Dispersion was further ensured by stirring the blends within TGA sample holders to prevent settling. This was continued up till the point where the samples were loaded into the analysers. These procedures helped to ensure reproducibility of greater than 98% between repeated runs. Blends were analysed at 5, 10, and 50 $^{\circ}\text{C min}^{-1}$ heating rates while single fuel samples were analysed at 5, 10, 20, 30, 40, 50 and 150 $^{\circ}\text{C min}^{-1}$. All analysis were conducted in duplicate. Variation of the sample residual mass with respect to time and temperature change (TG data) were collected automatically by the equipment and were analysed according to the method described in the next section.

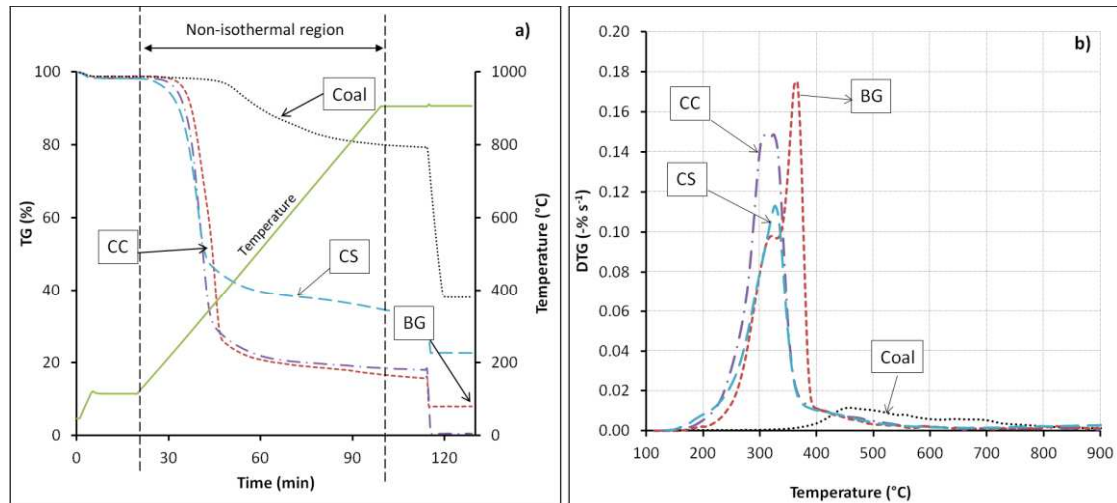


Figure 3-1: TG and DTG curves of individual fuel pyrolysis at 10 $^{\circ}\text{C min}^{-1}$ (dotted lines represent sample TG and DTG curves while unbroken line in 1a shows the time-temperature profile)

3.2.3 Kinetic analysis

The kinetic analysis of the thermal decomposition of biomass is usually based on the rate equation for solid state decomposition processes [9]:

$$\frac{d\alpha}{dt} = A \exp\left[-\frac{E}{RT}\right] f(\alpha) \quad (1)$$

Where α is the reacted fraction of the sample or conversion, A and E are the Arrhenius parameters - pre-exponential factor and activation energy respectively, and $f(\alpha)$ is the reaction model. Conversion, α , is derived from the equation $\alpha = (m_0 - m)/(m_0 - m_f)$ where m_0 and m_f are the initial and final mass in the non-isothermal temperature range used for the analysis (Fig. 4-1). The model-free or isoconversional approach does not require the choosing of a specific reaction model, or $f(\alpha)$ as was the case for model-fitting shown above. Isoconversional techniques allow the estimation of E as a function of conversion, or α based on data from multiple heating rates. Results obtained from the slow heating rates $5-50^\circ\text{Cmin}^{-1}$ were used in the analysis. The analysis was conducted using the AKTS Thermokinetics software [35] and a detailed description of the method used is given in Aboyade et al [16]. Simulation of experimental curves were obtained from the following expression [7,10];

$$t_\alpha = \frac{\frac{1}{\beta} \int_{T_0}^{T_\alpha} \exp\left(\frac{-E\alpha}{RT}\right) dT}{\exp\left(\frac{-E\alpha}{RT_0}\right)} \quad (2)$$

where t refers to the time and T_0 refers to initial temperature. The obtained quality of fit (QOF) between simulated and experimental curves was evaluated via the expression [36]:

$$QOF(\%) = 100 \times \sum_{i=1}^{N_k} \sqrt{\frac{\left\{ \left(\frac{d\alpha}{dt} \right)_{exp} - \left(\frac{d\alpha}{dt} \right)_{calc} \right\}^2}{N_k}} / \text{Max} \left| \frac{d\alpha}{dt} \right|_{exp} \quad (3)$$

where N_k is the number of experimental points employed.

3.3 Results

3.3.1 Characteristics of TGA curves

3.3.1.1 *Single fuels*

Fig. 4-1 shows the non-isothermal mass loss (TG) and derivative of mass loss (DTG) curves for BG, CC, CS and Coal single fuels at $10^{\circ}\text{C min}^{-1}$. Fig. 4-1a is a plot of mass loss against time and includes a temperature versus time plot, on which the temperature program used in the analysis is illustrated. The initial small reduction in mass just before the beginning of the dynamic section of the time/temperature plot could be attributed to the demoinsturation of the samples. Because the kinetic modelling in this paper is based on non-isothermal kinetics, all analysis henceforth will be focused on the temperature range corresponding to the dynamic region of the plot in Fig. 4-1a. Consequently the DTG versus temperature plots shown in Fig. 4-1b only cover this region.

Significant weight loss due to devolatilization in the biomass fuels started at 210, 200, and 170°C for BG, CC and CS, respectively, which was considerably lower than the temperature corresponding to the start of coal devolatilization (390°C). Rapid weight loss in the biomass samples occurred in a narrower temperature range (approximately $200\text{-}400^{\circ}\text{C}$) than for coal ($\sim 400\text{-}900^{\circ}\text{C}$). The maximum devolatilization rate for biomass ($0.15\text{-}0.18\ \%/s$) depicted on the DTG curves (Fig. 4-1b) were one order of magnitude greater than the maximum rates for coal ($0.02\ \%/s$). Four peaks for coal, two peaks each for the BG and CC, and one peak for CS was observed in the DTG curves (Fig. 4-1b). The CC peaks occurred at the lowest temperatures, and were of almost equal dimensions. The BG peaks were of unequal dimensions, with the first, smaller peak occurring at 210°C and the larger one at 365°C . The shoulder at the end of the last biomass peaks started at just under 400°C , marking the end of rapid weight loss. On the other hand, 400°C was only the start of the significant mass loss rates for coal, such that only 15 wt% of coal devolatilization had occurred at this temperature compared to 89 wt% and 88 wt% for BG and CC, respectively. Coal devolatilization continued up to 900°C with a total volatile content loss of 20 wt% (30 wt% on dry and ash free basis), and exhibited 4 overlapping peaks with successively

lower maximum reaction rates. By the end of the non-isothermal temperature region in Fig. 4-1a (at temperature of 900°C), total mass loss due to devolatilization on dry and ash free basis were 90.8%, 82.7%, 80.3% and 31% for BG, CC, CS and coal, respectively. In line with previous reports [37,38], there was no correlation observed between heating rate and total weight loss during devolatilization. The change in volatile yield as heating rates increased from 5 to 150°C min⁻¹ was negligible with deviation of less than 1% for all materials (data not shown).

3.3.1.2 Blends

Fig. 4-2 shows DTG curves of Coal-BG and Coal-CC blends at various mix ratios obtained at a heating rate of 10°C min⁻¹. At all mix ratios, peaks corresponding to biomass and coal fractions of the blended fuels maintained essentially the same shape and position on the temperature axis as was observed during individual pyrolysis. For each of the blend type, the two peaks representing the biomass fraction were visible in the same temperature range (approximately 200-400°C) as when biomasses were pyrolyzed individually (Fig. 4-1). Similarly, DTG peaks for coal as single fuel and as a component of a biomass-blend occurred in the same temperature range of 400-900°C. In other words, the shapes and position of the biomass and coal peaks in the DTG curves in the blends remained relatively unaltered compared to DTG curves of single fuels. However, blending did affect the peak height or maximum reaction rate of the section of the curves corresponding to both coal and biomass; increasing the biomass fraction in the blend caused an increase in the maximum devolatilization rate of the peaks representing coal, while reducing the maximum devolatilization rates of peaks corresponding to biomass. At the 90:10 coal biomass mix ratio, the maximum devolatilization rates of the biomass fraction of the blends was reduced to almost matching the values of the coal fraction (Figs. 4-1 and 4-2). Therefore, the maximum devolatilization rate of each material in a coal-biomass blend was a function of its relative contribution to the blends.

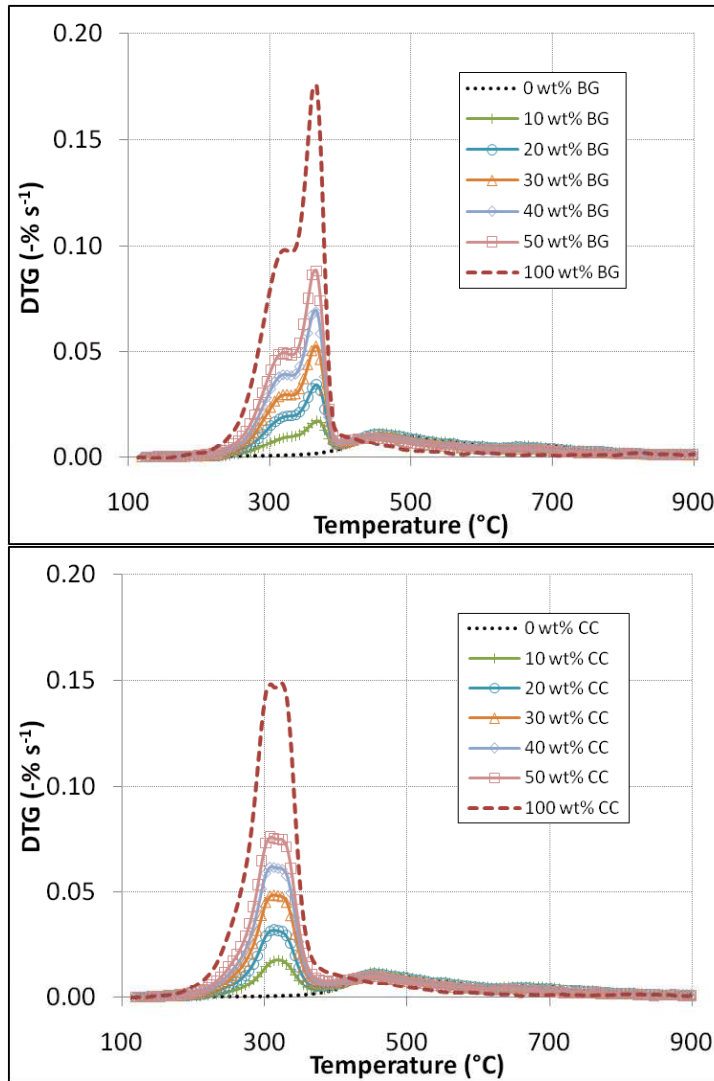


Figure 3-2: DTG curves of various mix ratios of Coal-BG and Coal-CC blends obtained at $10^{\circ}\text{C min}^{-1}$

The influence of mix ratio on the yield of volatiles is illustrated in Fig. 4-3, which depicts experimental and predicted weight loss due to devolatilization for different mix ratios of coal and biomass. To take account of the varying ash and moisture content (Fig. 4-1), dry and ash free values were used. Experimental values presented are the averages obtained from multiple heating rates, and as was the case for individual fuels, volatile yields from the blends were independent of heating rates, with negligible variation between experiments. Predicted weight loss was calculated as the weighted sum of the yields of the contributing coal and biomass fractions obtained under the same conditions.

$$Y = [x_c Y_c + x_b Y_b] / 100 \quad (4)$$

where Y = predicted yield for the blended sample; Y_c = observed yield of 100% coal; x_c = fraction (%) of coal in the blend sample; Y_b = observed yield of 100% biomass; x_b = fraction (%) of biomass in the blend.

Fig. 4-3 shows that as the biomass fraction in the blend was increased, a corresponding increase in volatiles yield was observed, beyond what would be expected assuming a simple additive behaviour in volatiles yield between the contributing fuels. However this increase was not directly proportional to the mix ratio. The difference between calculated and observed yields in coal-CC blends increased from 8.9% at 90:10 coal-biomass mix ratio, to a maximum of 12.3% at 70:30 mix ratio, and then reduced marginally to 11.9% at 50:50 mix ratio. The trend was similar for coal-BG blends, except that the maximum difference between calculated and observed yields (11 %) was observed at 60:40 mix ratio having increased from 6.6% at 90:10 mix ratio. Therefore, a point exists (approximately 40 wt% for BG and 30 wt% for CC) beyond which further addition of biomass to the blend did not lead to a corresponding increase in volatile yields.

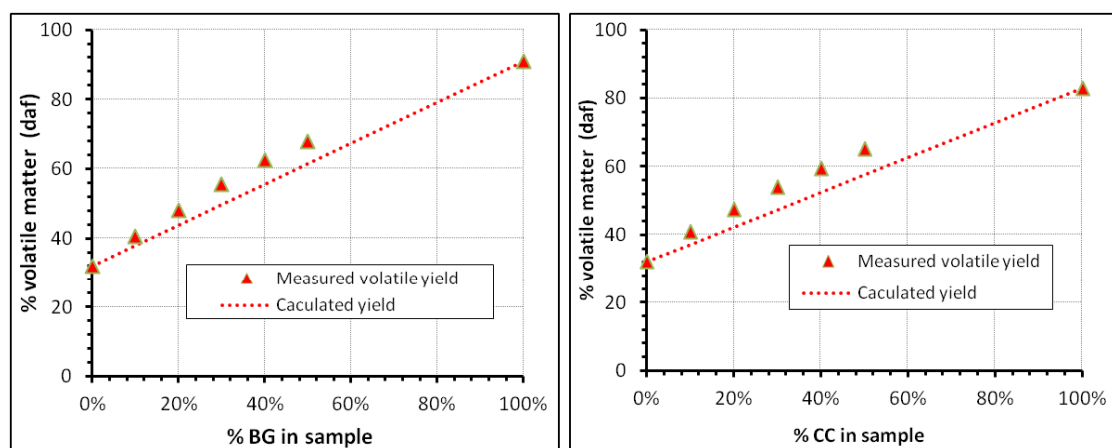


Figure 3-3: Influence of mix ratio on volatile yields (data shown are average of values from 5, 10 and 50°C min-1 heating rates)

Fig. 4-4 compares the experimental and calculated mass loss and DTG versus temperature curves for both coal-BG and coal-CC blends. Calculated curves were based on weighted average of the contributing fractions as detailed in eqn (4). It shows how the disparity between experimental and weighted average values (or

synergy) evolved as the pyrolysis process progressed. The experimental and calculated TG curves were closely matched for temperatures below 300°C for both blend types indicating the absence of synergy up to this point. This shows that the difference in final volatile yield observed in Fig. 4-3 was caused by deviations from the ‘expected’ mass loss trends that started around 300°C. However, reaction rate data on the DTG curves show that deviations from normality only lasted until 500°C, after which the calculated reaction rates again matched experimental data points for both coal-BG and coal-CC blends. This indicated that synergy during co-pyrolysis, as measured by the difference in experimental and calculated values of final volatile yields, was due to an ‘abnormal’ change in devolatilization rates that occurred in the 300-500°C range.

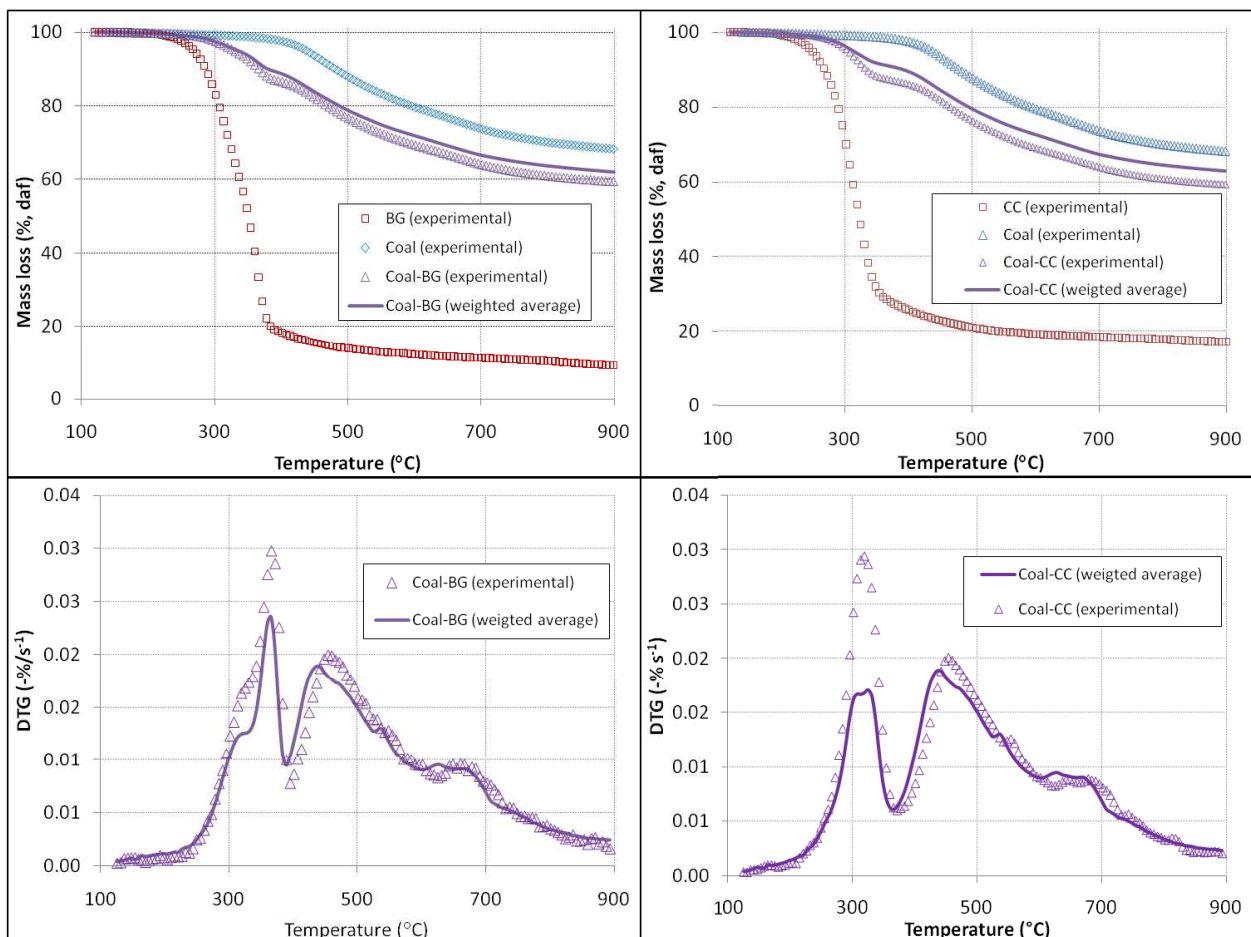


Figure 3-4: Comparing experimental and calculated (weighted average) TG and DTG curves of coal-biomass blends at 90:10 mix ratio

3.3.2 Kinetic analysis

3.3.2.1 Single fuels

Results of the model free analysis for single fuels are presented in Fig. 4-5. The figure depicts the change in apparent E and $\ln(A * f(\alpha))$ values for the samples studied. The plots also show correlation coefficients for the parameters calculated over the entire conversion range. In the 0.1 to 0.8 conversion range, where the correlation coefficient was high (>0.95), the apparent activation energy E for the biomass fuels, increased from 165 kJmol^{-1} , 162 kJmol^{-1} , and 160 kJmol^{-1} for BG, CC and CS, respectively to a maximum of 180 kJmol^{-1} , 190 kJmol^{-1} and 175 kJmol^{-1} , respectively. Within the biomass fuels, variation of apparent E at 3.4% with conversion in the range of 0.1-0.8 was lowest for BG, followed by 3.6%, and 6.6% for CC, and CS, respectively. Apparent E for coal was more or less constant, only varying by 4.6% with an average of $245.6 \text{ kJ mol}^{-1}$ over the 0.1-0.8 conversion range.

3.3.2.2 Blends

Apparent $E(\alpha)$ and $\ln(A * f(\alpha))$ for the blends are shown in Figs. 4-6 and 4-7. As for the DTG curves, the conversion range in which biomass devolatilized was easily distinguishable from the range corresponding to coal devolatilization, according to the values obtained for pyrolysis of the individual fuels which for biomass was generally less than 200 kJ mol^{-1} . The biomass fraction of the blend was responsible for the initial stages of conversion while transition to the range of conversion corresponding to predominantly coal pyrolysis was marked by an abrupt change in the trend of apparent E values. The conversion at which this transition occurred for both coal-BG and coal-CC blends, with 10 wt%, 20 wt%, and 40wt% biomass fractions, were at approximately 0.32-0.33, 0.5-0.52 and 0.7-0.73, respectively. These conversion values also indicated the mass contribution that biomass made to

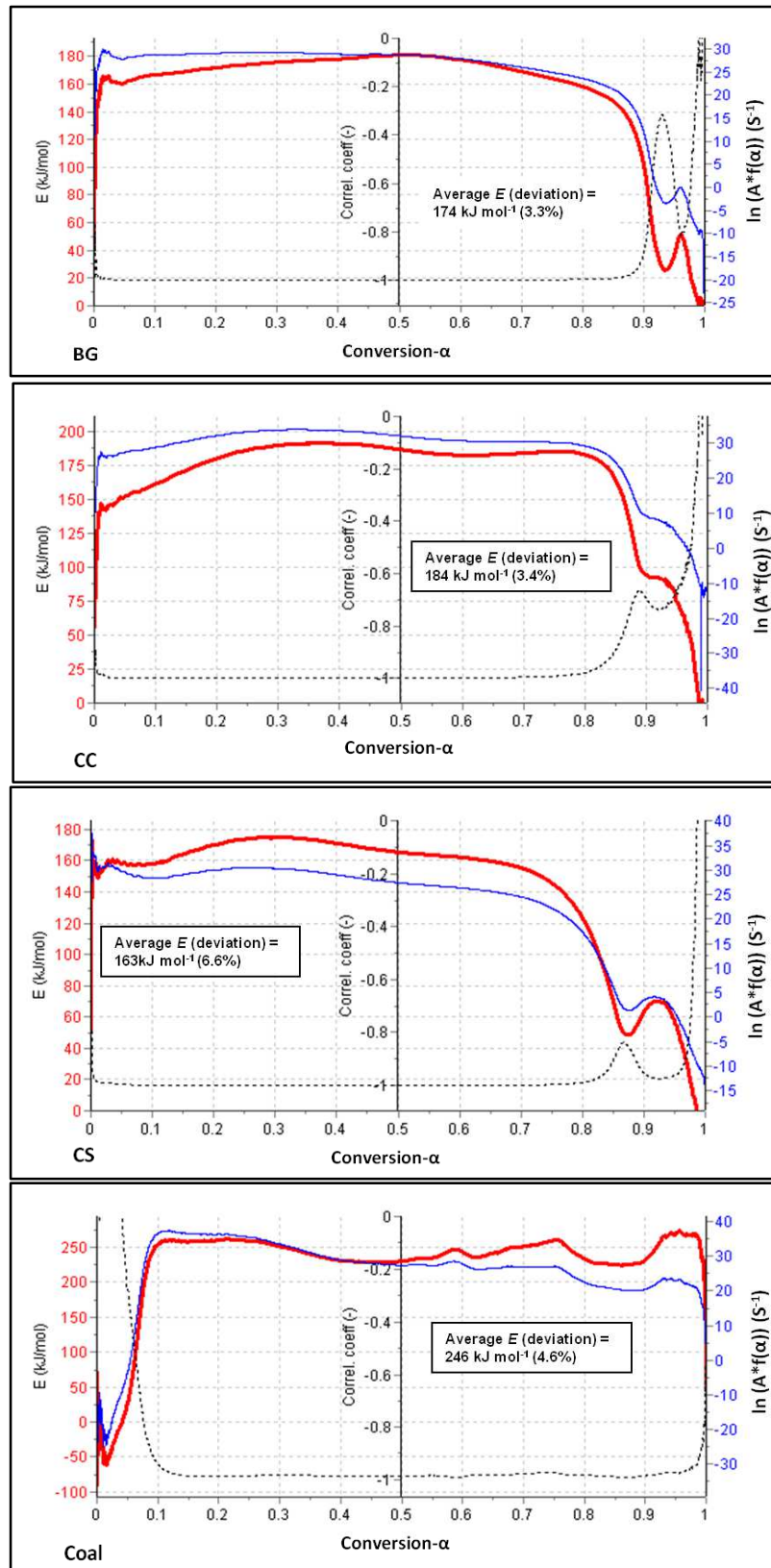


Figure 3-5: Isoconversional kinetic parameters of individual fuels. Also shown are average apparent E values and deviation (%); Maximum conversion $\alpha=1$ corresponds to 90.8%, 82.7%, 80.3% and 31% dry and ash free volatile yields in BG, CC, CS, and coal respectively; (Bold lines depict apparent E, thin lines depict $\ln(A \cdot f(\alpha))$ (S⁻¹) and dotted lines show the correlation coefficient of the calculated parameters)

the total volatile yields; at 10 wt% biomass, the BG and CC fractions accounted for about 34% conversion while at 80:20 and 60:40 mix ratios the contribution of biomass fraction of the blends to total conversion was approximately 50% and 70% respectively.

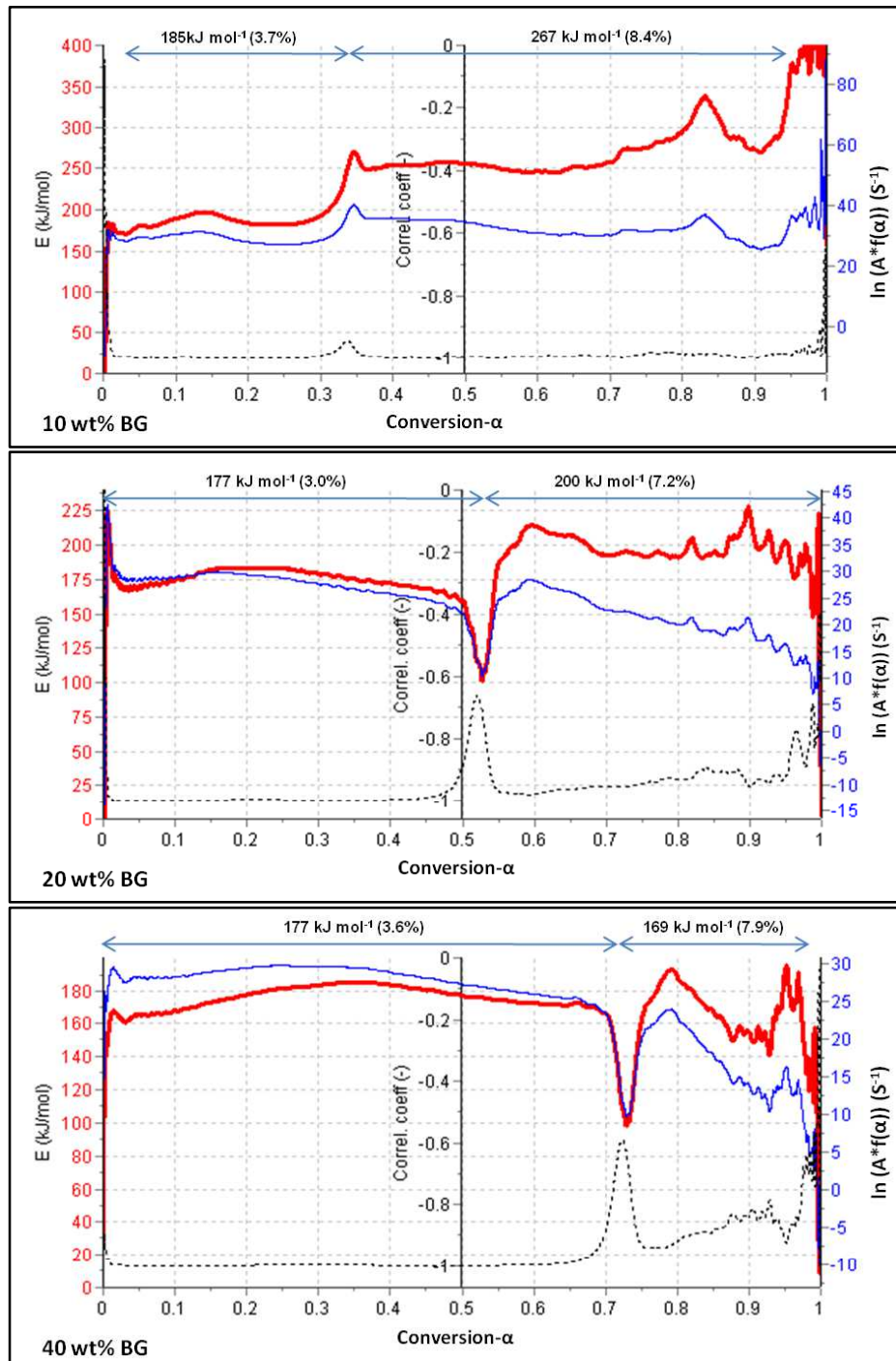


Figure 3-6: Isoconversional kinetic parameters for Coal-BG blends at 10, 20, and 40 wt% biomass mix ratio. Also shown are average apparent E values and deviation (%); (Bold lines depict apparent E values and thin lines depict $\ln(A \cdot f(\alpha))$ (s⁻¹) and dotted lines show the correlation coefficient of the calculated parameters)

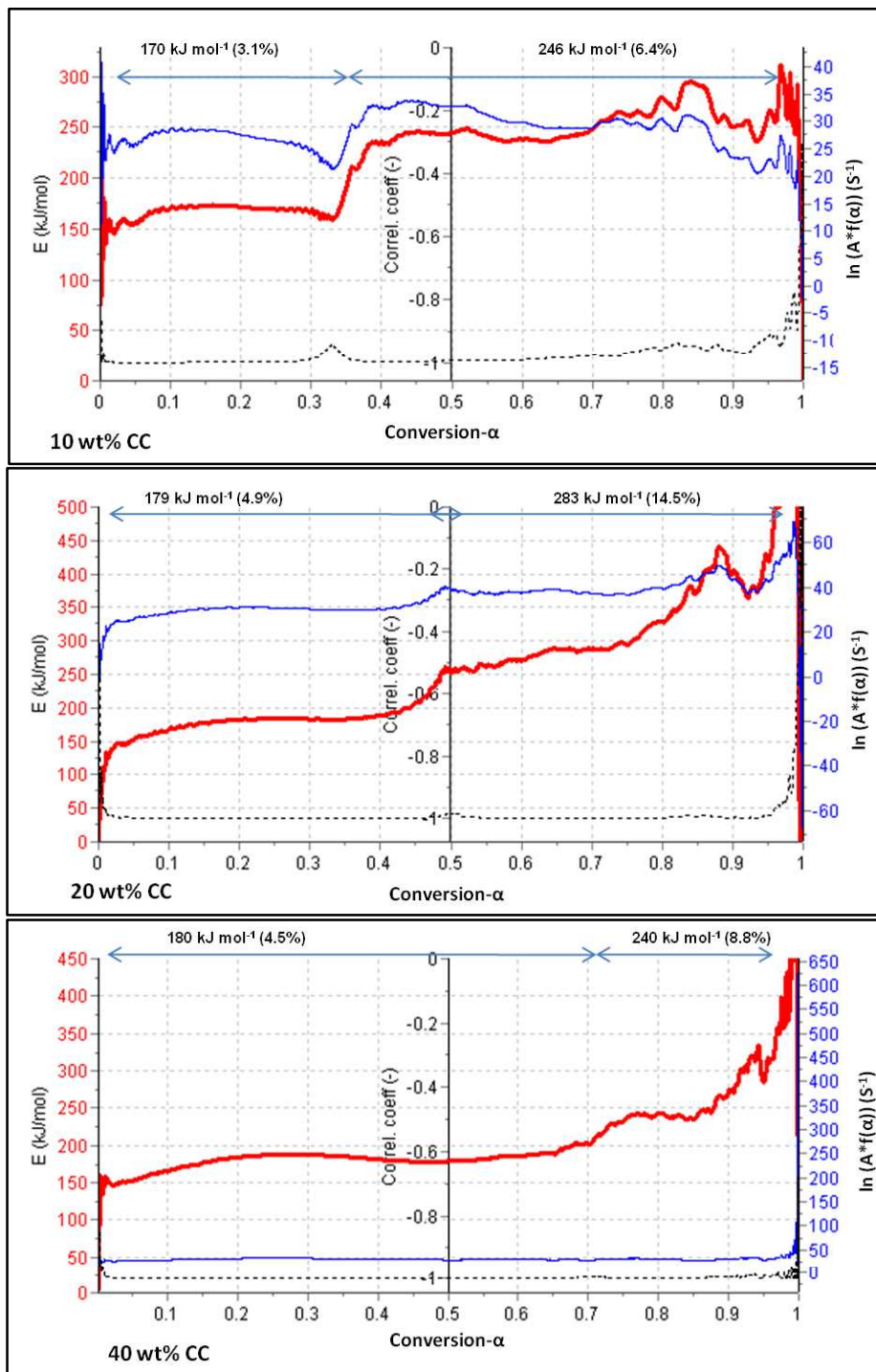


Figure 3-7: Isoconversional kinetic parameters for Coal-CC blends at 10, 20, and 40 wt% biomass mix ratio. Also shown are average apparent E values and deviation (%); (Bold lines depict apparent E, thin lines depict ln(A*f(α)) (s⁻¹) and dotted lines show the correlation coefficient of the calculated parameters)

Apparent E values for the biomass fraction of the blends followed similar trends to those observed for individual biomass pyrolysis as earlier described (Fig. 4-5).

However, the change in apparent E for the range of conversion corresponding to predominantly coal decomposition ($\alpha > 0.3$, 0.5 and 0.7 for 90:10, 80:20 and 60:40 mix ratios respectively), varied more significantly compared to how $E(\alpha)$ behaved when coal was pyrolyzed individually; $E(\alpha)$ values for coal alone varied by about 4.6% while in blends with BG and CC the variation ranged from 7.2 to 8.4% and 6.4 to 14.5% respectively (Figs. 4-5, 4-6 and 4-7). Additionally, the average E values for the coal fraction of the blends decreased during co-pyrolysis with increasing biomass fractions in the blends. For instance, in blends with BG, average E values corresponding to coal decomposition fell from 267 kJ mol^{-1} to 200 kJ mol^{-1} and 170 kJ mol^{-1} as the BG fraction was increased from 10 wt% to 20 wt% and 40 wt% respectively.

3.3.3 Validation of kinetic approach

According to Vyzovkin [9] and Varhegyi [39], kinetic analysis should also include the practical ability to simulate and predict degradation rates which helps in the design and sizing of thermochemical process reactors. For the current paper, validation was achieved by simulating the heating rate curves employed in the analysis, and by predicting the reaction rate progress at a different heating rate ($50^\circ\text{C min}^{-1}$) not used in the kinetic analysis.

In traditional kinetic analysis, it is ordinarily expected that all three parameters that form the kinetic triplets – activation energy (E), pre-exponential factors (A), and decomposition function ($f(\alpha)$) – are needed in order to simulate/predict TG or DTG curves using equation (1). However, Vyazovkin [10] showed that it was not necessary to derive these parameters when model-free analysis is applied. In the first place the theoretical relevance of the kinetic triplets as a tool for interpreting reaction mechanism has been questioned [7]. Furthermore their practical relevance in terms of simulating or predicting reaction progress or reaction rate data are rendered redundant (during isoconversional analysis) as reaction curve predictions can be readily obtained from eqn (2). Figs. 4-8 and 4-9 compares the simulated and experimental DTG curves for single fuels and blends for the range of heating rates (i.e. $5\text{-}50^\circ\text{C min}^{-1}$) used in the kinetic analysis. The calculated quality of fit, or

deviation between the simulated and experimental DTG curves for the single fuels are shown in Table 4-2. A similar range of deviation values were obtained for the blends (not shown). The fit values obtained were generally less than 2% and compared favourably to those resulting from conventional model fitting approaches found in previous reports [38,40,41]. Branca et al. [40] employed multi-heating rate, multi-component model fitting on wood devolatilization, and obtained fits ranging from 3-26%, using a 1, 2, and 3 independent parallel reaction model. However, Gronli et al. [41] obtained better fits ranging from 0.6-2.2% by using a 5 parallel reaction model.

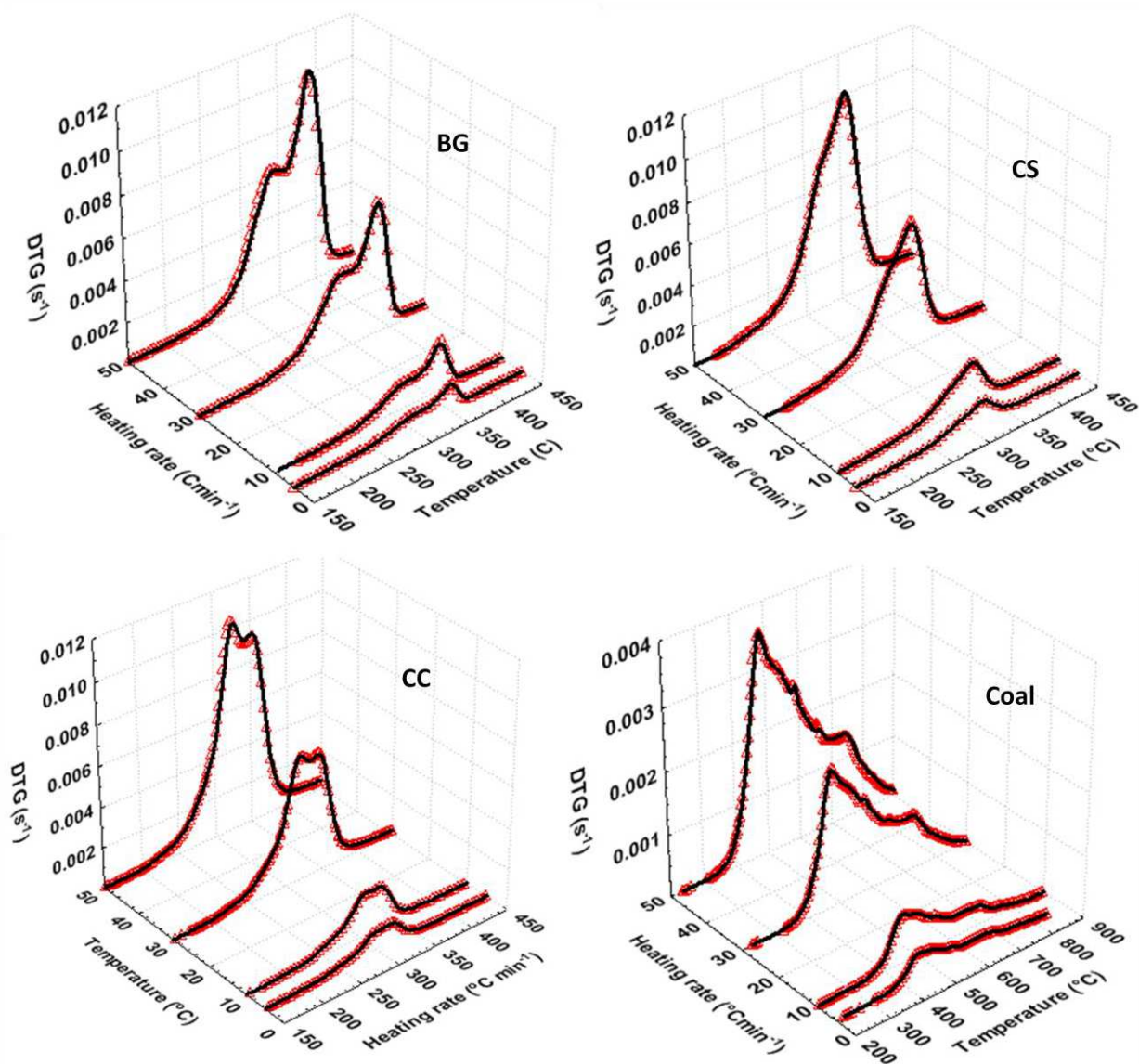


Figure 3-8: Experimental and simulated reaction rate curves at 5, 10, 30 and 50°C min⁻¹ (Experimental curves depicted by shaped markers and predicted curve depicted by lines)

Table 3-2: Deviation between experimental and calculated curves for individual fuels

Heating rate (°C min ⁻¹)	Deviation (%)			
	CC	BG	CS	Coal
5	1.05	1.87	0.26	0.89
10	0.89	1.94	0.36	1.07
20	0.97	0.99	0.50	0.86
30	0.84	1.17	0.52	0.42
40	0.92	1.32	0.28	0.81
50	1.14	1.87	0.66	0.94
Global*	0.40	0.67	0.25	0.33
150	3.28	4.60	3.39	2.78

*Global refers to combined data from 5-50°C min⁻¹ heating rates

Another indication of the reliability of the kinetic analysis approach employed in this paper was the ability to predict reaction progress for heating rates outside the range used in the analysis. Fig. 4-10 shows good agreement between the predicted and experimental TG and DTG curves for the individual samples at 150°C min⁻¹, which was 3 times as fast as the quickest heating rate used in the analysis. The deviations between experimental and predicted curves are also shown in Table 4-2. Reasonable fits of 2.8-4.6% were achieved, although not quite at the same levels of accuracy as was obtained for curves simulated within the experimental range of conditions.

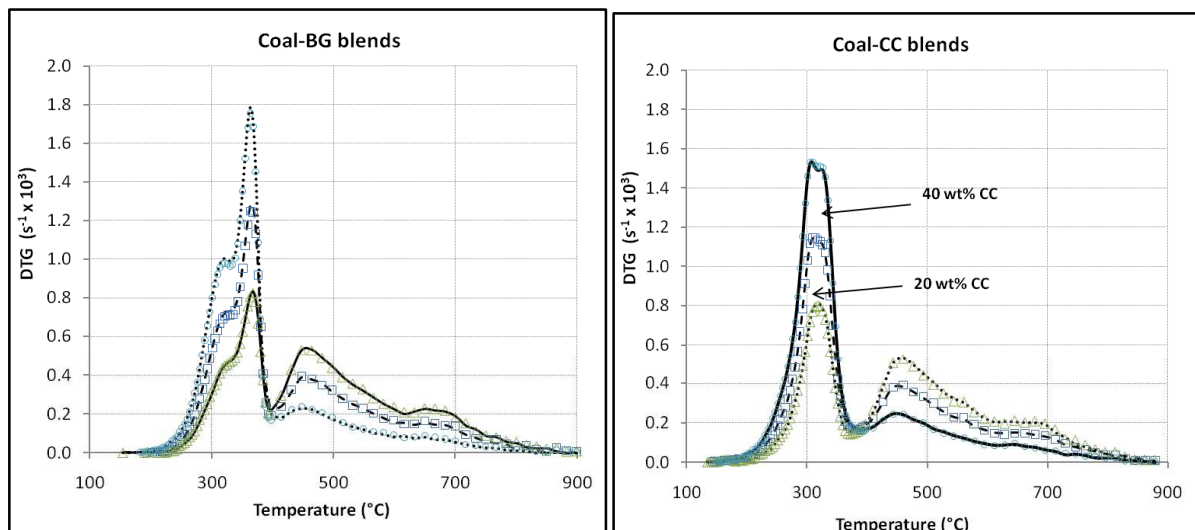


Figure 3-9: Experimental and simulated reaction rate curves for various mix ratios of Coal-BG and Coal-CC blends at 10°C min⁻¹ (Experimental curves depicted by shaped markers and predicted curve depicted by lines)

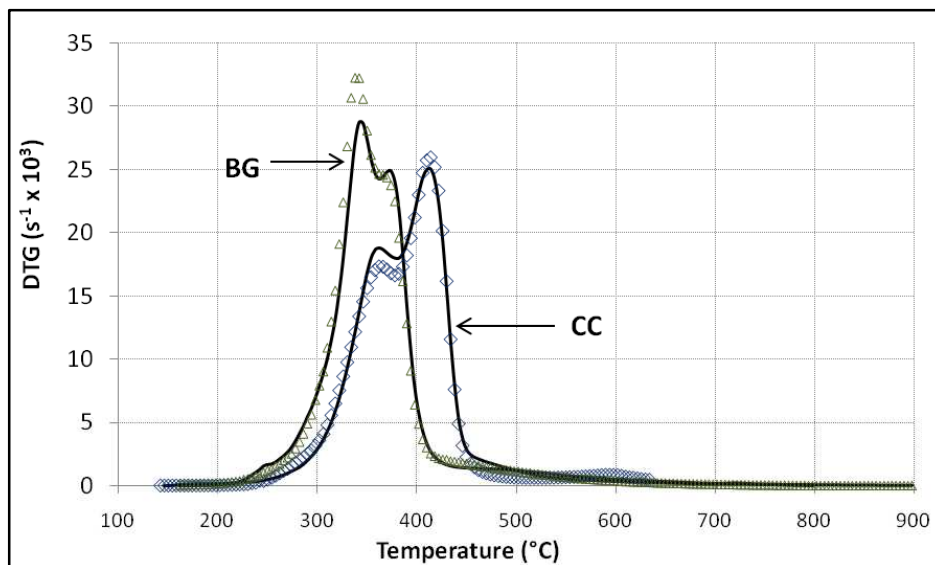


Figure 3-10: Experimental and predicted reaction rate curves at $150^{\circ}\text{Cmin}^{-1}$ based on kinetics obtained at $5\text{-}50^{\circ}\text{C min}^{-1}$ (Experimental curves depicted by shaped markers and predicted curve depicted by lines)

3.4 Discussions

The experimental results suggested that corn residues (CC and CS) were more reactive than sugarcane bagasse, and this is likely due to the higher hemicellulose content in the former (Table 4-1). Of the three main lignocellulosic polymers known to constitute biomass, hemicellulose is the most reactive as its decomposition starts at the lowest temperature [42]. For this reason, it is widely accepted that the lower temperature peak in biomass DTG curves can be ascribed to hemicelluloses, whereas the higher temperature peak represents cellulose [20,42]. Based on the foregoing, it can be seen from Fig. 4-1 that the peak representing hemicelluloses had a comparatively larger size in CC than in BG (for CS both peaks are completely merged). This observation for CC and BG was supported by the reported composition of the constituents in the original raw materials (Table 4-1, Refs [11,43]). Similar conclusions were reached in previous work by the authors using BG and CC samples sourced from the same region (but different farms) as those used in this work [16].

The results also showed that despite these observed differences in the biomass fuels, the overall trend of the devolatilization reaction occurred in a similar range of temperatures (200-400°C) and had similar maximum devolatilization rates (0.15-0.18 %/s), as depicted by the TG and DTG curves in Fig. 4-1. According to results of the isoconversional kinetic analysis (Fig. 4-5) the dependence of E on conversion followed a similar trend for the biomass fuels as well. Apparent E increased from the start of conversion up to a point about ($\alpha=0.5$ for BG and $\alpha=0.3$ for CC and CS) when it started to decrease. The lower $E(\alpha)$ values at early stages of conversion for the biomass fuels apparently corresponded to the degradation of hemicelluloses, since according to the literature, apparent activation energy for hemicelluloses (80-116 kJ mol⁻¹) is usually lower than for cellulose (195-286 kJ mol⁻¹)[40]. Based on the foregoing, the lower E values at low conversion for BG compared to CC and CS (Fig. 4-5), suggested that hemicelluloses in BG are apparently of a less reactive type than that found in the corn residues. This was consistent with the observation by Shafizadeh [44] that the nature of hemicellulose is known to vary significantly between different biomass types. Lignin, with activation energy known to range from 18-65 kJ mol⁻¹ [40], decomposed throughout the duration of pyrolysis over a much wider temperature range. It was mainly responsible for the later part of conversion after polysaccharides have decomposed, as represented by the long tail in the DTG curves at temperatures above 400°C (Fig. 4-1). The lower activation energy of lignin may have caused the relatively low activation energy values observed at higher conversion in Fig. 4-4.

Unlike model fitting approaches, the model-free kinetics allows for the relationship between apparent activation energy and conversion to be observed by way of the $E(\alpha)$ curves shown in Figs. 4-5, 4-6 and 4-7. The degradation trend for coal, as represented by the $E(\alpha)$ values in Fig. 4-4, were distinctly different from the biomass fuels. The average apparent E value for coal between 0.1 and 0.8 conversion was close to 250 kJ mol⁻¹, compared to 163 kJ mol⁻¹ to 183 kJ mol⁻¹ for the biomass fuels, which was consistent with previous reports [21,45].

Comparing the $E(\alpha)$ results for individual feedstocks (Fig. 4-5) and their blends (Figs. 4-6 and 4-7), the effect of blending on the variation in apparent $E(\alpha)$ trends could be identified. There was little difference in the $E(\alpha)$ trends for much of the conversion range corresponding to the decomposition of the biomass fraction of the blends compared to the $E(\alpha)$ trend for devolatilization of biomass alone. However towards the end of conversion associated with biomass decomposition ($\alpha > 0.3$, 0.5 and 0.7 for 90:10, 80:20 and 60:40 mix ratios respectively), a more significant variation of $E(\alpha)$ could be observed. Consequently, the calculated deviation in E for the range of conversion under which coal decomposes (7.2-8.4% in Coal-BG blends and 6.4-14.5% in Coal-CC blends) was higher than the deviation in $E(\alpha)$ observed during individual coal pyrolysis (4.6%). This suggests that there may be some reactions between coal and devolatilized biomass vapours – already present when coal decomposition started – which would not have occurred when coal was reacted individually.

The presence of synergy, or interactions between the coal and biomass fractions during co-pyrolysis, was confirmed by the higher than expected volatile yields (dry and ash free basis) of between 7-12% as the biomass fraction in the blend was increased from 10-50 wt% (Fig. 4-3). This finding contradicted previous reports indicating the absence of synergistic interaction between biomass and coal during co-pyrolysis [20-23], but confirmed more recent results of Ulloa et al. [24] and Haykiri-Acma et al. [25]. The exact mechanism by which interactions between coal and biomass causes synergistic behaviour during co-pyrolysis is not very clear [46]. It has been suggested that increased volatile yields or synergy may be due to inorganic matter in coal and biomass chars, which catalyses demethoxylation reactions. This causes an increase in the production of methoxyphenols which under normal conditions repolymerize to form char. However in the presence of aliphatics found in evolved coal volatiles, the methoxyphenols are thought to undergo secondary reactions that produce volatiles instead [24]. On the other hand, significant volatile release from coal only starts at temperatures greater than 400°C (Fig. 4-1) therefore the above mechanism does not fully account for the synergistic behaviour observed in Fig. 4-4 which occurred between 300-500°C. In hard coals, the main reactions

occurring below 350°C are due to the distillation and diffusion of small molecules trapped in the narrow pore structure of coal [47]. This is closely followed by the cracking of the coal's aromatic ring structure and the formation of CH_2^* , CH_3^* , OH^* and O^* radicals groups, which recombine to form either char (via repolymerisation) or volatiles such as methane water vapour and tar [47,48]. The presence of hydrogen during this process significantly favours the formation of volatiles over char production by partially saturating the radicals thereby preventing recombination reactions [46,49]. Biomass has a higher H/C ratio than coal (Table 4-1), therefore another explanation for synergy could be the increased availability of hydrogen around the coal particles during co-pyrolysis.

It is also important to note that the level of synergistic behaviour as indicated by the disparity between experimental and calculated volatile yields in Fig. 4-3 was not linearly dependent on the amount of biomass in the blends. The level of synergy increased as the biomass fraction of the blends increased up to a certain point – 40 wt% for BG and 30 wt% for CC – beyond which further addition of biomass did not lead to a corresponding increase in the severity of synergistic behaviour. A similar kind of inflection point was observed by Cao et al. [50] in their study of polycyclic aromatic hydrocarbons (PAHs) production from the co-pyrolysis of waste tyre and wood. It was deduced that this was due to competition between oxygenates (such as phenols, alcohols and ketones) and PAH production from biomass derived free radicals. As the availability of these radicals increase (due to addition of biomass), the balance between this two competing reactions shifts towards the production of oxygenates causing a reduction in PAH yields [50,51]. It is possible that a similar sort of balance exists between reactions that favour overall char and volatile production during the co-pyrolysis of biomass and coal. Further studies will be required to confirm and determine the exact nature of the synergy, based on the alternatives presented here.

3.5 Conclusions

The thermokinetics of the co-pyrolysis of two different types of coal biomass blends have been investigated via non-isothermal thermogravimetric analysis. The individual devolatilization behaviour of each of the fuels used – coal, sugarcane bagasse and corn residue – were compared with the behaviour of coal-biomass blends in order to identify synergistic behaviour that point to the existence of chemical interactions between the coal and biomass fraction of the blends.

The devolatilization of the biomass materials occurred in a narrow temperature interval (200-400°C) and with higher decomposition rates than coal, of which the decomposition occurred between 380-900°C. Isoconversional kinetic analysis revealed the dependence of apparent activation energy on conversion, $E(\alpha)$, from which very good predictions of reaction progress could be obtained for both individual samples and blends. The study also revealed that adding biomass to coal caused about 7-11% higher volatile yields (on dry and ash free basis) than would be expected assuming a purely additive behaviour and that much of this increase was due to synergistic interactions that occurred mainly between 300°C and 500°C. Co-pyrolysis also caused higher variability in $E(\alpha)$ values for the coal fraction of the blends compared to what was observed when the fuels were pyrolyzed separately, which provides further evidence of non-additive or synergistic behaviour during the co-pyrolysis process. It can also be concluded that the model-free method is a good approach for evaluating the kinetics of solid fuels and their blends. The method allows for changes in apparent E during conversion to be clearly observed, such that abnormal variations caused by chemical interaction between components of the blend can be detected. The method also gives comparably reliable predictions of reaction rates compared to the more traditional model fitting kinetic approaches.

3.6 References

- [1] International Energy Agency, Key world energy statistics, IEA, www.iea.org/stats/index.asp, 2010.
- [2] G. Couch, Coal to liquids, IEA Clean Coal Centre, 2008.

- [3] World Coal Institute, Coal: Liquid Fuels, <http://www.worldcoal.org/resources/wca-publications/>, 2006.
- [4] R. Davidson, A. Doig, J. Ekmann, R. Fernando, N. Harding, R. Moreea-Taha, et al., Cofiring coal with other fuels, IEA Clean Coal Centre, 2007.
- [5] N. Koukouzas, A. Katsiadakis, E. Karlopoulos, E. Kakaras, Co-gasification of solid waste and lignite—A case study for Western Macedonia, *Waste Management*. 28 (2008) 1263-1275.
- [6] P. Havlík, U.A. Schneider, E. Schmid, H. Böttcher, S. Fritz, R. Skalský, et al., Global land-use implications of first and second generation biofuel targets, *Energy Policy*. doi:10.1016/j.enpol.2010.03.030 (2011).
- [7] S. Vyazovkin, Model-free kinetics, *Journal of Thermal Analysis and Calorimetry*. 83 (2006) 45-51.
- [8] A. Kemmler, M.E. Brown, M. Maciejewski, S. Vyazovkin, R. Nomen, J. Sempere, et al., Computational aspects of kinetic analysis Part A: The ICTAC kinetics project-data, methods and results, *Thermochimica Acta*. 355 (2000) 125-143.
- [9] S. Vyazovkin, Computational aspects of kinetic analysis Part C: The ICTAC Kinetics Project—the light at the end of the tunnel?, *Thermochimica Acta*. 355 (2000) 155–163.
- [10] S. Vyazovkin, A unified approach to kinetic processing of nonisothermal data, *International Journal of Chemical Kinetics*. 28 (1996) 95-101.
- [11] M. Garcí`a-Pèrez, A. Chaala, J. Yang, C. Roy, Co-pyrolysis of sugarcane bagasse with petroleum residue. Part I: thermogravimetric analysis, *Fuel*. 80 (2001) 1245-1258.
- [12] E. Biagini, A. Fantei, L. Tognotti, Effect of the heating rate on the devolatilization of biomass residues, *Thermochimica Acta*. 472 (2008) 55-63.
- [13] J.M. Cai, L.S. Bi, Kinetic analysis of wheat straw pyrolysis using isoconversional methods, *J Therm Anal Calorim*. 98 (2009) 325-330.
- [14] V. Leroy, D. Cancellieri, E. Leoni, J.-L. Rossi, Kinetic study of forest fuels by TGA: Model-free kinetic approach for the prediction of phenomena, *Thermochimica Acta*. 497 (2010) 1-6.
- [15] A.G.D. Santos, A.S. Araujo, V.P.S. Caldeira, V.J. Fernandes Jr., L.D. Souza, A.K. Barros, Model-free kinetics applied to volatilization of Brazilian sunflower oil, and its respective biodiesel, *Thermochimica Acta*. 506 (2010) 57-61.
- [16] A.O. Aboyade, T.J. Hugo, M. Carrier, E.L. Meyer, R. Stahl, J.H. Knoetze, et al., Non-isothermal kinetic analysis of the devolatilization of corn cobs and sugar cane bagasse in an inert atmosphere, *Thermochimica Acta*. 517 (2011) 81-89.
- [17] K. Muira, A New and Simple Method to Estimate $f(E)$ and $ko(E)$ in the Distributed Activation Energy Model from Three Sets of Experimental Data, *Energy & Fuels*. 9 (1995) 302-307.
- [18] J.L. Hillier, T.H. Fletcher, Pyrolysis Kinetics of a Green River Oil Shale Using a Pressurized TGA, *Energy Fuels*. 25 (2010) 232-239.
- [19] G.W. Collett, B. Rand, Thermogravimetric investigation of the pyrolysis of pitch materials. A compensation effect and variation in kinetic parameters with heating rate, *Thermochimica Acta*. 41 (1980) 153-165.
- [20] D. Vamvuka, N. Pasadakis, E. Kastanaki, P. Grammelis, E. Kakaras, Kinetic Modeling of Coal/Agricultural By-Product Blends, *Energy & Fuels*. 17 (2003) 549-558.

- [21] H.B. Vuthaluru, Investigations into the pyrolytic behaviour of coal/biomass blends using thermogravimetric analysis, *Bioresource Technology*. 92 (2004) 187-195.
- [22] E. Biagini, F. Lippi, L. Petarca, L. Tognotti, Devolatilization rate of biomasses and coal–biomass blends: an experimental investigation, *Fuel*. 81 (2002) 1041-1050.
- [23] B. Moghtaderi, C. Meesri, T.F. Wall, Pyrolytic characteristics of blended coal and woody biomass, *Fuel*. 83 (2004) 745-750.
- [24] C.A. Ulloa, A.L. Gordon, X.A. García, Thermogravimetric study of interactions in the pyrolysis of blends of coal with radiata pine sawdust, *Fuel Processing Technology*. 90 (2009) 583-590.
- [25] H. Haykiri-Acma, S. Yaman, Synergy in devolatilization characteristics of lignite and hazelnut shell during co-pyrolysis, *Fuel*. 86 (2007) 373-380.
- [26] L.R. Lynd, H. Von Blottnitz, B. Tait, J. de Boer, I.S. Pretorius, K. Rumbold, et al., Converting plant biomass to fuels and commodity chemicals in South Africa: a third chapter?, *South African Journal of Science*. 99 (2003) 499-507.
- [27] Department of Minerals and Energy, White Paper on the Renewable Energy Policy of the Republic of South Africa, Department of Minerals and Energy, 2003.
- [28] European Committee for Standardization, Solid biofuels. Methods for sample preparation, 2005.
- [29] American Society for Testing Materials, ASTM D5373 - Standard Test Methods for Instrumental Determination of Carbon, Hydrogen, and Nitrogen in Laboratory Samples of Coal, 2002.
- [30] American Society for Testing Materials, ASTM D4239 - Standard Test Methods for Sulfur in the Analysis Sample of Coal and Coke Using High-Temperature Tube Furnace Combustion Methods, 2000.
- [31] British Standards Institute, Solid biofuels. Determination of calorific value, 2009.
- [32] American Society for Testing Materials, ASTM E1131 - Standard Test Method for Compositional Analysis by Thermogravimetry, 1998.
- [33] H. Yang, H. Chen, F. Ju, R. Yan, S. Zhang, Influence of Pressure on Coal Pyrolysis and Char Gasification, *Energy & Fuels*. 21 (2007) 3165-3170.
- [34] M.J. Antal, G. Varhegyi, Cellulose pyrolysis kinetics: the current state of knowledge, *Industrial and Engineering Chemistry Research*. 34 (1995) 703-717.
- [35] AKTS, AKTS Advanced Thermal Analysis Software - <http://www.akts.com/>, (2010).
- [36] J.A. Caballero, J.A. Conesa, Mathematical considerations for nonisothermal kinetics in thermal decomposition, *Journal of Analytical and Applied Pyrolysis*. 73 (2005) 85-100.
- [37] O. Senneca, Kinetics of pyrolysis, combustion and gasification of three biomass fuels, *Fuel Processing Technology*. 88 (2007) 87-97.
- [38] S. Sharma, A.K. Ghoshal, Study of kinetics of co-pyrolysis of coal and waste LDPE blends under argon atmosphere, *Fuel*. 89 (2010) 3943-3951.
- [39] G. Varhegyi, Aims and methods in non-isothermal reaction kinetics, *Journal of Analytical and Applied Pyrolysis*. 79 (2007) 278-288.
- [40] C. Branca, A. Albano, C. Di Blasi, Critical evaluation of global mechanisms of wood devolatilization, *Thermochimica Acta*. 429 (2005) 133-141.

- [41] M.G. Gronli, G. Varhegyi, C. Di Blasi, Thermogravimetric Analysis and Devolatilization Kinetics of Wood, *Industrial & Engineering Chemistry Research*. 41 (2002) 4201-4208.
- [42] G. Varhegyi, M.J. Antal, T. Szekely, P. Szabo, Kinetics of the thermal decomposition of cellulose, hemicellulose, and sugarcane bagasse, *Energy & Fuels*. 3 (1989) 329-335.
- [43] O. Ioannidou, A. Zabaniotou, E.V. Antonakou, K.M. Papazisi, A.A. Lappas, C. Athanassiou, Investigating the potential for energy, fuel, materials and chemicals production from corn residues (cobs and stalks) by non-catalytic and catalytic pyrolysis in two reactor configurations, *Renewable and Sustainable Energy Reviews*. 13 (2009) 750-762.
- [44] F. Shafizadeh, Introduction to pyrolysis of biomass, *Journal of Analytical and Applied Pyrolysis*. 3 (1982) 283–305.
- [45] D. Vamvuka, E. Kakaras, E. Kastanaki, P. Grammelis, Pyrolysis characteristics and kinetics of biomass residuals mixtures with lignite, *Fuel*. 82 (2003) 1949–1960.
- [46] T. Sonobe, N. Worasuwannarak, S. Pipatmanomai, Synergies in co-pyrolysis of Thai lignite and corncob, *Fuel Processing Technology*. 89 (2008) 1371-1378.
- [47] H. Jüntgen, Review of the kinetics of pyrolysis and hydrolysis in relation to the chemical constitution of coal, *Fuel*. 63 (1984) 731-737.
- [48] A. Radjenović, Pyrolysis of Coal, *Kemija U Industriji*. 55 (2006).
- [49] D.K. Park, S.D. Kim, S.H. Lee, J.G. Lee, Co-pyrolysis characteristics of sawdust and coal blend in TGA and a fixed bed reactor, *Bioresource Technology*. Article in Press (n.d.).
- [50] Q. Cao, L. Jin, W. Bao, Y. Lv, Investigations into the characteristics of oils produced from co-pyrolysis of biomass and tire, *Fuel Processing Technology*. 90 (2009) 337–342.
- [51] R.J. Evans, T.A. Milne, Molecular characterization of the pyrolysis of biomass, *Energy and Fuels*. 1 (1987) 123-137.

4 Model fitting kinetics of the co-pyrolysis of coal blends with corn and sugarcane residues

Submitted to *Thermochimica Acta* in July 2011 using the following details:

Title: “Model fitting kinetic analysis and characterisation of the devolatilization of coal blends with corn and sugarcane residues”

Authors: Akinwale O. Aboyade^{a,b}, Johann F. Görgens^a, Marion Carrier^a, Edson L. Meyer^b, Johannes H Knoetze^a,

^aDepartment of Process Engineering, Stellenbosch University, Stellenbosch, South Africa

^bFort Hare Institute of Technology, University of Fort Hare, Alice, South Africa

In this chapter, single and multi-component model fitting was used to determine the pyrolysis reaction kinetics of coal, corn cobs, and sugarcane bagasse, as well as blends of coal with each of the biomasses based on the same TGA data used in the previous chapter for model free analysis.

4.1 Introduction

Existing industrial scale thermochemical conversion processes are currently almost entirely coal based [1]. However, there has been a growing interest in combining the current coal feedstock with biomass and wastes, as a way to harness the energy potential of biomass fuels, while avoiding the cost of dedicated biomass plants. Recognizing that devolatilization is a fundamental step in all the main thermochemical conversion processes such as pyrolysis, combustion and gasification, has led to increased research focus on the pyrolysis kinetics of coals, biomass and their blends. Various procedures for evaluating devolatilization kinetic parameters of solid fuels from data derived from non-isothermal thermogravimetric analysis (TGA) have been developed, and the vast majority of them can be classified as either ‘model-free’ or ‘model-fitting’. The conventional approach for estimating kinetic parameters (activation energy, pre-exponential factor and reaction order) from TGA data via model-fitting analysis usually involves assuming a certain reaction order, and then manipulating the differential or integral form of the ensuing rate equation until a straight line plot can be obtained from where the remaining unknown parameters can be obtained by linear regression. Examples of this method are those due to

Coats and Redfern [2], Freeman and Carroll [3], and Duvvuri et al. [4]. However, it is widely recognised that these approaches suffer from two main deficiencies, particularly in cases where data from only a single heating rate is applied [5,6]: i) it can often yield different values of the kinetic parameters describing the same thermogravimetric curve, leading to an ambiguity in terms of interpretation of the results; ii) it generally tends to yield one set of kinetic parameters for the whole range of conversion, therefore not taking into account the complexity of mechanisms involved during pyrolysis of plant biomasses. More recently, due to increased availability of low-cost computing power, a more complicated but more accurate method involving non-linear least squares optimization of multiple heating rate data has been increasingly considered [7,8].

Model fitting kinetics of biomass materials is traditionally based on the assumption that pyrolysis weight loss occurs via a 1st order decomposition process which is modelled either as a single reaction, or as the weighted summation of multiple pseudo-mechanistic reactions representing decomposition of the main reactive constituents of biomass namely cellulose, hemicellulose, lignin and extractives [9–11]. While kinetic parameters derived in this way allow reasonably accurate simulations and predictions of experimental data, other reports have shown that even more accurate simulations can be achieved by nth order modelling where, the reaction order is not confined to any particular value, but is rather considered as one of the unknown parameters to be optimized [12,13]. The pyrolysis kinetics of coal is more frequently analysed using either the nth order or distributed activation energy model (DAEM) [14]. The DAEM is a form of the multi-component nth order reaction, where it is assumed that the reactivity distribution is represented by a set of parallel (usually 1st order) reactions each with its own activation energy but a common pre-exponential factor [14,15]. The activation energy is expressed as a continuous distribution function, more frequently of a Gaussian type, although Weibull and Gamma distributions have been employed as well [14].

A number of studies are available where the model fitting approach was applied to the kinetics of coal-biomass blends. Biagini et al. [16] combined a DAEM for coal with a 3 pseudocomponent 1st order reaction model for the biomass to predict reaction curves of the blends. Vamvuka et al. [17] on the other hand employed multi-pseudocomponent 1st order models for both coal and biomass, assuming 5 and 3 pseudocomponents respectively. Both studies indicated that reasonable visual fits could be obtained between predicted and experimental rate curves, but did not provide quantitative values of the fit quality. Rather than use the individual kinetic parameters of the coal and biomass components to predict behaviour of the blends, Vultharu et al. [18] calculated separate kinetic parameters for the blends and the contributing coal and biomass components using linear regressions of single nth order reaction models.

On the question of synergistic interactions between the reacting coal and biomass during co-pyrolysis, all the aforementioned studies concluded that no such interactions exist and that the components behaved in the same manner as when pyrolyzed alone. However Hayciri-Acma et al. [19], Ulloa et al. [20] and Aboyade et al. [21] have challenged this view, showing that there are indeed significant interactions between the coal and biomass fractions during TGA co-pyrolysis. This assertion is also supported by results of non-TGA co-pyrolysis experiments where the influence of blending ratio on the yield of specific volatile products was investigated [22–25]. There are a few possible mechanisms by which interactions between coal and biomass may cause synergistic behaviour during co-pyrolysis [23]. It has been suggested that increased volatile yields or synergy may be due to inorganic matter in biomass, which promote demethoxylation reactions, which in turn combines with the aliphatics found in coal derived volatiles, thereby causing increased occurrence of volatile producing secondary reactions [20]. Another explanation for the increased volatiles could be the effect of the increased presence of hydrogen arising from the higher H/C ratio in biomass. Hydrogen may prevent repolymerization and cross-linking of free radicals that increase char formation consequently leading to the formation of more volatiles instead [23,24].

The present work investigates the devolatilization behaviour and kinetics of individual samples and blends of hard South African coal, corn cobs and sugarcane bagasse. It is a continuation of a previous effort involving model-free analysis of the same data [21]. This is in keeping with recommendations from the Kinetics Committee of the International Confederation for Thermal Analysis and Calorimetry [26], that model fitting analysis be performed to supplement model-free approaches, especially where there is significant variation of model-free derived kinetic parameters with conversion, which was the case for the materials under investigation in this work [21]. Model fitting was achieved via non-linear optimization of multiple independent parallel 1st and nth order reaction models. Parameters obtained from the previously conducted model-free analysis were used as first estimate as part of the optimization procedure. Results of the 1st and nth order fitting procedures were compared with each other and with values obtained from the model free approach.

Table 4-1: Proximate, Ultimate and biochemical (biomass only) characteristics of feedstock samples

Properties	BG [18]	CC [18]	CS	Coal [18]
<u>Ultimate analysis (wt%, daf)</u>				
C	51.9±0.6	50±0.5	49.9±0.5	79.1±0.8
H	6.9±0.1	6.6±0.1	7.1±0.1	5.2±0.1
N	0.4±0.0	0.2±0.0	0.9±0.0	1.9±0.1
S	0.5±0.0	0.4±0.0	0.3±0.0	1.8±0.1
O*	40.5±0.5	43±0.5	42.1±0.5	12.2±0.2
HHV (MJ/kg)	16.6±0.2	18.0±0.2	13.2±0.1	79.1±0.8
<u>Proximate analysis (wt%)</u>				
Moisture	6.7±0.1	7.0±0.1	6.9±0.1	4.0±0.1
Ash (db)	10.3±0.1	1.6±0.1	24.5±0.1	38.6±0.2
Volatiles (daf)	91.7±0.3	84.3±0.3	84.1±0.3	31.7±0.1
Fixed carbon (daf)	8.3±0.1	15.7±0.1	15.9±0.1	68.3±0.3
<u>Lignocellulosic composition (wt%, daf)</u>				
Cellulose	44.2±0.6	35.9±0.8	34.0±0.5	
Hemicellulose	23.8±0.4	38.1±0.8	26.8±0.8	
Lignin	22.4±0.3	16.7±0.2	20.1±0.4	
Extractives and others	9.7±0.6	9.5±0.8	19.2±0.8	

*Obtained by difference; db=dry basis; daf=dry and ash free basis

4.2 Material and methods

Samples and experimental methods used in this chapter were the same ones presented in the previous chapter (section 4.2.1) and will not be repeated here. The results of the ultimate and proximate analysis for the samples used, as well as the biochemical characteristics of the biomasses are reproduced in Table 5-1.

4.2.1 Kinetic analysis

The kinetic analysis of the thermal decomposition of solid fuels is usually based on the rate equation for solid state decomposition processes [7,33,34];

$$\frac{d\alpha}{dt} = A \exp\left[-\frac{E}{RT}\right] f(\alpha) \quad (1)$$

where $f(\alpha)$ is the reaction model. Conversion, α , is derived from the equation $\alpha = (m_0 - m)/(m_0 - m_f)$ where m_0 and m_f are the initial and final mass in the non-isothermal temperature range used for the analysis [21].

Data from 5, 10, 20, 30, 40, and 50°C min⁻¹ were fitted simultaneously to 1st and nth order reaction model via non-linear least squares optimization. In selecting the data points to fit, 200 evenly spaced representative points were extracted for each experimental run according to the recommendation by Caballero and Conesa [8]. This was done by normalizing the total variation in both temperature and TG/DTG axis (units of measure in both axis range between zero and one), and then choosing the points such that length of the arc or curve between two consecutive points is constant, using an adaptation of the *curvspace* syntax in MATLAB [35]. Devolatilization was assumed to proceed through multiple independent parallel reactions corresponding to the assumed number of pseudocomponents that make up the sample [7,11,15]. The term pseudocomponent refers to a group of reactive species that exhibit similar reactivity e.g. cellulose, hemicellulose, lignin for biomass [7]. Under this scenario equation (1) becomes;

$$\frac{d\alpha}{dt} = \sum \gamma_i \frac{d\alpha_i}{dt} = \sum \gamma_i A_i \exp\left[-\frac{E_i}{RT}\right] f(\alpha_i) \quad (2)$$

where γ_i is the contribution of pseudocomponent i to the total mass loss. Eqn (2) can be rearranged after substituting dt with dT/β (where β is the heating rate), and integrating as follows

$$\int_0^\alpha \frac{d\alpha}{f(\alpha)} = \sum \gamma_i \frac{A_i}{\beta} \int_{T_0}^{T_\alpha} \exp\left(-\frac{E_i}{RT}\right) dT \quad (3)$$

The temperature integral in eqn (3) takes the following form

$$\int_{T_0}^{T_\alpha} \exp\left(-\frac{E_i}{RT}\right) dT = \frac{E_i}{RT} \left[\frac{\exp(-x_i)}{x_i} - \int_x^\infty \frac{\exp(-x_i)}{x_i} dx \right] \quad (4)$$

where $x_i = E_i/RT$. Eqn (3) can then be solved for an n^{th} order model, i.e. $f(\alpha) = (1-\alpha)^n$ as follows;

$$\alpha_i = 1 - \left[1 - (1 - n_i) \frac{A_i}{\beta} I(E_i, T) \right]^{\frac{1}{1-n_i}} \quad (5)$$

$I(E_i, T)$ represents the temperature integral function defined in eqn (4). Eqn (5) is only true for $n \neq 1$ and to perform 1st order modelling, one approach is to solve eqn (3) for $f(\alpha) = (1-\alpha)$. The alternative approach which according Burnham and Braun [14] gives equivalent results is to use $n = 1.0001$ in eqn (5). This latter technique was adopted in this study. Optimization was conducted by multidimensional non-linear regression, which involved searching for values of A_i , E_i , n_i , and γ_i that minimized the objective function given in eqn (6).

$$F = \sum_{k=1}^{N_k} \sum_{j=1}^{N_j} \left[\left(\frac{d\alpha}{dt} \right)_{exp} - \left(\frac{d\alpha}{dt} \right)_{calc} \right]^2 \quad (6)$$

where da/dt_{exp} and da/dt_{calc} stand for the experimental and calculated TG curves respectively for N_j data points in each of N_k experiments conducted at varying heating rates. Differential data was chosen for optimization as it magnifies the

features and peaks of TG curves [7]. Initial estimates used were obtained from previously conducted model-free analysis of the same samples [21]. The deviation between the predicted and experimental curves, or quality of fit (QOF) for each heating rate is given by eqn (7). A global QOF was also calculated for the combined data across all heating rates by replacing N_j in eqn (7) by the product of N_j and N_k .

$$QOF(\%) = 100 \times \sum_{j=1}^{N_j} \sqrt{\left[\frac{\left\{ \left(\frac{d\alpha}{dt} \right)_{exp} - \left(\frac{d\alpha}{dt} \right)_{calc} \right\}^2}{N_j} \right]} / \text{Max} \left| \frac{d\alpha}{dt} \right|_{exp} \quad (7)$$

4.3 Results and Discussions

4.3.1 Single fuels

Fig. 5-1 shows the non-isothermal mass loss (TG) curves for BG, CC, and Coal single fuels at $10^\circ\text{C min}^{-1}$ under an inert atmosphere. The figure also includes a temperature versus time plot, on which the temperature program used in the analysis is illustrated. The initial small reduction in mass just before the beginning of the dynamic section of the time/temperature plot could be attributed to the demoiustrization of the samples. Because the kinetic modelling in this paper is based on non-isothermal kinetics, all analysis henceforth will be focused on the temperature range corresponding to the non-isothermal (or dynamic) region of the plot in Fig. 5-1. A background description of the experimental TG and DTG curves of the single fuel samples can be found in Section 4.3.1.1.

Table 5-2 shows the kinetic parameter values for the slow pyrolysis of single biomass and coal fuels obtained via 1st and nth order model-fitting. Model fitting for biomass data was done based on the assumption of 1, 3 and 4 parallel reactions, while coal was modelled based on the 1, 3, 4 and 5 component approach, with the number of pseudocomponents corresponding to the number of assumed independent reactions occurring in parallel. Table 5-3 shows the quality of fit (QOF) values for each heating rate employed in the analysis, as well as global QOF for all the heating rate data ($5\text{-}50^\circ\text{C min}^{-1}$) combined. Graphical illustrations of DTG fits obtained from 3- and 4-

pseudocomponent, n^{th} order modelling for biomass are shown Fig. 5-2 while Fig. 5-3 shows results of the analysis for coal based on 3-, 4-, and 5- pseudocomponent, n^{th} order fitting.

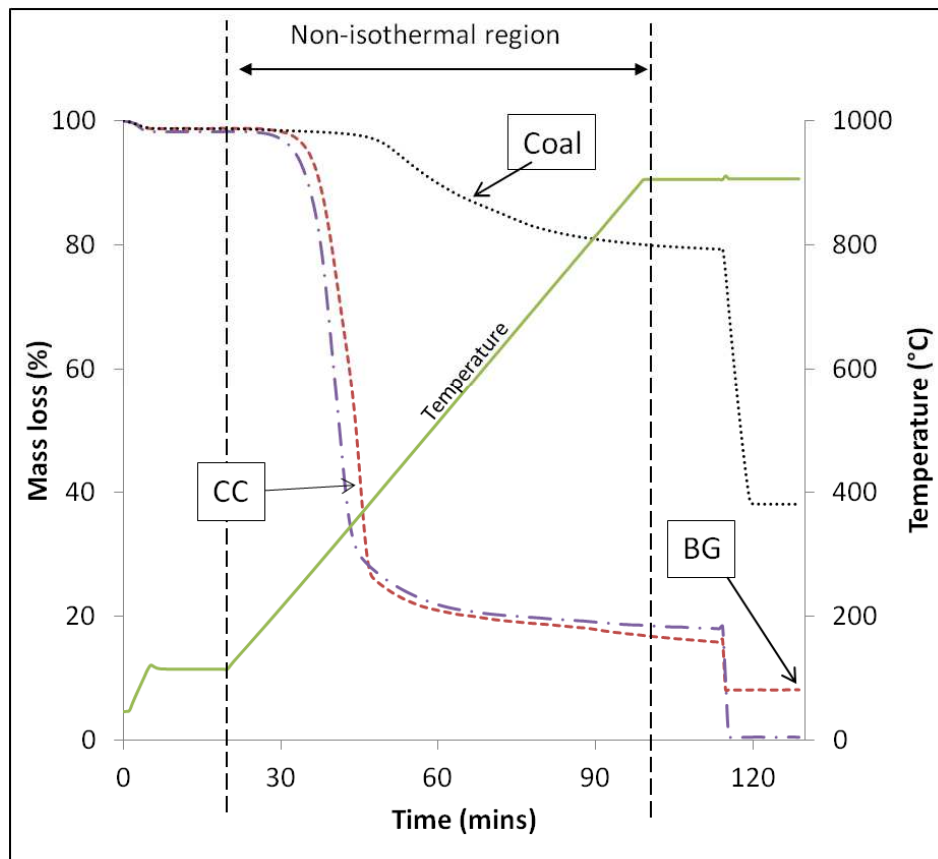


Figure 4-1: DTG curves of individual fuel pyrolysis at $10^{\circ}\text{C min}^{-1}$ (dotted lines represent sample TG and DTG curves while unbroken line in 1a shows the time-temperature profile)

Under the single component assumption ($i=1$), the quality of fit between experimental and simulated reaction rate curves (Table 5-3) was relatively poor for the biomass fuels (global QOF \approx 4.5-6%) and slightly worse for coal (7-10%). On the other hand global QOF values of just over 1% were achieved for the 3 pseudocomponent models ($i=3$) for biomass. Further increasing i for the biomasses from 3 to 4 gave slightly better fit values for all single fuels via both 1^{st} and n^{th} order analyses. Using multi-component analysis for coal led to similar improvements in QOF values compared to the single component fitting. Going from $i = 1$ to $i = 3$ resulted in a corresponding enhancement of QOF values from 4.7 to 3.0% for the 1^{st}

order model and 6.7 to 2.2% for n^{th} order modelling. However, only by fitting with $i = 5$ and higher could the fit qualities in coal match values observed for the biomass fuels. Higher i values required considerably longer computation times and did not result in remarkable improvements in fit quality, hence there was a risk of overfitting [36]. Consequently, discussions from here on will focus mainly on results of 3 pseudocomponent fitting, as the QOF values it produced were considered satisfactory. Additionally, the assumption of 3 parallel reactions is consistent with generally accepted decomposition mechanisms for biomass [9–11] and coal [15].

Table 5-3 shows that fit quality deteriorates with decrease in heating rates. For instance, the QOFs at $5^{\circ}\text{C min}^{-1}$ and $10^{\circ}\text{C min}^{-1}$ were usually significantly higher than those at 40 and $50^{\circ}\text{C min}^{-1}$. This observation can also be visualized in Figs. 5-2 and 5-3. The higher disparity between experimental and simulated peaks at $20^{\circ}\text{C min}^{-1}$ compared to $40^{\circ}\text{C min}^{-1}$ were a consequence of the simultaneous fitting of multiple heating rates which often resulted in poorer fits for slower heating rates. A similar trend was to some extent observed by Branca et al. [9]. The reason for this trend is proposed as follows; biomass and coal are complex materials consisting of more components than can be practically represented in kinetic models. For instance each of the hemicelluloses, cellulose and lignin sub-components are in turn made up of numerous other simpler components [37]. In general, this means that the greater the number of components assumed during multi-component kinetic analysis, the better the quality of the fits obtained. This is particularly true for lower heating rates where there is likelier to be a better separation of the individual component reactions [38]. Consequently, analysis of slower heating rates requires more pseudocomponents to achieve the same level of fit as faster heating rates. As Table 5-3 shows, the gap between the QOF at $5^{\circ}\text{C min}^{-1}$ and higher heating rates tends to reduce as the number of pseudocomponents increases.

Table 4-2: Kinetic parameters for single fuels based obtained from nth order model fitting based on multiple heating rate data (5, 10, 20, 30, 40 and 50°C min⁻¹)

pseudocomponents	BG				CC				Coal										
	1st order				nth order				1st order				nth order						
	1	3	4		1	3	4		1	3	4	5	1	3	4	5			
E₁ (kJ/mol)	116.4	211.4	212.1	197.0	212.4	212.4	215.8	172.3	214.9	214.8	44.7	190.8	190.8	190.8	189.9	91.8	251.8	232.4	234.5
A₁ (min⁻¹)	5.5E+09	3.0E+17	3.6E+17	8.5E+16	3.6E+17	3.6E+17	7.2E+18	5.5E+09	7.2E+18	7.2E+18	2.5E+02	4.2E+13	4.2E+13	4.2E+13	4.2E+13	1.0E+06	2.2E+18	7.1E+16	4.6E+18
n₁	1.0	1.0	1.0	3.5	1.0	1.0	1.0	1.0	1.3	1.2	1.0	1.0	1.0	1.0	1.0	2.9	4.4	4.4	6.0
V₁	-	0.46	0.46	-	0.45	0.45	0.32	-	0.40	0.41	-	0.56	0.56	0.56	0.51	-	0.42	0.47	0.05
E₂ (kJ/mol)	-	108.3	169.6	-	187.6	188.4	188.9	-	188.5	189.7	-	102.4	102.9	105.5	105.5	-	146.7	148.6	233.6
A₂ (min⁻¹)	-	5.5E+09	1.5E+15	-	8.5E+16	8.5E+16	2.6E+17	-	2.6E+17	3.5E+17	-	1.8E+06	1.8E+06	1.8E+06	1.8E+06	-	1.5E+09	2.8E+09	7.1E+16
n₂	-	1.0	1.0	-	1.4	1.3	1.0	-	1.0	1.0	-	1.0	1.0	1.0	1.0	-	3.9	2.6	4.1
V₂	-	0.37	0.26	-	0.23	0.20	0.27	-	0.24	0.23	-	0.11	0.12	0.07	0.07	-	0.50	0.32	0.45
E₃ (kJ/mol)	-	50.3	48.6	-	94.3	44.2	37.6	-	98.9	98.9	-	65.2	65.3	65.7	65.7	-	377.2	223.4	149.6
A₃ (min⁻¹)	-	3.3E+03	3.3E+03	-	3.3E+08	3.3E+03	1.2E+03	-	2.2E+09	2.2E+09	-	1.3E+03	1.3E+03	1.3E+03	1.3E+03	-	2.5E+20	5.1E+12	2.8E+09
n₃	-	1.0	1.0	-	4.2	2.3	1.0	-	4.6	4.7	-	1.0	1.0	1.0	1.0	-	2.8	2.6	2.1
V₃	-	0.17	0.23	-	0.32	0.17	0.28	-	0.36	0.36	-	0.44	0.28	0.04	0.04	-	0.10	0.11	0.27
E₄ (kJ/mol)	-	-	185.8	-	-	188.9	40.1	-	-	188.7	-	-	225.1	221.1	221.1	-	-	360.2	224.7
A₄ (min⁻¹)	-	-	3.5E+17	-	-	3.5E+17	7.1E+02	-	-	2.6E+17	-	-	6.9E+11	6.9E+11	6.9E+11	-	-	1.3E+19	5.1E+12
n₄	-	-	1.0	-	-	5.2	1.0	-	-	1.0	-	-	1.0	1.0	1.0	-	-	2.9	2.8
V₄	-	-	0.06	-	-	0.18	0.12	-	-	0.02	-	-	0.02	0.18	0.18	-	-	0.10	0.14
E₅ (kJ/mol)	-	-	-	-	-	-	-	-	-	-	-	-	-	201.1	201.1	-	-	-	360.2
A₅ (min⁻¹)	-	-	-	-	-	-	-	-	-	-	-	-	-	5.1E+12	5.1E+12	-	-	-	1.3E+19
n₅	-	-	-	-	-	-	-	-	-	-	-	-	-	1.0	1.0	-	-	-	2.9
V₅	-	-	-	-	-	-	-	-	-	-	-	-	-	0.20	0.20	-	-	-	0.10

Table 4-3: Quality of fit or percentage deviation for simulated curves based on assumption of various numbers of pseudocomponents

Number of pseudocomponents	BG				CC				Coal												
	1st order		nth order		1st order		nth order		1st order												
	1	3	4		1	3	4		1	3	4	5	1	3	4	5					
5°C min ⁻¹	15.8	7.2	6.3	1.3	1.0	1.0	1.0	15.8	7.2	6.9	11.3	8.5	8.2	10.2	16.0	15.1	7.1	26.7	6.1	5.1	4.4
10°C min ⁻¹	13.4	6.3	3.3	2.6	1.1	1.0	1.0	13.4	5.0	4.8	10.5	5.0	5.0	9.7	13.1	12.4	6.9	21.3	4.7	5.3	4.2
20°C min ⁻¹	9.7	3.0	3.5	4.5	0.9	0.9	0.9	9.7	2.3	3.9	11.2	3.6	3.0	8.0	7.0	6.6	4.2	13.6	4.2	3.8	2.6
30°C min ⁻¹	8.3	1.7	2.6	6.0	0.6	0.5	0.5	8.3	1.8	2.1	9.7	2.5	1.7	8.1	4.4	4.3	4.4	10.1	7.8	4.9	4.8
40°C min ⁻¹	7.8	1.4	2.6	7.6	1.2	1.2	1.2	7.8	2.0	1.4	8.9	2.7	1.8	6.7	2.4	2.3	1.9	9.5	4.8	2.7	1.2
50°C min ⁻¹	8.4	2.1	1.7	9.2	0.7	0.6	0.6	8.4	1.4	2.1	7.8	2.5	2.1	7.2	3.1	2.9	2.1	9.7	4.6	2.8	1.6
Global*	5.3	1.5	1.2	5.8	0.9	0.9	0.9	4.5	1.5	1.3	5.3	0.9	0.9	4.7	3.0	2.7	2.5	6.7	2.2	1.8	1.5
150°C min ⁻¹	12.5	7.6	6.5	10.5	5.0	3.5	3.5	11.3	6.0	5.0	4.4	3.2	3.2	20.0	12.3	10.9	9.5	22.3	6.5	5.2	5.0

*Global refers to the combined QOF for all heating rates

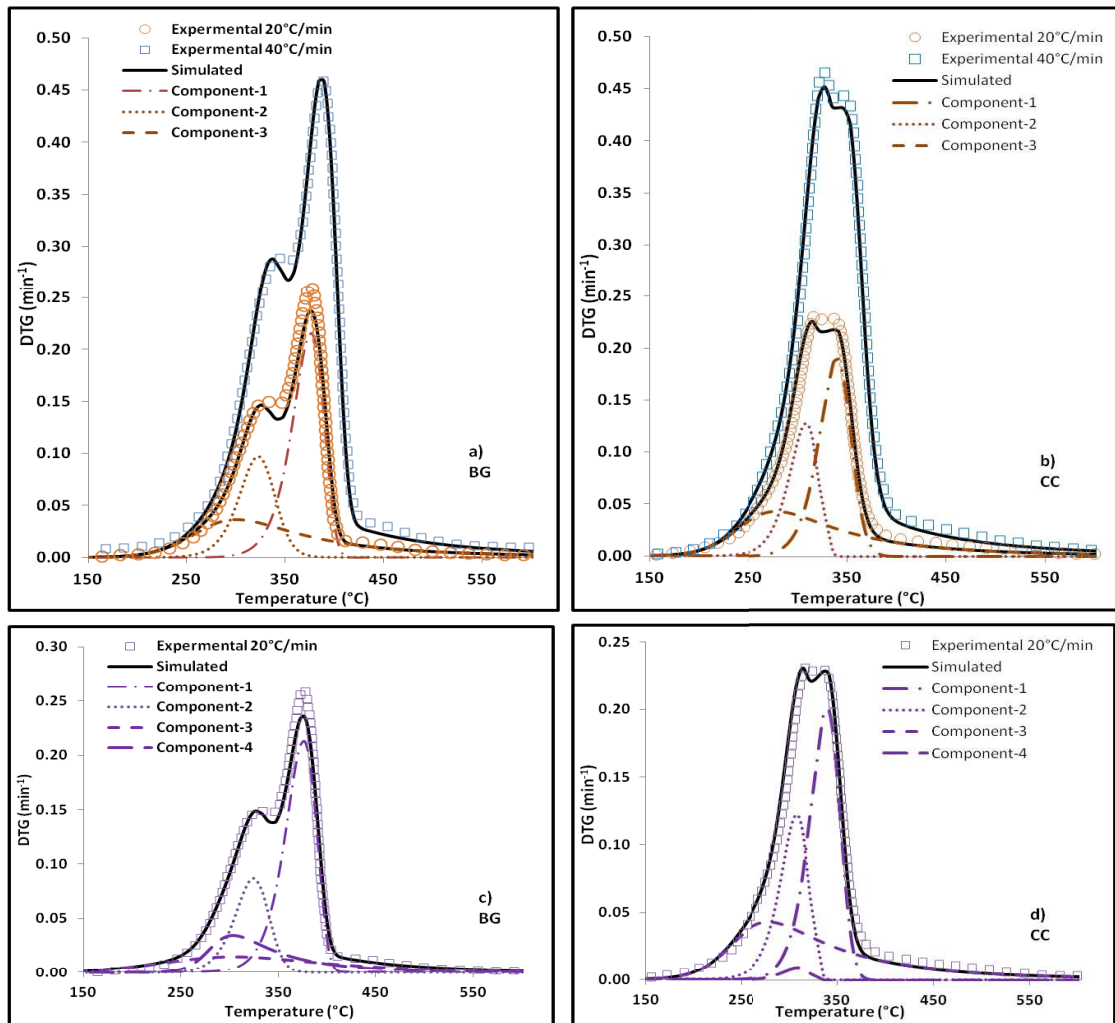


Figure 4-2: Simulated reaction rate curves for BG and CC based on nth order model for 3- pseudocomponent (plots a and b) and 4-pseudocomponent (plots c and d) fitting.

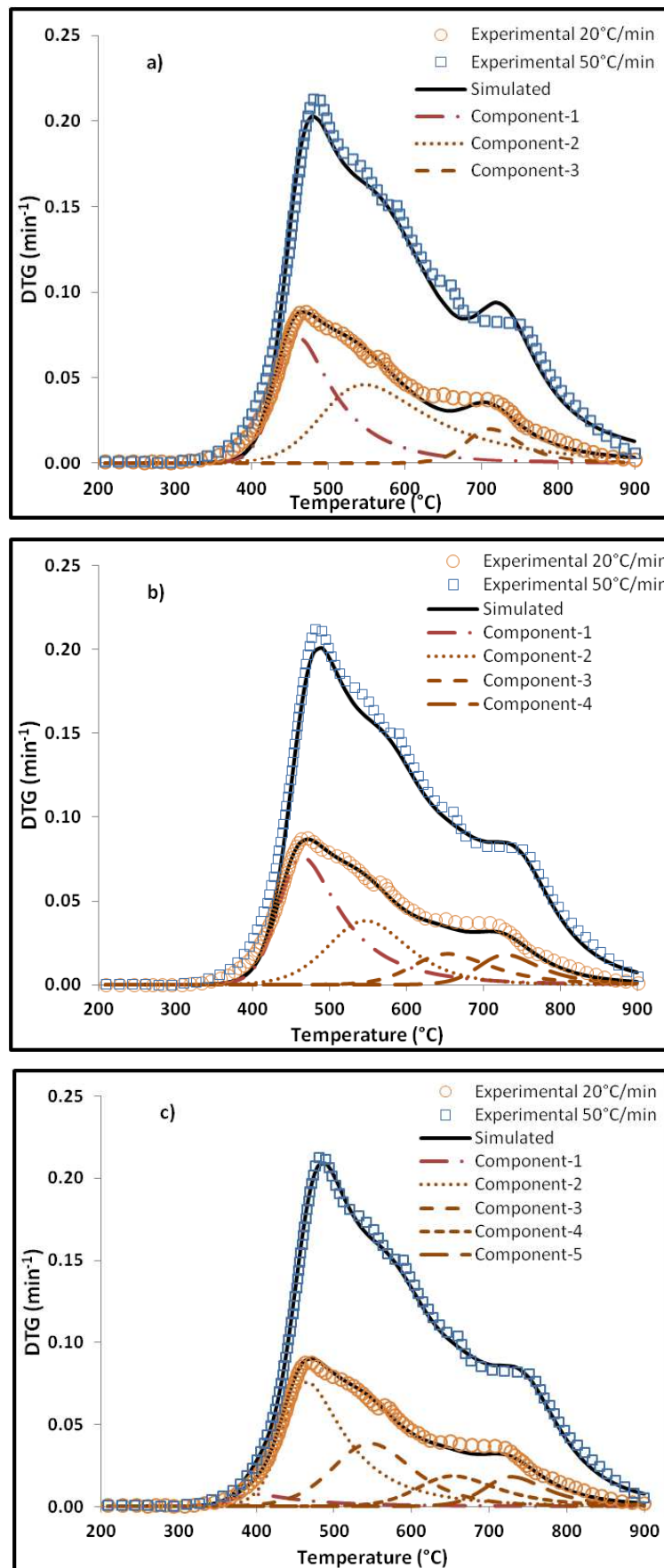


Figure 4-3: Simulated reaction rate curves for coal obtained from 3 (a), 4 (b) 5 (c) pseudocomponent fitting

In order to assess the effect of changes in the fitted kinetics parameters on the quality of fit of simulated curves, a sensitivity analysis was conducted for the 3-component, n th order modelling as shown in Table 5-4. Each parameter E_i , A_i , n_i was changed by $\pm 25\%$ and $\pm 50\%$ from its optimized value (Table 5-1), and the sensitivity was calculated as;

$$S = \left| \frac{\% \text{ change in global QOF}}{\% \text{ change in the specific parameter}} \right|$$

Table 5-4 shows that apparent E_i was the most sensitive parameter, whilst reaction order was the least sensitive. This was in agreement with results from Kuofopanos et al [54]. This also corresponds to observations by Vyazovkin on the relative importance of apparent activation energy in the interpretation of thermal kinetics.

Table 4-4: Sensitivity analysis for parameters obtained from 3-component n th order modelling

<u>% change in E_i</u>	S		
	BG	CC	Coal
50%	34.49	62.44	64.78
25%	65.67	119.98	119.40
-25%	70.94	124.80	102.97
-50%	33.93	59.81	64.08
<u>% change in A_i</u>			
50%	8.58	10.59	4.26
25%	8.56	10.14	3.05
-25%	10.82	13.86	5.23
-50%	13.41	18.32	9.26
<u>% change in n_i</u>			
50%	4.16	7.07	8.63
25%	4.17	7.01	7.76
-25%	3.67	5.21	9.35
-50%	1.84	2.60	17.25

In all samples and for all values of i , it was clear that n^{th} order modelling produced simulations with better fits than 1^{st} order models. This would suggest therefore that the former is a more reliable representation of the pyrolysis behaviour of these materials. However, n^{th} order fitting (for $i > 1$) of biomass still yielded reaction order

values close to 1 for components-1 and -2, which represents the bulk total conversion (Table 5-2). This suggests on the one hand that the 1st order model used in many biomass studies [9–11] is indeed not an unreasonable approximation of the devolatilization kinetics of biomass fuels. On the other hand, it highlights the utility of the nth order model in determining unknown reaction orders.

Table 5-2 further shows that a similar range of kinetic parameters and reaction orders were found for both BG and CC suggesting that both materials exhibit similar devolatilization behaviour. The 3 pseudocomponent model is consistent with the theory that biomass decomposition behaviour approximates to a combination of the decomposition trends of its three major lignocellulosic components namely, cellulose, hemicellulose and lignin [9–11]. Fig. 5-2 shows the simulated reaction rates for the various pseudocomponent fractions of BG and CC resulting from nth order modelling. For BG, component-1 reacted mainly between 300 and 400°C, as indicated by the location of the peak shoulders (Fig. 5-2a) and can be attributed to cellulose which is known to decompose within that temperature range [39]. Component-2 started to decompose at a lower temperature but over a slightly wider range (220-360°C) and for similar reasons as component-1, can be attributed to hemicellulose and extractives decomposition [39,40]. As Fig. 5-2 also shows, the peaks attributed to cellulose and hemicellulose overlapped to a greater degree for CC than for BG. Kinetic parameters obtained from 1st and nth order analysis for the first two components (corresponding to cellulose and hemicellulose) were consistent with values found in previous reports for these components; activation energy for cellulose pyrolysis is generally reported as falling between 192 and 250 kJ mol⁻¹ and for hemicellulose it is in the 154–200 kJ mol⁻¹ range [9,41]. There are a number of other studies on the pyrolysis kinetics of pure cellulose and hemicellulose that confirm these values [32,42,43] even though it is recognized that the processes involved in separating these substances might alter their structure and thermal behaviour.

The third component in both BG and CC decomposed throughout the pyrolysis temperature range (200-500°C) and is customarily attributed in part to lignin, which exhibits a similar behaviour [44,45]. Activation energies calculated from 1st order modelling was 51 and 43 kJ mol⁻¹ for BG and CC, respectively, which are consistent with often quoted activation energies for pure lignin devolatilization in previous reports similarly based on 1st order models (18-65 kJ mol⁻¹ [9,41]). However, higher *E* values (95 and 100 kJ mol⁻¹ for BG and CC, respectively) and reaction orders (2.4 and 4.5 for BG and CC) were obtained from the more accurate nth order modelling. The reaction order is a partial reflection of the width of the reaction rate curve [14], therefore the relatively high reaction orders obtained for component-3 is consistent with the much wider spread of its peak (Fig. 5-2). The fractional contribution of component-3 to total conversion (γ_3), was 32% and 36% for BG and CC, respectively, which was significantly higher than the determined lignin content for both materials shown in Table 5-1 (22.4% and 16.7%, respectively). Therefore, it is likely that component-3 represents a combination of lignin and some of the hemicellulose that was not already accounted for in component-2 as previously observed by Branca et al. [9] and Caballero et al. [42]. It can also be envisaged that 3rd component also included the decomposition of extractives and other compounds which as Table 5-1 shows account for about 10% of both CC and BG [40]. On the other hand, it is equally possible that component-3 is a reflection of a combination of lignin and some of the cellulose as noted by Cordero et al. [46] and Worasuwanarak et al. [47]. The result suggests that this method of analysis is not particularly suitable for determining lignocellulosic composition of biomass, in contrast to the observations by Garcia-Perez et al. [40]. A similar comparison of the contributions of component 1 and 2, to the measured cellulose and hemicelluloses composition shown in Table 5-1 further emphasizes this point. The respective percentage contributions of component-1 and component-2 to the global devolatilization rate curve for BG is 45% and 23%, while for CC it is 40% and 24%. However, Table 5-1 shows cellulose and hemicelluloses composition for BG as 44.2 and 24%, and for CC as 36% and 38%, respectively. This shows that while the BG composition for cellulose is well represented by the kinetic analysis results for component-1, there is significant disparity between the measured

compositional values and the kinetically derived contributions of the other pseudocomponents. This further suggests that for CC, component-3 could be made up of a combination of parts of the cellulose and hemicelluloses fraction of the sample, whereas for BG cellulose can be ruled out as a contributor to component-3. It is more difficult to compare pre-exponential factor (A) values as even the slightest changes cause variations typically up to 10 orders of magnitude. Hu et al. [13] reported A values corresponding to the cellulosic and hemicellulosic pseudocomponents as ranging between 4.2×10^{11} - 5.0×10^{21} and 4.86×10^8 - 2.1×10^{18} , respectively. While the corresponding values obtained for CC and BG in this study both lie within this range (Table 5-2), it has been argued that the variation inherent in A values are too large for any meaningful analysis, leading to recommendations that interpretative efforts should be focused on the value of E as it is more 'stable' [5].

Similar to biomass, coal decomposition rates could also be satisfactorily described by assuming 3 pseudocomponents, in accordance with the model by Alonso et al. [15], based on the description of coal pyrolysis mechanisms by van Heek and Hodek [48]. It was observed that the three pseudocomponents could be ascribed to macromolecular reaction steps that occurred between 400-450°C, 500-550°C, and at approximately 700°C. The first two steps corresponded to the release of tars and gases, while the third was attributed to the completion of the structural breakdown of the coal sample, coupled with char formation and the release of methane and carbon monoxide [15]. Simulations derived from 3 pseudocomponent fitting in the present study were consistent with these coal pyrolysis mechanisms, since the aforementioned temperature ranges corresponded to the position of the peaks of the simulated coal fractions shown in Fig. 5-3. Activation energy values calculated via the 1st order model for coal ranged from approximately 65 to 225 kJ mol^{-1} , which was more or less in the same range of activation energies obtained for the biomass fuels using the same 1st order model (Table 5-2). This result was contrary to the view that biomass is a significantly more reactive fuel than coal, due to denser and more heat resistant structure of the latter [17]. Biomass macromolecules are linked

together by relatively weak R-O-R bonds with energies in the 380-420 kJ mol⁻¹ range, in contrast to coal where bond energies are as high as 1000 kJ mol⁻¹ [49]. Besides, the coal used in this study is mainly composed of primarily inertinite macerals which are known to be one of the least reactive types of coal [15]. In theory, therefore, it should be expected that the activation energy values for coal should be higher than biomass. Activation energy is known to be linearly correlated to the pre-exponential factor via the artificial isokinetic relationship [15] such that high E values generally corresponded to relatively high A values for both coal and biomass (Table 5-2).

Compared to 1st order results, a significantly higher range for E was obtained from n^{th} order modeling (150-380 kJ mol⁻¹), along with higher reaction orders ranging from 2.8-4.4 for the 3 pseudocomponents of coal (Table 5-2). These range of E values are more consistent with results from previous studies obtained via DAEM and n^{th} order techniques [14,50] and can be considered more reliable than the 1st order assumption. This view is further corroborated by the observation that n^{th} order fitting yielded simulations with better quality of fit than 1st order (Table 5-3). The disparity between the 1st order and n^{th} order E results was likely due to a previous observation by Burnham and Braun [14] that when reactions mechanism with orders greater than 1 that are force fitted to 1st order kinetic model, there is a tendency to obtain activation energy values lower than the true mean value. As Table 5-2 shows, unrealistically high reaction orders are frequently obtained during n^{th} order fitting for both coal [14] and biomass fuels [12,13] which limits the physical significance of the results. However, as observed by Vyazovkin [26] and White [11], the Arrhenius based kinetic evaluation of complex heterogenous solid state processes (such as coal and biomass pyrolysis) are of limited theoretical relevance to start with. The main purpose in the global kinetic analysis of pyrolysis lies in its practical use in the design of reactors [7,26].

The kinetic results obtained via model fitting could be compared with those obtained via isoconversional methods applied to the same dataset [21], within the limitations and differences of the two approaches; model fitting methods yielded a single

activation energy value for the whole conversion process for the sample or its pseudocomponents, while the isoconversional method has a functional dependence of E_α on conversion [51,38]. Nevertheless, the activation energies obtained by n^{th} order model-fitting compared favourably to those obtained from isoconversional analysis, which yielded slightly lower average apparent E values of 174 kJ mol^{-1} for BG compared to 184 kJ mol^{-1} for CC, in the 0.2-0.8 conversion range [21]. Similarly, as Table 5-2 shows, the values of E derived from model fitting for BG ($95\text{-}210 \text{ kJ mol}^{-1}$) was lower than for CC ($100\text{-}216 \text{ kJ mol}^{-1}$) based on both 1 and 3-pseudocomponent models. In a similar manner, the E values for coal derived via both model-free and model fitting methods was higher than for the biomass fuels. Both methods show reasonable fit qualities, although the QOF values obtained by the model-free were slightly better (<2%) than the model fitting methods whose fits ranged from 1-6% for heating rates between 5 and $50^\circ\text{C min}^{-1}$. The same trend was observed when predicting reaction rates at heating conditions outside the range used in the kinetic analysis. The global QOFs for the n^{th} order predictions at 150°C (based on the 3 pseudocomponent assumptions) were 5%, 3.3%, and 5.7% for BG, CC and coal respectively. Model-free analysis for the same samples gave slightly better fits at 4.6, 3.3 and 2.8%, respectively.

4.3.2 Blends

Fig. 5-4 shows the TG/DTG curves of coal-BG and coal-CC blends at various mix ratios obtained at a heating rate of $50^\circ\text{C min}^{-1}$. At all mix ratios, peaks corresponding to biomass and coal fractions of the blended fuels maintained essentially the same shape and position on the temperature axis as was observed during individual pyrolysis. This is consistent with observations by Bonelli et al. [52], Idris et al. [53] and Ulloa et al. [20] based different types of coals and biomasses. However, blending affected the peak height or maximum reaction rate of the section of the curves corresponding to both coal and biomass; increasing the biomass fraction in the blend caused an increase in the maximum devolatilization rate of the peaks representing coal, while reducing the maximum devolatilization rates of peaks corresponding to biomass. Further description of the TG and DTG curves for the coal-BG and coal-CC blends can be found in Section 4.3.1.2.

The kinetic analysis of blends was approached in two ways. The first was to subject the blends to the same type of model fitting analysis as the individual fuels, based on n^{th} order parallel reactions. In this manner, reasonable fits could be achieved by assuming 6 pseudocomponents ($i=6$), corresponding to 3 parallel reactions each for coal and biomass fraction of the blends. Parameters obtained for the individual pyrolysis of coal and biomasses (Table 5-2) were used as initial estimates for the optimization procedure. During fitting, a linear constraint was applied to ensure that the relative mass contributions of the pseudocomponents corresponding to biomass fraction in the blends (γ_1 to γ_3) was not less than the calculated contribution of biomass to volatile yield, based on weighted averages. For coal-BG blends, the fractional contribution of biomass to the volatile yields at 90:10, 80:20 and 60:40 sample mix ratio was thus 0.33, 0.53 and 0.75 respectively, while for coal-CC it was estimated as 0.32, 0.52 and 0.74, respectively.

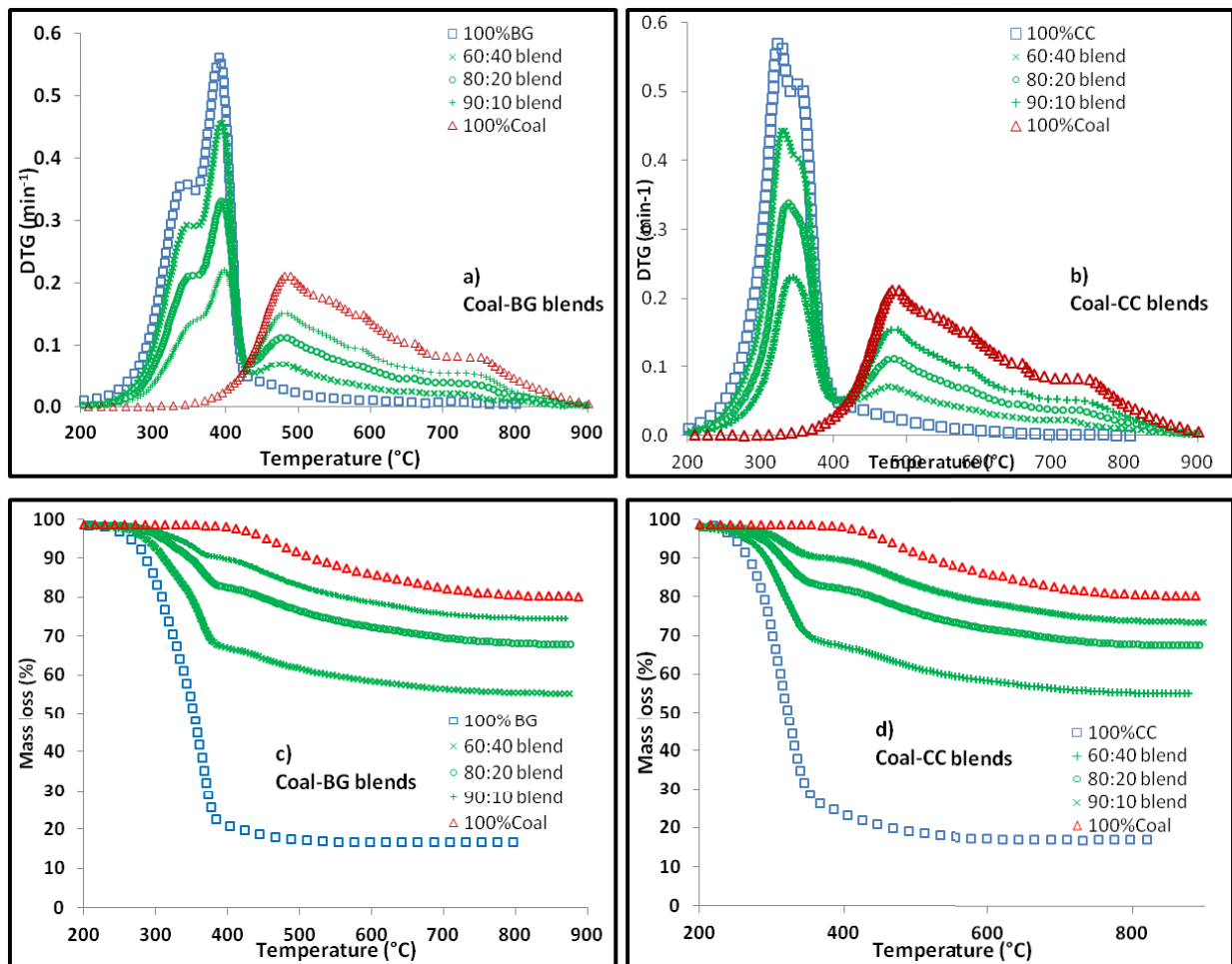


Figure 4-4: DTG and TG curves of various mix ratios of Coal-BG and Coal-CC blends obtained at 50°C min⁻¹

The kinetic parameters thus obtained are shown in Table 5-5 for the coal-biomass blends at 90:10, 80:20 and 60:40 mix ratios, while the QOFs between simulated and experimental curves are shown in Table 5-5. Fig. 5-5 shows the plots of the simulated and experimental reaction rate curves (at 90:10 mix ratio) based on the kinetic data presented. Compared to the results of the individual pyrolysis (Table 5-2), apparent activation energy values for the pseudocomponents ascribed to cellulose, hemicelluloses, and lignin (component-1, -2, and -3) differed only slightly at 207-209, 183-189 and 101-105 kJ mol⁻¹ respectively for BG and 210-216, 189-191, and 103-106 kJ mol⁻¹ for CC. There was no clear correlation between mix ratio and the deviation between these parameters from those observed for the contribution of the single fuels. The same trend could be observed for the other kinetic parameters, i.e. reaction order and pre-exponential factor.

Table 4-5: Kinetic parameters obtained from 6-pseudocomponent, nth order model fitting of coal biomass blends based on multiple heating rate DTG data (5, 10 and 50°C min⁻¹). Given wt% represents percentage of biomass in the blends

	Coal-BG			Coal-CC		
	10wt%	20wt%	40wt%	10wt%	20wt%	40wt%
E₁ (kJ mol⁻¹)	209.4	209.6	207.5	215.5	212.8	210.3
A₁ (min⁻¹)	1.4E+17	1.7E+17	1.2E+17	4.4E+18	2.5E+18	1.6E+18
n₁	1.0	1.0	1.0	1.0	1.0	1.0
γ₁	0.15	0.24	0.34	0.05	0.06	0.13
E₂ (kJ mol⁻¹)	191.3	184.6	182.9	189.2	189.8	191.2
A₂ (min⁻¹)	1.1E+17	3.4E+16	2.7E+16	9.8E+16	1.2E+17	2.3E+17
n₂	1.3	1.2	1.2	1.2	2.1	2.1
γ₂	0.05	0.09	0.12	0.10	0.34	0.41
E₃ (kJ mol⁻¹)	101.8	101.1	104.8	105.6	102.7	102.8
A₃ (min⁻¹)	5.4E+08	6.1E+08	1.8E+09	2.0E+09	4.5E+09	3.9E+09
n₃	3.3	3.4	2.6	2.0	4.9	5.8
γ₃	0.21	0.27	0.31	0.21	0.16	0.27
E₄ (kJ mol⁻¹)	256.1	255.4	260.8	253.1	255.4	253.0
A₄ (min⁻¹)	3.1E+18	2.7E+18	7.1E+18	2.2E+18	3.3E+18	2.6E+18
n₄	5.4	5.3	5.3	5.6	5.8	4.3
γ₄	0.35	0.23	0.14	0.39	0.28	0.11
E₅ (kJ mol⁻¹)	154.2	152.7	157.0	153.9	161.6	165.1
A₅ (min⁻¹)	3.3E+09	2.7E+09	5.9E+09	3.8E+09	9.9E+09	3.0E+10
n₅	2.9	2.8	2.8	3.0	3.1	2.2
γ₅	0.18	0.12	0.06	0.19	0.11	0.06
E₆ (kJ mol⁻¹)	417.3	404.8	390.5	416.8	423.4	390.2
A₆ (min⁻¹)	3.0E+22	9.3E+21	2.8E+21	2.7E+22	7.5E+22	3.7E+21
n₆	2.8	3.3	3.8	3.1	3.2	3.9
γ₆	0.07	0.05	0.03	0.06	0.04	0.03

The most significant deviation between the behaviour of these pseudocomponents in single fuel pyrolysis and blend co-pyrolysis was observed for the 3rd coal component. Apparent activation energies for the group of reactions represented by this pseudocomponent increased in a similar way for both coal-BG and coal-CC blends from 377 kJ mol⁻¹ to between 390-417 kJ mol⁻¹. According to Alonso et al. [15] this component corresponded to secondary char, methane and carbon monoxide formation. Table 5-5 also reveals higher total γ values for the biomass fraction of the blends (0.41, 0.65 and 0.84 for coal-BG blends; 0.45, 0.62, and 0.81 for coal-CC blends), compared to the fractional contributions calculated based on a

weighted average of coal and biomass volatile yields. The foregoing suggests non-additive or synergistic behaviour between the coal and biomass fractions of the blend. This is in contrast to conclusions by some previous authors [17,18,53], but in agreement with results by some others [19,20].

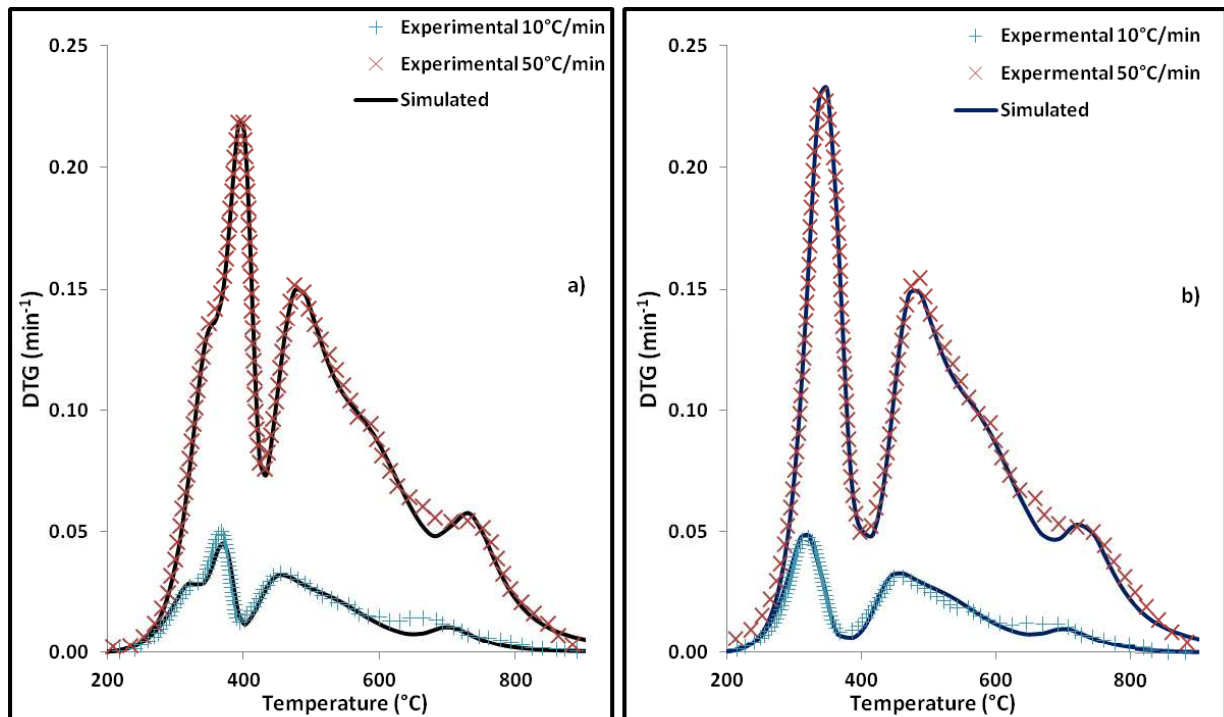


Figure 4-5: Simulated DTG curves of coal-BG (a) and coal-CC (b) blends based on 6 pseudocomponent model fitting for 90:10 coal-biomass mix ratio

Table 4-6: Quality of fit values for simulated DTG curves of blends obtained via nth order model fitting

Heating rate (°C min ⁻¹)	Coal-BG			Coal-CC		
	10wt%	20wt%	40wt%	10wt%	20wt%	40wt%
5	7.0	5.4	5.3	5.6	6.1	5.5
10	6.5	3.2	4.3	4.2	4.4	4.1
50	1.2	0.8	1.1	1.6	1.2	1.7
Global	1.3	1.3	1.8	1.1	0.9	1.1

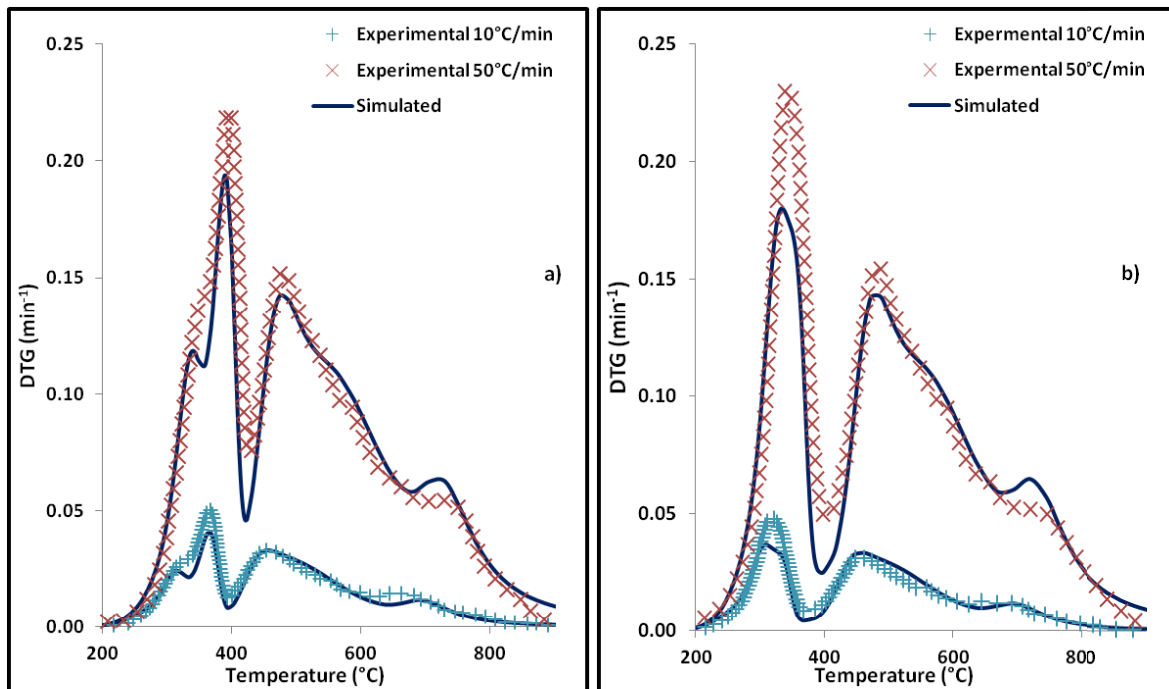


Figure 4-6: Simulated DTG curves for Coal-BG (a) and Coal-CC (b) blends based on kinetic parameters obtained from pyrolysis of individual fuels for 90:10 coal-biomass mix ratio

Table 4-7: Quality of fit values for DTG predictions recreated from simulated coal and biomass curves

Heating rate (°C min ⁻¹)	Coal-BG			Coal-CC		
	10wt%	20wt%	40wt%	10wt%	20wt%	40wt%
5	9.2	10.4	10.4	8.9	5.4	4.4
10	9.7	7.8	8.4	8.5	6.0	4.1
50	14.0	11.8	9.2	11.9	9.5	6.6
Global	8.2	6.9	5.5	6.9	5.5	3.9

The second approach to performing kinetic analysis of the blends was based on employing the kinetic parameters derived for the individual samples (Table 5-2). These were used to predict conversion progress for coal and biomass components of the blends. The simulated curves were then added together taking into account the relative contributions to the blend mix ratio. In this way simulated curves for coal-CC and coal-BG blends for mix ratios, 90:10, 80:20 and 60:40 were obtained. The quality of fits for these simulations is shown in Table 5-7 while the plot of simulated versus experimental DTG curves at 90:10 mix ratios are presented in Fig. 5-6. Much poorer fits (8-13% for individual curves and 6-8% for global fits) were obtained by this

method than in the first approach (Table 5-6). This suggests that imposing the characteristics of the individual fuels on the blends does not give the best predictions of co-pyrolysis behaviour; therefore supporting the view that synergistic interactions do exist between the biomass and coal making up the blend. Plausible explanations for the synergistic mechanism was given in Aboyade et al. [21], based on model free analysis of the same data. The approach of supplementing model free analysis with model fitting was recommended by ICTAC [26] and helps to give confidence that the kinetic parameters obtained for pyrolysis and co-pyrolysis reactions for the materials under investigation are in fact reliable representations of the actual process taking place.

4.4 Conclusions

Single and multi-component model fitting was used to evaluate the pyrolysis kinetics of coal, corn cobs, and sugarcane bagasse, and the co-pyrolysis behaviour of mixtures of the coal and biomasses. The results showed that single component kinetics was a poor representation of the decomposition behaviour of all of the samples, regardless of whether a 1st or nth order reaction model was assumed. Conversely, reasonable approximate simulations of reaction rates could be obtained by adopting the simpler 1st order model when 3 or more parallel reactions were assumed in the biomass fuels, but less so for coal. The nth order provided simulations and predictions with better fits to the experimental data, particularly for coal where a larger deviation from 1st order behaviour was observed. Kinetic analysis of the coal blends with biomass revealed non-additive synergistic interactions as indicated by the relatively poor quality of fit achieved when the parameters of the contributing single fuels were used to predict co-pyrolysis reaction rate curves.

4.5 References

- [1] International Energy Agency, Key world energy statistics, IEA, www.iea.org/stats/index.asp, 2010.
- [2] A.W. Coats, J.P. Redfern, Kinetic parameters from thermogravimetric data. II., *Journal of Polymer Science Part B: Polymer Letters*. 3 (1965) 917-920.

- [3] E.S. Freeman, B. Carroll, The application of thermoanalytical techniques to reaction kinetics: the thermogravimetric evaluation of the kinetics of the decomposition of calcium oxalate monohydrate, *J. Phys. Chem.* 62 (1958) 394-397.
- [4] M.S. Duvvuri, S.P. Muhlenkamp, K.Z. Iqbal, J.R. Welker, Pyrolysis of natural fuels, *Journal of Fire & Flammability.* 6 (1975) 468-477.
- [5] S. Vyazovkin, Model-free kinetics, *Journal of Thermal Analysis and Calorimetry.* 83 (2006) 45-51.
- [6] A. Kemmler, M.E. Brown, M. Maciejewski, S. Vyazovkin, R. Nomen, J. Sempere, et al., Computational aspects of kinetic analysis Part A: The ICTAC kinetics project-data, methods and results, *Thermochimica Acta.* 355 (2000) 125-143.
- [7] G. Varhegyi, Aims and methods in non-isothermal reaction kinetics, *Journal of Analytical and Applied Pyrolysis.* 79 (2007) 278-288.
- [8] J.A. Caballero, J.A. Conesa, Mathematical considerations for nonisothermal kinetics in thermal decomposition, *Journal of Analytical and Applied Pyrolysis.* 73 (2005) 85-100.
- [9] C. Branca, A. Albano, C. Di Blasi, Critical evaluation of global mechanisms of wood devolatilization, *Thermochimica Acta.* 429 (2005) 133-141.
- [10] C. Di Blasi, Modeling chemical and physical processes of wood and biomass pyrolysis, *Progress in Energy and Combustion Science.* 34 (2008) 47-90.
- [11] J.E. White, W.J. Catallo, B.L. Legendre, Biomass pyrolysis kinetics: A comparative critical review with relevant agricultural residue case studies, *Journal of Analytical and Applied Pyrolysis.* 91 (2011) 1-33.
- [12] Z. Li, W. Zhao, B. Meng, C. Liu, Q. Zhu, G. Zhao, Kinetic study of corn straw pyrolysis: Comparison of two different three-pseudocomponent models, *Bioresource Technology.* 99 (2008) 7616-7622.
- [13] S. Hu, A. Jess, M. Xu, Kinetic study of Chinese biomass slow pyrolysis: Comparison of different kinetic models, *Fuel.* 86 (2007) 2778-2788.
- [14] A.K. Burnham, R.L. Braun, Global Kinetic Analysis of Complex Materials, *Energy & Fuels.* 13 (1999) 1-22.
- [15] M.J.G. Alonso, D. Alvarez, A.G. Borrego, R. Menéndez, G. Marbán, Systematic Effects of Coal Rank and Type on the Kinetics of Coal Pyrolysis, *Energy & Fuels.* 15 (2001) 413-428.
- [16] E. Biagini, F. Lippi, L. Petarca, L. Tognotti, Devolatilization rate of biomasses and coal-biomass blends: an experimental investigation, *Fuel.* 81 (2002) 1041-1050.
- [17] D. Vamvuka, N. Pasadakis, E. Kastanaki, P. Grammelis, E. Kakaras, Kinetic Modeling of Coal/Agricultural By-Product Blends, *Energy & Fuels.* 17 (2003) 549-558.
- [18] H.B. Vuthaluru, Investigations into the pyrolytic behaviour of coal/biomass blends using thermogravimetric analysis, *Bioresource Technology.* 92 (2004) 187-195.
- [19] H. Haykiri-Acma, S. Yaman, Synergy in devolatilization characteristics of lignite and hazelnut shell during co-pyrolysis, *Fuel.* 86 (2007) 373-380.
- [20] C.A. Ulloa, A.L. Gordon, X.A. García, Thermogravimetric study of interactions in the pyrolysis of blends of coal with radiata pine sawdust, *Fuel Processing Technology.* 90 (2009) 583-590.

- [21] Aboyade, J. Gorgens, M. Carrier, E.L. Meyer, J.H. Knoetze, Thermogravimetric study of the devolatilization characteristics and kinetics of coal blends with corn and sugarcane residues, *Fuel Processing Technology*. (n.d.).
- [22] J.M. Jones, M. Kubacki, K. Kubica, A.B. Ross, A. Williams, Devolatilisation characteristics of coal and biomass blends, *Journal of Analytical and Applied Pyrolysis*. 74 (2005) 502-511.
- [23] T. Sonobe, N. Worasuwannarak, S. Pipatmanomai, Synergies in co-pyrolysis of Thai lignite and corncob, *Fuel Processing Technology*. 89 (2008) 1371-1378.
- [24] D.K. Park, S.D. Kim, S.H. Lee, J.G. Lee, Co-pyrolysis characteristics of sawdust and coal blend in TGA and a fixed bed reactor, *Bioresource Technology*. Article in Press (n.d.).
- [25] L. Zhang, S. Xu, W. Zhao, S. Liu, Co-pyrolysis of biomass and coal in a free fall reactor, *Fuel*. 86 (2007) 353-359.
- [26] S. Vyazovkin, A.K. Burnham, J.M. Criado, L.A. Pérez-Maqueda, C. Popescu, N. Sbirrazzuoli, ICTAC Kinetics Committee recommendations for performing kinetic computations on thermal analysis data, *Thermochimica Acta*. 520 (2011) 1-19.
- [27] American Society for Testing Materials, ASTM D5373 - Standard Test Methods for Instrumental Determination of Carbon, Hydrogen, and Nitrogen in Laboratory Samples of Coal, 2002.
- [28] American Society for Testing Materials, ASTM D4239 - Standard Test Methods for Sulfur in the Analysis Sample of Coal and Coke Using High-Temperature Tube Furnace Combustion Methods, 2000.
- [29] British Standards Institute, Solid biofuels. Determination of calorific value, 2009.
- [30] American Society for Testing Materials, ASTM E1131 - Standard Test Method for Compositional Analysis by Thermogravimetry, 1998.
- [31] H. Yang, H. Chen, F. Ju, R. Yan, S. Zhang, Influence of Pressure on Coal Pyrolysis and Char Gasification, *Energy & Fuels*. 21 (2007) 3165-3170.
- [32] M.J. Antal, G. Varhegyi, Cellulose pyrolysis kinetics: the current state of knowledge, *Industrial and Engineering Chemistry Research*. 34 (1995) 703-717.
- [33] S. Vyazovkin, Computational aspects of kinetic analysis Part C: The ICTAC Kinetics Project—the light at the end of the tunnel?, *Thermochimica Acta*. 355 (2000) 155–163.
- [34] M.E. Brown, Introduction to thermal analysis: techniques and applications, Kluwer Academic Publishers, 2001.
- [35] Y. Fukushima, MATLAB Central - File Exchange (2005). Obtained from <http://www.mathworks.com/matlabcentral/fileexchange/7233> on 15th Sept 2011.
- [36] B. Roduit, Computational aspects of kinetic analysis Part E: The ICTAC Kinetics Project—numerical techniques and kinetics of solid state processes, *Thermochimica Acta*. 355 (2000) 171–180.
- [37] F. Shafizadeh, Introduction to pyrolysis of biomass, *Journal of Analytical and Applied Pyrolysis*. 3 (1982) 283–305.
- [38] A.O. Aboyade, T.J. Hugo, M. Carrier, E.L. Meyer, R. Stahl, J.H. Knoetze, et al., Non-isothermal kinetic analysis of the devolatilization of corn cobs and sugar cane bagasse in an inert atmosphere, *Thermochimica Acta*. 517 (2011) 81-89.

- [39] G. Varhegyi, M.J. Antal, T. Szekely, P. Szabo, Kinetics of the thermal decomposition of cellulose, hemicellulose, and sugarcane bagasse, *Energy & Fuels*. 3 (1989) 329-335.
- [40] M. Garcí'a-Pèrez, A. Chaala, J. Yang, C. Roy, Co-pyrolysis of sugarcane bagasse with petroleum residue. Part I: thermogravimetric analysis, *Fuel*. 80 (2001) 1245-1258.
- [41] M.G. Gronli, G. Varhegyi, C. Di Blasi, Thermogravimetric Analysis and Devolatilization Kinetics of Wood, *Industrial & Engineering Chemistry Research*. 41 (2002) 4201-4208.
- [42] J.A. Caballero, J.A. Conesa, R. Font, A. Marcilla, Pyrolysis kinetics of almond shells and olive stones considering their organic fractions, *Journal of Analytical and Applied Pyrolysis*. 42 (1997) 159-175.
- [43] J.A. Conesa, J. Caballero, A. Marcilla, R. Font, Analysis of different kinetic models in the dynamic pyrolysis of cellulose, *Thermochimica Acta*. 254 (1995) 175-192.
- [44] H. Haykiri-Acma, S. Yaman, S. Kucukbayrak, Comparison of the thermal reactivities of isolated lignin and holocellulose during pyrolysis, *Fuel Processing Technology*. In Press, Corrected Proof (2010).
- [45] G. Varhegyi, M.J. Antal, E. Jakab, P. Szabó, Kinetic modeling of biomass pyrolysis, *Journal of Analytical and Applied Pyrolysis*. 42 (1997) 73-87.
- [46] T. Cordero, J.M. RodrÃ-guez-Maroto, J. RodrÃ-guez-Mirasol, J.J. RodrÃ-guez, On the kinetics of thermal decomposition of wood and wood components, *Thermochimica Acta*. 164 (1990) 135-144.
- [47] N. Worasuwannarak, T. Sonobe, W. Tanthapanichakoon, Pyrolysis behaviors of rice straw, rice husk, and corncob by TG-MS technique, *Journal of Analytical and Applied Pyrolysis*. 78 (2007) 265-271.
- [48] K.H. Van Heek, W. Hodek, Structure and pyrolysis behaviour of different coals and relevant model substances, *Fuel*. 73 (1994) 886-896.
- [49] C. Meesri, B. Moghtaderi, Lack of synergetic effects in the pyrolytic characteristics of woody biomass/coal blends under low and high heating rate regimes, *Biomass and Bioenergy*. 23 (2002) 55-66.
- [50] T. Maki, A. Takatsuno, K. Miura, Analysis of Pyrolysis Reactions of Various Coals Including Argonne Premium Coals Using a New Distributed Activation Energy Model, *Energy & Fuels*. 11 (1997) 972-977.
- [51] S. Vyazovkin, C.A. Wight, Model-free and model-fitting approaches to kinetic analysis of isothermal and nonisothermal data, *Thermochimica Acta*. 340-341 (1999) 53-68.
- [52] P.R. Bonelli, E.L. Buonomo, A.L. Cukierman, Pyrolysis of Sugarcane Bagasse and Co-pyrolysis with an Argentinean Subbituminous Coal, *Energy Sources-Part A Recovery Utilization and Environmental Effects*. 29 (2007) 731-740.
- [53] S.S. Idris, N.A. Rahman, K. Ismail, A.B. Alias, Thermal behaviour and kinetics investigations of malaysian oil palm biomass, low rank coal and their blends during pyrolysis via thermogravimetric analysis (TGA), in: 25th Annual International Pittsburgh Coal Conference, PCC - Proceedings, 2008.
- [54] C.A. Koufopoulos, A. Lucchesi, G. Maschio, Kinetic modelling of the pyrolysis of biomass and biomass components, *The Canadian Journal of Chemical Engineering*. 67 (1989) 75-84.

5 Characterization of devolatilized products from the pyrolysis of coal and agricultural residues

Adapted version was submitted to Energy Conversion and Management in September 2011 using the following details:

Title: “Slow and pressurized co-pyrolysis of coal and agricultural residues”

Authors: Akinwale O. Aboyade^{a,b}, Marion Carrier^a, Edson L. Meyer^b, Johannes H Knoetze^a, Johann F. Görgens^a

^aDepartment of Process Engineering, Stellenbosch University, Stellenbosch, South Africa

^bFort Hare Institute of Technology, University of Fort Hare, Alice, South Africa

In order to obtain information about devolatilization products obtained during updraft fixed bed gasification of coal and biomass, experiments to simulate the pyrolysis conditions in Sasol’s fixed bed gasifiers were conducted on coal and biomass samples. The yield and composition of volatile pyrolysis products from coal were compared with those obtained from the biomass fuels (i.e. sugarcane bagasse, corn cobs and corn stover). Particular attention was paid to liquid phase products which were separated into aqueous and non-aqueous fractions before being chemically characterized by GC-MS.

5.1 Introduction

One of the main technological routes for the conversion of fossil fuels, to fuels and chemicals is thermochemical processing. Thermochemical processes include pyrolysis, combustion, liquefaction, and gasification. The predominant end use application for thermochemical technology is the production of chemicals, Fischer-Tropsch (FT) liquid fuels, power, and gaseous fuels in that order [1]. Much of the chemicals and FT fuels currently produced are obtained via updraft fixed bed gasification of coal feedstock [2]. The largest of such operations is the Sasol coal-to-liquids conversion plants based in Secunda and Sasolburg, South Africa [1]. The pyrolysis or devolatilization step in updraft gasification is particularly important because its products – tars, oils, and water – are released in significant quantities along with the produced gas [3,4]. These condensates are produced in the

devolatilization reaction zone of updraft gasifiers and are normally considered an unwanted by-product of gasification that has to be minimised [5-7]. In the Sasol process, they have chosen to utilize the hydrocarbon fraction of these liquids via conventional refining processes to produce commercially valuable chemicals such as naphtha, creosotes, and phenols [3,8]. Naphtha and creosotes are produced from the heavier tar fraction and phenols from the light oil fraction of the condensates [9]. Coal tars in fact currently represent one of the most important feedstock for these aromatic chemicals, particularly the multi-ring aromatics such as quinoline and thiophene which are considered high value specialty chemicals [10].

When considering the potential for biomass to be used as feedstock based on the existing coal based fixed-bed gasification processes, the devolatilization step becomes even more important as volatile matter content in biomass is known to be significantly higher than in coal. The composition of produced liquids are also known to differ, with biomass derived tars consisting of a higher fraction of oxygenates due to the higher O/C ratios compared to coal [11,12]. To evaluate the effect of substituting biomass for coal on tar quality in updraft gasification, identification and quantification of the hydrocarbons components is necessary at conditions at least similar to what obtained within the reactor. Pyrolysis in updraft gasification is believed to occur at relatively low temperatures (400-600°C) and at slow heating rates [6,13-15]. It has also been shown that tars from updraft gasification are quantitatively and qualitatively similar to tars from conventional pyrolysis [13,14]. However, as previously observed by Branca et al. [13], the literature is very limited on the chemical characterization of tars from slow pyrolysis [13,16,17], compared to fast pyrolysis processes [5,18-23]. There are even fewer studies available that investigate the composition of condensates from both biomass and coal feedstock under similar experimental conditions [5,11]. Also, few of these studies have been conducted at elevated pressures. This is noteworthy considering that it has been shown that pressure can influence the composition of volatile products during pyrolysis [24,25] and the majority of modern industrial scale thermochemical processes are operated at elevated pressures [26-29]. This lack of experimental data

from pressurized pyrolysis conditions also limits the potential for applying process models to pressurized updraft gasification [14], where as pointed out earlier, devolatilization reactions are important.

In this chapter, the yield and composition of pyrolysis products from coal were compared with those obtained from sugarcane bagasse, corn cobs and corn stover. A fixed bed batch reactor was employed for simulating the devolatilization zone in updraft gasifiers under the following operating condition; heating rate of $10^{\circ}\text{C min}^{-1}$, 26 bars pressure, and final temperature of 600°C . Particular attention was paid to liquid phase products which were separated into aqueous and non-aqueous fractions before being chemically characterized by GC-MS.

5.2 Experimental

5.2.1 Feedstock

The coal sample used was a blend of various typical South African hard coals that can be described as low grade, high ash and inertinite rich coal. The biomass types used in the study were sugarcane bagasse (BG) and corn residues separated into cobs (CC), and corn stover (CS), all obtained from farms in the Free State region of South Africa. CS was received already shredded while CC was received in whole pieces. Both types of corn residues were received already dried with moisture content less than 7%. BG was received relatively untreated with 35-40% moisture content and then air dried for 48 hours to a moisture content of approximately 10%. Representative sub-samples for experiments were obtained for all samples according to CEN/TS 14780/2005 [30]. CC was size-reduced by grinding to <20 mm for fixed-bed pyrolysis experiments, BG was milled to <2 mm and CS was used as received (Table 6-1). The overarching aim was to subject the samples to minimal pre-treatment and preparation and using size distributions that are relevant to industrial applications for each sample. The bulk density of the air dried samples was determined according to CEN/TS 15103:2005 as $80\text{-}90$ kg/m^3 , $200\text{-}220$ kg/m^3 , $100\text{-}130$ kg/m^3 , and $800\text{-}850$ kg/m^3 for BG, CC CS and coal respectively. Proximate and

ultimate analysis methods and results have already been presented in Chapter 4 (section 4.2.1).

Table 5-1: Size distribution of feedstock

Size range (mm)	BG	CC	CS	Coal
13.2-20.0		15.0		29.2
9.5-13.2		29.9		26.7
6.7-9.5		31.6		24.2
3.35-6.7		13.6		18.3
2.3-3.35		3.5	29.1	1.7
1.0-2.3	30.3	2.5	30.5	
0.5-1.0	37.3	2.2	40.4	
<0.5	32.4	1.8		

5.2.2 Pyrolysis products generation

Pyrolysis products were obtained using the fixed bed reactor set-up depicted in Fig. 6-1. The equipment is able to produce gas, condensates and char under pressurized slow pyrolysis conditions. The apparatus consists of a steel autoclave heated by surrounding heating elements to 600°C at 10°C min⁻¹ and 26 bars.

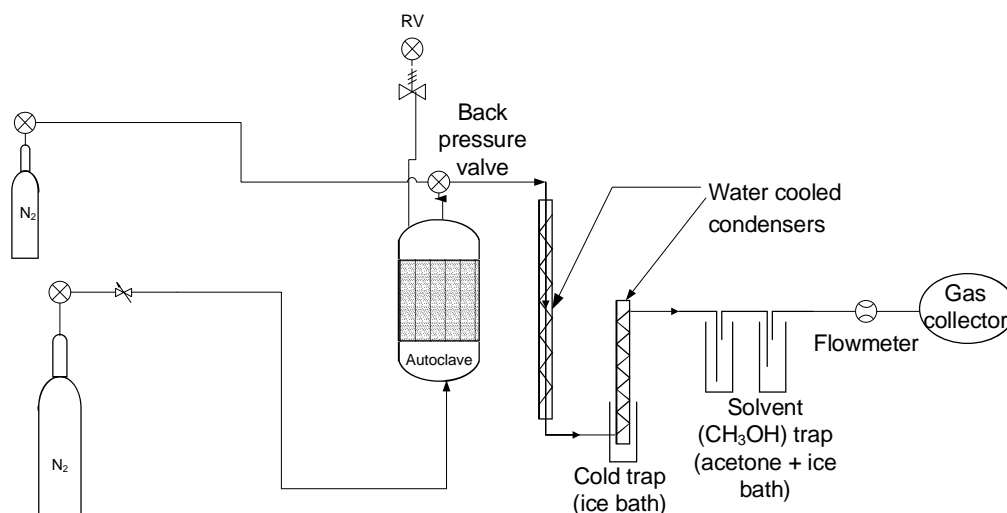


Figure 5-1: Schematic of fixed bed pyrolysis experimental setup

The pressure is controlled by the back pressure valve. Samples are loaded in the 2 L autoclave and sealed with the help of gaskets and steel bolts. The carrier gas, nitrogen flows through the reactor from the bottom at about 200 ml/min. The inert

gas flow continues for the duration of the experiment and afterwards while the reactor is allowed to cool until no further volatile effluence is observed (usually 2-4 hours). Two separate condensate traps were employed. The first cold trap collected heavier molecular liquids which condensed at 0-2.5°C in an ice bath. Lighter condensables in the form of aerosols that escaped this trap were then collected using a methanol solvent trap placed in an acetone and ice bath with temperature of -15°C. This gas-cleaning system guarantees a gas clean enough for subsequent compositional analysis. Non-condensable gas is directed into a gas bag; however, samples were also taken at selected temperature ranges during the duration of the tests by using a bypass valve. The heavy molecular weight condensates trapped in the first ice bath consisted of an aqueous and oily (water-insoluble) phase. The phases were separated according to ASTM D244 (Dean and Stark distillation) with toluene as solvent. According to this method, 100g of toluene is added to the sample in a reaction vessel to cause the separation of the aqueous phase in the sample. Upon heating toluene and water vaporises but the toluene falls back into the reaction vessel because of the difference in density (azeotropic distillation). In this way the entire aqueous fraction is separated, and then the 100g of toluene can also be recovered. The non-aqueous tar fraction is obtained by difference. All vessels and samples are weighed before and after the process to ensure a mass balance which was always achieved within 5% error. The purity of toluene recovered was verified by GC-MS to be more than 95%. The tar, aqueous phase, and condensed aerosols were analysed by GC-MS.

5.2.3 Volatile product analysis

5.2.3.1 Gas

Pyrolysis gas produced was analysed using the Agilent Technologies 6890N gas chromatograph system connected to a flame ionization detector. Dioxane was used as the external standard with hydrogen used as the carrier gas at 1.3 ml min⁻¹ flowrate. The GC was equipped with a 100 m x 0.25 mm column with film thickness of 0.5 µm. The inlet and detector temperature were kept at 225°C and 250°C,

respectively, and the maximum oven temperature was fixed at 250°C. Gases tested for were H₂, CH₄, CO, CO₂ and N₂. Gas was collected and analysed at different temperature ranges 200-300°C, 300-400°C, 400-500°C and 500-600°C.

5.2.3.2 Liquids

GC analysis was done using an Agilent 7890A Gas Chromatography system equipped with an Agilent 5973 mass spectrometer (MS). For analysis of the aqueous fraction liquids and light condensates, hydrogen was used as the carrier gas at 1.3ml/min flowrate. The GC column used was a FFAP with dimensions (50 m X 0.2mm X 0.33 µm). The oven was programmed for an initial temperature of 60°C to hold at 5 min, ramp at 6°C/min to 240°C and hold for 20 min. The injector temperature was 220°C and the split ratio was set to 100:1. The MS was equipped with ion source and interface temperature of 260°C and 29-300 scan mode. For identification of compounds in the tar phase, A PONA GC column with dimensions (50 m X 0.2 mm X 0.5 µm) was used with Helium as carrier gas flowing at 1 ml min⁻¹. The oven was set to hold for 1 min at the initial temperature of 50°C, ramp at 4°C min⁻¹ to 290°C. Inlet temperature was set at 250°C and the split ratio set to 100:1. Injector volume for both phases was 1 µl. Dioxane was used as the internal standard for all liquid fractions. Identification of compounds was done using the NIST mass spectrum library. Quantification was done based on calculated response factors for each identified component.

5.3 Results

The proximate and elemental analyses values of the samples used are presented in Table 4.1. Apart from the margins of error values shown in the table, an indication of the accuracy of these experimentally obtained elemental and HHV values is their closeness to predictions obtained from Channiwala and Parikh's [35] multivariate correlation. According to the correlation, HHV for BG, CC, CS and Coal are predicted as 17.4, 18.2, 13.4 and 17.5 MJ kg⁻¹ respectively.

The coal used in this study is a hard, low grade coal, and as such has relatively low carbon and high ash content as shown in the Table 4-1. The heating value of the coal is also lower than what generally obtained for higher coal grades, which generally tends to be higher than most biomass heating values [38].

5.3.1 Kinetic and transport dynamics

Pyrolysis behaviour is a consequence of the chemical (kinetics) and physical (heat and mass transport) processes that exist between (extra-particle) and within (intra-particle) feedstock particles [40]. During pyrolysis, evolution rates of volatiles escaping the particles surface are determined by internal transport mechanisms and intrinsic chemical reaction rates. Transport processes are strongly influenced by particle size of the feedstock [41], which in this study ranged from ≤ 2 mm for BG and CS to ≤ 20 mm for CC and coal (Table 6-1).

Table 5-2: Characteristic time-scales of major physical and chemical processes during devolatilization of wood and coal

		Characteristic time scale (s)					
		Biomass				Coal	
		L=2mm		L=20mm		L=20mm	
		T=200°C	T=600°C	T=200°C	T=600°C	T=200°C	T=600°C
Diffusion	L^2/D_{eff}	4	1.2	400	120	10	<10
Intraparticle fluid flow	$\mu L^2/PK$	10^{-3}	10^{-3}	0.1	0.1	10^{-2}	< 10^{-2}
Convective heat transfer	$Ld(\rho c)/h$	0.01	>0.01	0.1	>0.1	10	>10
Conduction heat transfer	$L^2(\rho c)/k$	4	>4	400	>200	100	>100
Devolatilization	$1/[A \exp(-E/RT)]$	10^5-10^6	10^4-10^5	10^5-10^6	10^4-10^5	10^{10}	10^{-3}

D_{eff}	effective mass diffusivity	*coal($10^{-7} \text{ m}^2 \text{ s}^{-1}$); biomass ($10^{-6} \text{ m}^2 \text{ s}^{-1}$)
μ	Viscosity	coal (10^{-5} Pa s); biomass(10^{-5} Pa s)
P	Pressure	2.6 MPa
K	Permeability	coal (10^{-15} m^2); biomass(10^{-14} m^2)
d	characteristic diameter	coal (0.1 μm); biomass(10 μm)
(ρc)	volumetric thermal capacity of the solid	coal ($4 \times 10^5 \text{ J m}^{-1} \text{ K}^{-1}$); biomass($10^3 \text{ J m}^{-1} \text{ K}^{-1}$)
h	heat transfer coefficient	coal ($10 \text{ J m}^{-2} \text{ s}^{-1} \text{ K}^{-1}$); biomass($10 \text{ J m}^{-2} \text{ s}^{-1} \text{ K}^{-1}$)
k	thermal conductivity	coal ($0.7 \text{ J m}^{-2} \text{ s}^{-1} \text{ K}^{-1}$); biomass($10^{-1} \text{ J m}^{-2} \text{ s}^{-1} \text{ K}^{-1}$)

*parameters for biomass based on values of wood obtained from Refs [42-44], while coal parameters were derived from Ref [49,50].

External heat transfer to the surface of the particle generally occurs either via the convective heat transport between the particle and the gas flow, or by radiation from the furnace walls and between particles [40,45]. Convective heat transfer coefficient for the conditions used in this study was estimated in the order of 5-30 W m⁻² using the Ranz Marshall correlation $h_{cond} = \left[2.0 + 0.6 Re^{\frac{1}{2}} Pr^{\frac{1}{3}}\right] k_f / L$ [46,47]. Obtained values for the radiative heat transfer coefficient were significantly higher at 120-130 W m⁻² using the expression $h_{rad} = \varphi \sigma 4T^3$, [40,48]. This is consistent with the practice where convective heat transfer is neglected in systems heated primarily by an external radiative flux, as opposed to heating by a hot gas injection [40,48].

The relative importance of internal and external heat transfer resistance is measured by the Biot number which for radiative systems is given by $B = (h_{rad}L/k)$. At 600°C, the Biot numbers for 20 mm coal and biomass particles were calculated as approximately 4 and 12 respectively, while for the 2 mm biomass particles it was estimated at an order of magnitude less at 1.2. This shows that intra-particle processes were much more prominent for coal and CC samples (20 mm) than for BG (2 mm).

Estimates of the relative characteristic times for intra-particle phenomena occurring within the coal and biomass feedstock are given in Table 6-2, according to differences in particle sizes and temperatures. Calculated values were based on analysis similar to that of Chan et al. [42], Moghtaderi et al. [43] and Russell et al. [49]. Heat and mass transfer parameters and their temperature and size dependencies for biomass were based on values for wood obtained from [42-44], while those for coal were obtained from [49,50]. Chemical reaction time-scales were calculated based on global reaction rate constants obtained from a previous kinetic study on the same materials by the authors [51]. At low temperatures for all particle sizes and fuels, transport processes were several orders of magnitude faster than reaction times, whereas the opposite trend was observed at high temperature (600°C). This means that transport processes were the controlling mechanism at

high temperatures. The large temperature sensitivity of devolatilization time-scales was a consequence of the Arrhenius relationship between activation energy, temperature and chemical reaction rates [52]. In contrast, changes in mass and energy transport times-scales due to increase in temperature from 200°C to 600°C were usually within one order of magnitude. Overall, mass transfer times scales increased with increase in particle size, and were slower in coal than in biomass. This is due to the difference in permeability and effective diffusivity of coal and biomass which are in turn dependent on characteristic pore sizes. Pore sizes for coal range was estimated as 0.1 μm [49,53] while in biomass values in the order of 10 μm have been reported [42].

5.3.2 Pyrolysis products distribution

Overall distribution of the lumped solid, liquid and gas phase product yields are presented in Fig. 6-2. The values shown are average of three runs and the error bars represent the standard deviations. The higher observed deviation in measured yields for CS could be attributed to the relatively higher heterogeneity of the feedstock samples.

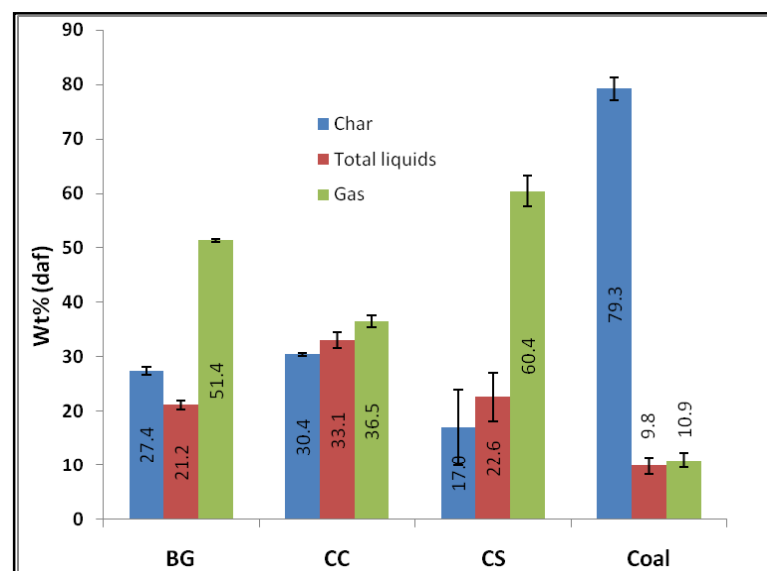


Figure 5-2: Lumped product distribution

The results shows that during fixed bed pyrolysis at 600°C and 26 bars, volatile yields (pyrolysis gas and liquids) were higher for biomass than for coal, a result that is

consistent with the earlier reported proximate characteristics for these materials. CS yielded the highest quantities of volatile products (83%) - and consequently lower char- than the other two biomasses (69.6% and 72.6% for CC and BG respectively). On the other hand, CC produced the highest condensate yield (31%). BG and CS produced significantly higher gas yields relative to the total volatiles quantities, compared to CC or coal.

When compared to results from previous work by other authors (Table A-1, Appendix A) – most of which are obtained at atmospheric pressure – the results here show that gas and char yields were generally higher with correspondingly lower liquid yields. Pressure affects pyrolysis product yields in two important ways; mass transport and secondary reactions [9]. At high pressures, primary pyrolysis reactions are suppressed due to the restricted transport of volatiles from the site of formation to surface of the fuel particle and into the bulk volatile phase. This is caused by the reduced pressure drop in the particle pores which occurs at elevated external pressures. The extended residence time of intra particle volatiles favours secondary reactions (tar cracking, char-forming) between volatiles that have already escaped leading to the increased production of lighter, more stable gas products and char at the expense of tar [66,67]. This effect has been noticed for coal [27,28,65] and biomass [25,29] in both slow and fast pyrolysis conditions [26,68]. In addition to pressure, it should also be noted that the type of reactor used, heating rate and pyrolysis temperature are also major factors that could cause the relatively low liquid and high gas yield observed. Slow heating rates and fixed bed reactor configuration tend to favour repolymerisation of volatiles leading to increased secondary char production. At fast heating rates and in vacuum, fluidized and flash pyrolysis conditions, impediments to each particle's devolatilization are lower and higher conversion generally occurs [68].

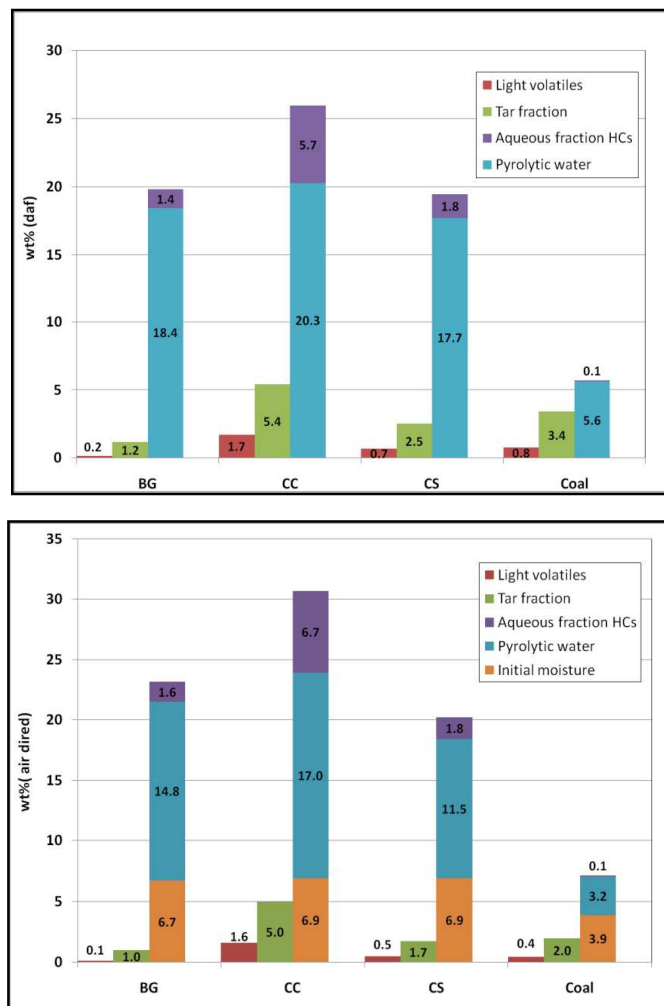


Figure 5-3: Distribution of liquid fractions on air dried and daf basis

Fig. 6-3 reports the relative distribution of the separate liquid phases on an air dried and dry and ash free (daf) basis. The columns representing the aqueous fraction have been split to show the influence of initial water content ('free' water) and/or pyrolytic (or 'bound') water. The data shows that pyrolysis liquids from all fuels are dominated by the aqueous fraction which represents about 95, 84, 88 and 73 wt% of total liquid product for BG, CC, CS and coal respectively. The figures also show that water soluble organics are produced in higher quantities from biomass than from coal, as is the case for water insoluble organics (tar and light condensates). Whilst overall liquid production was higher for biomass than for coal, yields of the tar fraction for coal was actually higher (on a daf basis) than for CS and BG.

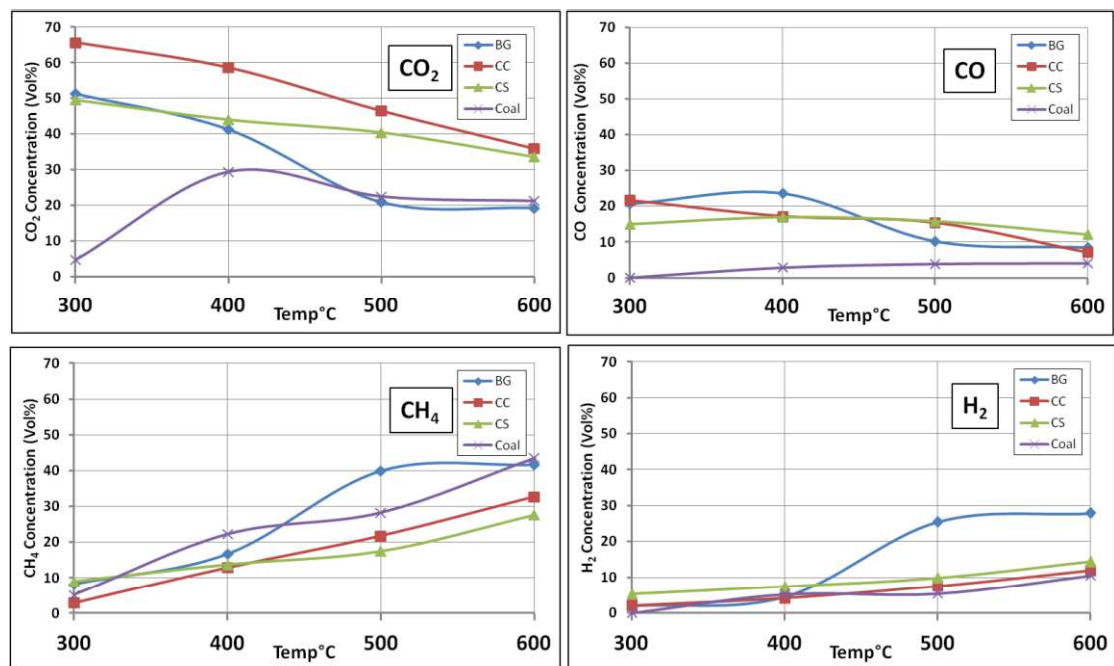


Figure 5-4: Evolution of CO, CO₂, CH₄, and H₂ yields as pyrolysis proceeds

5.3.3 Compositional analysis of volatile products

5.3.3.1 Gas

Gas samples were obtained at various temperature intervals over the duration of the experiment and analysed to provide an indication of dynamics of the gas phase component production. Fig. 6-4 reports the concentrations of CO, CO₂, CH₄ and H₂ in the gas samples as pyrolysis proceeded. In addition to CH₄, some other C₂-C₄ aliphatics are produced during pyrolysis but the quantities are small enough to be justifiably left out in this analysis, in accordance with many other literature [17,18,69,70]. It can be observed from Fig. 6-4 that the gas composition changes significantly over the temperature range under which pyrolysis occurred. For the biomasses, pyrolysis gas is composed of mainly carbon oxides at 300°C. As pyrolysis temperature increases, the concentration of CO and CO₂ falls as the quantities of CH₄ and H₂ increases. Gas release from coal pyrolysis generally follows the same trend, although the concentration of CO and CO₂ starts off from lower concentrations.

Fig. 6-5 displays the composition of gas products collected over the whole duration of pyrolysis as a fraction of the feedstock. The data shows non-hydrocarbon gas

species represented a higher fraction of total gas yields from biomass than coal. On the other hand, CH₄ represented a higher proportion of gas products from coal than is the case for biomass.

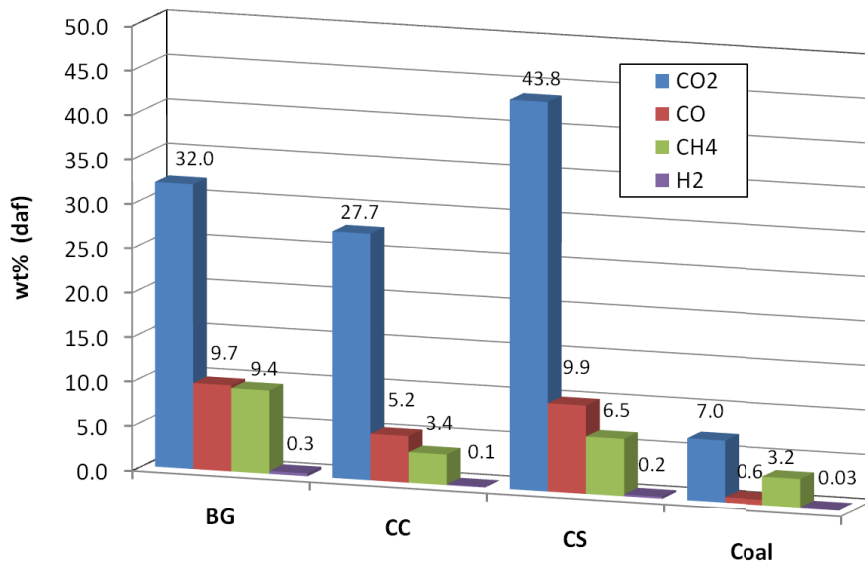


Figure 5-5: Overall yields of CO, CO₂, CH₄, and H₂ of total feedstock

5.3.3.2 Liquids

Results of the chemical characterization of pyrolysis liquid hydrocarbons (HCs) from all four feedstock can be found in Table A-2 (Appendix A). The column named NF represents compounds identified in the non-aqueous fraction – consisting the tar and condensed aerosol fraction, while the column AF refers to the aqueous fraction of condensates. The identified compounds are categorised into functional groups and the fractional distribution of these groups are graphically presented in Fig. 6-6. It should be noted that the compounds identified here represent only the volatile fraction of condensates collected, as GCMS technique cannot detect non-volatile compounds i.e. compounds with boiling points greater than 300°C [71]. The results show that volatile liquid hydrocarbons in biomass derived condensates consisted of a wider variety of chemical species mostly dominated by oxygenates such as acids (consisting mainly acetic and propanoic acid), alcohols (methanol, ethanol, 1-propanol), phenolics (phenol, cresols, and guaiacols), ketones (acetone, methyl ethyl ketone, and methyl isobutyl ketone) and furans (furfural, 2,5-dimethyl-furan, and furfuryl alcohol). PAHs (mainly naphthalene, methyl naphthalene, toluene and

anthracene) and other monocyclic aromatics such as benzene and o-xylene were also prominent, but represented a lower fraction of total HCs than was found in coal.

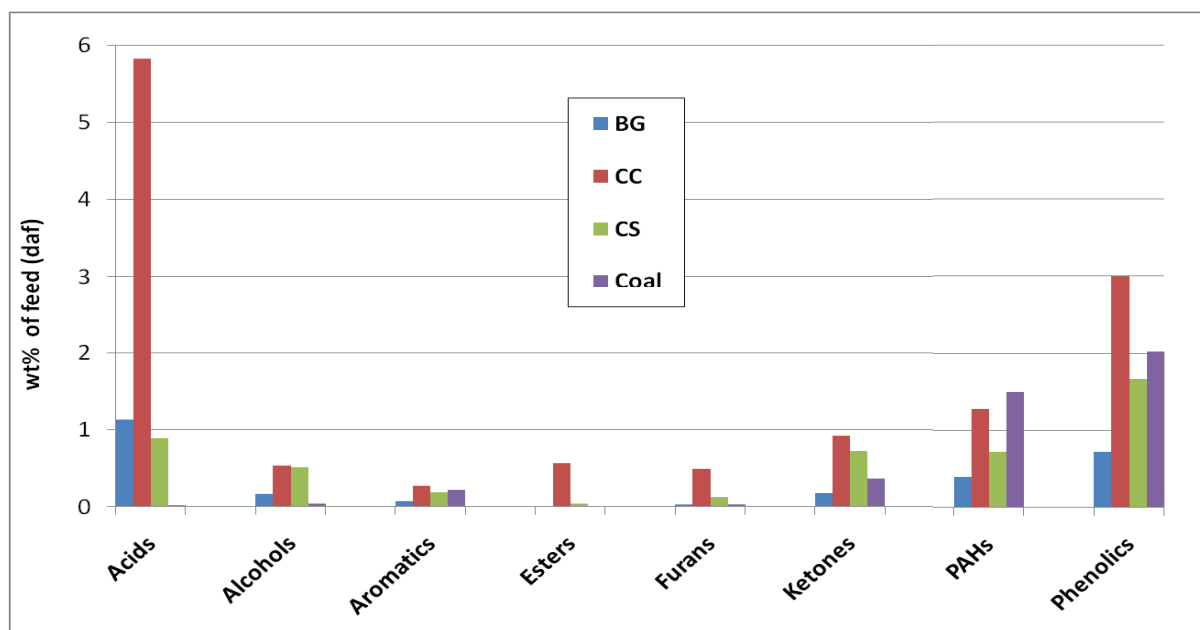


Figure 5-6: Distribution of main functional groups identified in the combined condensates

The most prominent hydrocarbons in CC condensates (as percentage of total feedstock mass) were acetic acid (5.9 wt%), naphthalene (1.1 wt%), phenol (0.85 wt%), *p*-ethyl-methyl-phenol (0.6 wt%), methanol (0.52 wt%), methyl acetate (0.51 wt%), and acetone (0.49 wt%). In BG condensates, they are acetic acid (1.05 wt%) and naphthalene (0.3 wt%). For CS condensates, they are acetic acid (0.8 wt%), naphthalene (0.62 wt%) acetone (0.52 wt%), methanol (0.49 wt%), and *m*-cresol (0.4 wt%). Carboxylic acids (mainly acetic acid) were prominent in condensates from all the biomass fuels in keeping with generally reported values for both slow [13,16,17] and fast pyrolysis conditions [18,19,21,23,72]. Interestingly, the only biomass tar composition study found that was conducted under pressurized pyrolysis conditions reported negligible acid yields from wheat straw tars obtained at 1-3 bars [73]. In general, the overall distribution of functional groups is qualitatively consistent with the observed trend reported by previous reports which all point to significant yields of carboxylic acids, ketones, alcohols, as well as lignin derived aromatics such as phenols and PAHs [13,21]. Acetic acid is known to derive from all three

lignocellulosic components of biomass, but the main contributors are cellulose and hemicellulose via a number of competing pathways including the elimination of acetyl groups within the polysaccharide structures [72,74]. The results also show significant yields of phenolics and aromatics. This is not surprising given that these substances are known to derive from the lignin fraction of biomass and the decomposition of lignin is known to be prominent during secondary reactions [75]. The pressurized conditions under which this study is undertaken and the associated long vapour residence times provide an environment that encouraged secondary reactions. One other notable difference between these results and what is generally reported in the literature based on experiments under atmospheric pressure [17,18,21], is the generally lower molecular weight (32 -202 g/mol) of compounds identified in this study. Studies in the literature (largely based on atmospheric pyrolysis conditions) tend to show prominent yields of high molecular compounds such as levoglucosan, and longer chain lignin derivatives such as dimethoxyphenols (guaicols), and catechols [76]. These compounds are known precursors to the lower molecular weight species reported here and their decomposition is due to the increased residence times caused by elevated pressure which encourages the severity of secondary vapour reactions [77].

The results also show that coal derived liquid hydrocarbons are mainly composed of PAHs and phenolics. The compounds with the highest yields are naphthalene, phenol and m-cresol representing 1.3, 0.5, and 0.47 wt% of the dry and ash free feedstock (or 30%, 11.7 and 11.2 wt% of the liquid hydrocarbons fraction only). In addition to these, heterocyclic aromatics containing nitrogen and sulphur are present in small amounts. Compared to biomass, there are fewer recent studies that quantitatively describe the composition of coal tars at either atmospheric or pressurized conditions. Qualitatively however, the findings here are in line with the reported trend in the literature [10,71,78,79].

In general for all fuels, much of the cyclic compounds including single chain aromatics, PAHs, furans and phenolics were found in the water insoluble or tarry

fraction of the condensates, while the aqueous fractions comprised most of the acids, alcohols, aldehydes, ketones and esters. More of the latter group were detected in biomass in accordance with the observed higher fraction of aqueous fraction liquids (Fig. 6-3). Table 6-3 reports some characteristics (derived from the list of compounds quantified by GCMS) of the combined liquids hydrocarbons and of the separate liquid fractions. Put together, these results show that there are also significant differences between the pyrolysis liquids composition of the biomass fuels. CC-derived liquids consisted of considerably higher variety of compounds in higher quantities than the other two biomasses. Also many more of the species detected in BG and CS condensates had very low yields (<0.5 wt%) compared to CC.

Table 5-3: Key characteristics of the combined and separate liquid phases

	BG	CC	CS	Coal
Combined Liquids				
Total liquid HCs (wt% of feedstock, daf)	2.71	13.23	4.98	4.20
% of total condensates that are HCs	12.82	39.95	21.97	42.74
wt % of oxygenates in HCs	82.75	87.44	80.94	59.04
No of total detected HCs	63	85	69	44
Pyrolytic water produced (wt%, daf)	18.43	20.26	17.70	5.62
non-Aqueous HCs				
No of compounds detected	70	90	71	43
Weighted average molecular weight (g/mol)	116.90	106.09	116.99	118.85
BP°C (weighted average)	208	184	202	207
% oxygenates	63.25	73.75	76.02	50.04
Total HC yield (wt%, daf)	1.32	7.53	3.25	4.16
Aqueous HCs				
No of compounds detected	15	27	15	10
Weighted average molecular weight (g/mol)	56.88	58.32	52.20	59.52
BP°C (weighted average)	105.09	108.31	83.83	83.13
Total HC yield (wt%, daf)	1.38	5.70	1.74	0.053

5.4 Discussions

The differences in the observed yield distribution between coal and biomass can be largely attributed to the differing structural and chemical characteristics of coal and biomass. Coal has a higher fixed carbon and carbon content than biomass (Table 4-1) which leads to higher char and lower volatile yields. Biomass comprises of hemicellulose, cellulose and lignin macromolecules linked together by relatively weak R-O-R bonds (bond energy ca. 380-420 kJ/mol) which are almost completely degraded at 600°C [66]. In contrast, coal produces comparatively less volatile yields because it comprises denser aliphatics, aromatics and polycyclic aromatic hydrocarbons (PAHs), held together by stronger C-C bonds which are more heat resistant (bond energy ca. 1000 kJ/mol)[66,80]. The higher temperatures required for producing gas species from coal as observed in Fig. 6-4 can be linked to the difference in their chemical structure. Initially, CO and CO₂ dominate the gas phase of all the fuels, produced via primary decomposition of the carbohydrates in biomass, and bond scission, depolymerization and cracking in coal. However, the higher reactivity and lower bond energy of biomass [66,67] cause the release of these gases to start at lower temperatures than for coal as shows. As pyrolysis severity increases, CO₂ concentration is progressively reduced partly via mild char gasification, while the concentration of H₂ and CH₄ increases. CH₄ is obtained via the partial saturation of alkyl free radicals with H₂, and from gas phase methanation reactions [81].

The weaker macromolecular structure of biomass and its relatively high oxygen content, which is in turn a result of the high oxygen content of the cellulose and hemicellulose building blocks, is also responsible for the larger fraction of oxygenates detected in biomass derived liquids compared to coal (50%, 75% and 10% for BG, CC and coal respectively). The weaker structure and high oxygen content of lignocellulosic biomass also yields higher quantities of reactive oxygen containing free radicals, leading to a more complex mix of products and could explain the detection of 65-85 species in biomass tars, compared to 44 in coal. Cellulose and hemicellulose are precursors to the formation of acids, esters, aldehydes, ketones,

and furans yields while lignin decomposes to forms phenol and cresol derivatives and also some of the furans [13,21]. On the other hand, the generally lower reactivity of coal led to lower liquid hydrocarbon yields, and a lesser variety of products than was obtained from biomass. Coal liquid hydrocarbons were dominated by PAH's and phenolics. A number of reaction pathways have been suggested for the production of PAHs including the decomposition of long chain aromatics within the coal structure [82] and via the Diels-Alder reaction which involves aromatization and dehydrogenation of aliphatics liberated during coal devolatilization [76,83]. PAHs can also be produced via the deoxygenation of phenols and cresols or via recombination of phenyl and other aromatic radicals [75,84,85]. Phenols are derived from the catechol isomers (o,m,p dihydroxybenzene) within the coal [86]. Catechols are also found in lignin which is responsible for the phenol and cresol derivatives produced from lignocellulosic biomass [86-88].

Comparisons between the biomass fuels lead to some notable observations that possibly highlight the significance of particle size differences between the samples. CC consists of larger woody type particles crushed to <20 mm sizes, compared to CS and BG which had straw and fibrous type constitutions and was shredded to <2 mm. As the characteristic time-scales for chemical and transport processes presented in Table 6-2 shows, particle size did not affect intrinsic devolatilization rates, but caused significant changes in mass and energy transfer time scales. Intra-particle energy transfer by convection were about one order of magnitude faster for 2 mm particles compared to 20 mm particles while conduction rates occurred at about 2 orders of magnitude faster, which means that the core of smaller particles are heated up significantly faster. For similar change in particle size, time scales of intra-particle bulk flow of volatiles increased by about 2 orders of magnitude for biomass. The faster occurrence of transport phenomena in smaller sized particle means that primary volatiles are released quicker from small particle sized fuels thereby encouraging secondary decomposition or cracking of heavier volatiles to more stable gas products and lighter volatiles [40]. In larger particles however, transport limitations will cause lower severity of secondary reactions due to increased

residence time of intra-particle volatiles resulting from higher mass and heat transfer resistances [40,41]. These processes, in addition to differences in chemical structure, may explain the higher ratio of gas to liquid yields for BG and CS (2.4 and 2.7 respectively) compared with 1.1 for CC (Fig. 6-2), and the higher tar phase yields in CC (Fig. 6-3). Secondary reactions lead to increased cracking of condensable volatiles and tars to lighter and more stable gas products [89].

The predominance of transport processes in the experimental conditions employed in this study could also explain some of the observed difference in gas species production from the feedstocks studied. Small particle size and low bed porosity aids mass and energy transfer to active sites within the devolatilizing particle and encourages secondary reactions leading to increased decomposition or cracking of heavier volatiles to gas and lighter volatiles. This may be responsible for the relatively higher total gas yields seen in the straw fuels, BG and CS, compared to the more woody and dense CC (Fig. 6-2). According to Park et al. [69], H₂ is a product of extensive secondary depolymerization of lignin derived tars. The reported lignin composition of BG (about the highest of the three biomasses as shown in Table 4-1), coupled with the straw-like nature of the feedstock and associated high bed porosity very likely explains the high H₂ concentrations observed for BG in Fig. 6-4. The relatively reduced occurrence of secondary and tertiary reactions for CC caused by its generally larger particle size, can also partly account for the significantly higher variety and quantity of organic compounds produced, compared to the other two biomasses (Fig. 6-5 and Table A-2). Increased extra-particle or vapour phase secondary and tertiary reactions cracks the primary oxygenates to more stable gaseous products leading to higher gas yields and lower liquid yields [75]. It probably accounts for the lower acetic acid yields in BG and CC as its production is known to be negatively correlated with the severity of pyrolysis conditions [21].

As further evidence of the influence of transport processes, volatile yields for CC and CS reported in this paper were compared with those obtained from thermogravimetric analysis (TGA) of the same samples where kinetic control was

maintained as heat and mass transfer effects were limited [90]. The TGA study produced dry and ash free volatile yields of 83% and 80% for CC and CS, respectively, compared to 70% and 83% derived from the present study. Compared to the ultimate volatile content of these fuels presented in Table 4-1 (84.3% for CC and 84.1% for CS), this shows that almost 100% of ultimate conversion was achieved in this study for CS, similar to the conversion levels obtained via TGA. In contrast, approximately 84% conversion was obtained for CC in this study compared to the near complete conversion obtained in the TGA. This potentially highlights the heat and mass transfer limitations imposed by larger particle sizes of CC, compared to the smaller particle sized CS, where transports effects are limited and chemical reactions are able to proceed to near completion.

5.5 Conclusions

In order to obtain information about devolatilization products obtained during updraft fixed bed gasification of coal and biomass, experiments to simulate the pyrolysis conditions in Sasol's fixed bed gasifiers were conducted. It can be concluded that differences between biomass and coal in terms of the overall distribution of char, condensates and gas phase product yields are correlated with the significantly differing proximate and chemical properties of the fuels. This is reflected in the generally higher yield, variety and oxygen content of biomass volatile products compared to coal. While the fact that coal produced higher char and lower gas and liquid products than any of the biomass considered are to be expected, there were significant differences in pyrolysis behaviour between the biomass fuels as well that merit mentioning. The dissimilarity observed between biomass fuels corresponds to the differences in their particle size and the ensuing effect on transport dynamics within the reactor. Such differences were manifested in terms of overall gas/liquid of volatile phase products and in the composition and distribution of the volatiles as well. This results reflect behaviour than can be expected from these fuels in an updraft fixed bed gasification process were similar pyrolysis conditions as used in this study generally occur.

5.6 Nomenclature

A	pre-exponential factor (s^{-1})
c	specific heat capacity ($kJ\ kg^{-1}\ K^{-1}$)
D	mass diffusivity ($m^2\ s^{-1}$)
E	Activation energy ($kJ\ mol^{-1}$)
h	heat transfer coefficient ($W\ m^{-2}\ K^{-1}$)
k	thermal conductivity coal ($W\ m^{-1}\ K^{-1}$)
K	permeability (m^2)
Pr	Prandtl number
P	pressure (Pa)
Re	Reynolds number
R	Gas constant ($8.314\ J\ mol^{-1}$)
d	characteristic diameter (m)
ρ	density ($kg\ m^{-3}$)
φ	emissivity
σ	Stefan–Boltzman constant ($5.67 \times 10^{-8}\ W\ m^{-2}\ K^{-4}$)
μ	dynamic viscosity (Pa s)

Subscripts

eff	effective
f	fluid
$cond$	conduction
rad	radiation

5.7 References

- [1] C. Higman, M. van der Burgt, Introduction, in: Gasification (Second Edition), Gulf Professional Publishing, Burlington, 2008: pp. 1-9.
- [2] NETL, Worldwide Gasification Database, (2007).
- [3] H. Boerrigter, A. Van Der Drift, J.H. Hazewinkel, G. Kupers, BIOSYNGAS; Multifunctional intermediary for the production of renewable electricity, gaseous energy carriers, transportation fuels, and chemicals from biomass, Energy Research Centre of the Netherlands (ECN), 2004.

- [4] C. Higman, M. van der Burgt, Gasification Processes, in: Gasification (Second Edition), Gulf Professional Publishing, Burlington, 2008: pp. 91-191.
- [5] C. Brage, Q. Yu, G. Chen, K. Sjöström, Tar evolution profiles obtained from gasification of biomass and coal, *Biomass and Bioenergy*. 18 (2000) 87-91.
- [6] J. Leppälahti, T. Koljonen, Nitrogen evolution from coal, peat and wood during gasification: Literature review, *Fuel Processing Technology*. 43 (1995) 1-45.
- [7] E. Kurkela, P. Ståhlberg, Air gasification of peat, wood and brown coal in a pressurized fluidized-bed reactor. I. Carbon conversion, gas yields and tar formation, *Fuel Processing Technology*. 31 (1992) 1–21.
- [8] S. Mangena, Effective Utilisation of Coal in Sasol – A SasolFBDB Gasification Technology Perspective, in: SACPS International Conference “Coal Powering the Future,” Secunda, South Africa, 2009.
- [9] A. de Klerk, Fisher-Tropsch Refining, PhD Thesis, University of Pretoria, 2008.
- [10] C. Li, K. Suzuki, Resources, properties and utilization of tar, *Resources, Conservation and Recycling*. 54 (2010) 905-915.
- [11] J.M. Jones, M. Kubacki, K. Kubica, A.B. Ross, A. Williams, Devolatilisation characteristics of coal and biomass blends, *Journal of Analytical and Applied Pyrolysis*. 74 (2005) 502-511.
- [12] T. Sonobe, N. Worasuwannarak, S. Pipatmanomai, Synergies in co-pyrolysis of Thai lignite and corncob, *Fuel Processing Technology*. 89 (2008) 1371-1378.
- [13] C. Branca, P. Giudicianni, C. Di Blasi, GC/MS characterization of liquids generated from low-temperature pyrolysis of wood, *Ind. Eng. Chem. Res.* 42 (2003) 3190–3202.
- [14] C. Di Blasi, G. Signorelli, G. Portoricco, Countercurrent Fixed-Bed Gasification of Biomass at Laboratory Scale, *Industrial & Engineering Chemistry Research*. 38 (1999) 2571-2581.
- [15] J.R. Bunt, J.P. Joubert, F.B. Waanders, Coal char temperature profile estimation using optical reflectance for a commercial-scale Sasol-Lurgi FBDB gasifier, *Fuel*. 87 (2008) 2849-2855.
- [16] F. Ateş, M.A. Işıkdağ, Evaluation of the Role of the Pyrolysis Temperature in Straw Biomass Samples and Characterization of the Oils by GC/MS, *Energy & Fuels*. 22 (2008) 1936-1943.
- [17] Z. Wang, J. Cao, J. Wang, Pyrolytic characteristics of pine wood in a slowly heating and gas sweeping fixed-bed reactor, *Journal of Analytical and Applied Pyrolysis*. 84 (2009) 179-184.
- [18] C.A. Mullen, A.A. Boateng, Chemical Composition of Bio-oils Produced by Fast Pyrolysis of Two Energy Crops†, *Energy & Fuels*. 22 (2008) 2104-2109.
- [19] C.A. Mullen, A.A. Boateng, N.M. Goldberg, I.M. Lima, D.A. Laird, K.B. Hicks, Bio-oil and bio-char production from corn cobs and stover by fast pyrolysis, *Biomass and Bioenergy*. 34 (2010) 67-74.
- [20] M. Garcia-Perez, A. Chaala, H. Pakdel, D. Kretschmer, C. Roy, Characterization of bio-oils in chemical families, *Biomass and Bioenergy*. 31 (2007) 222-242.
- [21] A. Demirbas, The influence of temperature on the yields of compounds existing in bio-oils obtained from biomass samples via pyrolysis, *Fuel Processing Technology*. 88 (2007) 591-597.

- [22] W.T. Tsai, M.K. Lee, Y.M. Chang, Fast pyrolysis of rice straw, sugarcane bagasse and coconut shell in an induction-heating reactor, *Journal of Analytical and Applied Pyrolysis*. 76 (2006) 230-237.
- [23] J. Yanik, C. Kornmayer, M. Saglam, M. Yüksel, Fast pyrolysis of agricultural wastes: Characterization of pyrolysis products, *Fuel Processing Technology*. 88 (2007) 942-947.
- [24] T.P. Griffin, J.B. Howard, W.A. Peters, Pressure and temperature effects in bituminous coal pyrolysis: experimental observations and a transient lumped-parameter model, *Fuel*. 73 (1994) 591-601.
- [25] W.S.-L. Mok, M.J. Antal, Effects of pressure on biomass pyrolysis. I. Cellulose pyrolysis products, *Thermochimica Acta*. 68 (1983) 155-164.
- [26] P. Arendt, K.-H. van Heek, Comparative investigations of coal pyrolysis under inert gas and H₂ at low and high heating rates and pressures up to 10 MPa, *Fuel*. 60 (1981) 779-787.
- [27] R. Gadiou, Y. Bouzidi, G. Prado, The devolatilisation of millimetre sized coal particles at high heating rate: the influence of pressure on the structure and reactivity of the char, *Fuel*. 81 (2002) 2121-2130.
- [28] H. Chen, Z. Luo, H. Yang, F. Ju, S. Zhang, Pressurized Pyrolysis and Gasification of Chinese Typical Coal Samples, *Energy & Fuels*. 22 (2008) 1136-1141.
- [29] M.R. Hajaligol, J.B. Howard, W.A. Peters, An experimental and modeling study of pressure effects on tar release by rapid pyrolysis of cellulose sheets in a screen heater, *Combustion and Flame*. 95 (1993) 47-60.
- [30] European Committee for Standardization, *Solid biofuels. Methods for sample preparation*, 2005.
- [31] American Society for Testing Materials, *ASTM D5373 - Standard Test Methods for Instrumental Determination of Carbon, Hydrogen, and Nitrogen in Laboratory Samples of Coal*, 2002.
- [32] American Society for Testing Materials, *ASTM D4239 - Standard Test Methods for Sulfur in the Analysis Sample of Coal and Coke Using High-Temperature Tube Furnace Combustion Methods*, 2000.
- [33] British Standards Institute, *Solid biofuels. Determination of calorific value*, 2009.
- [34] American Society for Testing Materials, *ASTM E1131 - Standard Test Method for Compositional Analysis by Thermogravimetry*, 1998.
- [35] S.A. Channiwala, P.P. Parikh, A unified correlation for estimating HHV of solid, liquid and gaseous fuels, *Fuel*. 81 (2002) 1051-1063.
- [36] M. Garcìa-Pèrez, A. Chaala, J. Yang, C. Roy, Co-pyrolysis of sugarcane bagasse with petroleum residue. Part I: thermogravimetric analysis, *Fuel*. 80 (2001) 1245-1258.
- [37] O. Ioannidou, A. Zabaniotou, E.V. Antonakou, K.M. Papazisi, A.A. Lappas, C. Athanassiou, Investigating the potential for energy, fuel, materials and chemicals production from corn residues (cobs and stalks) by non-catalytic and catalytic pyrolysis in two reactor configurations, *Renewable and Sustainable Energy Reviews*. 13 (2009) 750-762.
- [38] R. Davidson, A. Doig, J. Ekmann, R. Fernando, N. Harding, R. Moreea-Taha, et al., *Cofiring coal with other fuels*, IEA Clean Coal Centre, 2007.

- [39] O. Senneca, Kinetics of pyrolysis, combustion and gasification of three biomass fuels, *Fuel Processing Technology*. 88 (2007) 87-97.
- [40] C. Di Blasi, Modeling chemical and physical processes of wood and biomass pyrolysis, *Progress in Energy and Combustion Science*. 34 (2008) 47-90.
- [41] C. Di Blasi, Kinetic and heat transfer control in the slow and flash pyrolysis of solids, *Ind. Eng. Chem. Res.* 35 (1996) 37-46.
- [42] W.-C.R. Chan, M. Kelbon, B.B. Krieger, Modelling and experimental verification of physical and chemical processes during pyrolysis of a large biomass particle, *Fuel*. 64 (1985) 1505-1513.
- [43] B. Moghtaderi, The state-of-the-art in pyrolysis modelling of lignocellulosic solid fuels, *Fire and Materials*. 30 (2005) 1-34.
- [44] F.P.L. (U.S.), *Wood handbook: wood as an engineering material*, Forest Products Society, 1999.
- [45] E. Schröder, A. Class, L. Krebs, Measurements of heat transfer between particles and gas in packed beds at low to medium Reynolds numbers, *Experimental Thermal and Fluid Science*. 30 (2006) 545-558.
- [46] K. Papadikis, S. Gu, A.V. Bridgwater, H. Gerhauser, Application of CFD to model fast pyrolysis of biomass, *Fuel Processing Technology*. 90 (2009) 504-512.
- [47] D. Kunii, *Fluidization Engineering*, Wiley, New York, N.Y, 1969.
- [48] K.M. Bryden, K.W. Ragland, C.J. Rutland, Modeling thermally thick pyrolysis of wood, *Biomass and Bioenergy*. 22 (2002) 41-53.
- [49] W.B. Russel, D.A. Saville, M.I. Greene, A model for short residence time hydrolysis of single coal particles, *AIChE Journal*. 25 (1979) 65-80.
- [50] O.J. Hahn, M.W. Akhtar, R.C. Birkebak, Thermo-physical properties of coal under transient conditions, *Fuel Processing Technology*. 8 (1984) 241-252.
- [51] A.O. Aboyade, M. Carrier, E.L. Meyer, J. Gorgens, J.H. Knoetze, Model fitting kinetic analysis and characterisation of the devolatilization of coal blends with corn and sugarcane residues, *Thermochimica Acta*. (2011).
- [52] H.S. Fogler, *Elements of Chemical Reaction Engineering*, 4th ed., Prentice Hall, 2005.
- [53] J.H. Slaghuis, *Coal gasification*, Sasol Technology, Sasolburg, SA, 1993.
- [54] P.R. Bonelli, E.L. Buonomo, A.L. Cukierman, Pyrolysis of Sugarcane Bagasse and Co-pyrolysis with an Argentinean Subbituminous Coal, *Energy Sources-Part A Recovery Utilization and Environmental Effects*. 29 (2007) 731-740.
- [55] J. Zanderons, J. Gravitis, A. Kokorevics, A. Zhurinsh, O. Bikovens, A. Tardenaka, et al., Studies of the Brazilian sugarcane bagasse carbonisation process and products properties, *Biomass and Bioenergy*. 17 (1999) 209-219.
- [56] M. Asadullah, M.A. Rahman, M.M. Ali, M.S. Rahman, M.A. Motin, M.B. Sultan, et al., Production of bio-oil from fixed bed pyrolysis of bagasse, *Fuel*. 86 (2007) 2514-2520.
- [57] S. Al Arni, B. Bosio, E. Arato, Syngas from sugarcane pyrolysis: An experimental study for fuel cell applications, *Renewable Energy*. 35 (2010) 29-35.
- [58] M.F. Parihar, M. Kamil, H.B. Goyal, A.K. Gupta, A.K. Bhatnagar, An Experimental Study on Pyrolysis of Biomass, *Process Safety and Environmental Protection*. 85 (2007) 458-465.

- [59] M. Garcìa-Pèrez, A. Chaala, C. Roy, Co-pyrolysis of sugarcane bagasse with petroleum residue. Part II. Product yields and properties, *Fuel*. 81 (2002) 893-907.
- [60] M.R. Islam, M. Parveen, H. Haniu, Properties of sugarcane waste-derived bio-oils obtained by fixed-bed fire-tube heating pyrolysis, *Bioresource Technology*. In Press, Corrected Proof (2010).
- [61] Q. Cao, K.-C. Xie, W.-R. Bao, S.-G. Shen, Pyrolytic behaviour of waste corn cob, *Bioresource Technology*. 94 (2004) 83-89.
- [62] F. Yu, P.H. Steele, R. Ruan, Microwave Pyrolysis of Corn Cob and Characteristics of the Pyrolytic Chars, *Energy Sources, Part A: Recovery, Utilization, and Environmental Effects*. 32 (2010) 475.
- [63] B.P. Baruah, P. Khare, Pyrolysis of High Sulfur Indian Coals, *Energy & Fuels*. 21 (2007) 3346-3352.
- [64] C. Li, J. Zhao, Y. Fang, Y. Wang, Pressurized Fast-Pyrolysis Characteristics of Typical Chinese Coals with Different Ranks, *Energy & Fuels*. 23 (2009) 5099-5105.
- [65] C.W. Lee, A.W. Scaroni, R.G. Jenkins, Effect of pressure on the devolatilization and swelling behaviour of a softening coal during rapid heating, *Fuel*. 70 (1991) 957-965.
- [66] C. Meesri, B. Moghtaderi, Lack of synergetic effects in the pyrolytic characteristics of woody biomass/coal blends under low and high heating rate regimes, *Biomass and Bioenergy*. 23 (2002) 55-66.
- [67] B. Moghtaderi, C. Meesri, T.F. Wall, Pyrolytic characteristics of blended coal and woody biomass, *Fuel*. 83 (2004) 745-750.
- [68] R.V. Pindoria, A. Megaritis, R.C. Messenböck, D.R. Dugwell, R. Kandiyoti, Comparison of the pyrolysis and gasification of biomass: effect of reacting gas atmosphere and pressure on Eucalyptus wood, *Fuel*. 77 (1998) 1247-1251.
- [69] D.K. Park, S.D. Kim, S.H. Lee, J.G. Lee, Co-pyrolysis characteristics of sawdust and coal blend in TGA and a fixed bed reactor, *Bioresource Technology*. Article in Press (n.d.).
- [70] T. Hosoya, H. Kawamoto, S. Saka, Pyrolysis gasification reactivities of primary tar and char fractions from cellulose and lignin as studied with a closed ampoule reactor, *Journal of Analytical and Applied Pyrolysis*. 83 (2008) 71-77.
- [71] P. Wang, L. Jin, J. Liu, S. Zhu, H. Hu, Analysis of coal tar derived from pyrolysis at different atmospheres, *Fuel*. In Press, Corrected Proof (n.d.).
- [72] D.K. Shen, S. Gu, A.V. Bridgwater, Study on the pyrolytic behaviour of xylan-based hemicellulose using TG-FTIR and Py-GC-FTIR, *Journal of Analytical and Applied Pyrolysis*. 87 (2010) 199-206.
- [73] N. Mahinpey, P. Murugan, T. Mani, R. Raina, Analysis of Bio-Oil, Biogas, and Biochar from Pressurized Pyrolysis of Wheat Straw Using a Tubular Reactor, *Energy & Fuels*. 23 (2009) 2736-2742.
- [74] G.J. Lv, S.B. Wu, R. Lou, Characteristics of corn stalk hemicellulose pyrolysis in a tubular reactor, *BioResources*. 5 (2010).
- [75] R.J. Evans, T.A. Milne, Molecular characterization of the pyrolysis of biomass, *Energy and Fuels*. 1 (1987) 123-137.

- [76] M.E. Sánchez, J.A. Menéndez, A. Dominguez, J.J. Pis, O. Martinez, L.F. Calvo, et al., Effect of pyrolysis temperature on the composition of the oils obtained from sewage sludge, *Biomass and Bioenergy*. 33 (2009) 933–940.
- [77] S. Thomas, M.J. Wornat, Polycyclic aromatic hydrocarbons from the co-pyrolysis of catechol and 1,3-butadiene, in: *Proceedings of the Combustion Institute*, 2009: pp. 615-622.
- [78] E.B. Ledesma, P.F. Nelson, J.C. Mackie, The formation of nitrogen species and oxygenated PAH during the combustion of coal volatiles, *Symposium (International) on Combustion*. 27 (1998) 1687-1693.
- [79] E.B. Ledesma, N.D. Marsh, A.K. Sandrowitz, M.J. Wornat, An experimental study on the thermal decomposition of catechol, *Proceedings of the Combustion Institute*. 29 (2002) 2299–2306.
- [80] M.J.G. Alonso, D. Alvarez, A.G. Borrego, R. Menéndez, G. Marbán, Systematic Effects of Coal Rank and Type on the Kinetics of Coal Pyrolysis, *Energy & Fuels*. 15 (2001) 413-428.
- [81] H. Jüntgen, Review of the kinetics of pyrolysis and hydrolysis in relation to the chemical constitution of coal, *Fuel*. 63 (1984) 731-737.
- [82] K.H. Van Heek, W. Hodek, Structure and pyrolysis behaviour of different coals and relevant model substances, *Fuel*. 73 (1994) 886–896.
- [83] K. Unapumnuk, A Study of the Pyrolysis of Tire Derived Fuels and an Analysis of Derived Chars and Oils, PhD Thesis, University of Cincinnati, 2006.
- [84] T. McGrath, R. Sharma, M. Hajaligol, An experimental investigation into the formation of polycyclic-aromatic hydrocarbons (PAH) from pyrolysis of biomass materials, *Fuel*. 80 (2001) 1787-1797.
- [85] R.K. Sharma, M.R. Hajaligol, Effect of pyrolysis conditions on the formation of polycyclic aromatic hydrocarbons (PAHs) from polyphenolic compounds, *Journal of Analytical and Applied Pyrolysis*. 66 (2003) 123-144.
- [86] M.J. Wornat, E.B. Ledesma, N.D. Marsh, Polycyclic aromatic hydrocarbons from the pyrolysis of catechol (ortho-dihydroxybenzene), a model fuel representative of entities in tobacco, coal, and lignin, *Fuel*. 80 (2001) 1711–1726.
- [87] T. Hosoya, H. Kawamoto, S. Saka, Pyrolysis behaviors of wood and its constituent polymers at gasification temperature, *Journal of Analytical and Applied Pyrolysis*. 78 (2007) 328-336.
- [88] T. Hosoya, H. Kawamoto, S. Saka, Secondary reactions of lignin-derived primary tar components, *Journal of Analytical and Applied Pyrolysis*. 83 (2008) 78-87.
- [89] C. Di Blasi, C. Branca, A. Santoro, E. Gonzalez Hernandez, Pyrolytic behavior and products of some wood varieties, *Combustion and Flame*. 124 (2001) 165-177.
- [90] Aboyade, J. Gorgens, M. Carrier, E.L. Meyer, J.H. Knoetze, Thermogravimetric study of the devolatilization characteristics and kinetics of coal blends with corn and sugarcane residues, *Fuel*. (2011).

6 Characterization of devolatilized products from co-pyrolysis of coal-biomass blends

Adapted version was submitted to Energy Conversion and Management in September 2011 using the following details:

Title: “Slow and pressurized co-pyrolysis of coal and agricultural residues”

Authors: Akinwale O. Aboyade^{a,b}, Marion Carrier^a, Edson L. Meyer^b, Johannes H Knoetze^a, Johann F. Görgens^a

^aDepartment of Process Engineering, Stellenbosch University, Stellenbosch, South Africa

^bFort Hare Institute of Technology, University of Fort Hare, Alice, South Africa

In this chapter, the influence of mix ratio, pressure and temperature on the yield and composition of volatile products obtained from pressurized co-pyrolysis of coal and biomass was investigated based on a 2³ factorial design.

6.1 Introduction

A number of researchers have reported co-pyrolysis studies using a range of pyrolysis conditions, reactor types and fuel types. There has been some contradictions in the conclusions from these studies. Some have reported significant interactions between the contributing fuels [1,2] and others describe mainly additive effects [3-6]. Few of these studies [1-3] focused on the effects of co-processing on the composition and quality of volatiles products. However, the quality and composition of liquid hydrocarbon is important for industrial processes where tar is recovered and used for commercial applications. The composition of tar is also of concern with regards to its safe and environmentally sustainable disposal. Jones et al. [1] determined that co-pyrolyzing pinewood with coals of different rank ranging from lignite to sub-bituminous coal, results in a decrease in aromatics and increase in phenols during atmospheric, slow heating rate pyrolysis. They did not however provide quantitative yields of these compounds or the effect of temperature or pressure on such yields. The majority of co-pyrolysis studies were conducted under atmospheric conditions, whereas high pressure is required for most industrial processes. Collot et al's [16] work on the co-pyrolysis of Daw Mill coal and Silver Birch wood under pressures ranging from 1-20 bars is one of the few works on

pressurized co-pyrolysis of coal and biomass. However, the effect of co-pyrolysis conditions on the composition of the gas or liquid products obtained was not included in their study.

The yield and composition of volatile products from of individual pressurized pyrolysis of both coal and selected agricultural residue have been presented Chapter 5, under conditions similar to what obtains in an updraft, fixed-bed gasifier. This chapter investigates the yields of volatiles of various mix ratios of coal-biomass blends under the same conditions, with a view to detecting possible synergistic behaviour. The influence of operating parameters such as pressure and temperature has also been investigated. The experimental plan was based on a 2^3 factorial design with mix ratio, pressure and temperature as the three factors. Factorial designs allow for studying the influence of multiple factors using a reduced number of experimental runs than would normally be required [9]. Observed devolatilization behaviour was discussed in the context of the relative importance of kinetic and transport phenomena on the process. The influence of varying operating conditions such as temperature and pressure on co-pyrolysis behaviour were also considered.

6.2 Experimental

The description and characteristics of feedstock and apparatus used in the experiments have been provided in Chapter 5.

6.3 Experimental design

This study is based on a two-level (2^k) factorial design (Table 7-1) employed to study the effect of three factors ($k=3$), namely temperature, pressure, and the percentage biomass added to the feed (coal-biomass mix ratio), on a number of response variables relating to the yield and composition of volatile (gas and liquid) products. The temperature range chosen for experiments was 400-600°C, whereas pressure ranged from 1 to 26 bars. This range is typical of conventional pyrolysis processes for both biomass and coal [10], and covers the temperature and pressure conditions

observed in updraft fixed bed reactors [11,12]. Percentage biomass added to the coal feed varied from 5 to 50 wt%. The full design gives a total of 8 tests performed. Additional centre-point runs (500°C, 13 bars and 27.5 wt% biomass in feed) were conducted in duplicate resulting in a total of 10 tests performed for each of coal-BG and coal-CC blends.

Table 6-1: Experimental plan (values in parenthesis represents coded factors in factorial design)

Exp/no	Biomass composition (%)	Temperature (°C)	Pressure (bars)
1	(+1) 50	(+1) 600	(+1) 26
2	(+1) 50	(+1) 600	(-1) 1
3	(+1) 50	(-1) 400	(+1) 26
4	(-1) 5	(+1) 600	(+1) 26
5	(-1) 5	(-1) 400	(+1) 26
6	(-1) 5	(+1) 600	(-1) 1
7	(-1) 5	(-1) 400	(-1) 1
8	(+1) 50	(-1) 400	(-1) 1
9	(0) 27.5	(0) 500	(0) 13
10	(0) 27.5	(0) 500	(0) 13
11*	0	600	26
12*	100	600	26

*runs not part of factorial experimental plan

Analysis of the experimental data obtained from the factorial experimental plan was done using the Statistica software package (v. 9.0) by Statsoft Inc., USA. The software determines which of the independent input factors have significant effects on the response (dependent) variables using Analysis of Variance (ANOVA). Experimental data was also fitted to a regression model of the form [9]:

$$Y = \beta_0 + \sum_{i=1}^n \beta_i x_i + \sum_{i=1}^n \beta_{ii} x_i^2 + \sum_{i=1}^n \sum_{j>i}^n \beta_{ij} x_i x_j$$

Where Y is the response variable parameter pertaining to yields of the various products, the β s are the coefficients of the main effects and interactions, and x_1 to x_k are the scaled independent variables. The first order terms describe the main effects

and the second order term describes non-linear effects and interactions. Response surface plots were used to visualize the effects of the input factors on selected yields.

6.3.1 Influence of coal-biomass mix ratio

In addition to the factorial experimental plan, further pyrolysis experiments were conducted on individual samples of BG, CC, CS and coal at 26 bars and 600°C (runs #11 and #12). This in combination with runs at the same temperature and pressure obtained from the factorial experimental plan (run #1 and #4 in Table 7-1) helped to separately highlight the influence of coal-biomass mix ratio and to address the question of synergy between the blend materials. In this way, product distribution and composition of coal-biomass blends with mix of 100:0, 95:5, 50:50, and 0:100 could be compared.

Measured yields from the coal-biomass blends were compared with predictions calculated on the assumption that no interactions occurred between the feedstocks during pyrolysis. Predicted yield values are thus given by the weighted sum of the individual yield values of the contributing fuels as the expression below shows [10]:

$$PY = [(c_{100\%} \times c_m) + (b_{100\%} \times b_m)]/100$$

where PY = predicted yield value for the mixture; $c_{100\%}$ = coal value from single fuel pyrolysis; c_m = share (%) of coal in the mixture during co-pyrolysis; $b_{100\%}$ = biomass value from single fuel pyrolysis; b_m = share (%) of biomass in the mixture during co-pyrolysis.

6.4 Results and Discussions

Table 7-2 shows ANOVA p-values reflecting the relative significance of the three process variables and their interactions on the yields of char, gases, total liquids, tar, and chemical groups such as acids, phenolics, ketones, and PAHs from coal-CC and coal-CC blends. Among the factors, the blend mix ratio (represented by wt% biomass

values) had the highest statistical significance for all of the measured responses. Factors with p-values lower than 0.05 were considered highly significance while values greater than 0.15 are insignificant. Values between 0.05 and 0.15 indicated low significance of the associated process variable. Consequently it could be observed that wt% biomass had a statistically high significance on the phase distribution of products into char, liquids and gases. With respect to the yield of specific fractions or chemical groups such as tar, acids, phenolics and PAHs, the effects of wt% biomass was generally less significant.

Table 6-2: ANOVA results and measures of model adequacy for both coal-BG and coal-CC blends

	<i>p-values</i>								R^2 ***
	<i>(wt%)*</i>	<i>(T)</i>	<i>(P)</i>	$(T)^2$ **	<i>(wt%)(T)</i>	<i>(wt%)(P)</i>	<i>(T)(P)</i>	<i>Lack of Fit</i>	
Coal-BG									
<i>Char</i>	0.0237	0.0669	0.3008	0.1335	0.2389	0.1533	0.3714	0.3708	0.9962
<i>Liquids</i>	0.0414	0.0741	0.1044	0.2872	0.2198	0.1361	0.2750	0.6738	0.9966
<i>Gas</i>	0.0144	0.0584	0.0450	0.0728	0.2748	0.1896	0.6953	0.1338	0.9904
<i>Tar</i>	0.0629	0.4730	0.0948	0.1550	0.2304	0.0788	0.1435	0.2494	0.9736
<i>Acids</i>	0.0733	0.0867	0.0837	0.0817	0.1463	0.0083	0.0135	0.0243	0.9922
<i>PAHs</i>	0.3520	0.9632	0.4310	0.7740	0.6897	0.8459	0.8366	0.8744	0.8201
<i>Phenols</i>	0.0112	0.1474	0.0485	0.0800	0.0264	0.0559	0.0206	0.3841	0.9997
<i>Ketones</i>	0.4534	0.8208	0.3619	0.4907	0.3844	0.7919	0.5416	0.6369	0.8497
Coal-CC									
<i>Char</i>	0.0063	0.0205	0.2583	0.2698	0.0858	0.0932	0.0637	0.2004	0.9991
<i>Liquids</i>	0.0120	0.0730	0.0752	0.3965	0.0899	0.1356	0.1791	0.1605	0.9947
<i>Gas</i>	0.0304	0.0611	0.1144	0.7925	0.9208	0.5527	0.2067	0.6810	0.9978
<i>Tar</i>	0.1009	0.5833	0.2186	0.8863	0.7036	0.2137	0.9484	0.9575	0.9824
<i>Acids</i>	0.0628	0.1307	0.1170	0.1399	0.4982	0.1299	0.2212	0.3593	0.9833
<i>PAHs</i>	0.0364	0.0416	0.0680	0.1806	0.0726	0.0736	0.1157	0.7053	0.9985
<i>Phenols</i>	0.3490	0.3117	0.3350	0.4134	0.3284	0.3901	0.3530	0.4167	0.8731
<i>Ketones</i>	0.0246	0.0529	0.0450	0.0492	0.0888	0.1206	0.2244	0.5211	0.9985

*wt% biomass in feedstock blend

** coefficients of the other quadratic terms $(wt\%)^2$ and $(P)^2$ were redundant and thus not shown. Their effects were linear combinations of other effects and cannot be estimated

***squared multiple correlation coefficient for the regression model

Table 7-2 also shows that for both coal-CC and coal-BG blends, temperature was the next most significant factor influencing the yields of the major product classes, although the significance levels ranged mostly from low to negligible except for char and PAH yields obtained from coal-CC blends. The ANOVA results confirmed the relative significance of mix-ratio compared to process variables. However, in order to properly investigate the effect of blending coal and biomass during co-pyrolysis, and to address the question of synergy, product yields obtained from pyrolysis of the individual fuels were presented and then compared directly with results of coal-biomass blends from runs in the factorial experimental plan that were conducted under the same conditions.

6.5 Influence of mix ratio

6.5.1 Products yields/distribution

Fig. 7-1 compares product distribution of the lumped gas, liquid and solid phase products for various mix ratios of coal and biomass at 26 bars and 600°C. It shows yield values for individual coal and biomass compared with coal-biomass blends of 95:5, 50:50 mix ratios (corresponding to runs #1 and #4 in the factorial plan shown in Table 7-1). The results reveal approximate proportionality between product yields and blend ratios. Measured gas production increased by 68% and 350% when 5% and 50% respectively of BG was added compared to 49% and 300% increases from CC. This means a significantly higher fraction of the volatiles released were converted to gas in coal-BG blends than in coal-CC blends. On the other hand, the increase in total volatiles as a result of adding biomass to the feed mixture was higher for coal-CC blends than for coal-BG blends, due to the significantly higher liquid condensate yield from CC. This result is generally in line with previous findings from other authors using various types of coals and biomass, as well as pyrolysis apparatus [2,4,6,13].

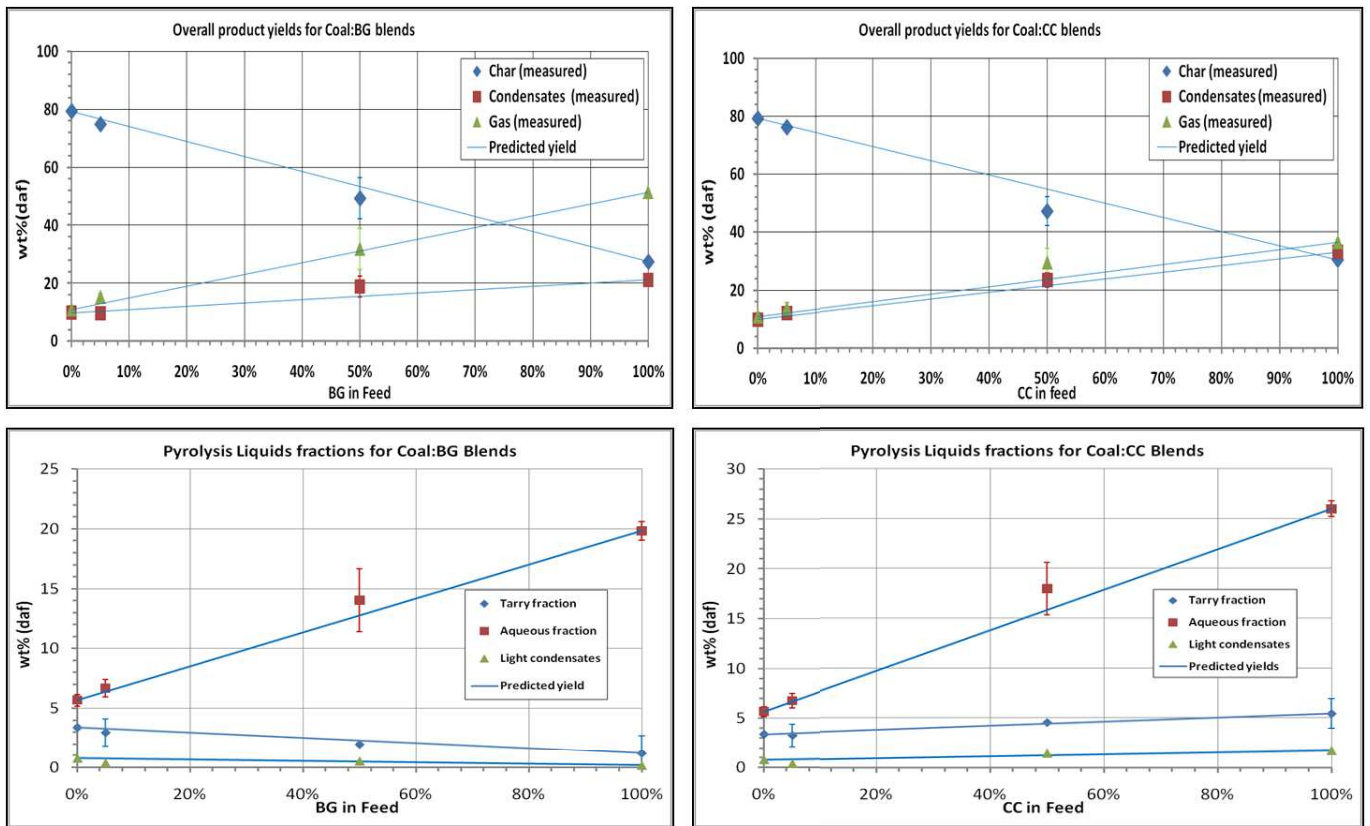


Figure 6-1: Influence of mix ratio on overall product distribution and the distribution of liquid phase fractions

Furthermore, the study revealed that measured gas and condensate yields were slightly higher than predicted for the blends, and the disparity was higher for 50:50 blends compared to 95:5 blends. This is likely due to the higher hydrogen content in biomass causing increased liquefaction during co-pyrolysis. It has previously been observed in liquefaction studies that hydrogen increases liquid yields [15-20]. As a consequence of synergies noted from volatile products, experimental results for char best matched predicted values for 95:5 mix ratios, while 50:50 blends showed higher disparity between experimental and expected values. Park et al. [13], conducted *atmospheric* fixed bed pyrolysis on mixtures of sub-bituminous coal and sawdust, and observed similar trends for the measured and predicted char and gas yields.

The deviation between measured and predicted values of overall product yield were generally within experimental error, except for the char yield values for 50:50 coal-CC blends. On the one hand, this may suggest that deviations between experimental and predicted values can be ascribed to experimental errors, and may lead to the

conclusion that there are no interactions or synergy between the coal and biomass samples during co-processing. This view is supported by previous findings from other authors found in the literature [3,4,6,21,22]. On the other hand, the consistent, systemic nature of such deviations for both mixture types studied here and in some other studies [1,2,13], lends weight to the opposing view that synergies do occur during co-pyrolysis of coal and biomass.

Pyrolysis condensates comprise of water soluble (pyrolytic water phase) and water insoluble (tarry phase) fraction both of which condensed in the first ice bath. In addition was a light volatile fraction consisting aerosols trapped in a solvent impinger train. Fig. 7-1 shows the relative distribution of these fractions for the blends pyrolyzed at 26 bars and 600°C. The production of all liquid fractions increased with addition of CC to coal. In contrast, for coal-BG blends, the non-aqueous tar and light condensates decreased with increase in the proportion of biomass in the feed blend, implying that the aqueous fraction was mostly responsible for the increase in total liquid products observed for same blends.

Deviations between experimental and predicted yield values of the various liquid condensate fractions were most significant for 50:50 blends, particularly for the aqueous fractions. As was the case for overall product distribution, the disparity between experimentally obtained yields of the condensates fractions and the predicted results was within experimental error. This highlights the uncertainty regarding whether or not co-pyrolysis of coal and biomass proceeds in a non-additive manner. Results of the analysis of volatile products presented in the following sections will shed more light on possible synergistic reactions.

6.5.2 Compositional analysis of volatile products

6.5.2.1 Gas composition

Fig. 7-2 shows the composition of gas species produced during pyrolysis. It has been shown from the previous chapter that biomass produces gas in higher yields than coal. This is reflected in the approximately linear increase in CO₂, CO, CH₄ and H₂

yields that result from increase in the biomass fraction in the fuel. This observation agrees with previous findings by Meesri and Moghtaderi [3] from the atmospheric co-pyrolysis of coal and sawdust, and by Sonobe et al. [2] from the atmospheric co-pyrolysis of lignite and corn cobs. On the other hand, Zhang et al. [23] observed higher levels of synergy in gas production, indicated by deviation from predicted values.

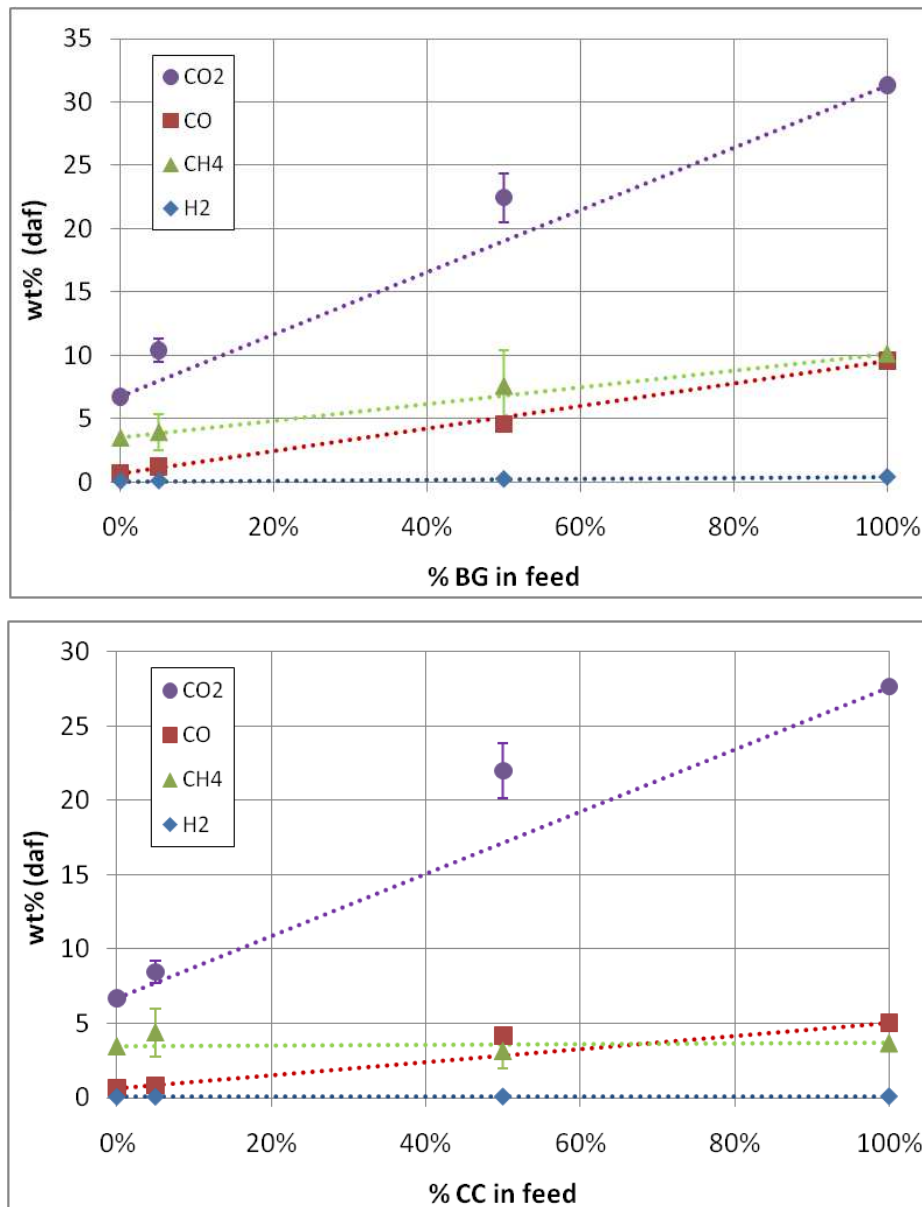


Figure 6-2: Influence of mix ratio on yields of gas species

Gas phase production at all mix ratios during pyrolysis is dominated by the carbon oxides, CO₂ and CO. The results show that the higher than predicted gas yields observed in Fig. 7-2 is mainly due to increases in CO₂ production. CO₂ is mainly derived from the decomposition of mainly carboxylic compounds [24]. The higher quantities of these oxides produced as a result of biomass addition highlights the increased availability of unstable carboxylic precursors [2]. As have been shown in the previous chapter, CH₄ and H₂ are produced at later stages of pyrolysis mainly due to secondary and tertiary reactions. CH₄ is formed from the cracking of primary tar and aromatics [2]. During both coal and biomass pyrolysis, reactions that produce H₂ (cracking of heavy molecular weight aromatics, depolymerization of phenyl groups [25,26]) occur at high temperatures which explains the relatively low yields observed in section 6.6.3.

6.5.2.2 Liquids composition

The chemical components in the combined condensate fractions obtained from the blends were identified and quantified by GC-MS. Detected compounds were grouped into the following functional groups; acids, alcohols, aldehydes, esters, furans, ketones, nitriles, single ring aromatics, PAHs, and phenolics. The influence of coal-biomass blend ratios on the yields of identified compounds by is shown in Table A-3 (Appendix A). In Table 7-3, percentage differences between experimental and predicted values for some variables derived from the quantification results have been presented along with yields. Predicted values were calculated based on the additive model explained earlier. The almost complete lack of linearity in yield trends of the components shown for either of the biomass blends is symptomatic of strong synergistic behaviour or chemical interactions between volatiles during pyrolysis. The elevated pressure at which these results were obtained ensures sufficiently high residence times which will in turn encourage secondary reactions making it likely for interactions to occur. However the possibility that these chemical interactions occurred after condensation, i.e. outside the reactor, cannot be ruled out.

Yields of phenolics and PAHs were substantially lower than should otherwise be expected assuming additive behaviour at 5 wt% addition of either BG or CC in the feedstock, while acids yields were higher. The proportion of the yield of acids, alcohols, ketones, phenolics and other oxygenated groups represented in the total liquid hydrocarbons produced are described by the term 'oxygenates' in Table 7-2. Upon addition of 5 wt% of BG and CC to the feed, oxygenate yield obtained was higher than predicted by 24% and 34%, respectively. PAH's and aromatics which make up the bulk of the remaining organic condensates are 0.5 and 3.5 times lower than expected at the same level of BG and CC addition, respectively. The increase in oxygenate yield at 5 wt% biomass content despite the observed decrease in phenolics (and ketones for coal-BG blends) is mainly due to the strong increase in acid yields. The decrease in yield of phenolics and other oxygenates at the seeming expense of PAHs is in agreement with previous observations by Jones et al. [1] in their study of the atmospheric, slow heating rate co-pyrolysis. They observed that PAH production was suppressed when coal and pinewood was pyrolyzed in combination, resulting in predominantly oxygenated condensates. PAHs from coal are formed from the repolymerisation of liberated phenyl derivatives and other hydrocarbon radicals released during bond scission [14]. The reduction in PAH yields as a result of pyrolysis in combination is likely due to the action of reactive oxygenated free radicals from biomass reacting with the unsaturated aromatics from coal and preventing them from recombining to form long chain hydrocarbons such as PAHs.

For both blends, the yields of acids were relatively more proportional with mix ratio, even though the observed yields were consistently higher than predicted. Acids (mainly acetic, propanoic, and butanoic acid) in tar are mainly derived from carboxylic fractions of cellulose and hemicellulose in biomass. The increase in acids beyond what would be expected from purely additive behaviour of the combined feedstocks implies that reactions pathways that produce these acids are favoured. These reactions include carbonylation, hydrocarboxylation of phenolics, and oxidation of aldehydes [26].

Table 6-3: Influence of mix ratio on composition and some other key characteristics of liquid phase hydrocarbons (% diff refers to relative disparity between measured and predicted values)

daf (g/kg)	BG fraction in blend						CC fraction in blend					
	0%	5%		50%		100%	0%	5%		50%		100%
		Exp	% Diff	Exp	% Diff			Exp	% Diff	Exp	% Diff	
Acids	0.25	3.87	79.19	7.27	20.66	11.28	0.25	6.48	51.29	57.55	49.17	58.25
Alcohols	0.40	0.40	-15.72	1.00	-1.85	1.63	0.40	0.75	13.34	5.41	46.51	5.38
Aldehydes	0.00	0.01	29.72	0.01	-431.29	0.07	0.00	0.02	-118.44	0.18	-146.64	0.87
Aromatics	2.15	3.54	41.30	4.35	67.43	0.68	2.15	1.96	-11.14	1.12	-118.10	2.74
Furans	0.27	1.53	82.34	1.60	80.88	0.34	0.27	2.39	79.23	8.25	68.83	4.88
Heterocyclics	0.10	0.09	-11.98	0.12	41.85	0.03	0.10	0.00	-12.33	0.01	-3390.09	0.82
Ketones	3.71	2.47	-46.06	5.06	46.31	1.72	3.71	4.48	11.00	6.58	1.85	9.21
Nitriles	0.01	0.05	69.93	0.05	55.07	0.03	0.01	0.03	58.12	0.04	48.19	0.03
PAHs	14.96	1.79	-704.52	1.54	-513.54	3.93	14.96	0.45	3167.00	1.83	-659.13	12.85
Phenolics	20.20	13.09	-49.36	16.85	18.68	7.21	20.20	10.89	-90.04	30.60	17.92	30.04
Pyrolytic water	56.18	68.97	9.26	150.36	20.02	184.33	56.18	73.26	13.32	132.10	2.07	202.55
Total HCs	42.06	26.97	-53.19	38.12	9.23	27.14	42.06	27.89	-66.99	112.71	22.67	132.26
wt% oxygenates in total HCs	59.04	79.23	23.99	83.37	14.96	82.75	59.04	91.11	33.64	97.30	24.73	87.44
wt % PAH and aromatics in total HCs	40.69	19.78	-99.78	15.46	-86.54	17.00	40.69	8.67	-352.64	2.62	-901.48	11.78

Furthermore, Table 7-3 also reveals that suppression of polycyclic and monocyclic aromatics can also be observed in the 50:50 blends. Interestingly, decrease in PAH yields due to addition of biomass was less severe in the 50:50 blend (7 and 31 times less than predicted for BG and CC respectively) than in the 95:5 blend where the yields are 5 and 6.5 times less than predicted. On initial inspection, this leads to the seemingly paradoxical conclusion that the severity of synergistic reactions is lower at higher biomass mix ratios. It must however be considered that the same oxygenated radicals that suppress PAH production are also in demand during secondary reactions of biomass vapours for the production of oxygenates [26,27]. The balance between this two competing reactions is likely shifted towards the production of oxygenates at higher biomass composition in the feedstock mix and would explain why higher biomass mix ratios do not necessarily lead to higher levels of synergy in terms of PAH suppression. It may also explain the observed reduction in yield of oxygenates like phenolics, ketones and aldehydes (Table 7-2 and 7-3) for blends with lower biomass composition.

6.6 Influence of process variables

6.6.1 Product distribution

Fig. 7-3 shows the normal probability plot for total liquid yields. It can be observed that for both coal-BG and coal-CC blends, the main positive influence on total condensate production was wt% biomass in the feedstock. Standardized t-values of approximately 15 and 52 respectively imply a stronger effect on liquid yields when BG and CC are added to coal. This is in accordance with the previously reported influence in mix ratio presented in Fig. 7-1. This section will focus more on the influence of the other two factors studied; temperature and pressure.

Temperature produced similarly significant positive impact to a lesser extent on both coal-cc and coal cc blends as indicated by the standardized t-values (x-axis of Fig. 7-

3). Pressure on the other hand is shown to have a negative effect on liquids production from both blends. Interaction between mix ratio and pressure and interactions between temperature and mix ratio were the next important influences. The former caused a reduction in liquid yield and the later had a positive effect. Relative significance levels for these factors and their interactions are confirmed by the p-values given in Table 7-2.

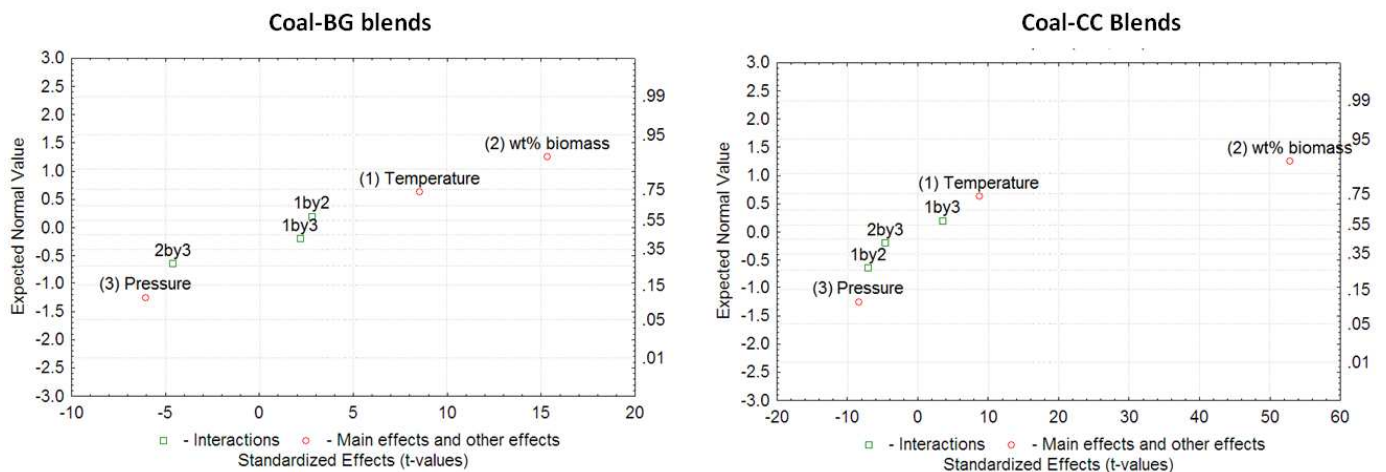


Figure 6-3: Normal probability plot for total liquid yields

It is clear that mix ratio had a far more significant effect on devolatilization characteristics than temperature and pressure within the range studied. However, studying in more detail the effects of temperature and pressure on devolatilization behaviour of the blends can still be of interest. Particularly because these factors are known to vary during gasifier operation, and it would be helpful to know what impact such variation might have on the yield and composition of volatile products. To investigate the influence of pressure and temperature in more detail therefore, response surface plots have been generated from the regression model based on the factors that has been identified to have significant effects (Table 7-2) for both coal-BG and coal-CC blends. An indication of the reliability of the response model is given by the LOF values in Table 7-2. The p-values of 0.67 for coal-BG and 0.16 for coal-CC indicate that it is not significant relative to pure error.

Fig. 7-4 shows the response surface of liquid yields from 95:5 wt% and 75:25 wt% coal-BG and coal-CC blends, as a function of the pyrolysis variables, temperature and pressure. Liquid yields from all mix ratios increases with temperature and decreases with pressure at a lesser rate. The observed increase in pyrolysis liquid yield from coal-biomass blends due to temperature in the range 400-600°C is in line with previous findings from literature [2,3,28,29]. Studies on the influence of pressure are much less available. Collot et al. [6] on the fast pyrolysis of 50:50 coal-wood blends at 850°C observed a decrease in liquid yields from 29 wt% to 23 wt% when pressure was increased from 5 to 20 bars.

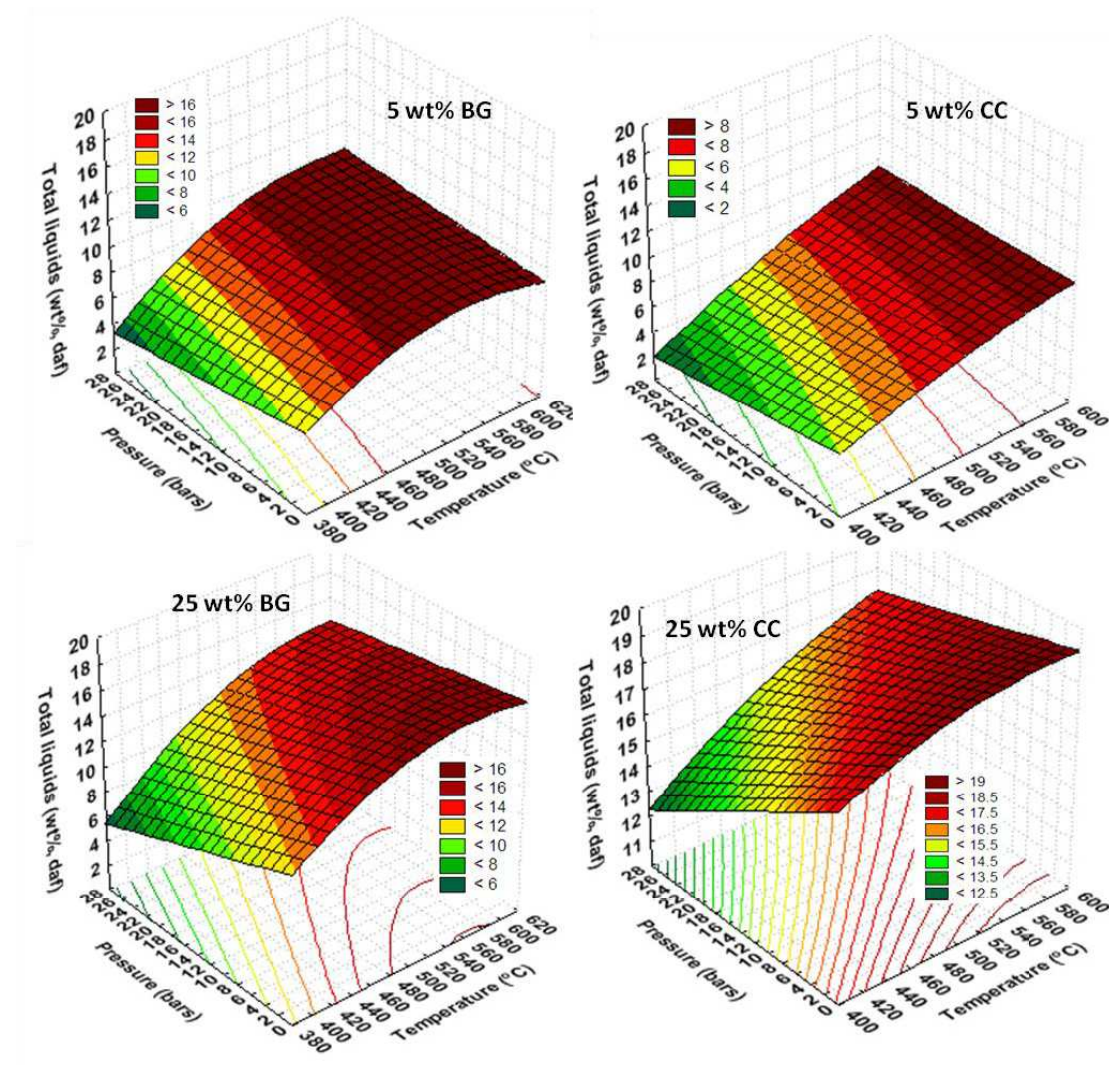


Figure 6-4: Influence of temperature and pressure on total liquid yields at 5 wt% and 25 wt% biomass blends

As mentioned in earlier sections, the total liquid yields in this study were made up of a tar, aqueous and light condensate fraction. The tar phase contains the bulk of hydrocarbons of the most commercial value i.e. phenolics and PAHs [30]. Fig. 7-5 shows the response surface plots for yields of the tar fraction of 5 wt% and 25 wt% blends. The most significant factors influencing tar production in order of decreasing importance are wt% of biomass, pressure, and temperature (Table 7-2). Again focusing on factors related to operating conditions, temperature had a positive effect on tar yields from coal-CC blends, but the effect on yields from coal-BG blends was less obvious. Tar production from BG blends peaked on or before 400°C, decreased slightly at 500°C and increased again as temperatures approached 600°C. This is consistent with the observation in Fig. 7-1 that showed that at 600°C, BG produced lower yields of tar fraction liquids than CC. This varying behaviour between the biomasses can again be linked to the differences in the physical characteristics of the fuels. BG devolatilizes more rapidly than CC as a result of its smaller particle size distribution and consequently the escaped volatiles are more readily cracked into lower molecular weight gases as pyrolysis temperatures increase beyond 400°C. This behaviour combined with the fact that tar production from coal starts at higher temperatures (closer to 600°C) explains the dip in tar production between 400 and 600°C for Coal-BG blends. The larger CC particles decompose more slowly such that tar production steadily rises through the temperature range studied.

The results also show that pressure has a stronger, albeit negative, effect on tar production (quadrupling from <1 wt% to approximately 4 wt% at 75:25 coal-BG mix ratio) compared to total liquid yields (7-12 wt% at same mix ratio). This indicates that at elevated pressures more cracking of the heavier hydrocarbons is prominent due to the extended residence times. A similar trend can be noticed for coal-CC blends. This is confirmed by the p-values in Table 7-2 which shows pressure had a more significant effect on tar production than temperature.

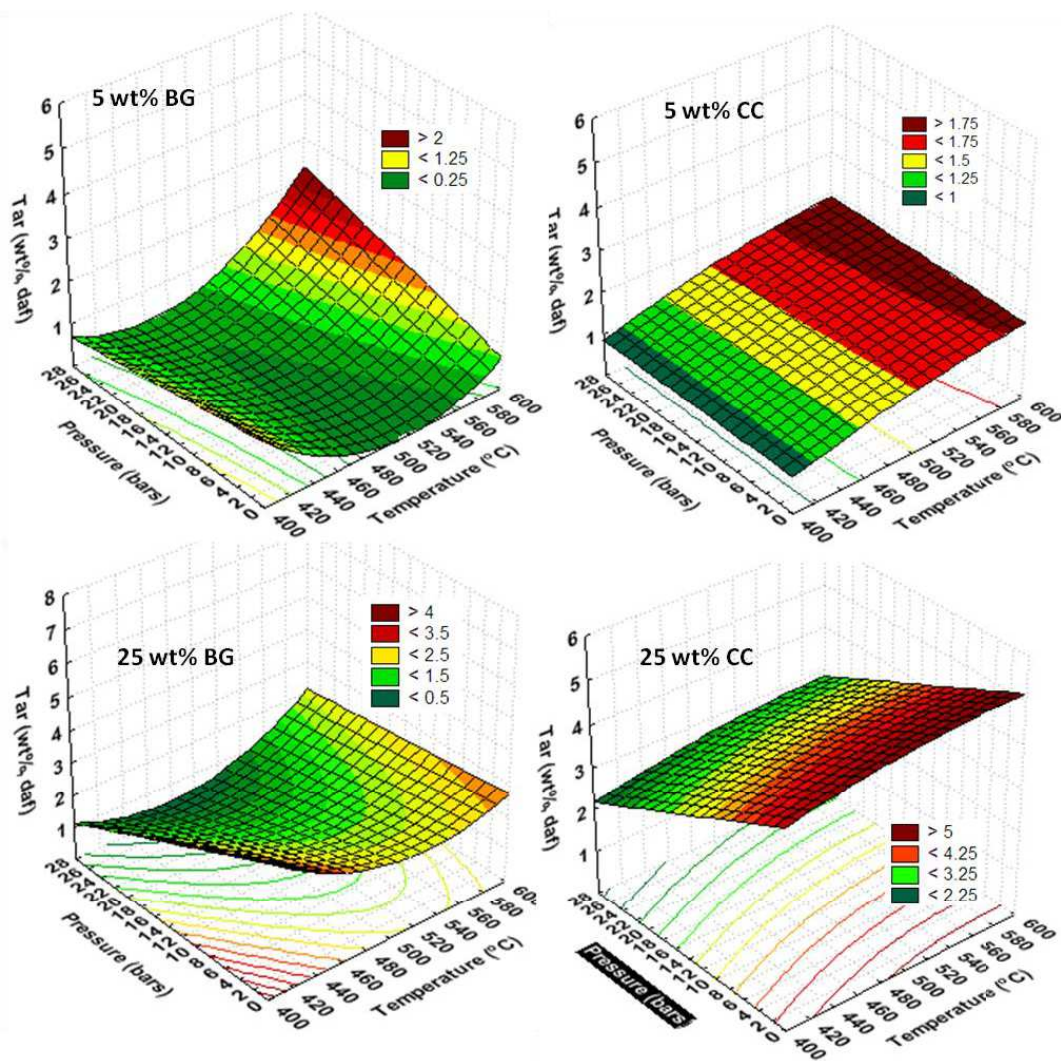


Figure 6-5: Influence of temperature and pressure on tar yields at 5 wt% and 25 wt% biomass blends

6.6.2 Compositional analysis of volatile products

6.6.2.1 Gas composition

The influence of operating parameters – pressure and temperature – on the production of CO_2 , CO , CH_4 , and H_2 from 95:5 wt % coal-biomass blends are shown in Figs. 7-6 and 7-7. It must be noted that there was significant lack of fit for much of the gas specie yields (Table 7-2) indicating a relatively poor fit of the model in predicting gas yields and/or pure error variability. Nevertheless, the trends observed are reasonable and are largely consistent with the literature. The results show that the production of all gas species was positively correlated with temperature and pressure in the 400-600°C and 1-26 bars range for the coal-BG blend. As has earlier

been established, high pressure favour gas production as a consequence of increased residence times which allow for more cracking of volatiles. High temperatures also favour the decomposition of volatiles and mild gasification of chars [31]. High CO₂ production could be the results of secondary carboxylation reactions which are encouraged by long vapour residence times allowed under the pressurized experimental conditions employed.

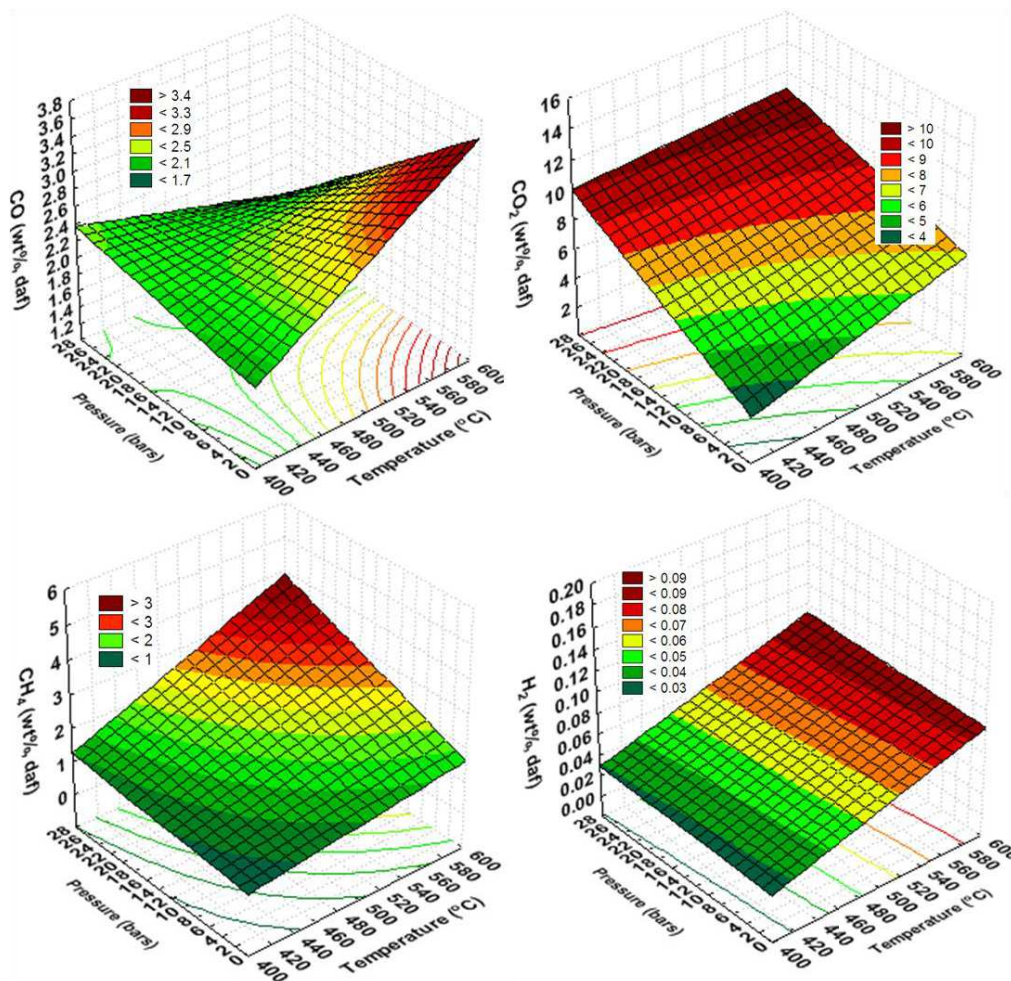


Figure 6-6: Influence of temperature and pressure on gas species production from 25 wt% BG blends

A similar trend of higher gas specie yields with increase in pressure was observed for coal-CC blends except for CO whose production dipped with increasing pressure (Fig. 7-9). Mok and Antal [32] reported increases in CO₂ and H₂ yields with pressure from the pyrolysis of cellulose, but noted decreases in CO and CH₄. On the other hand, Arendt et al. [33] noted increases in CH₄ yields from coal pyrolysis due to pressure.

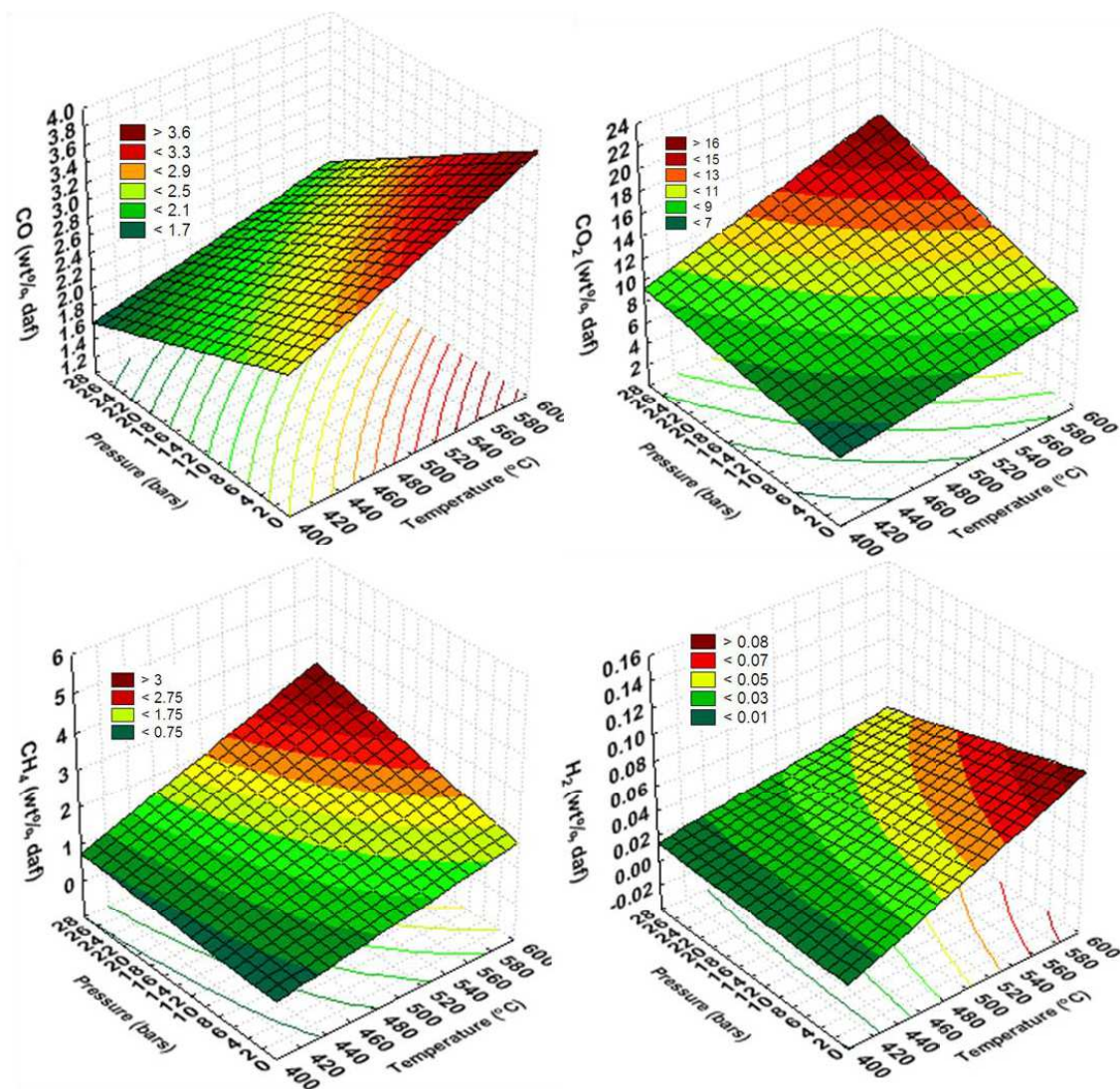


Figure 6-7: Influence of final temperature and pressure on gas species production from 25 wt% CC blends

6.6.2.2 Liquids composition

Figs. 7-8 and 7-9 shows the influence of temperature and pressure on the composition of combined liquid phase hydrocarbons in both coal-BG and coal-CC blends. The relative significance of factors for each of the responses shown can be found in Table 7-2 as indicated by the p-values. It can be observed that acid yields for coal-BG was relatively unaffected by temperature while from coal-CC blends, acid yields increased at first and then decreased after 500°C. Temperature had a generally positive influence on the production phenolics from coal-CC as did pressure, in contrast to coal-BG blends where a reduction in yields was observed.

The literature also shows mixed results for the influence of temperature on yields of phenolics. Sanchez et al. [34] observed a decrease in phenols production while other authors observed a decrease [35]. Phenols are derived mainly from the decomposition of lignin in biomass [26,36]. Phenols from coal are produced via the recombination of phenyl radicals liberated during primary devolatilization [37]. The presence of phenyl groups in coal – in common with lignocellulosic biomass – is not surprising given that coal is thought to be the product of long term decomposition of biomass [38]. Similarities between coal and lignin have led to the hypothesis that the bulk of coal in fact originates mainly from the lignin fraction in biomass [39].

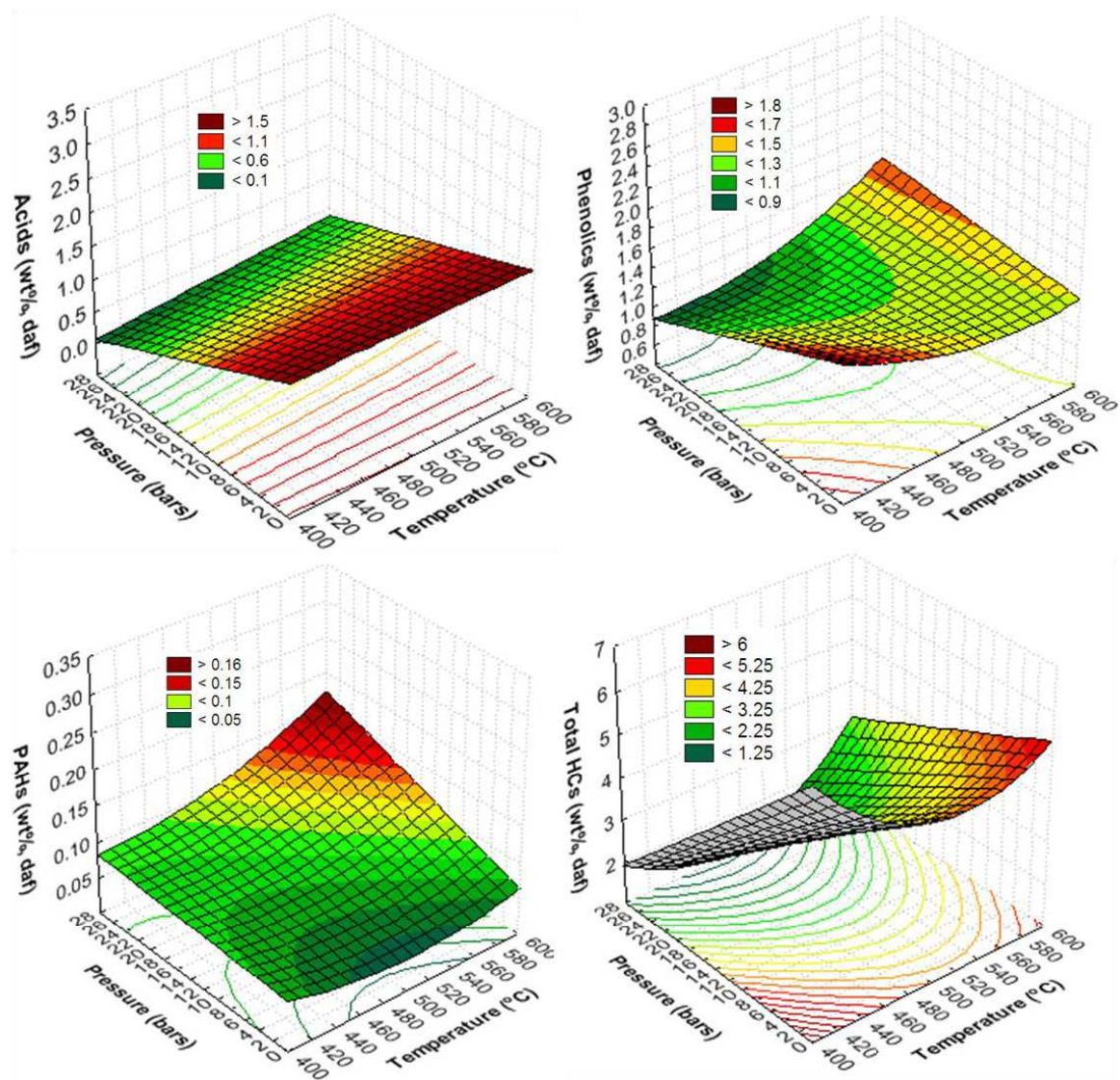


Figure 6-8: Influence of temperature and pressure on key aspects of liquids composition from 25 wt% BG blends

Overall, total liquid hydrocarbon yields for coal-CC tended to increase slightly before levelling out over the temperature range studied, whereas for coal-BG blends, an initial decrease was mostly observed. This can again be linked to their differing densities and particle size. The smaller BG particles are already mostly fully devolatilized (primary decomposition) at 400°C such that at higher temperatures than that, secondary and tertiary reactions are favoured leading to less liquid hydrocarbons. On the other hand, the larger particle sizes of CC sees primary devolatilization occurring for longer, up till 500°C, after which secondary and tertiary decomposition takes place as shown by the dip in liquid hydrocarbons productions between 500 and 600°C. The effect of pressure on the other hand was mostly negative for production of liquid hydrocarbons shown. This is to be expected as higher pressures and residences time implies more time for secondary decomposition reactions.

Figs. 7-8 and 7-9 also show the influence of operating parameters factors on yield of PAHs. The relatively higher p-values for LOF (Table 7-2) indicate the model's predictions are reasonably accurate for the range of temperature and pressure studied. It can be observed that pressure was more important for PAH yields than temperature, for both coal-BG and coal-CC blends. However, whereas the effect of pressure was positive on coal-BG blends, the opposite was true for coal-CC blends. PAHs constitute much of the heavy molecular hydrocarbons in tar [40]. A number of reaction pathways have been suggested for the production of PAHs. They may be formed via the decomposition of long chain aromatics within the coal structure [24]. PAHs can also be formed by Diels-Alder reaction [34,41] which involves aromatization and dehydrogenation of aliphatics liberated during coal devolatilization. PAHs can also be produced via the deoxygenation of phenols and cresols or via recombination of phenyl and other aromatic radicals [26,40,42]. Pressure/residence time and temperature have been known to have mixed effects on PAH production as reflected in these results. On the one hand, long residences times allow for the formation reactions described above leading to increased PAH

yields. On the other hand, severe pyrolysis conditions could lead to cracking of the phenyl rings into short chain aromatics which may be the case for the observed reduction in yields from coal-CC blends shown in Fig. 7-9. It may also be the case that PAHs production peaked quicker in coal-CC blends than in coal-BG blends. This may explain why increased residence times caused by elevated pressures led to increase in PAH production from coal-BG, in contrast to coal-CC.

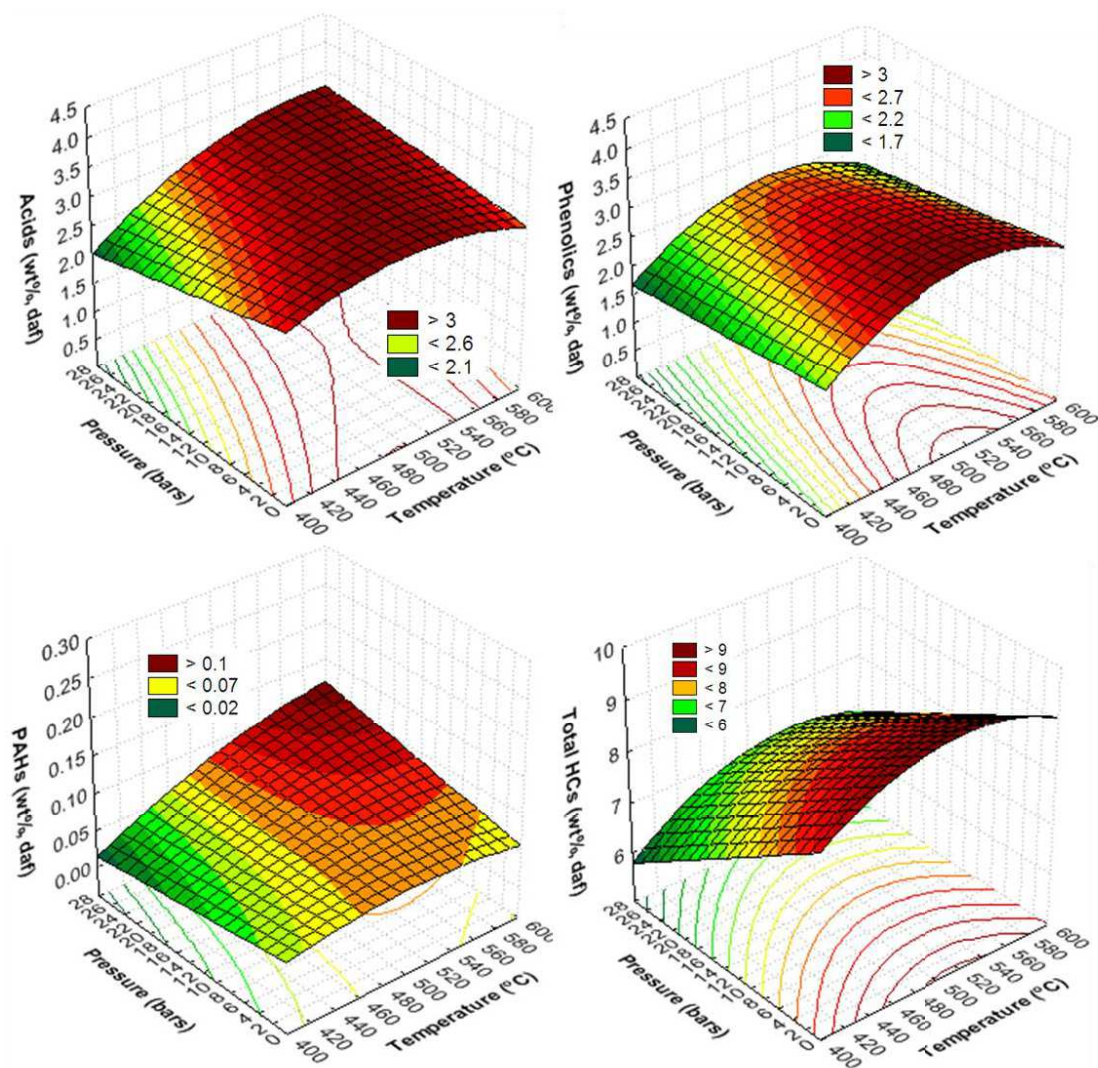


Figure 6-9: Influence of temperature and pressure on key aspects of liquids composition from 25 wt% CC blends

In the range of co-pyrolysis conditions employed in this work, product yields of the different condensate fractions and chemical groups revealed a generally much weaker dependence on process variables like temperature and pressure, compared to changes in the feedstock mix ratio. This implies that the impact of increasing the

biomass proportion in a coal-biomass mix on co-pyrolysis behaviour will be more significant than changes due to variation in process conditions between 1 and 26 bars and/or 400°C and 600°C. Nevertheless, some useful inferences can still be drawn on the influences of temperature and pressure on the co-pyrolysis process. Figs. 7-4, 7-8 and 7-9 show that, consistent with findings in the literature, temperature had a generally positive influence on the yields of the various liquid condensate fractions whilst pressure had a negative impact [14,43]. It is well known that as temperature increases during pyrolysis of a solid fuel, the yields of liquid products formed due to devolatilization increases up to a certain point, after which further heating will cause a reduction as more and more of the heavier volatiles are cracked into non-condensable gases [44]. The temperatures at which maximum liquid production occurs is generally higher for coal (600-700°C) than for biomass (300-500°C), although the exact values also depends on other factors such as feedstock type and particle size, reactor pressure, bed density, and residence time [14,43]. Fig. 7-8 demonstrates that in their respective blends with coal, the peak production of condensates occurs at a lower temperature for BG than for CC.

The effect of pressure on total condensate yield during devolatilization is generally negative as Fig. 7-8 confirms for both coal-BG and coal-CC feedstock blends. Pressure affects pyrolysis product yields in two important ways; mass transport and secondary reactions [32,45]. At high pressures, primary pyrolysis reactions are suppressed due to the restricted transport of volatiles from the site of formation to the surface of the fuel particle and into the bulk volatile phase. This is caused by the reduced pressure drop in the particle pores which occurs at elevated external pressures. The extended residence time of intra particle volatiles favours secondary reactions (tar cracking, char-forming) between volatiles that have already escaped leading to the increased production of lighter, more stable gas and solid products at the expense of the relatively less stable tar phase products [32].

It can also be observed that the various liquid fractions react differently to variations in temperature and pressure conditions. Whereas as Fig. 7-4 and Table 7-2 shows,

temperature had a higher significance level than pressure on total liquid yields, the yield of hydrocarbons represented by the tar fraction, as well as condensate groups such as acids, phenolics, and PAHs, showed the opposite trend. This means that pressure had the greater influence on the distribution of the fractions and chemical groups that make up the liquid condensates. Although it must be noted that both process based factors had overall very limited significance on these products. The main route by which pressure affects pyrolysis is to increase intra-particle and inter-particle residence times thereby allowing more time for vapour phase reactions [32,45]. This is largely consistent with the observation made earlier that the long residence times allowed by the conditions employed in the study which encouraged interactions which were sufficiently vigorous to affect the distribution of specific chemical components within the condensate phase.

6.7 Comments on synergistic behaviour

The present study demonstrates that the overall yields of chars, aqueous liquids, tar and gas products obtained from co-pyrolysis of coal with biomass of different particle sizes and structure, matched well with values calculated based on the absence of synergistic or additive effects, within experimental error. Many previous reports [3-6] based on experiments conducted mostly under atmospheric conditions show the same non-additive trend for volatile and char yields during co-pyrolysis. Indeed the same non-additive trend has been observed even between more closely mixed constituents such as maceral concentrates in coal [6,46-48] and lignocellulosic components in biomass [6]. This is in stark contrast to results of TGA experiments for the same samples where the effects of synergy were clearly observable [44]. This may be due to the more intimate mixing made possible by the micro-scale particles (<212 μm particles; 5-20 mg sample size) employed in the TGA experiments, compared to the macro-scale conditions (2-20 mm; 100 g) used in the present paper. At micro-scales, heat and/or mass transfer limitations are negligible thus posing no constraints to interactions between coal and biomass [47].

In contrast to lumped product yields, a distinct non-proportionality was observed between coal-biomass mix ratios and the observed yields of specific volatile species and functional groups such as H₂, CO, CO₂, CH₄, acids, furans, ketones, phenolics, PAHs and other mono and heterocyclic aromatics. This suggests the presence of significant chemical interactions in the vapour phase between volatiles obtained from the contributing feedstocks some of which were described in the previous section. For instance, the increase in acids was significantly beyond what would be expected assuming no interactions. There was also a comparably less drastic increase in the composition of total oxygenates at the various mix ratios, and a corresponding decrease in the percentage of mono and polycyclic aromatics. This trend is in agreement with previous observations by Jones et al. [1] in their study of the atmospheric, slow heating rate co-pyrolysis of coal and pinewood. PAHs from coal are mainly formed from the repolymerisation or cross-linking of liberated phenyl derivatives and other hydrocarbon radicals released during bond scission [14]. The reduction in PAH yields as a result of co-pyrolysis was likely due to the action of reactive oxygenated free radicals from biomass reacting with the unsaturated aromatics from coal and preventing them from recombining to form long chain hydrocarbons such as PAHs [1,27]. Table 7-3 also showed that on average, the yield of oxygenates (particularly acids and furans) and polycyclic aromatics deviate more severely from their predicted values at 95:5 than at 50:50 mix ratios. On initial inspection, this leads to the seemingly paradoxical conclusion that the severity of synergistic reactions is lower at higher biomass mix ratios. However, as Cao et al. [27] showed, the same oxygenated radicals that suppress PAH production are also in demand during secondary reactions of biomass vapours for the production of oxygenates. The balance between these two competing reactions is likely shifted towards the production of oxygenates at higher biomass composition in the feedstock mix and would explain why higher biomass mix ratios do not necessarily lead to higher levels of synergy in terms of PAH suppression [24,25]. There are numerous other such reactions during pyrolysis that highlights the complexity and heterogeneity of the process. The slow heating rate, fixed bed reactor design, and elevated pressure employed in this study ensures sufficiently

long residence times for these reactions to occur, further increasing the complexity of the process and reducing its predictability.

These observations may help to resolve the apparent contradiction in co-pyrolysis studies on whether or not there is synergy. Researchers who study the distribution of major products such as char, total liquids and gas tend to find no evidence of synergy [3-6] while those who study the composition of tars tend to conclude the opposite [1,2,50]. This study shows that this may be because while the vapour phase interactions outlined above are sufficiently significant to disrupt the proportionality expected between yields of specific volatile species and feedstock mix ratio (assuming no synergy), they do not seem to overtly influence phase equilibria or the overall distribution of gas, liquid and solid products. This is consistent with the common hypothesis made by a number of researchers that for engineering purposes, the distribution of lumped products (gases, liquids and solids) obtained from co-pyrolysis of coal and biomass can be reliably estimated based on the corresponding yields of the individual parent materials.

Effects of particle size differences and their influence on transport phenomena in the biomass fuels are also reflected in their behaviour when blended with coal during co-pyrolysis. It was observed from Fig. 7-5 that deviations between observed and predicted values were higher in coal-CC blends than in coal-BG blends, implying there is a higher level of non-additive or synergistic behaviour caused by vapour phase interactions in the former. The differences in the reaction of the various blends to increases in temperature as shown in the response surface plot for liquid and tar yields (Figs. 7-8 and 7-9 respectively) also reflect the differences in mass transfer rates in CC and BG particles. The different temperatures at which liquids are produced from the coal and BG fractions are visible on the coal-BG response plots. Substantial condensate production from coal starts at temperatures higher than 500°C when primary decomposition that produces condensates from BG is already nearly complete due to the more rapid devolatilization resulting from its smaller particle size. This was less obvious in the coal-CC plots where the larger particles of

CC ensures slower evolution rates of biomass (Chapter 6, Table 7-2) such that the evolution of liquids production rises steadily through the temperature range studied, thereby ensuring an almost uniform increase in liquid and tar production as temperature increases between 400°C and 600°C. Similar to liquid yields a curvature in the temperature axis of the tar yield response plots for coal-BG can also be observed in Figs. 7-8 and 7-9. The trend can again be explained by the smaller particle sizes of the BG fraction which ensure that volatile evolution rates occurred more rapidly than from CC. Consequently, the escaped volatiles are more readily cracked into lower molecular weight volatiles and gases as pyrolysis temperatures increase beyond 400°C. This behaviour combined with the fact that tar production from coal starts at higher temperatures (closer to 600°C) explains the dip in tar production between 400 and 600°C for Coal-BG blends. The larger CC particles release volatiles more slowly such that tar production rises steadily through the temperature range studied.

6.8 Conclusions

Results of investigation into the influence of mix ratio on pyrolysis yields show limited evidence of non-additive or synergistic behaviour on the overall distribution of solid liquid and gas yields. On the other hand, in terms of the distribution of specific liquid phase hydrocarbons, the evidence is in favour of synergistic pyrolysis behaviour. From these observations, it can be concluded that predicting the overall distribution of phases (solid liquid and gas products) from co-pyrolysis/co gasification is relatively straightforward according to a simple additive model. However, predicting specific gas and liquid compositions is a much harder task which cannot be predicted via additive models. The influence of temperature and pressure within the range of 400-600°C and 1-26 bars on the yield and composition of volatiles were also investigated via a factorial design. Elevated pressure generally led to lower liquid hydrocarbon yields while temperature had mixed effects depending on the biomass type in the blends.

6.9 References

- [1] J.M. Jones, M. Kubacki, K. Kubica, A.B. Ross, A. Williams, Devolatilisation characteristics of coal and biomass blends, *Journal of Analytical and Applied Pyrolysis*. 74 (2005) 502-511.
- [2] T. Sonobe, N. Worasuwannarak, S. Pipatmanomai, Synergies in co-pyrolysis of Thai lignite and corncob, *Fuel Processing Technology*. 89 (2008) 1371-1378.
- [3] C. Meesri, B. Moghtaderi, Lack of synergetic effects in the pyrolytic characteristics of woody biomass/coal blends under low and high heating rate regimes, *Biomass and Bioenergy*. 23 (2002) 55-66.
- [4] B. Moghtaderi, C. Meesri, T.F. Wall, Pyrolytic characteristics of blended coal and woody biomass, *Fuel*. 83 (2004) 745-750.
- [5] H. Rudiger, U. Greul, H. Spliethoff, K.R.G. Hein, Co-pyrolysis of Coal/Biomass and Coal/Sewage Sludge Mixtures in an Entrained Flow Reactor, APAS Clean Coal Technology Program. Volume 3, by European Commission, 1999.
- [6] A.G. Collot, Y. Zhuo, D.R. Dugwell, R. Kandiyoti, Co-pyrolysis and co-gasification of coal and biomass in bench-scale fixed-bed and fluidised bed reactors, *Fuel*. 78 (1999) 667-679.
- [7] Ž.R. Lazić, *Design of experiments in chemical engineering: a practical guide*, Wiley-VCH, 2004.
- [8] M.J. Antal, M. Gronli, The Art, Science, and Technology of Charcoal Production†, *Industrial & Engineering Chemistry Research*. 42 (2003) 1619-1640.
- [9] C. Di Blasi, G. Signorelli, G. Portoricco, Countercurrent Fixed-Bed Gasification of Biomass at Laboratory Scale, *Industrial & Engineering Chemistry Research*. 38 (1999) 2571-2581.
- [10] J.R. Bunt, J.P. Joubert, F.B. Waanders, Coal char temperature profile estimation using optical reflectance for a commercial-scale Sasol-Lurgi FBDB gasifier, *Fuel*. 87 (2008) 2849-2855.
- [11] D.K. Park, S.D. Kim, S.H. Lee, J.G. Lee, Co-pyrolysis characteristics of sawdust and coal blend in TGA and a fixed bed reactor, *Bioresource Technology*. Article in Press (n.d.).
- [12] H. Jüntgen, Review of the kinetics of pyrolysis and hydrolysis in relation to the chemical constitution of coal, *Fuel*. 63 (1984) 731-737.
- [13] F. Behrendt, Y. Neubauer, M. Oevermann, B. Wilmes, N. Zobel, Direct Liquefaction of Biomass, *Chemical Engineering & Technology*. 31 (2008) 667-677.
- [14] H. Heidecke, H.H. Oelert, L.H. Xiong, Copyrolysis and coliquefaction of blended mixtures from hardcoal, municipal waste and petroleum residue, *Erdoel Erdgas Kohle/EKEP*. 106 (1990) 456-460.
- [15] R. Kandiyoti, A.A. Herod, K.D. Bartle, Liquefaction: Thermal Breakdown in the Liquid Phase, in: *Solid Fuels and Heavy Hydrocarbon Liquids*, Elsevier Science Ltd, Oxford, 2006: pp. 161-198.
- [16] B.N. Kuznetsov, V.I. Sharypov, S.A. Kuznetsova, V.E. Taraban'ko, N.M. Ivanchenko, The study of different methods of bio-liquids production from wood biomass and from biomass/polyolefine mixtures, *International Journal of Hydrogen Energy*. 34 (2009) 7051-7056.

- [17] R. Malhotra, Direct Coal Liquefaction: Lessons Learned, in: Proceedings of the GCEP Advanced Coal Workshop, Morgantown, WV, USA, 2005.
- [18] R.H. Williams, E.D. Larson, A comparison of direct and indirect liquefaction technologies for making fluid fuels from coal, *Energy*. 103 (2003).
- [19] Y.G. Pan, E. Velo, L. Puigjaner, Pyrolysis of blends of biomass with poor coals, *Fuel*. 75 (1996) 412-418.
- [20] C. Storm, H. Rüdiger, H. Spliethoff, K.R.G. Hein, Co-pyrolysis of coal/biomass and coal/sewage sludge mixtures, *Journal of Engineering for Gas Turbines and Power*. 121 (1999) 55-63.
- [21] L. Zhang, S. Xu, W. Zhao, S. Liu, Co-pyrolysis of biomass and coal in a free fall reactor, *Fuel*. 86 (2007) 353-359.
- [22] K.H. Van Heek, W. Hodek, Structure and pyrolysis behaviour of different coals and relevant model substances, *Fuel*. 73 (1994) 886–896.
- [23] W. Hodek, J. Kirschstein, K.H. van Heek, Reactions of oxygen containing structures in coal pyrolysis, *Fuel*. 70 (1991) 424–428.
- [24] R.J. Evans, T.A. Milne, Molecular characterization of the pyrolysis of biomass, *Energy and Fuels*. 1 (1987) 123-137.
- [25] Q. Cao, L. Jin, W. Bao, Y. Lv, Investigations into the characteristics of oils produced from co-pyrolysis of biomass and tire, *Fuel Processing Technology*. 90 (2009) 337–342.
- [26] B. Moghtaderi, The state-of-the-art in pyrolysis modelling of lignocellulosic solid fuels, *Fire and Materials*. 30 (2005) 1–34.
- [27] S. Rodjeen, L. Mekasut, P. Kuchontara, P. Piumsomboon, Parametric studies on catalytic pyrolysis of coal-biomass mixture in a circulating fluidized bed, *Korean Journal of Chemical Engineering*. 23 (2006) 216-223.
- [28] C. Li, K. Suzuki, Resources, properties and utilization of tar, *Resources, Conservation and Recycling*. 54 (2010) 905-915.
- [29] D.L. Klass, Thermal Conversion: Pyrolysis and Liquefaction, in: *Biomass for Renewable Energy, Fuels, and Chemicals*, Academic Press, San Diego, 1998: pp. 225-269.
- [30] W.S.-L. Mok, M.J. Antal, Effects of pressure on biomass pyrolysis. I. Cellulose pyrolysis products, *Thermochimica Acta*. 68 (1983) 155-164.
- [31] P. Arendt, K.-H. van Heek, Comparative investigations of coal pyrolysis under inert gas and H₂ at low and high heating rates and pressures up to 10 MPa, *Fuel*. 60 (1981) 779-787.
- [32] M.E. Sánchez, J.A. Menéndez, A. Dominguez, J.J. Pis, O. Martinez, L.F. Calvo, et al., Effect of pyrolysis temperature on the composition of the oils obtained from sewage sludge, *Biomass and Bioenergy*. 33 (2009) 933–940.
- [33] P.A. Horne, P.T. Williams, Influence of temperature on the products from the flash pyrolysis of biomass, *Fuel*. 75 (1996) 1051–1059.
- [34] C. Brage, Q. Yu, G. Chen, K. Sjöström, Tar evolution profiles obtained from gasification of biomass and coal, *Biomass and Bioenergy*. 18 (2000) 87-91.
- [35] P.F. Britt, A.C.I.I.I. Buchanan, E.A. Malcolm, Thermolysis of Phenethyl Phenyl Ether: A Model for Ether Linkages in Lignin and Low Rank Coal, *The Journal of Organic Chemistry*. 60 (1995) 6523–6536.
- [36] G. Couch, Coal to liquids, IEA Clean Coal Centre, 2008.

- [37] R. Hayatsu, R.E. Botto, R.G. Scott, R.L. McBeth, R.E. Winans, Evaluation of lignin and cellulose contributions to low-rank coal formation by alkaline cupric oxide oxidation, *Fuel*. 65 (1986) 821-826.
- [38] T. McGrath, R. Sharma, M. Hajaligol, An experimental investigation into the formation of polycyclic-aromatic hydrocarbons (PAH) from pyrolysis of biomass materials, *Fuel*. 80 (2001) 1787-1797.
- [39] K. Unapumnuk, A Study of the Pyrolysis of Tire Derived Fuels and an Analysis of Derived Chars and Oils, PhD Thesis, University of Cincinnati, 2006.
- [40] R.K. Sharma, M.R. Hajaligol, Effect of pyrolysis conditions on the formation of polycyclic aromatic hydrocarbons (PAHs) from polyphenolic compounds, *Journal of Analytical and Applied Pyrolysis*. 66 (2003) 123-144.
- [41] C. Zaror, D. Pyle, The pyrolysis of biomass: A general review, *Sadhana*. 5 (1982) 269-285.
- [42] C. Di Blasi, G. Signorelli, C. Di Russo, G. Rea, Product Distribution from Pyrolysis of Wood and Agricultural Residues, *Industrial & Engineering Chemistry Research*. 38 (1999) 2216-2224.
- [43] H. Chen, Z. Luo, H. Yang, F. Ju, S. Zhang, Pressurized Pyrolysis and Gasification of Chinese Typical Coal Samples, *Energy & Fuels*. 22 (2008) 1136-1141.
- [44] C.-Z. Li, K.D. Bartle, R. Kandiyoti, Characterization of tars from variable heating rate pyrolysis of maceral concentrates, *Fuel*. 72 (1993) 3-11.
- [45] A. Megaritis, R.C. Messenböck, I.N. Chatzakis, D.R. Dugwell, R. Kandiyoti, High-pressure pyrolysis and CO₂-gasification of coal maceral concentrates: conversions and char combustion reactivities, *Fuel*. 78 (1999) 871-882.
- [46] J. Duxbury, Prediction of coal pyrolysis yields from BS volatile matter and petrographic analyses, *Fuel*. 76 (1997) 1337-1343.
- [47] Aboyade, J. Gorgens, M. Carrier, E.L. Meyer, J.H. Knoetze, Thermogravimetric study of the devolatilization characteristics and kinetics of coal blends with corn and sugarcane residues, *Fuel*. (2011).
- [48] I. Suelves, R. Moliner, M.J. Lázaro., Synergetic effects in the co-pyrolysis of coal and petroleum residues: influences of coal mineral matter and petroleum residue mass ratio, *Journal of Analytical and Applied Pyrolysis*. 55 (2000) 29-41.

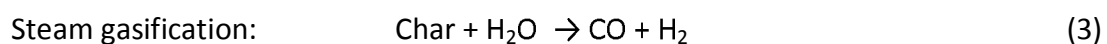
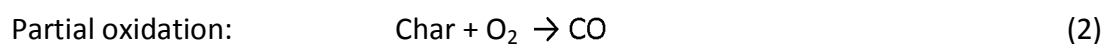
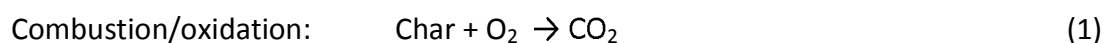
7 Gasification process modelling and economics

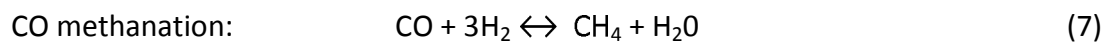
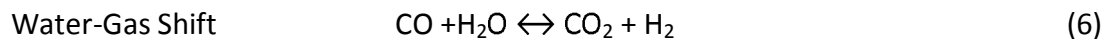
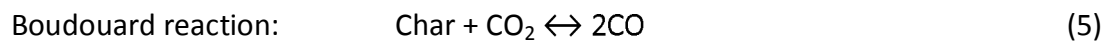
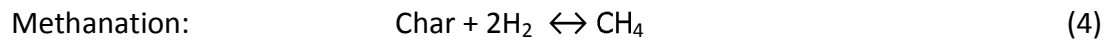
This chapter reports on the investigation of the thermal characteristics of char obtained from previously reported pressurized pyrolysis experiments. Also, a semi-empirical ASPEN model was developed to simulate gasification performance based partly on the char and volatiles characterization results, and on equilibrium modelling principles. Simulation results from the model informed an economic evaluation of the impact of co-gasification on syngas production costs.

7.1 Introduction

The possibility of co-gasifying of alternative feedstock with coal has received a lot of attention in recent decades as it offers a realistic approach to reducing GHG emissions, while diversifying fuel supply options [1–5]. Gasification of any solid feedstock (coal, petroleum coke, municipal waste or plant biomass) comprises of two main process steps – pyrolysis and conversion of residual chars in gasification reactions [6]. Pyrolysis takes place in parallel with drying of the feedstock and usually occurs in the 300-800°C range, resulting of the decomposition of the feedstock into solid, liquid and gas phase components. Results from the study of pyrolysis behaviour of the fuels used in this thesis – obtained under conditions relevant to industrial updraft gasification – were presented in Chapters 3-7. Chapters 6 and 7 in particular give the composition and yields of devolatilized products. Those results show that about 15 wt% of coal and 70 wt% of biomass are devolatilized during the pyrolysis process.

Pyrolysis is followed by the conversion of solid char products via a number of combustion and gasification reactions (eqns 1-7 [6]).





In practice, gasification generally occurs at temperatures (800-1300°C) high enough to minimize the effect of kinetic barriers [7]. Consequently, thermodynamic models based on the assumption of chemical equilibrium has often been successively employed to predict the gasification performance of both coal and biomass feedstock [8,9]. This has been done for a variety of gasifier types including entrained flow [10], fluidized bed [11], downdraft [12] and updraft reactors [13,14]. Equilibrium modelling is based on either stoichiometric or non-stoichiometric approaches. In the former approach, product yields are calculated from the stoichiometric reaction mechanism involved in the gasification process (eqns 1-7). The non-stoichiometric approach minimizes the Gibbs free energy of the system without specifying any particular reaction mechanism [11,12,15]. As have been previously shown, the two approaches give essentially equivalent results [15].

In this chapter, the non-stoichiometric equilibrium approach was applied to simulating the updraft gasification of coal, and blends of coal with corn cobs and sugarcane bagasse. In updraft gasifiers, only the char comes into contact with the oxidant as the volatiles would have been released higher up the gasifier. This is in contrast to fluidized and entrained flow reactors where both volatiles and char are oxidised [6]. As a result particular attention has been paid to assessing the thermal characteristics and reactivity of residual chars obtained from previous pyrolysis and co-pyrolysis experiments. The observed char properties, combined with yield distribution results from previous chapters are provided as inputs to an Aspen Plus model designed to simulate updraft gasification conditions.

7.2 Material and Methods

7.2.1 Char characterisation.

Chars of coal, sugarcane bagasse (BG) and corn cobs (CC) and their blends (at 95:5 and 50:50 mix ratios) obtained from pressurized pyrolysis experiments described in Chapter 6 were used. Representative char sub-samples for experiments were obtained according to CEN/TS 14780/2005 [16]. C, H, and N contents in the samples were determined according to ASTM D5373 [17]. Sulphur was determined according to ASTM D4239 [18]. Higher heating value was determined using BS EN 14918:2009 [19], while proximate analysis was conducted according to ASTM E1131 [20]. The results of the ultimate and proximate analyses for the samples used are presented in Table 8-1.

Table 7-1: Proximate and ultimate parameters of pyrolysis chars

Properties	BG Char	CC Char	Coal char
Ultimate analysis (wt%, daf)			
C	82.9	75.8	82.6
H	0.6	1.5	2.0
N	1.0	0.9	2.5
S	0.2	0.1	1.0
O ¹	15.5	21.9	12.2
HHV (MJ/kg)²	21.9	25.0	15.7
Proximate analysis (wt%)			
Initial moisture	0.9	1.2	0.7
Volatiles	9.1	10.6	12.0
Fixed Carbon	69.7	85.0	43.0
Ash	20.2	3.2	44.3

¹ obtained by difference

²Calculated via correlation with elemental values using the formula [5]:

$$\text{HHV} = 0.3491 * \text{C} + 1.1783 * \text{H} + 0.1005 * \text{S} - 0.1034 * \text{O} - 0.0151 * \text{N} - 0.0211 * \text{Ash}$$
(MJ/kg)

7.2.2 Char reactivity measurements

The CO₂ gasification reactivity of the char that was measured at isothermal condition by using a Mettler Toledo TGA/DCS 1 analyzer. The char samples were milled to particle sizes less than 200 μm. In an inert atmosphere of pure N₂, the char was heated from ambient temperature to 1200°C at a heating rate of 20°C min⁻¹ and

maintained at the temperature for 20 minutes to ensure complete drying and devolatilization of remnant volatiles. Thereafter the samples were cooled to the test temperature of 1000°C and the purge gas was switched to the reactive CO₂ gas flowing at 150 ml min⁻¹. The char was gasified until constant weight was achieved. Runs were repeated at least twice to ensure reproducibility. From the mass versus time data, conversion X, for each run was calculated as;

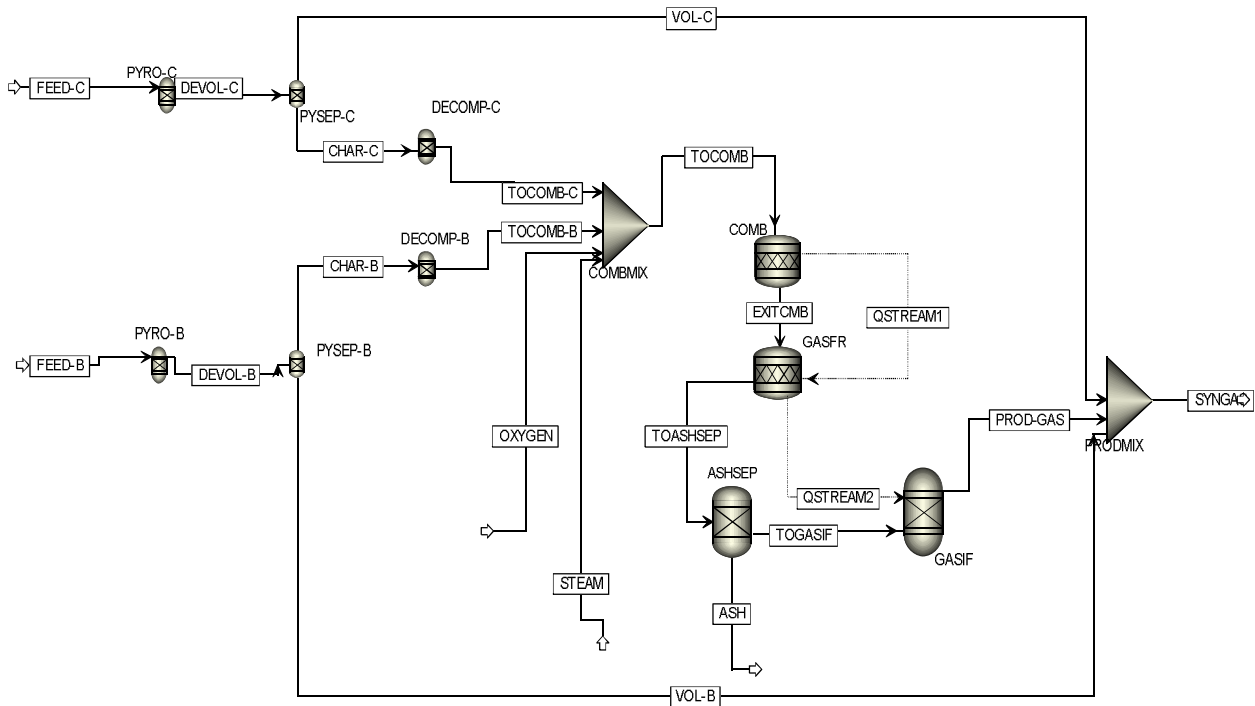
$$X = \frac{w_o - w_i}{w_o - w_{ash}}$$

where w_o , w_i and w_{ash} are the initial, instantaneous, and final mass values respectively. The instantaneous reactivity R_i was calculated using the formula;

$$R_i = \left(-\frac{dw_i}{dt} \right) / (w_i - w_{ash})$$

7.2.3 Aspen Plus modelling

An updraft, dry bottom (i.e non-slugging), fixed bed gasifier was modelled in Aspen Plus®, based on the thermodynamic equilibrium approach for char gasification, combined with empirical pyrolysis data. A block diagram of the model is shown in Fig. 8-1. The empirically based pyrolysis section was based on product yield data obtained from the previous sections, and the equilibrium modelling section simulated the equilibrium gasification of residual char leaving the pyrolysis zone. Residual char move downwards in an updraft gasifier countercurrent to meet the hot gases rising into the gasification and combustion zones. Properties such as volume, entropy, fugacity coefficients and Gibbs free energy for each component were based on the Redlick-Kwong-Soave equation of state [21,22]. Aspen Plus differentiates between conventional and non-conventional streams. Conventional streams comprise fluids defined as MIXED stream and pure solids (defined as CISOLIDS). Non-conventional streams such as coal, biomass, char, and ash cannot be processed directly in phase or chemical equilibrium calculations. In order to simulate non-conventional streams, the user must input details of the stream composition such as ultimate analysis, proximate analysis and sulphur analysis [23].



7-1: ASPEN PLUS model flowsheet

At the top of the updraft gasifier the feedstock is dried and devolatilized by the hot rising gases from the bottom. This section is represented by the blocks, DEVOL-C and DEVOL-B for the coal and biomass feedstock respectively. These devolatilization blocks are fed by the streams Feed-C and Feed-B. Coal-biomass mix ratio is controlled by a block where the user can set the biomass fraction from any value between 0 and 1. These RYIELD blocks simulate the drying and devolatilization of the feedstock into water, gases (CO, CO₂, CH₄, H₂), tarry phase liquids (naphtha, cresol, phenol), aqueous phase liquids (acetic acid, acetone), and char. The distribution of these devolatilization products were based on previously experimentally determined values presented in Chapter 6. It was assumed that the product distribution from devolatilization and subsequent char gasification of blends followed an additive rule, i.e. are the result of the weighted addition of the contributing coal and biomass values. As was previously shown in Chapter 7, synergistic interactions between coal and biomass during co-pyrolysis do not significantly influence the distribution of

lumped products (i.e gases, solids, aqueous and non- aqueous phase liquids) from their blends.

Table 7-2: Properties of Kentucky No. 9 coal [21]

Ultimate analysis (wt%, as received)	
C	59.6
H	5.3
N	1.2
S	3.5
O	15.0
Proximate analysis (wt%)	
Moisture	8.2
Fixed Carbon	43.4
Volatile Matter	33.0
Ash	15.4

Separators (PYSEP-C and PYSEP-B) remove the char (via streams CHAR-B and CHAR-C) from the volatiles (streams VOL-C and VOL-B) and sends the former to the combustion and gasification sections which are modelled in the following manner. The RYIELD reactors, DECOMP-C and DECOMP-B break down the chars into their elemental components and ash. The distribution of char into these components is achieved by means of the FORTRAN subroutine F-DECOMP based on ultimate and proximate analyses of the chars given in Table 8-1. The broken down char components from both biomass and coal fractions are mixed with the oxygen and steam reactants in COMBMIX before being passed to the RSTOIC reactor, COMB for combustion. Partial oxidation of the chars carbon content converts 100% of the oxygen feed to produce CO and CO₂ according to eqn (1) and (2). Combustion products are then passed to GASFR, where unreacted carbon undergoes steam gasification (eqn 3) and the Boudouard reaction (eqn 5), such that 90% of the CO₂ and 50% of the steam is converted [22]. The separator block ASHSEP removes the ash and sends the fluid components to the RGIBBS reactor GASEQUIL for equilibration based on the gas phase reactions shown in eqns (6) and (7). Product gas from GASEQUIL proceeds to the mixer, PRODMIX where they are combined with pyrolysis volatiles from PYSEP-C and PYSEP-B, to form the raw syngas.

Experimental conditions and results from a FBDB gasifier obtained from a previous study by Barker et al. [21] were used to calibrate the model. Kentucky No. 9 coal was used in that study with properties as shown in Table 8-2. A comparison of the results of the experimental and predicted gasifier outputs is given in Table 8-3. The results show that predictions reasonably matched actual gasifier output, especially considering that the elemental composition of tar from the gasifier (representing 5.6% of the dry and ash free coal [21]) was unknown and had to be assumed. Further details of the model and parameters used for each block can be found in Appendix A.

Table 7-3: Comparing actual gasifier outputs with model predictions

	Experimental [21]	This study
<u>Inputs</u>		
Oxygen/Feed kg/kg,daf)	0.413	0.413
Steam/Feed (kg/kg,daf)	1.66	1.66
Pressure (bars)	32	32
<u>Dry syngas composition (mol %)</u>		
H ₂	40.80	44.09
CO	15.90	16.11
CO ₂	30.60	28.47
CH ₄	9.40	9.34
C ₂ +	0.90	0.00
N ₂	0.90	0.79
H ₂ S	1.50	1.19

7.3 Results and Discussion

This section is divided into three main parts, results of the char characterisation and reactivity, results of the ASPEN gasification modelling and lastly an evaluation of the economics of syngas production based on results of the simulation.

7.3.1 Char properties and reactivity

Fig. 8-2 is a graphical illustration of the proximate analysis of chars relative to the raw feedstock properties. As expected a higher fraction of volatile matter was removed from the biomasses (CC and BG) than from coal during the pyrolysis. In coal, the reduced amounts of volatiles and fixed carbon found in the residual char

suggest that the pyrolyzed fraction was derived from both the volatiles and fixed carbon contents of the raw feedstock. In biomass however, the volatile content in the raw fuels was mainly responsible for weight loss during pyrolysis. In coal, part of the fixed carbon is also consumed during pyrolysis, such that its percentage contribution to the total dry mass drops from 43 wt% before pyrolysis (i.e. in the raw fuel) to 33 wt% afterwards (Fig. 8-2). There is on the other hand, a relative increase in fixed carbon content after pyrolysis in biomass (7-21 wt% for BG and 16-25 wt% for CC) which may indicate the extent of char forming secondary reactions of the devolatilized vapours in these materials. This is consistent with the view expressed in previous chapters that secondary reactions were more prominent in BG, followed by CC and then coal (Section 6.6.2 and 6.7). A slight reduction in the proportion of ash was also observed for the chars, which may be attributed to experimental error.

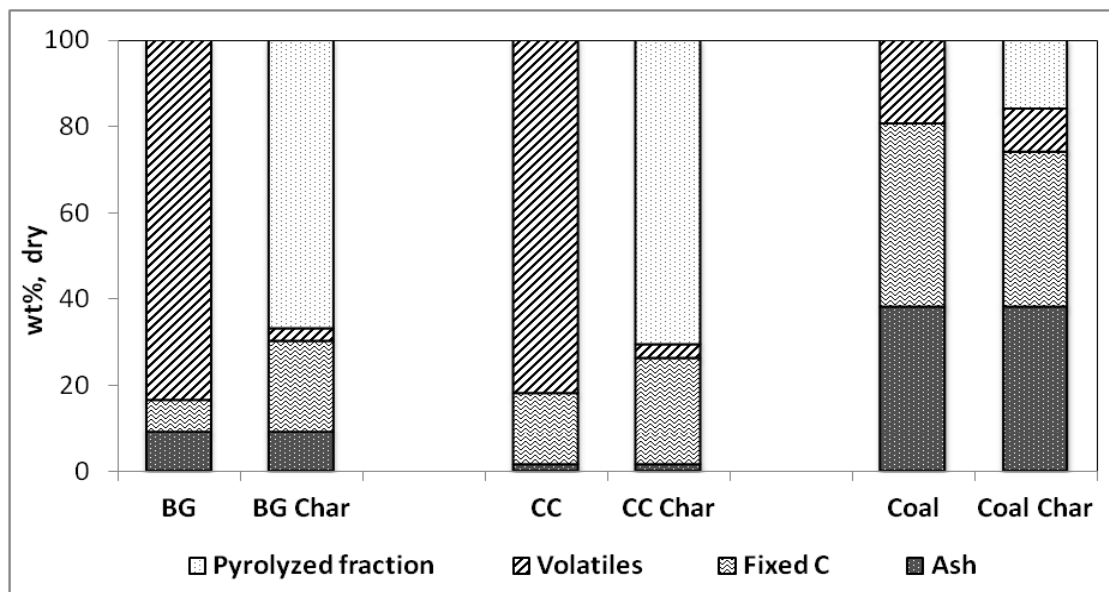


Figure 7-2: Comparing proximate analysis of raw fuels and their chars (obtained at 600°C and 26 bars)

Fig. 8-3 shows the effect of blending on the proximate analyses of the chars. Fixed carbon increased by 2 wt% and 10 wt% upon the addition of 5 wt% and 50 wt% BG and by 5 wt% and 15 wt% for the corresponding coal-CC mix ratios. The fixed carbon and volatile matter content generally follows an additive trend as indicated by the closeness between experimental and calculated values. Calculated results were based on the weighted sum of values for the individual contributing feedstock (see

section 7.3.1). This provides justification for treating char gasification of coal-biomass blends as a function of the mix ratio (by mass) as previously suggested by other authors [24,25].

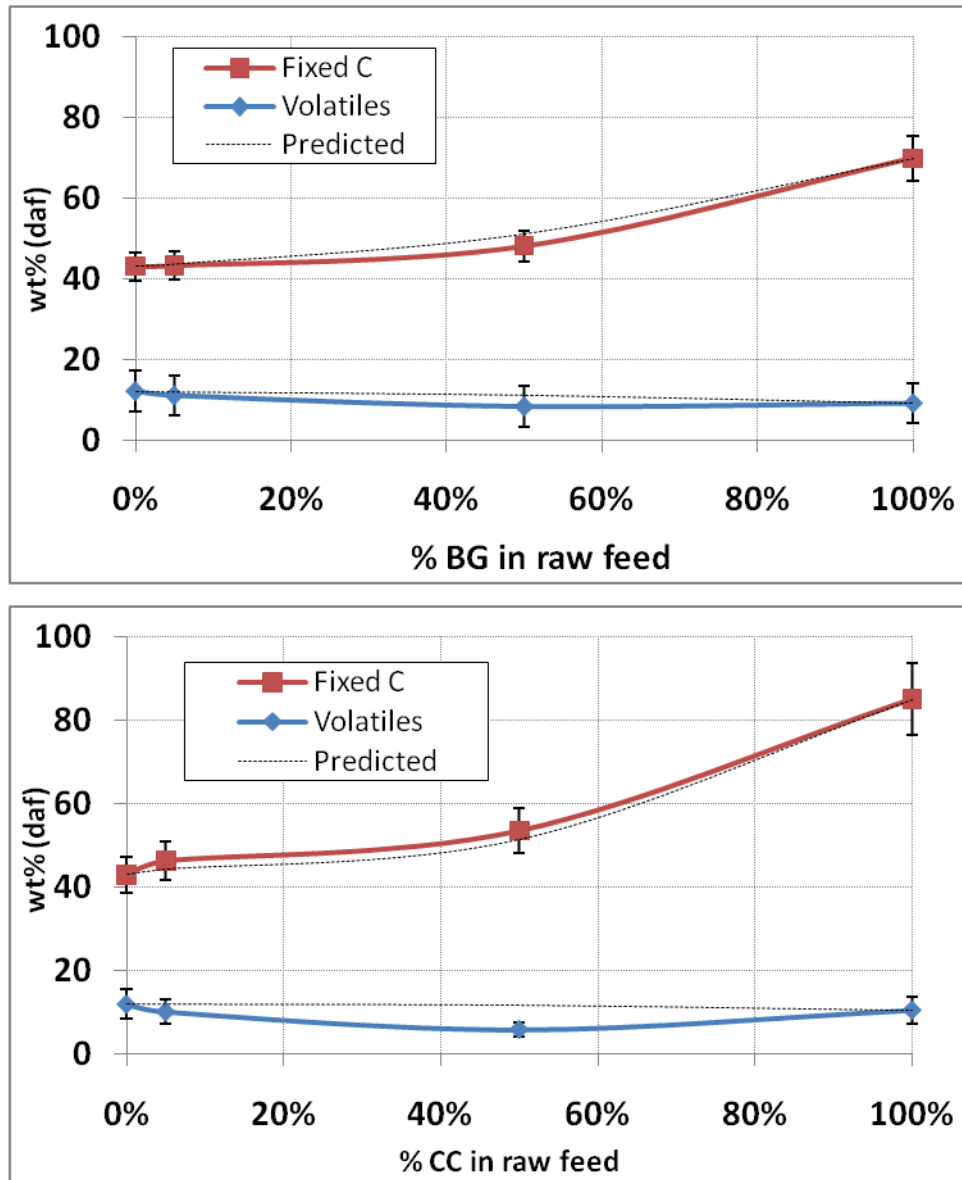


Figure 7-3: Influence of blending on proximate analysis results of coal-BG and coal-CC chars (Fixed-C = Fixed Carbon)

Conversion versus time graphs obtained from CO₂ gasification reactivity measurements of the single fuel and blends chars at 1000°C, are shown in Fig 8-4. It is recognized that char reaction with steam (eqn 3) also takes place during the FBDB gasification. Steam gasification, like CO₂ gasification, is a function of structural

properties such as the surface area and porosity, and the intrinsic reactivity dependant on the surface chemistry and catalytic effect of the inorganic compounds [53]. In this work however, only CO₂ gasification reactivities are presented.

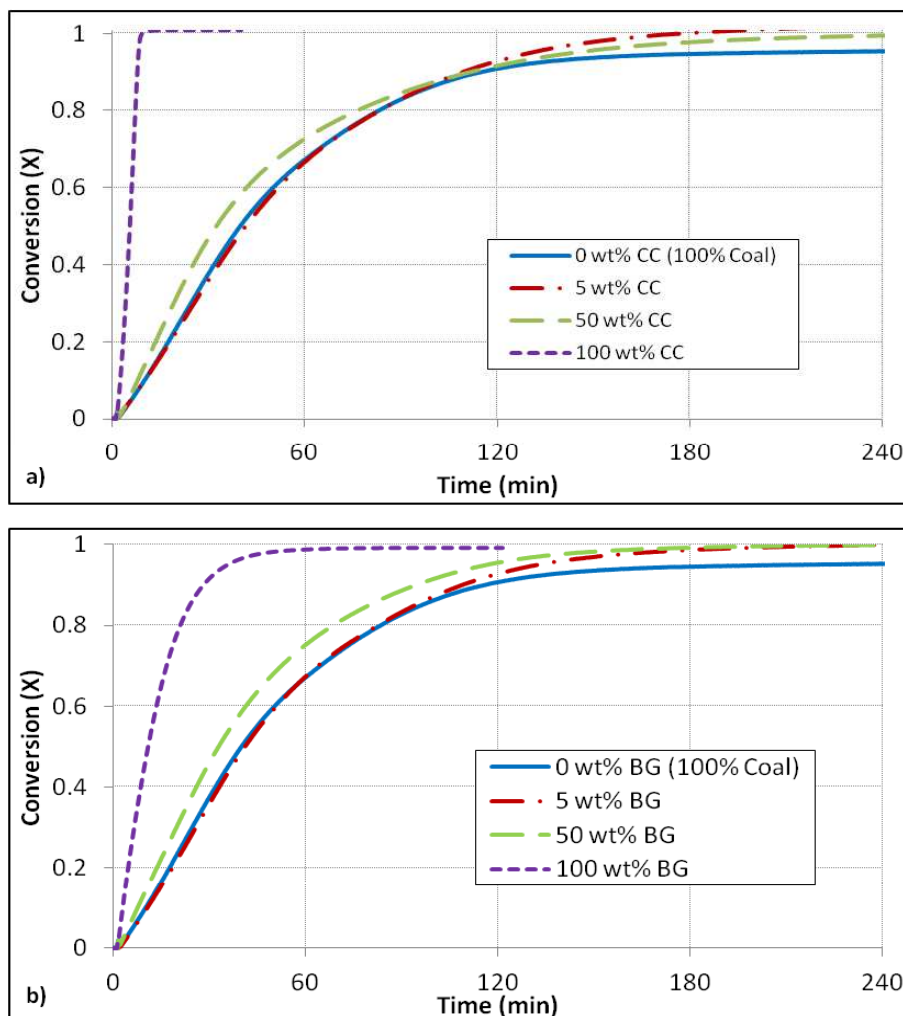


Figure 7-4: Conversion-time plots for Coal-BG and Coal-CC char blends

The figures illustrate that complete conversion of the biomass chars in reaction with CO₂ is achieved in less than 1 hour compared to over 4 hours for coal. The changes in instantaneous gasification reactivity with conversion are depicted in Fig 8-5. Reactivity in CC is about one order of magnitude greater than for BG and Coal. Also a drastic increase of reactivity can be observed as conversion proceeds in CC chars, compared to BG and coal where reactivity remained relatively constant for a while before dropping off towards the tail end of conversion.

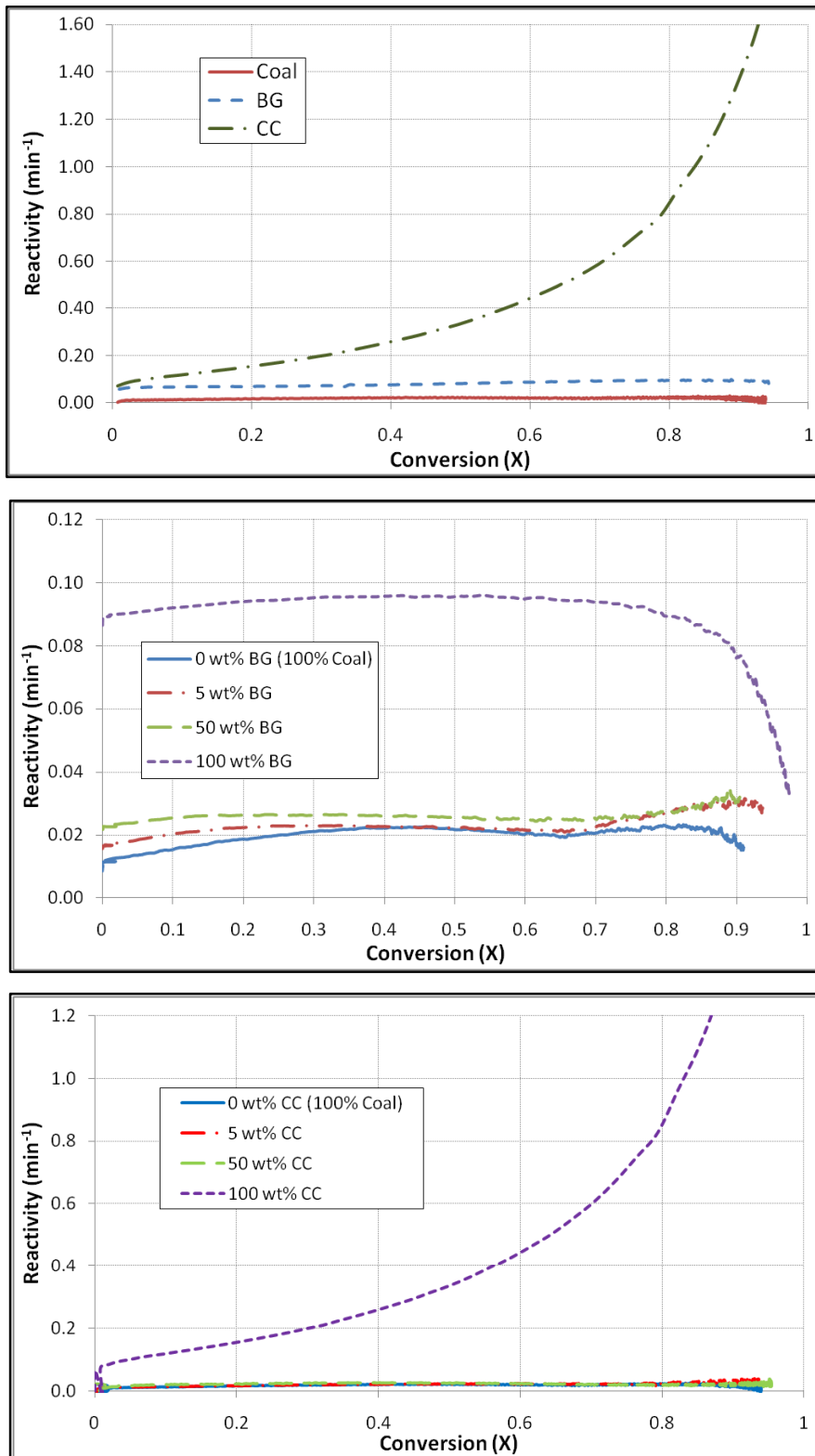


Figure 7-5: Instantaneous gasification rates versus conversion for single fuels as well as Coal-BG and Coal-CC char blends

The increase in char reactivity in CC could be the result of pore enlargement as the gasification reactions occurred, causing successively more active sites to be accessible for heterogeneous gas-char reactions to take place [28]. However, as Di Blasi et al. [27] cautioned, care must be taken in interpreting shape of the reactivity curves of biomass chars because of the absence of a regularity in their structure, compared to coal chars.

The results further show that the reactivity of char blends, even at 50:50 mix ratios, was close to that of pure coal char. This is to be expected because, based on yield distributions reported in Chapter 6, it can be estimated that 97-98% and 70-80% (dry and ash free mass) of the blended char at 95:5 and 50:50 mix ratio is coal derived. In other words, a disproportionately large part of the char from blended fuels is derived from coal, since most of the biomass material is removed in the devolatilization zone. These results suggest that the addition of biomass to coal does not impose any kinetic limitation on the gasification of blended chars, rather the blended char decomposes at approximately the same rate as 100% coal chars. Steam gasification is known to be affected by the same factors that affect CO₂ gasification; as such it can be assumed that the behaviour described above can be considered a reasonable qualitative indication of steam gasification [27].

7.3.2 Gasification modelling

The mass and energy balance obtained for modelling the coal samples in this study is presented in Fig. 8-6. The modelling was based on gasifier capacity of 44.4 t/hr, corresponding approximately to the capacity of a MK IV Sasol FBDB reactor [6], or the BGL² 1000 gasifier [29]. Steam-to-oxygen to feedstock ratios were targeted at levels required to produce FT grade syngas (H₂/CO ratio of approximately 1.8 [30]).

The ASPEN model used was based on the assumption that char gasification occurred under thermodynamic equilibrium. The model did not take into account the kinetics

² British Gas Lurgi gasifier - the slagging version of the Sasol-Lurgi fixed bed gasifier

of the process, although as previously shown from char characterization section, the presence of biomass in char does not significantly change the kinetics of gasification at fractions up to 50 wt%. The previous section also showed that the behaviour of char blends did not deviate significantly from the weighted average of the corresponding properties of the contributing fuels. Consequently, the gasification performance of blends was modelled based on the weighted average of previously described pyrolysis properties of coal and CC. The input conditions are shown in Table 8-4, along with key model outputs, some of which has been illustrated in Fig. 8-6. Steam-to-oxygen ratios were kept constant for all blend ratios, at levels required for 100% coal.

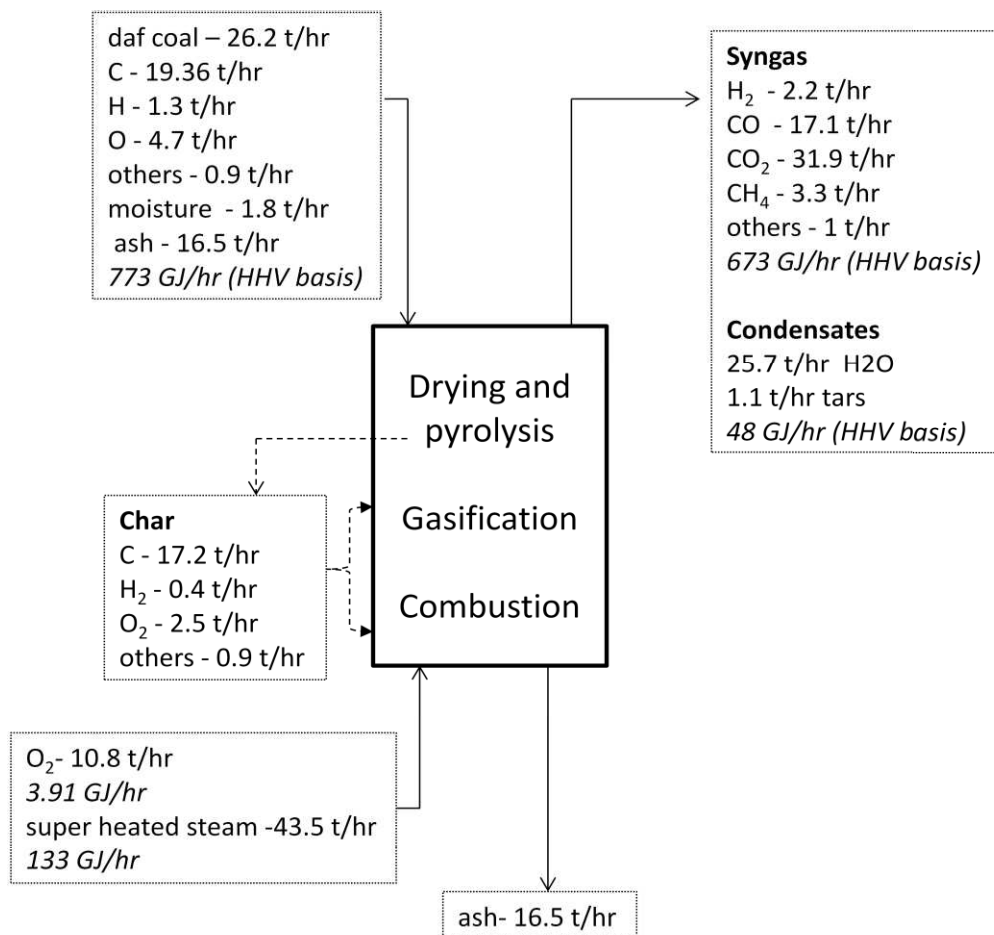


Figure 7-6: Simulated mass and energy flows for gasification of 100% coal feedstock

Results show a generally non-linear relationship between the percentage (by mass) of biomass in the gasification feedstock, and the distribution of syngas products. This is a reflection of the view that the composition of syngas is a function of many variables including combustion and gasification zone temperatures, relative abundance of oxygen and steam, and the elemental composition of the feedstock. As biomass fraction in the feedstock was increased, the fraction of CO₂ in the syngas also increased, while that of H₂ showed an overall decrease. As Fig. 8-7 illustrates, the decrease in H₂ coincides with an increase in CH₄, in agreement with results from other co-gasification studies based on different fuel and gasifier configurations [31–33]. This trend is likely to be partly caused by the successively net lower quantities of elemental hydrogen entering the reduction zone (due to the significantly lower charring rates of biomass). Furthermore, it is generally considered that production of H₂ and CH₄ are inversely linked via the CO methanation reaction in which CO reacts with H₂ to form CH₄ and water (eqn 7) [6].

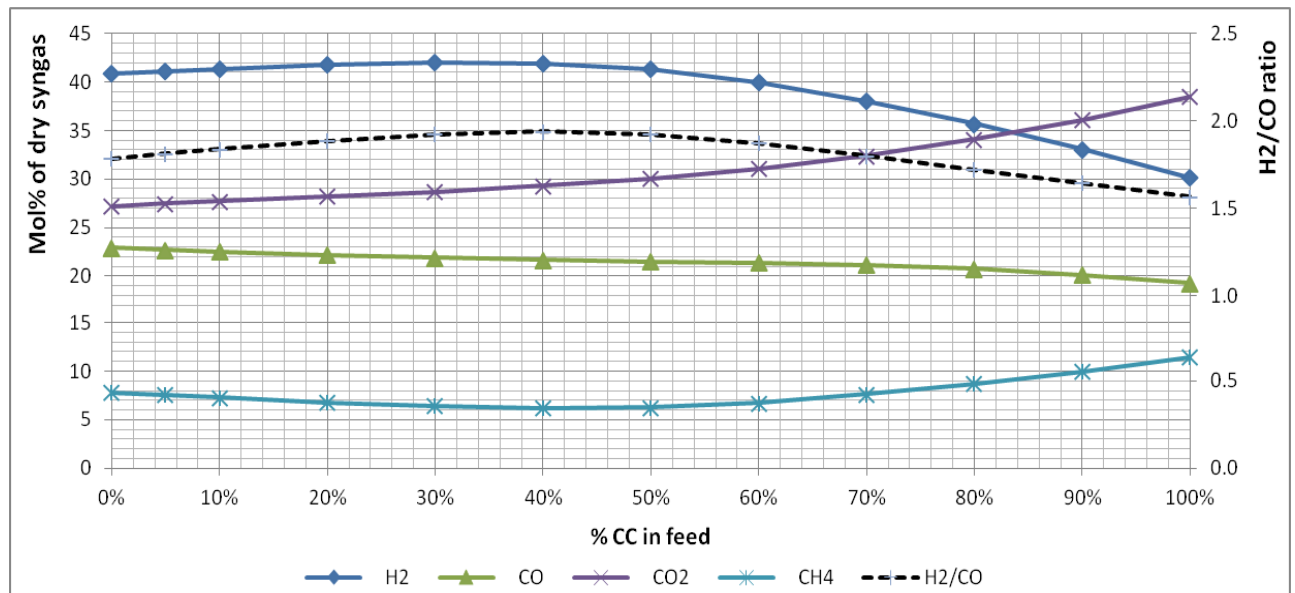


Figure 7-7: Influence of Coal-CC blend ratio on raw syngas composition and H₂/CO ratio

The addition of biomass also caused an increase in the combustion and gasification zone temperatures (1250°C to 1470°C from 0 to 100% biomass increase), as Table 8-4 further shows. The maximum reaction temperature is a key aspect of the non-

slagging gasifier performance, mainly in respect to the ash fusion temperatures and the occurrence slagging and ash sintering. The addition of superheated steam during the gasification process helps to moderate the temperature in the combustion zone, and is the reason why non-slagging fixed bed gasifiers such as the Sasol FBDB gasifier on which this study is modelled, generally require higher steam/feedstock ratios compared to the slagging versions [6,34]. The observed increase in reaction temperature was due to the increased availability of oxygen relative to char, leading to a higher propensity for complete combustion that produces CO₂ (compared to partial combustion which produces CO). The relatively low melting temperatures in biomass ashes (700-1000°C) compared to coal derived ash (1200-1700°C [34]), means that more quantities of steam will be required to moderate temperatures of the combustion zone when biomass is included as fuel.

The increased occurrence of complete combustion during biomass gasification may partly explain the increase in CO₂ concentrations at higher levels of biomass in the feedstock. However, a more likely explanation for the increase in CO₂ composition in the raw syngas at higher biomass/coal ratios is that, increasing the proportion of biomass in the feed led to a reduction in available carbon for gasification, in favour of the production of liquid hydrocarbons, water and pyrolysis gases from the preceding devolatilization step. Another cause of the increase in CO₂ production could be the reaction between CO and the extra oxygen made available through the addition of biomass, to form CO₂ [21]. Fig. 8-7 shows that the impact of biomass addition on the H₂/CO ratio was not very significant, although as Table 8-4 shows, the production of higher value gases (H₂, CO, CH₄) falls from 23 t/hr 100% coal to 19 t/hr at 50:50 mix ratio along with a matching increase in water and CO₂. This caused a corresponding decrease in the heating value of syngas from 12 MJ/kg to 11 MJ/kg. This also led to a reduction in the thermal efficiency of syngas production from 87% to 73% at 0:100 and 50:50 biomass ratios, respectively. Co-gasification also led to a reduction in H₂S production which is expected given the lower sulphur content in biomass compared to coal (Table 8-4).

Table 7-4: Influence of coal-biomass mix ratio on gasifier performance of a 44 ton/hr (input) installation

Input	% of CC in feedstock blend											
	0%	5%	10%	20%	30%	40%	50%	60%	70%	80%	90%	100%
input coal (ar)	44.38	42.16	39.95	35.51	31.07	26.63	22.19	17.75	13.32	8.88	4.44	0.00
input CC (ar)	0.00	2.22	4.44	8.88	13.32	17.75	22.19	26.63	31.07	35.51	39.95	44.38
Total input (daf)	26.18	26.90	27.63	29.08	30.53	31.97	33.42	34.87	36.32	37.77	39.22	40.66
HHV	17.40	17.43	17.46	17.52	17.58	17.64	17.70	17.76	17.82	17.88	17.94	18.00
Energy input flow	772.28	773.61	774.94	777.61	780.27	782.93	785.60	788.26	790.92	793.59	796.25	798.91
O2 feed	10.81	10.81	10.81	10.81	10.81	10.81	10.81	10.81	10.81	10.81	10.81	10.81
Steam feed	43.54	43.54	43.54	43.54	43.54	43.54	43.54	43.54	43.54	43.54	43.54	43.54
Output												
Combustion temp	1,250	1,258	1,267	1,285	1,304	1,324	1,345	1,367	1,391	1,416	1,443	1,471
Crude gas vol. f./rate	11,391	11,480	11,572	11,771	11,987	12,239	12,542	12,908	13,317	13,747	14,187	14,632
Organic condensates	1.09	1.33	1.57	2.05	2.53	3.01	3.49	3.97	4.45	4.93	5.41	5.89
H ₂ O	25.67	26.50	27.33	29.06	30.82	32.71	34.78	37.05	39.43	41.82	44.17	46.48
H ₂	2.20	2.20	2.20	2.19	2.17	2.12	2.03	1.88	1.69	1.50	1.30	1.11
N ₂	0.72	0.70	0.68	0.64	0.60	0.56	0.52	0.48	0.44	0.40	0.36	0.32
CO	17.11	16.87	16.63	16.15	15.71	15.22	14.65	13.94	13.08	12.10	11.03	9.88
CO ₂	31.93	32.06	32.17	32.31	32.40	32.36	32.16	31.83	31.48	31.22	31.06	31.03
CH ₄	3.34	3.21	3.08	2.83	2.64	2.49	2.44	2.52	2.70	2.91	3.13	3.36
H ₂ S	0.21	0.20	0.19	0.17	0.15	0.13	0.11	0.09	0.07	0.05	0.03	0.01
Syngas/feedstock	1.25	1.24	1.24	1.22	1.21	1.19	1.17	1.14	1.11	1.09	1.06	1.03
H ₂ /CO ratio	1.78	1.81	1.84	1.89	1.92	1.94	1.92	1.87	1.80	1.72	1.64	1.56
HHV Syngas	12.12	12.01	11.90	11.68	11.47	11.25	11.03	10.81	10.57	10.31	10.03	9.72
Syngas energy flow	672.94	663.55	654.12	634.07	615.41	594.86	572.76	548.62	523.00	496.83	470.50	444.15
Thermal efficiency	87.14	85.77	84.41	81.54	78.87	75.98	72.91	69.60	66.13	62.61	59.09	55.59
Coal derived CO ₂ emissions	255.46	242.69	229.91	204.37	178.82	153.28	127.73	102.18	76.64	51.09	25.55	0.00
CO ₂ emission savings*	0.00	12.77	25.55	51.09	76.64	102.18	127.73	153.28	178.82	204.37	229.91	255.46

*assuming net zero CO₂ emissions from biomass

7.3.3 Process Economics

A model is developed for the assessment of the economics of syngas production from the co-gasification of coal and biomass by retrofitting a hypothetical updraft coal gasifier to accept biomass fuel. Previous co-gasification and co-firing tests have revealed that existing coal plants can, in many cases, successfully co-process alternative fuels such as biomass without alterations to the gasification reactor (especially at coal-biomass mass ratios of less than 20-30%)[35–37]. The main cost of co-processing is therefore largely dependent on the separate fuel pre-treatment and feeding system that would have to be installed for processing the biomass fraction of the feedstock [38], although other factors such as site layout and plant design can also be of significance [1]. While some biomass types such as dried wood chips can conceivably be handled using the preparation and feeding system used by coal, in the majority of cases, this will not be possible due to significant differences in the handling properties (e.g. grindability) of biomass and coal. Both the samples types considered in this work (CC and BG) will, for instance, require a drying step not required for coal preparation. Furthermore, the fibrous nature of BG in particular makes it unsuitable to the size reduction equipment employed for coal. BG also contained a significant fraction of fines, which are not acceptable in the Sasol FBDB type gasifier [30]. It is therefore reasonable to assume that some kind of upgrading technology will be required for the biomasses. Various types of upgrading technologies have been considered for thermal processing of biomass, especially in existing coal combustors, boilers and gasifiers. These include pelletisation, torrefaction, torrefaction and pelletisation (TOP), as well as pyrolysis [39]. Pelletisation is selected in this study as it does not lead to significant changes in the chemical composition of the biomass, and hence, its behaviour during the gasification process will deviate the least from the experimentally determined pyrolysis behaviour of the fresh biomass on which the process model is based. However, it must be recognized that particle size differences caused by pelletisation may have non-negligible effect on char production to the effects of heat and transport phenomena (as was shown in Chapter 7), and thus gasification

performance. Densification via pelletisation also leads to reduction in the investment required for the feeding system [40].

Table 7-5: Capital cost estimate for fixed coal gasification system for a 44.5 t/hr capacity plant [29]

Module	Cost (US\$, 2011)
Coal preparation and feeding	4,399,496
ASU*	61,160,702
Gasifier and accessories	35,017,170
Gas cleanup	39,516,100
Steam generator	348,591
Cooling water system	2,304,754
Ash handling system	1,639,458
Accessory electric plant	6,113,637
Instrumentation and control	4,267,837
Site construction	3,140,112
Professional services	9,857,067
Other costs	7,342,106
Contingency	24,030,760
TCI	199,137,791
Annual TCI	
Operating and maintenance costs	

* Air Separation Unit- data obtained from Hamelinck and Faaij [41]

7.3.3.1 Estimating production costs

Capital costs of a hypothetical syngas production process from a coal-conversion facility (based on fixed bed gasification) were based on NETL estimates for a coal-based BGL 1000 gasifier [29]. The BGL gasifier is an extension of the original Lurgi FBDB gasifier developed by British Gas and Lurgi with the ash discharge designed for slagging conditions. Its configuration is sufficiently close enough to the Sasol FBDB gasifier for it to be used as basis for this study [6,33]. As previously mentioned, the BGL 1000 gasifier is roughly the same size (44 t/hr) as the Sasol FBDB Mark IV gasifier and their costs should therefore be considered comparable [29]. The NETL estimates did not include the costing of air separation unit (ASU) for oxygen production, and so the values from Hamelinck and Faaij [41] were adapted for this item, correcting for the difference in scale by using the scale factor of 0.85 [41]. The scale employed

were thoseAll costs were corrected to 2011 values using the CPI³ inflation calculator. The Total Capital Investment (TCI) consists of equipment and material costs, direct and indirect labour costs, engineering and construction costs, as well as contingencies for the total coal-based syngas project. The TCI however, excluded items like sales tax, escalation and owners costs for permits, land, etc. Operating and maintenance expenses for the coal based process were estimated as 64% of the annualized TCI based on the data from the NETL study [29]. The annualisation was based on 13.5% discount rate and 20 year average utilization period. Operating expenses included items such as non-feedstock consumables (such as water, chemicals, natural gas, nitrogen, etc), as well as operating, maintenance, and administrative staff costs, and waste disposal [29].

Table 7-6: Cost estimate for biomass processing scaled to 20% coal substitution*

Module	Cost (US\$, 2011)
General investments	1,958,508
Drying	1,788,319
Grinding	199,321
Pelletisation	450,846
Cooling	30,846
Storage	690,507
Peripheral equipment	1,186,438
Conveyers	288,234
Feeding system	258,883
TCI	6,851,902

*20% of coal input corresponds to 9 t/hr of pelletized feed, which requires 16.6 t/hr of wet biomass to produce.

A breakdown of the capital investment required for the base case plant is provided in Table 8-5 while those for the biomass handling and pre-treatment system are shown in Table 8-6. Capital cost estimates have been scaled to biomass feeding rates required to substitute 20% of coal with biomass on a mass basis. The pelletisation plant costs were estimated using data from Bergman et al. [42] and Thek and

³ United States Bureau of Labor Statistics' Consumer Price Index calculator -

<http://www.bls.gov/cpi/cpicalc.htm>

Obernberg [43], while other handling costs for biomass were obtained from Hamelinck and Faaij [41]. It is believed that higher than 20% blend ratios for co-gasification are unrealistic for a variety of factors including gasifier performance problems (mainly related to ash sintering and fouling), biomass supply constraints, impact on downstream tar processing (due to significantly increased volumetric flow rates, as well as acid and oxygenate content of biomass derived condensates). Operating expenses for the biomass processing module is comparatively much higher than the base case at 480% of annual TCI [42,43].

Production costs were calculated as the sum of the annualised TCI and operating costs. Consequently, the unit cost of syngas production for the coal only system (not including feedstock cost) amounted to \$128.5/t. This translates to an additional specific cost of about \$17/t, such that the unit cost for co-gasification becomes \$145.6/t (not including feedstock cost). In the case where the capital cost of biomass pre-treatment is pro-rated to the quantities of biomass input, the additional unit cost was \$6.8/t and \$10.7/t for 5% and 10% biomass input, respectively.

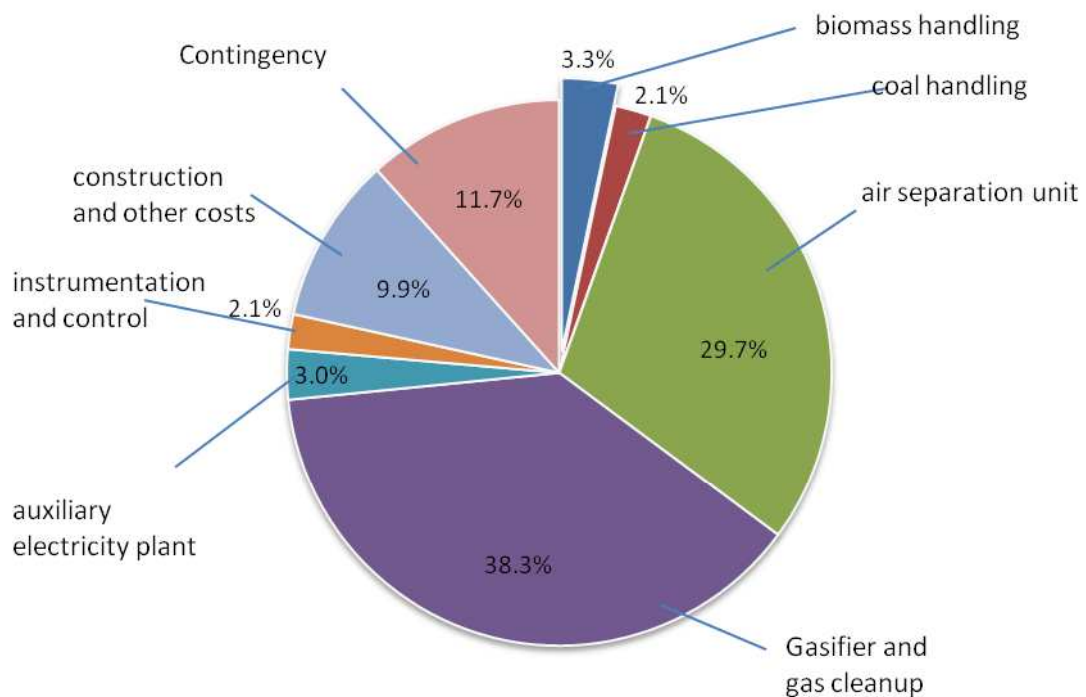


Figure 7-8: Distribution of capital costs for co-gasification (based on 20% biomass input)

Fig. 8-8 depicts the contribution of various process modules to the total capital investment costs for co-gasification. It shows that the absolute investment required for preparing and feeding biomass is only 1.1 % more than the coal handling costs. On the other hand, on a unit basis, the extra cost for handling biomass (\$14/t of pellets) is significantly higher than the corresponding costs for coal (\$1.8/t of coal). This shows that even without considering the costs of the feedstock, the extra investment required for retrofitting a coal-based syngas production facility is significant. However, it is widely recognised that feedstock cost is also an important component of the cost structure of many solid fuel conversion systems [40]. According to data from the Chamber of Mines of South Africa [44], FOB⁴ coal prices for the South African domestic market have risen steadily since 2001 from ZAR60/t to almost ZAR200/t in 2010. Eberhard [45] estimates that the costs coal supply to Eskom⁵ and Sasol in 2009 was less than ZAR 170/t and ZAR150/t for an average of respectively. Eberhard [45] further calculates that Eskom's coal prices rose to under ZAR200/t in 2010. Based on the two preceding sources, a 2011 price of ZAR 200/t (\$27/t) was employed in this study for coal. On an energy basis, this corresponds to a cost of \$1.6/GJ, which is not too far off from the \$1.8/GJ value used by Kreutz et al. [46]. In the manner of Leibrandt [47], the price of biomass in this study was set equal to that of coal on an energy basis, which based on average biomass heating value of 18 MJ/kg, is equivalent to \$28/t.

Table 7-7: Specific syngas production costs based on fixed retrofitting costs (at 20% coal substitution by mass)

		100% coal	5% biomass	10% biomass	20% biomass
Annualized TCI	\$	29,203,783	30,291,572	30,291,572	30,291,572
OPEX	\$	18,251,803	23,473,189	23,473,189	23,473,189
Feedstock cost	\$	9,954,350	9,968,571	9,982,791	10,011,232
Annual prod cost	\$	57,409,936	63,733,332	63,747,552	63,775,993
Prod cost per ton input	\$/tonne	155.43	172.55	172.59	172.66
Prod cost per tonne syngas	\$/tonne	129.27	144.22	145.00	146.82
Prod cost per GJ syngas	\$/GJ	10.66	12.01	12.18	12.57

⁴ free-on-board

⁵ Eskom: National power utility of South Africa

Based on the preceding cost assumptions, the specific production cost of syngas from coal alone is \$130/t or \$10.7/GJ (Table 8-7) which is comparable to the \$13/GJ estimate given by the IEA for IGCC systems based on entrained flow gasification technology [48]. Substituting 5, 10, and 20% of the coal feedstock mass with biomass resulted in specific production cost values shown in Table 8-7. Again, the values shown are based on retrofitting costs fixed at biomass capacity corresponding to 20% coal substitution. In the case where additional capital investment for retrofitting biomass is pro-rated to the quantities of biomass feed, the specific production cost for co-gasification at 95:5 and 90:10 feedstock mix ratios are reduced to \$11.3/GJ and \$11.7/GJ, respectively (Table 8-8).

Table 7-8: Specific production costs based on pro-rata retrofitting costs

		100% coal	5% biomass	10% biomass	20% biomass
Annualized TCI	\$	29,203,783	29,634,910	29,886,737	30,291,572
OPEX	\$	18,251,803	20,321,215	21,529,981	23,473,189
Feedstock cost	\$	9,954,350	9,968,571	9,982,791	10,011,232
Annual prod cost	\$	57,409,936	59,924,696	61,399,509	63,775,993
Prod. cost per ton input	\$/tonne	155.43	170.78	184.70	215.83
Prod. cost per tonne syngas	\$/tonne	129.27	135.60	139.66	146.82
Prod. cost per GJ syngas	\$/GJ	10.66	11.29	11.73	12.57

These results are consistent with the view that co-utilization of biomass with coal in thermal conversion systems makes little financial sense when the externalities such as the cost of mitigating pollutant emissions are not considered. If the avoided cost of CO₂ capture for instance is factored in, the economics of co-gasification is slightly improved. International prices for carbon emission credits (CER) are have ranged between \$13-\$20 in the last few years. According to the National Treasury in South Africa, a tax of ZAR75 – ZAR200/tCO₂ (\$10-\$26/tCO₂) would be “both feasible and appropriate” [49]. This corresponds to an extra cost ranging between \$0.5-\$1.2/GJ of syngas produced for coal only conversion. This cost is reduced successively according to the percentage of coal replaced with biomass, therefore at 20% biomass addition; the carbon tax is correspondingly 20% less. For the range of values given, the

avoided carbon tax due to co-feeding biomass can offset between 40-96% of the specific retrofitting cost at 20 wt% coal substitution. The effect of carbon tax (at a median value of ZAR117/tCO₂) on the production cost structure with increasing biomass ratio is further illustrated in Fig. 8-9. It can be observed that the reduction in carbon tax associated with substitution of coal with biomass could not offset the increasing pro-rata cost of retrofitting the base plant. Only at a carbon tax of \$30/tCO₂(ZAR242/tCO₂) or higher are the retrofitting costs completely covered (at 20 wt% coal substitution). Fig. 8-9 also shows that based on the assumed feedstock prices, there is little variability in the feedstock cost as the fuel blend ratio changes.

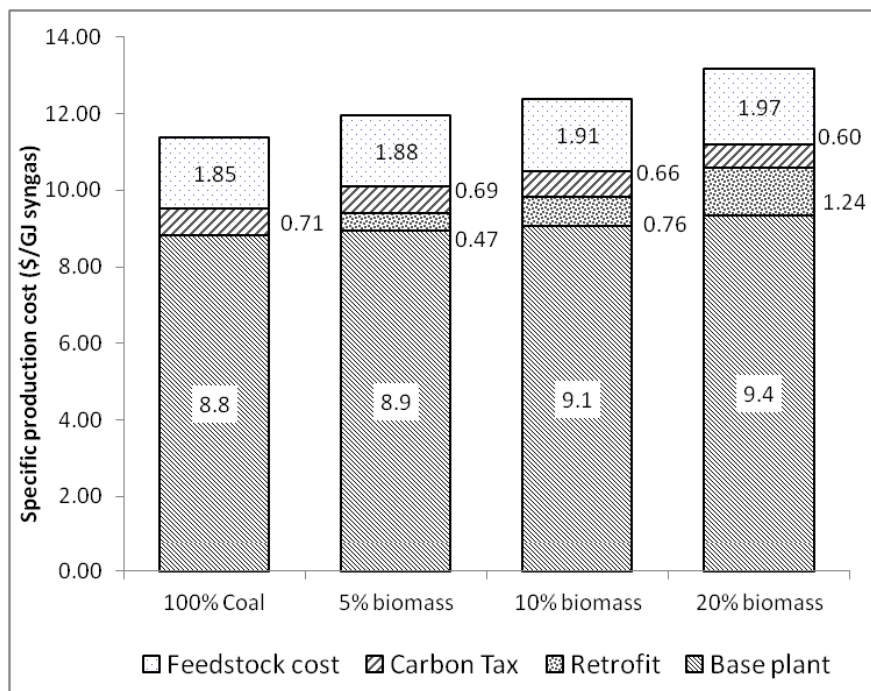


Figure 7-9: Influence of carbon tax on distribution of specific production cost.

7.3.3.2 Sensitivity analysis

The study so far has been based on a biomass price of \$28/t. Based on this value, the contribution of feedstock in the syngas production cost from the 80:20 coal-biomass blends is about 12%. However, biomass costs are notoriously hard to accurately estimate, consequently, a sensitivity analysis varying the cost of biomass feedstock from \$0-60/t was done and the results are shown in Fig. 8-10. Fig. 8-10a illustrates

the effect of varying biomass charges on the production cost of syngas at various feedstock mix ratios. The drastic increase in syngas cost from 0% to 5% biomass in the fuel mix, is a reflection of the cost of retrofitting the existing coal plant to handle biomass. Such that, even when there is no cost for obtaining biomass, the cost of syngas production still increases by approximately 10%. Nevertheless the cost of biomass is still an important component of production cost as Fig. 8-10b shows. Increasing the cost of biomass increased the percentage of syngas production cost represented by feedstock from 15-20% when the biomass price is varied from \$0/t to \$60/t.

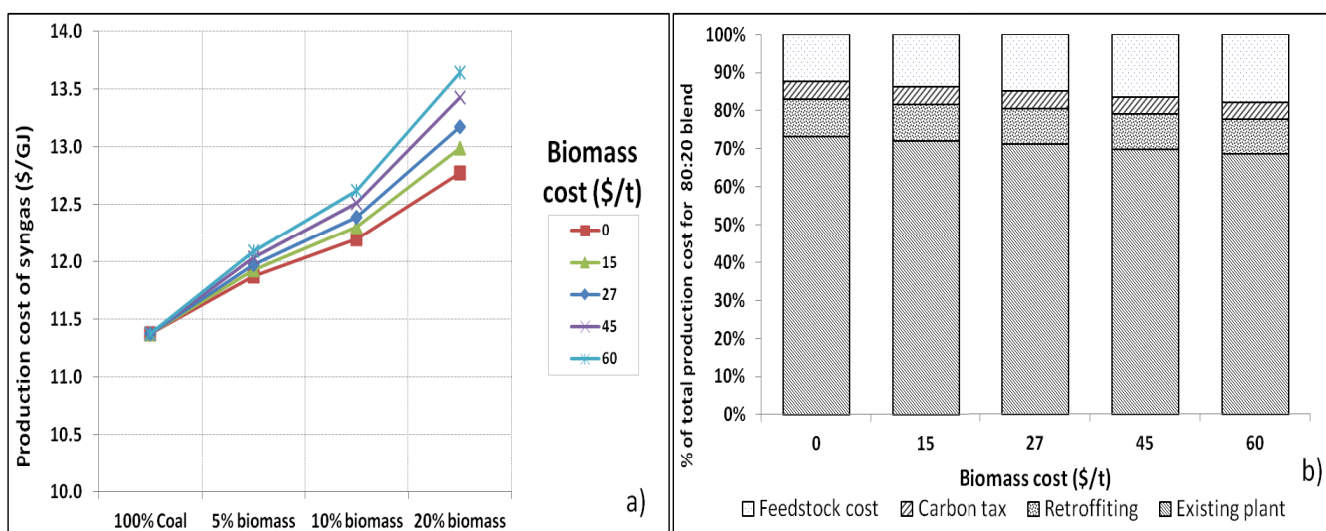


Figure 7-10: Sensitivity of syngas cost and cost distribution to biomass cost

7.4 Other industrial implications of simulation results

Considering that biomass devolatilizes 60-70 wt% of original material compared with approximately 20 wt% for coal during pyrolysis, it is no surprise that substituting biomass for coal at 5, 10 and 20 wt% caused a 22, 43 and 87 wt% increase in the production of hydrocarbon condensates (Table 8-4). This is likely to have significant implications on the downstream tar handling and utilization systems, from both a scale (throughput capacity) and quality perspective. Differences between coal and biomass derived condensates where outlined in Chapters 6 and 7 and can be summarised as follows: i) the overall higher production of condensates, ii) the higher

variety of compounds, iii) the higher oxygenates content, iv) significantly higher yields of strong acids, v) the considerable higher fraction of water soluble organics obtained from biomass liquids.

The increased pyrolysis condensate yield due to use of biomass feedstock would not necessarily lead to increased yields of tar derived chemicals. It was shown in Chapter 6 that only corn cobs produces larger naphtha yields than coal (naphtha and PAHs in general represent the bulk of coal derived tar).

The wide variety of compounds produced during biomass pyrolysis (Table 6.3 and Fig. 6.7) is likely to also pose a challenge, particularly with regards to the much higher oxygenate content found in biomass derived tars. Currently, condensates from coal in the Sasol CTL process are upgraded by hydrodeoxygenation – a procedure that involves extensive distillation under pressure in the presence of hydrogen and catalysts to remove phenols, as well as sulphur and nitrogen containing compounds [10,91]. The wider product variety in biomass is likely to reduce selectivity during separation of distillation products and/or affect the distilled product quality. Also, the drastic increase in oxygenates from the addition of biomass will at the very least increase the hydrogen demands for hydrotreating and hence, costs. Also, the high oxygenate content may reduce the activity and lifetime of catalysts normally employed in the process [92]. The high fraction of aqueous organics will also be of concern to the treatment of wastewater effluents. In addition, the higher acids content may lead to corrosion risks to piping and process equipment (~60g/kg for corn cobs compared to <1g/kg for coal, on air dried basis). The increased presence of strong acids and other aqueous phase condensates has been identified as contributing factor to the relative thermal instability of biomass pyrolysis oils [51,52], which will also negatively impact the tar upgrading process [53].

On the other hand acetic acid is a commercially valuable product stream (\$400-\$500/tonne⁶) that could be developed as a new product stream. The increased volume of other valuable chemicals such as alcohols (methanol, ethanol, 1-propanol), phenolics (phenol, cresols, and guaiacols), ketones (acetone, methyl ethyl ketone, and methyl isobutyl ketone) and furans (furfural, 2,5-dimethyl-furan, and furfuryl alcohol) could also be conceivably developed into value added products.

While this work is purely aimed at assessing impacts of co-gasification, the question may arise as to what the optimal coal-biomass blend ratio for gasification is. It is clear from this study that such a question is more complicated than it seems at first. From a financial and efficiency point of view, the optimal rate of biomass addition would be zero biomass since the inclusion of biomass reduces the efficiency and increases the cost of the coal gasification. This is based on the assumption that costs of handling the change in quality and quantity of biomass derived condensates do not outweigh the benefits from potentially new revenue streams as described in the last paragraph. It is clear that this particular assumption needs to be confirmed from further studies. From a net GHG reduction point of view however, it will be desirable to have as much biomass as would be technically possible in the gasifiers. Previous studies show that up to 20-30 wt% of coal can be replaced with biomass in gasifiers [35–37]. However there is little point in discussing environmental optimality in isolation from financial profitability, especially for commercial/industrial projects on the scale operated by Sasol. The financial justification for co-gasification becomes stronger under relatively high carbon tax regimes (of higher than \$30/tCO₂).

7.5 Conclusion

This chapter ties together results of the previous chapters (Chapters 6 and 7) to produce an assessment of the impact of coal and biomass co-gasification in fixed bed reactors. Fixed bed gasification is a stratified process with relatively distinct pyrolysis and char gasification steps. Results of the analysis of char obtained from the

⁶ As found on the trading website www.alibaba.com

pyrolysis of coal, biomass and coal-biomass blends revealed that the proximate characteristics of the blended chars approximates to the weighted average of the individual values for coal and biomass. Furthermore, analysis of the CO₂ reactivity of the fuel and their blends showed that the addition of biomass to coal does not impose any kinetic limitation on the gasification of blended chars. The blended chars decomposed at approximately the same rate as the char from 100% coal, even at higher biomass concentrations in the original feedstock blend. Based on these observations, an equilibrium based simulation of syngas production for co-gasification of coal-biomass blends at various mix ratios was implemented in Aspen Plus. The model showed that H₂/CO ratio was relatively unaffected by biomass addition to the coal fuel mix, whereas significant changes in syngas heating value and thermal efficiency was observed. Subsequent evaluation of the production cost of syngas at biomass input ranging between 0-20% of coal reflected the significant additional cost of pre-treating biomass. Syngas production costs from co-gasification remained significantly higher than coal only gasification, even at low to zero prices of the biomass feedstock. The reduction in carbon tax associated with substitution of coal with biomass could not offset the cost of retrofitting the base plant.

7.6 References

- [1] R. Davidson, A. Doig, J. Ekmann, R. Fernando, N. Harding, R. Moreea-Taha, et al., *Cofiring coal with other fuels*, IEA Clean Coal Centre, 2007.
- [2] N. Koukouzas, A. Katsiadakis, E. Karlopoulos, E. Kakaras, *Co-gasification of solid waste and lignite—A case study for Western Macedonia*, *Waste Management*. 28 (2008) 1263-1275.
- [3] C.A. Alzate, F. Chejne, C.F. Valdés, A. Berrio, J.D.L. Cruz, C.A. Londoño, *CO-gasification of pelletized wood residues*, *Fuel*. 88 (2009) 437-445.
- [4] R. Kandiyoti, *Bench-scale experiment design for developing co-pyrolysis and co-gasification technologies*, *International Journal of Power and Energy Systems*. 24 (2004) 205-214.
- [5] A. Valero, S. Usón, *Oxy-co-gasification of coal and biomass in an integrated gasification combined cycle (IGCC) power plant*, *Energy*. 31 (2006) 1643-1655.
- [6] C. Higman, M. van der Burgt, *Gasification*, Second Edition, 2nd ed., Gulf Professional Publishing, 2008.
- [7] Y.H. Zhao, H. Wen, Z.C. Guo, Z.H. Xu, *Development of a fuel-flexible co-gasification technology*, *Chin. J. Chem. Eng.* 13 (2005) 96–101.

- [8] M.R. Mahishi, D.Y. Goswami, Thermodynamic optimization of biomass gasifier for hydrogen production, *International Journal of Hydrogen Energy*. 32 (2007) 3831–3840.
- [9] P. De Filippis, C. Borgianni, M. Paolucci, F. Pochetti, Prediction of syngas quality for two-stage gasification of selected waste feedstocks, *Waste Management*. 24 (2004) 633-639.
- [10] C.M. van der Meijden, H.J. Veringa, L.P.L.M. Rabou, The production of synthetic natural gas (SNG): A comparison of three wood gasification systems for energy balance and overall efficiency, *Biomass and Bioenergy*. 34 (2010) 302-311.
- [11] X. Li, J.R. Grace, A.P. Watkinson, C.J. Lim, A. Ergüdenler, Equilibrium modeling of gasification: a free energy minimization approach and its application to a circulating fluidized bed coal gasifier, *Fuel*. 80 (2001) 195-207.
- [12] H.-J. Huang, S. Ramaswamy, Modeling Biomass Gasification Using Thermodynamic Equilibrium Approach, *Appl Biochem Biotechnol*. 154 (2009) 14-25.
- [13] A.P. Watkinson, J.P. Lucas, C.J. Lim, A prediction of performance of commercial coal gasifiers, *Fuel*. 70 (1991) 519-527.
- [14] C. Di Blasi, G. Signorelli, G. Portoricco, Countercurrent Fixed-Bed Gasification of Biomass at Laboratory Scale, *Industrial & Engineering Chemistry Research*. 38 (1999) 2571-2581.
- [15] M. Puig-Arnavat, J.C. Bruno, A. Coronas, Review and analysis of biomass gasification models, *Renewable and Sustainable Energy Reviews*. (2010).
- [16] European Committee for Standardization, Solid biofuels. Methods for sample preparation, 2005.
- [17] American Society for Testing Materials, ASTM D5373 - Standard Test Methods for Instrumental Determination of Carbon, Hydrogen, and Nitrogen in Laboratory Samples of Coal, 2002.
- [18] American Society for Testing Materials, ASTM D4239 - Standard Test Methods for Sulfur in the Analysis Sample of Coal and Coke Using High-Temperature Tube Furnace Combustion Methods, 2000.
- [19] British Standards Institute, Solid biofuels. Determination of calorific value, 2009.
- [20] American Society for Testing Materials, ASTM E1131 - Standard Test Method for Compositional Analysis by Thermogravimetry, 1998.
- [21] R.E. Barker, J.M. Begovich, J.H. Clinton, P.J. Johnson, ASPEN modeling of the Tri-State indirect-liquefaction process, Oak Ridge National Lab., TN (USA), 1983.
- [22] J.M. Stefano, Evaluation and modification of ASPEN fixed-bed gasifier models for inclusion in an integrated gasification combined-cycle power plant simulation, USDOE Morgantown Energy Technology Center, WV, 1985.
- [23] Aspen Technology Inc, Getting Started Modeling Processes with Solids, 2000.
- [24] W. Zhu, W. Song, W. Lin, Catalytic gasification of char from co-pyrolysis of coal and biomass, *Fuel Processing Technology*. 89 (2008) 890-896.
- [25] A.G. Collot, Y. Zhuo, D.R. Dugwell, R. Kandiyoti, Co-pyrolysis and co-gasification of coal and biomass in bench-scale fixed-bed and fluidised bed reactors, *Fuel*. 78 (1999) 667-679.
- [26] C. Di Blasi, Combustion and gasification rates of lignocellulosic chars, *Progress in Energy and Combustion Science*. 35 (2009) 121-140.

- [27] J.H. Slaghuis, Coal gasification, Sasol Technology, Sasolburg, SA, 1993.
- [28] L.M. Bartone, J. White, Industrial Size Gasification for Syngas, Substitute Natural Gas and Power Production - DOE/NETL-401/040607, National Energy Technology Laboratory (NETL), 2007.
- [29] J.C. van Dyk, M.J. Keyser, M. Coertzen, Syngas production from South African coal sources using Sasol-Lurgi gasifiers, International Journal of Coal Geology. 65 (2006) 243-253.
- [30] F. Pinto, C. Franco, R.N. Andre, M. Miranda, I. Gulyurtlu, I. Cabrita, Co-gasification study of biomass mixed with plastic wastes, Fuel. 81 (2002) 291-297.
- [31] F. Pinto, C. Franco, R.N. Andre, C. Tavares, M. Dias, I. Gulyurtlu, et al., Effect of experimental conditions on co-gasification of coal, biomass and plastics wastes with air/steam mixtures in a fluidized bed system, Fuel. 82 (2003) 1967-1976.
- [32] F. Pinto, R.N. Andre, H. Lopes, M. Dias, I. Gulyurtlu, I. Cabrita, Effect of Experimental Conditions on Gas Quality and Solids Produced by Sewage Sludge Cogasification. 2. Sewage Sludge Mixed with Biomass, Energy & Fuels. 22 (2008) 2314-2325.
- [33] R.A. Meyers, Handbook of Synfuels Technology, McGraw Hill Higher Education, 1984.
- [34] IEA Bioenergy Task 32, Technical status of biomass co-firing, IEA, Arnhem, 2009.
- [35] J. Koppejan, B. Gerrit, Cofiring and co-processing biomass with coal, Thermalnet, Netherlands, 2008.
- [36] A. Maciejewska, H. Veringa, J. Sanders, S.D. Peteves, Co-firing of biomass with coal: constraints and role of biomass pre-treatment, Petten, The Netherlands: Institute for Energy. (2006).
- [37] S. De, M. Assadi, Impact of cofiring biomass with coal in power plants – A techno-economic assessment, Biomass and Bioenergy. 33 (2009) 283-293.
- [38] A. Uslu, Pre-treatment technologies, and their effect on international bioenergy supply chain logistics: Techno-economic evaluation of torrefaction, fast pyrolysis and pelletisation, Masters Thesis, Utrecht University, 2005.
- [39] F.S. Lau, D.A. Bowen, R. DiHu, S. Doong, E.E. Hughes, R. Remick, et al., Techno-Economic Analysis of Hydrogen Production by Gasification of Biomass, US DOE Contract Number: DE-FC36-01GO11089, USA, 2002.
- [40] C.N. Hamelinck, A.P.C. Faaij, Future prospects for production of methanol and hydrogen from biomass, Journal of Power Sources. 111 (2002) 1–22.
- [41] P.C.A. Bergman, A.R. Boersma, R.W.R. Zwart, J.H.A. Kiel, Torrefaction for biomass co-firing in existing coal-fired power stations, Energy Research Centre of the Netherlands, ECN-C-05-013, 2005.
- [42] G. Thek, I. Obernberger, Wood pellet production costs under Austrian and in comparison to Swedish framework conditions, Biomass and Bioenergy. 27 (2004) 671-693.
- [43] Chamber of Mines of South Africa, Fact and Figures:2010, Chamber of Mines of South Africa, Pretoria, 2010.
- [44] A. Eberhard, The future of South African coal: market, investment, and policy challenges, Freeman Spogli Institute for International Studies, Stanford University, Stanford, 2011.

- [45] T.G. Kreutz, E.D. Larson, G. Liu, R.H. Williams, Fischer-Tropsch fuels from coal and biomass, in: Princeton Environmental Institute, Princeton University, Prepared for 25th Annual International Pittsburgh Coal Conference, Pittsburgh, Pa, 2008.
- [46] N. Leibrandt, Technoeconomic study for sugarcane bagasse to liquid fuels in South Africa: A comparison between biological and thermochemical process routes, PhD Thesis, Stellenbosch University, 2010.
- [47] IEA - Energy Technology Systems Analysis Programme, Syngas Production from Coal, IEA ETSAP Technology Brief. S01 (2010).
- [48] SA National Treasury, Reducing Greenhouse Gas Emissions: The Carbon Tax Option, National Treasury, South Africa, 2010.
- [49] A. de Klerk, Fisher-Tropsch Refining, PhD Thesis, University of Pretoria, 2008.
- [50] E. Churin, Upgrading of pyrolysis oils by hydrotreatment, in: Biomass Pyrolysis Liquids Upgrading and Utilization, Hardcover, Springer, 1991: pp. 219 -225.
- [51] M. Rupp, Utilisation of pyrolysis liquids in refineries, in: Biomass Pyrolysis Liquids Upgrading and Utilization, Hardcover, Springer, 1991: pp. 219 -225.
- [52] M.E. Boucher, A. Chaala, H. Pakdel, C. Roy, Bio-oils obtained by vacuum pyrolysis of softwood bark as a liquid fuel for gas turbines. Part II: Stability and ageing of bio-oil and its blends with methanol and a pyrolytic aqueous phase, Biomass and Bioenergy. 19 (2000) 351-361.
- [53] A.V. Bridgwater, S.A. Bridge, Review of biomass pyrolysis technologies, in: Biomass Pyrolysis Liquids Upgrading and Utilization, Hardcover, Springer, 1991: pp. 11-92.
- [53] R.C. Everson, H.W.J.P. Neomagus, H. Kasaini, D. Njapha, Reaction kinetics of pulverized coal-chars derived from inertinite-rich coal discards: Gasification with carbon dioxide and steam, Fuel. 85 (2006) 1076–1082

8 Conclusions and recommendations

Gasification provides a proven alternative to the dependence on petroleum for the production of high value products such liquid fuels and chemicals. Syngas, the main product from gasification can be converted to fuels and chemicals via a number of possible synthesis processes. Coal and natural gas are currently the main feedstock used for syngas production. In South Africa (SA), Sasol operates the largest commercial coal-to-liquids conversion process in the world, based on updraft fixed bed gasification of low grade coal to syngas. Co-utilizing alternative and more sustainable feedstock (such as biomass and wastes) with coal in existing coal-based plants offers a realistic approach to reducing the costs and risks associated with setting up dedicated biomass conversion plants.

In updraft gasification, the pyrolysis or devolatilization step is particularly important because liquid condensates produced during this step – comprising tars, oils, and water – are released in significant quantities along with syngas [1,2]. These condensates are produced in the devolatilization reaction zone of updraft gasifiers and are normally considered an unwanted by-product of gasification that has to be minimised [3–5]. In the Sasol process, however, they have chosen to utilize the hydrocarbon fraction of these liquids via conventional refining processes to produce commercially valuable chemicals such as naphtha, creosotes, and phenols [1,6]. When considering the potential for biomass to be used as feedstock based on the existing coal based fixed-bed gasification processes, the devolatilization step becomes even more important as volatile matter content in biomass is known to be significantly higher than in coal, and with considerably different composition [7,8].

8.1 Main conclusions

8.1.1 Pyrolysis kinetics

Based on the aforementioned, substantial attention was devoted in this work to the investigation of the pyrolysis behaviour of selected coal and biomass samples, and their

blends. The coal sample used was a blend of various typical South African hard coals that can be described as low grade, high ash and inertinite rich coal [9]. Biomass samples comprised of corn and sugar cane biomass residues, which represent the bulk of agricultural waste in South Africa [10,11].

The pyrolysis thermokinetics of the samples and their blends were investigated via non-isothermal thermogravimetric analysis (TGA). An atmospheric TGA was employed, but as Hillier and Fletcher [12] showed, pyrolysis kinetic parameters obtained under atmospheric conditions are also applicable to pressurized conditions of up to 40 bars. The devolatilization of the biomass materials occurred in a narrow temperature interval (200-400°C) and with higher decomposition rates than coal, where decomposition occurred between 380-900°C. Isoconversional kinetic analysis revealed the dependence of apparent activation energy on conversion, $E(\alpha)$, from which very good predictions of reaction progress could be obtained for both individual samples and blends. Synergistic interactions in the blends resulted in higher than expected volatile yields. The interactions occurred between 300°C and 500°C, corresponding to the end of biomass devolatilization and the start of coal decomposition. Isoconversional kinetic analysis revealed the dependence of apparent activation energy (E) on conversion (α) from which reliable predictions of reaction progress could be obtained for both individual samples and blends. Apparent activation energy values varied between 165-180, 162-190, 160-175, and 225-260 kJ mol⁻¹ for sugarcane bagasse, corn cobs, corn stover, and coal in the 0.1 to 0.8 conversion range. A comparison of $E(\alpha)$ for single fuels and coal-biomass blends gave further evidence of synergistic behaviour as demonstrated by larger variation in $E(\alpha)$ for the biomass and coal fractions the blends in contrast to the level of variation in $E(\alpha)$ observed when these components were pyrolyzed separately.

Single and multi-component model fitting kinetics was also applied to the TGA data. The results showed that single component kinetics was a poor representation of the decomposition behaviour of all of the samples, regardless of whether a 1st or nth order reaction model was assumed. Conversely, reasonably approximate simulations of reaction rates could be obtained by adopting the simpler 1st order model when 3 or

more parallel reactions were assumed in the biomass fuels. However, not all the reactive pseudocomponents in biomass strictly followed the first order model. In comparison, the n^{th} order model was found to be a more robust and flexible approach providing simulations and predictions with better fits to the experimental data, particularly for coal where a larger deviation from 1^{st} order reaction behaviour was observed. Apparent activation energy values obtained for n^{th} order model fitting with 3 pseudocomponents were 212, 188, and 94 kJ mol^{-1} for sugarcane bagasse; 215, 189, and 99 kJ mol^{-1} for corn cobs; and 252, 147 and 377 kJ mol^{-1} for coal. Corresponding pre-exponential factor values obtained were 3.6×10^{17} , 8.5×10^{16} , $3.3 \times 10^{08} \text{ min}^{-1}$ for bagasse, 7.2×10^{18} , 2.6×10^{17} , $2.2 \times 10^{09} \text{ min}^{-1}$, for corn cobs, and 2.2×10^{18} , 1.5×10^{09} , $2.5 \times 10^{20} \text{ min}^{-1}$ for coal, respectively. These results, along with the corresponding reaction order values, produced reaction rate simulations with less than 2% deviation from experimental observations. The activation energies obtained also compared well with values derived previously in a model free analysis of the same data.

8.1.2 Pyrolysis product distribution

In Chapter 6, pyrolysis experiments under conditions that simulate industrial updrafts gasifiers revealed the relevance of the chemical reaction rates determined in the kinetics chapters. At low temperatures for all particle sizes and fuels, transport processes were several orders of magnitude faster than chemical reaction times, whereas the opposite trend was observed at high temperature (600°C). This means that reaction kinetics was the controlling mechanism at high temperatures. Overall, mass transfer times scales increased with increase in particle size, and were slower in coal than in biomass. This is due to the difference in permeability and effective diffusivity of coal and biomass which are in turn dependent on characteristic pore sizes. Investigation of the pyrolysis product distribution showed that differences between biomass and coal in terms of the overall distribution of char, condensates and gas phase product yields are correlated with the significantly differing physical and chemical properties of the fuels. This is reflected in the generally higher yield, variety and oxygenates content of biomass volatile products compared to coal. While the fact that coal produced higher char and lower gas and liquid products than any of the

biomass considered are to be expected, significant differences in pyrolysis behaviour between the biomass fuels were observed as well. The dissimilarity observed between biomass fuels could be linked to the differences in their particle size and the ensuing effect on transport dynamics within the reactor. Such differences were manifested in terms of overall gas/liquid of volatile phase products and in the composition and distribution of the volatiles as well.

Results of investigation into the influence of mix ratio on pyrolysis yields show limited evidence of non-additive or synergistic behaviour on the overall distribution of solid liquid and gas yields. On the other hand, in terms of the distribution of specific liquid phase hydrocarbons, the evidence is in favour of synergistic pyrolysis behaviour. From these observations, it can be concluded that predicting the overall distribution of phases (solid, liquid and gas products) from co-pyrolysis/co gasification is relatively straightforward according to a simple additive model. However, predicting specific gas and liquid compositions is a much harder task which cannot be predicted via additive models. The influence of temperature and pressure within the range of 400-600°C and 1-26 bars on the yield and composition of volatiles were also investigated via a factorial design. Elevated pressure generally led to lower liquid hydrocarbon yields while temperature had mixed effects depending on the biomass type in the blends.

8.1.3 Gasification modelling and process economics

Fixed bed gasification is a stratified process with relatively distinct pyrolysis and char gasification steps. Results of the analysis of char obtained from the pyrolysis of coal, biomass and coal-biomass blends revealed that the proximate characteristics of the blended chars approximates to the weighted average of the individual values for coal and biomass. Furthermore, analysis of the CO₂ reactivity of the fuel and their blends showed that the addition of biomass to coal does not impose any kinetic limitation on the gasification of blended chars. The blended chars decomposed at approximately the same rate as when coal was gasified alone, even at higher biomass concentrations in the original feedstock blend. Based on these observations, an equilibrium based simulation of syngas production for co-gasification of coal-biomass blends at various

mix ratios was implemented in Aspen Plus. The model showed that H₂/CO ratio was relatively unaffected by biomass addition to the coal fuel mix, whereas syngas heating value and thermal efficiency were negatively affected. Subsequent evaluation of the production cost of syngas at biomass input ranging between 0-20% of coal reflected the significant additional cost of pre-treating biomass. Syngas production costs from co-gasification remained significantly higher than coal only gasification, even at low to zero prices of the biomass feedstock. The reduction in carbon tax associated with co-gasification could not offset the cost of retrofitting the base plant to handle the biomass feedstock. These results are in agreement with the observation by the IEA co-firing study group (Bioenergy Task 32) that economic advantages for co-firing of biomass with coal so far do not exist [13]. Instead, the main motivations behind the concept are the potential CO₂ emission reduction and the global climate change mitigation [13]. Nevertheless, co-utilization of biomass with coal still remains among the “lowest-risk, least expensive, most efficient and shortest-term option” for renewable energy production [14].

8.2 Recommendations

In summary, this dissertation has showed that co-feeding of biomass in existing coal based updraft gasification plants poses significant challenges in terms of impacts on condensates and syngas quality, and production costs. Many assumptions have been made during the study that need to be verified, either experimentally or by obtaining quoted costs from local industry.

The TGA based kinetic study in this work showed the difference in the overall reaction rates of coal and biomass decomposition. Further investigation of the kinetics of specific volatile products is necessary to better understand the reaction mechanisms responsible for their production. This can be achieved using thermal analysis equipment employed in tandem with an ancillary analytical tool that can evaluate the chemical composition and structure of evolved products, such as the FTIR, GCMS, or HPLC [15]. This will allow a better understanding of the synergistic reaction

mechanisms, which will in turn improve the ability to predict the composition of devolatilized products.

The modelling of syngas production was based on a fixed steam-to-oxygen ratio suited to producing FT grade syngas (H/C ratio of 1.8). This led to changes in syngas quality summarised in the previous section and detailed in section 8.3.2. Another possibility is to adapt gasifier operating conditions to produce syngas of fixed quality. It can be envisaged that the higher oxygen content of biomass fuels will lead to higher combustion temperatures, which will in turn increase the steam demand. As Valero and Uson [16] observed, this can only be done by using a multi-dimensional non-linear model based on operational data maps of real life plant outputs. Such a model could include the optimization of other desired operational outputs such as lower combustion temperatures necessary to prevent the slagging of biomass derived ash. Further experimental investigation is also required to confirm the assumption made that pelletized biomass behave in a similar manner to untreated biomass. In addition, the effect of other biomass pre-treatment technologies on pyrolysis and gasification performance would be useful for obtaining a better assessment of the range of syngas production costs from co-gasification.

There are other relevant issues relating to the industrial scale application of biomass co-gasification that need further investigation. These include life cycle assessments (LCA), availability of a biomass supply stream, and the extra treatment requirements of mixed biomass and coal condensates. An LCA point of view is required to holistically assess the life cycle efficiencies, emissions and environmental impacts of the co gasification process. Knowledge of biomass availability is vital when deciding the optimum scale of investment in co-gasification infrastructure, after allowing for the technical limits related to gasifier performance. The benefits of maximising cost savings due to economies of scale must be balanced against the availability and cost of biomass supply. Although significant effort has been devoted to research on the upgrading and utilization of biomass derived and coal derived condensates, there is virtually no literature on the handling of condensates from blended coal and biomass feedstock.

The study highlighted the possibility of ameliorating some of the financial impacts of co-gasification by developing new high value product streams (such as acetic acid) from the significant fraction of condensates derived from biomass. Further research is essential to quantify the effects of the significantly higher quantities of high acid and oxygenate content condensate produced from biomass, on the existing piping and processing equipment devoted to coal derived tar. A process optimization study that investigates tradeoffs between the financial implications of such effects, and the potential revenues from developing new product lines, will also be of considerable interest.

8.3 References

- [1] H. Boerrigter, A. Van Der Drift, J.H. Hazewinkel, G. Kupers, BIOSYNGAS; Multifunctional intermediary for the production of renewable electricity, gaseous energy carriers, transportation fuels, and chemicals from biomass, Energy Research Centre of the Netherlands (ECN), 2004.
- [2] C. Higman, M. van der Burgt, Gasification Processes, in: Gasification (Second Edition), Gulf Professional Publishing, Burlington, 2008: pp. 91-191.
- [3] C. Brage, Q. Yu, G. Chen, K. Sjöström, Tar evolution profiles obtained from gasification of biomass and coal, Biomass and Bioenergy. 18 (2000) 87-91.
- [4] J. Leppälähti, T. Koljonen, Nitrogen evolution from coal, peat and wood during gasification: Literature review, Fuel Processing Technology. 43 (1995) 1-45.
- [5] E. Kurkela, P. Ståhlberg, Air gasification of peat, wood and brown coal in a pressurized fluidized-bed reactor. I. Carbon conversion, gas yields and tar formation, Fuel Processing Technology. 31 (1992) 1-21.
- [6] S. Mangena, Effective Utilisation of Coal in Sasol – A SasolFBDB Gasification Technology Perspective, in: SACPS International Conference “Coal Powering the Future,” Secunda, South Africa, 2009.
- [7] J.M. Jones, M. Kubacki, K. Kubica, A.B. Ross, A. Williams, Devolatilisation characteristics of coal and biomass blends, Journal of Analytical and Applied Pyrolysis. 74 (2005) 502-511.
- [8] T. Sonobe, N. Worasuwannarak, S. Pipatmanomai, Synergies in co-pyrolysis of Thai lignite and corncob, Fuel Processing Technology. 89 (2008) 1371-1378.
- [9] A. Eberhard, The future of South African coal: market, investment, and policy challenges, Freeman Spogli Institute for International Studies, Stanford University, Stanford, 2011.
- [10] L.R. Lynd, H. Von Blottnitz, B. Tait, J. de Boer, I.S. Pretorius, K. Rumbold, et al., Converting plant biomass to fuels and commodity chemicals in South Africa: a third chapter?, South African Journal of Science. 99 (2003) 499-507.

- [11] Department of Minerals and Energy, White Paper on the Renewable Energy Policy of the Republic of South Africa, Department of Minerals and Energy, 2003.
- [12] J.L. Hillier, T.H. Fletcher, Pyrolysis Kinetics of a Green River Oil Shale Using a Pressurized TGA, *Energy Fuels*. 25 (2010) 232-239.
- [13] IEA Bioenergy Task 32, Technical status of biomass co-firing, IEA, Arnhem, 2009.
- [14] A. Maciejewska, H. Veringa, J. Sanders, S.D. Peteves, Co-firing of biomass with coal: constraints and role of biomass pre-treatment, Petten, The Netherlands: Institute for Energy. (2006).
- [15] J.E. White, W.J. Catallo, B.L. Legendre, Biomass pyrolysis kinetics: A comparative critical review with relevant agricultural residue case studies, *Journal of Analytical and Applied Pyrolysis*. 91 (2011) 1-33.
- [16] A. Valero, S. Usón, Oxy-co-gasification of coal and biomass in an integrated gasification combined cycle (IGCC) power plant, *Energy*. 31 (2006) 1643-1655.

Appendix A – Data relating to chapters 6 & 7

Table A-1: Phase distribution of products from pyrolysis studies found in literature

Fuel	Reactor type	Experimental conditions	Char (wt%)	Liquids (wt%) Total	Gas (wt%)	yield basis	Reference
BG	Fixed bed	HR:10°C/min;T:600°C;P:atm	25			ar	Bonelli et al. [54]
	Stirred Fixed bed	HR: Isothermal; F:1.2kg(wet);T:520°C;P:atm	20.7	57.7	21.6	db	Zandersons et al. [55]
	Fixed bed	HR:50°C/min; F:200g; T:500°C;P:atm	23	60	18	ar	Asadullah et al. [56]
	Fixed bed	HR:1°C/min; F:30g; T:700°C;P:atm	23	20	48	ar	Arni et al. [57]
	Fixed bed	HR:25°C/min;T:550°C;P:atm	22	45	20	ar	Parihar et al. [58]
	Vacuum pyrolysis	HR:2.5°C/min;F:20kg;T:530°C	26	51	22	db	Garcia-Perez et al. [59]
	Vacuum pyrolysis	HR:12°C/min;F:80g; T:500°C;P:atm	20	62	18	db	Garcia-Perez et al. [59]
Fixed bed	HR: fast; F:250g; T:575°C; P:atm	33	48	19	db	Islam et al. [60]	
CC	Fixed bed	HR:30°C/min;T:600°C;P:atm	25	35	42	ar	Cao et al. [61]
	Microwave oven	F:150g;T:600°C;P:atm	22			ar	Yu et al. [62]
	Fixed bed	F:1.5g; T:500°C;P:atm	38	40	17	ar	Ioannidou et al. [37]
CS	Fixed bed	F:1.5g; T:500°C;P:atm	33	42	15	ar	Ioannidou et al. [37]
Coal	Fixed bed	HR:28°C/min;T:600°C;P:atm	68-73.7	24.8-16.8	7.1-19.8	db	Baruah et al. [63]
	Wire mesh	HR:60°C/min;T:600°C;P:atm	65	18	17	daf	Li et al. [64]
	Thermobalance	HR:3°C/min; T:600°C; P:25 bars		7		ar	Arendt et al [26]

	Entrained flow	HR:very fast; T:900°C; P:23 bars		10		daf	Lee et al[65]
--	----------------	-------------------------------------	--	----	--	-----	---------------

HR- heating rate; F-feed size/rate; T-temperature; P-pressure; atm-atmospheric pressure (~1 bar); ar-as received; db-dry basis; daf-dry and ash free basis

Table A-2: Chemical composition of hydrocarbons in pyrolysis condensates (NF=non-aqueous fraction; AF=aqueous fraction of condensates) expressed on daf (wt%) basis of feedstock

Group	Compound	Formula	Structure	BP (°C)	MW (g/mol)	BG			CC			CS			Coal		
						NF	AF	Total	NF	AF	Total	NF	AF	Total	NF	AF	Total
Acid	Acetic acid	C ₂ H ₄ O ₂	Linear	117.1	60.1		1.048	1.048	1.069	4.627	5.695		0.803	0.803	0.803	0.021	0.021
	Propanoic acid	C ₃ H ₆ O ₂	Linear	141.7	74.1		0.070	0.070		0.124	0.124		0.075	0.075	0.075	0.003	0.003
	Butanoic acid	C ₄ H ₈ O ₂	Linear	164.3	88.1		0.009	0.009		0.005	0.005		0.009	0.009	0.009	0.001	0.001
	Iso-butanoic acid	C ₄ H ₈ O ₂	Linear	155.2	88.1					0.001	0.001						
Alcohol	Methanol	C ₁ H ₄ O	Linear	48.1	32.0		0.151	0.151		0.519	0.519		0.485	0.485	0.485	0.001	0.001
	Ethanol	C ₂ H ₆ O	Linear	72.6	46.1	0.009	0.001	0.010	0.012	0.003	0.015		0.006	0.019	0.038		0.038
	2-propen-1-ol	C ₃ H ₆ O	Linear	99.0	58.1		0.000	0.000					0.002	0.002			
	1-propanol	C ₃ H ₈ O	Linear	95.8	60.1		0.001	0.001		0.003	0.003		0.003	0.003		0.001	0.001
	2-propanol	C ₃ H ₈ O	Linear	73.0	60.1		0.000	0.000		0.000	0.000		0.002	0.002			
Aldehyde	Acetaldehyde	C ₂ H ₄ O	Linear	18.6	44.1		0.001	0.001		0.010	0.010		0.020	0.020		0.000	0.000
	Propanal	C ₃ H ₆ O	Linear	49.3	58.1	0.002	0.000	0.003	0.031	0.003	0.034		0.005	0.005			
	Butanal	C ₄ H ₈ O	Linear	77.6	72.1	0.001		0.001	0.012	0.000	0.012			0.005			
	Iso-butanal	C ₄ H ₈ O	Linear	67.1	72.1				0.016		0.016			0.005			
	3-methyl-butanal	C ₅ H ₁₀ O	Linear	93.5	86.1	0.002		0.002	0.016		0.016			0.005			
Aromatic	1,3-cyclopentadiene	C ₅ H ₆	Cyclic	41.5	66.1				0.009	0.009							
	Methyl-cyclopentene	C ₆ H ₁₀	Cyclic	229.0	82.1				0.009	0.009							
	Benzene	C ₆ H ₆	Cyclic	78.8	78.1	0.004		0.004	0.037		0.037			0.025	0.005	0.005	0.005
	Toluene	C ₇ H ₈	Cyclic	110.6	92.1	0.021		0.021	0.024	0.002	0.026			0.025	0.020	0.020	0.020
	Ethyl-benzene	C ₈ H ₁₀	Cyclic	136.2	106.2	0.007		0.007	0.026		0.026			0.025	0.025	0.025	0.025
	M-xylene	C ₈ H ₁₀	Cyclic	140.6	106.2	0.017		0.017	0.100		0.100			0.051	0.079	0.079	0.079
	O-xylene	C ₈ H ₁₁	Cyclic	145.9	106.2	0.008		0.008	0.036		0.036			0.026	0.032	0.032	0.032
	Ethyl-methyl-benzene	C ₉ H ₁₂	Cyclic	163.0	120.2	0.002		0.002	0.021		0.021			0.017	0.010	0.010	0.010
	Propyl-benzene	C ₉ H ₁₂	Cyclic	160.5	120.2	0.004		0.004	0.013		0.013			0.010	0.020	0.020	0.020

	Trimethyl-benzene	C ₉ H ₁₂	Cyclic	168.0	120.2	0.006		0.006	0.017	0.011	0.011	0.024	0.024	0.024
Ester	Methyl-formate	C ₂ H ₄ O ₂	Linear	26.0	60.1		0.012	0.012	0.012	0.016				
	Methyl-acetate	C ₃ H ₆ O ₂	Linear	44.0	74.1	0.004	0.432	0.080	0.512	0.016	0.026			
	1,1-dimethoxy-ethane	C ₄ H ₁₀ O ₂	Linear	63.0	90.1		0.008		0.008					
	Methyl-propanoate	C ₄ H ₈ O ₂	Linear	67.9	88.1		0.029		0.029					
	Methyl-butanoate	C ₅ H ₁₀ O ₂	Linear	104.2	102.1		0.008		0.008					
	1,1-dimethoxy-propane	C ₅ H ₁₂ O ₂	Linear	89.8	104.2	0.001	0.012		0.012	0.003				
	2,2-dimethoxy-propane	C ₅ H ₁₂ O ₂	Linear	83.0	104.2	0.010	0.106		0.106	0.019				
	2,2-dimethoxy-butane	C ₆ H ₁₄ O ₂	Linear	99.8	118.2	0.002	0.016		0.016	0.005				
	Furan	C ₄ H ₄ O	Cyclic	31.4	68.1		0.031		0.031	0.002				
	Tetrahydrofuran (thf)	C ₄ H ₈ O	Cyclic	68.3	72.1		0.018		0.018	0.002				
Furan	Furfural	C ₅ H ₄ O ₂	Cyclic	161.8	96.1	0.006	0.062		0.062	0.012		0.005		0.005
	2-methyl-furan	C ₅ H ₆ O	Cyclic	64.5	82.1	0.000	0.196		0.196	0.012				
	2-furanmethanol	C ₅ H ₆ O ₂	Cyclic	170.0	98.1		0.048	0.000	0.048	0.046				
	2,5-dimethyl-furan	C ₆ H ₈ O	Cyclic	93.1	96.1	0.001	0.035		0.035	0.004				
	2-ethyl-furan	C ₆ H ₈ O	Cyclic	94.5	96.1		0.016		0.016	0.002				
	2-ethyl-5-methyl-furan	C ₇ H ₁₀ O	Cyclic	119.1	110.2	0.002	0.015		0.015	0.015				
	Benzofuran	C ₈ H ₆ O	Cyclic	174.0	118.1	0.011	0.024		0.024	0.013				
	2,3-dihydro-benzofuran	C ₈ H ₈ O	Cyclic	188.2	120.2	0.006	0.018		0.018	0.014				
	Methyl-benzofuran	C ₉ H ₈ O	Cyclic	190.0	132.2	0.008	0.025		0.025	0.015				
	Heterocyclics	Acetonitrile	C ₂ H ₃ N	Cyclic	63.5	41.1		0.003	0.003	0.003		0.007		0.001
1h-pyrrole		C ₄ H ₅ N	Cyclic	129.8	67.1		0.031		0.031	0.002				
Pyridine		C ₅ H ₅ N	Cyclic	115.3	79.1	0.001	0.017		0.017	0.008				
Methyl-pyridine		C ₆ H ₇ N	Cyclic	128.0	93.1	0.002	0.022		0.022	0.014		0.004		0.004
Dimethyl-pyridine		C ₇ H ₉ N	Cyclic	142.5	107.2		0.013		0.013	0.003		0.006		0.006
Acetone		C ₃ H ₆ O	Linear	46.5	58.1	0.048	0.310	0.166	0.476	0.236	0.288	0.343	0.024	0.368
1-hydroxy-2-propanone		C ₃ H ₆ O ₂	Linear	145.5	74.1			0.034	0.034					

2,5-xyleneol	C ₈ H ₁₀ O	Cyclic	211.1	122.2	0.015	0.070	0.043	0.043	0.070	0.104	0.104	0.104
2,6-xyleneol	C ₈ H ₁₀ O	Cyclic	201.1	122.2	0.010	0.048	0.030	0.030	0.048	0.028	0.028	0.028
3,5-xyleneol	C ₈ H ₁₀ O	Cyclic	221.7	122.2	0.001	0.112	0.059	0.059	0.112			
m-ethyl-phenol	C ₈ H ₁₀ O	Cyclic	211.7	122.2	0.024					0.195	0.195	0.195
o-ethyl-phenol	C ₈ H ₁₀ O	Cyclic	204.5	122.2	0.007	0.067	0.031	0.031	0.067	0.028	0.028	0.028
p-ethyl-phenol	C ₈ H ₁₀ O	Cyclic	219.0	122.2	0.064	0.626	0.307	0.307	0.626	0.117	0.117	0.117
Vinyl guaiacol	C ₉ H ₁₂ O ₂	Cyclic	246.5	152.2	0.003	0.122	0.036	0.036	0.122	0.014	0.014	0.014
Ethyl-methyl-phenol (cresol)	C ₉ H ₁₂ O	Cyclic	228.0	136.2	0.023	0.172	0.089	0.089	0.172	0.071	0.071	0.071

Table A-3: Yields (wt%, daif) of chemical components detected in the condensates from Coal-BG and Coal-CC blends

Group	Compound	Structure	Formula	BP °C	MW	Coal-BG Blends (wt% biomass)			Coal-CC blends (wt% biomass)				
						0%	5%	50%	100%	0%	5%	50%	100%
Acid	Acetic acid	linear	C ₂ H ₄ O ₂	117.10	60.05	0.021	0.276	0.575	1.048	0.021	0.450	4.835	5.695
Acid	Butanoic acid	linear	C ₄ H ₈ O ₂	164.30	88.11	0.001	0.087	0.112	0.009	0.001	0.160	0.723	0.005
Acid	Iso-butanoic acid	linear	C ₄ H ₈ O ₂	155.20	88.11		0.002	0.002					0.001
Acid	Propanoic acid	linear	C ₃ H ₆ O ₂	141.70	74.08	0.003	0.021	0.035	0.070	0.003	0.035	0.192	0.124
Alcohol	1-propanol	linear	C ₃ H ₈ O	95.80	60.10	0.001	0.001	0.001	0.001	0.001	0.002	0.005	0.003
Alcohol	2-propanol	linear	C ₃ H ₈ O	73.00	60.10		0.000	0.000	0.000				0.000
Alcohol	Ethanol	linear	C ₂ H ₆ O	72.60	46.07	0.038	0.001	0.001	0.010	0.038	0.001	0.013	0.015
Alcohol	Methanol	linear	C ₁ H ₄ O	48.10	32.04	0.001	0.037	0.096	0.151	0.001	0.072	0.461	0.519
Aldehyde	3-methyl-butanal	linear	C ₅ H ₁₀ O	93.50	86.13				0.002				0.016
Aldehyde	Acetaldehyde	linear	C ₂ H ₄ O	18.60	44.05	0.000	0.001	0.001	0.001	0.000	0.002	0.014	0.010
Aldehyde	Butanal	linear	C ₄ H ₈ O	77.60	72.11				0.001				0.012
Aldehyde	Iso-butanal	linear	C ₄ H ₈ O	67.10	72.11								0.016
Aldehyde	Propanal	linear	C ₃ H ₆ O	49.30	58.08				0.003				0.034
Alkane	Nonadecane	linear	C ₁₉ H ₄₀	330.10	268.52		0.176	0.247					
Aromatic	1,3-cyclopentadiene	cyclic	C ₅ H ₆	41.50	66.10						0.025		0.009
Aromatic	Benzene	cyclic	C ₆ H ₆	78.80	78.11	0.005		0.008	0.004	0.005	0.021		0.037
Aromatic	Ethyl-benzene	cyclic	C ₈ H ₁₀	136.20	106.17	0.025	0.007	0.008	0.007	0.025	0.014	0.011	0.026
Aromatic	Ethyl-methyl-benzene	cyclic	C ₉ H ₁₂	163.03	120.19	0.010	0.014	0.011	0.002	0.010	0.017	0.018	0.021
Aromatic	Methyl-cyclopentene	cyclic	C ₆ H ₁₀	229.00	82.14								0.009
Aromatic	M-xylene	cyclic	C ₈ H ₁₀	140.60	106.17	0.079			0.017	0.079			0.100
Aromatic	O-xylene	cyclic	C ₈ H ₁₀	145.90	106.17	0.032			0.008	0.032			0.036
Aromatic	Propyl-benzene	cyclic	C ₉ H ₁₂	160.50	120.19	0.020	0.000	0.001	0.004	0.020	0.020		0.013
Aromatic	Toluene	cyclic	C ₇ H ₈	110.60	92.14	0.020	0.004	0.006	0.021	0.020	0.037	0.029	0.026
Aromatic	Trimethyl-benzene	cyclic	C ₉ H ₁₂	168.01	120.19	0.024	0.004	0.004	0.006	0.024	0.024	0.003	0.017
Aromatic	Xylene	cyclic	C ₈ H ₁₀	138.00	106.17		0.043	0.029			0.057	0.044	

Ester	1,1-dimethoxy-ethane	linear	C ₄ H ₁₀ O ₂	63.00	90.12				0.006	0.005	0.008
Ester	1,1-dimethoxy-propane	linear	C ₅ H ₁₂ O ₂	89.80	104.15	0.001					0.012
Ester	2,2-dimethoxy-butane	linear	C ₆ H ₁₄ O ₂	99.80	118.17	0.010	0.002				0.016
Ester	2,2-dimethoxy-propane	linear	C ₅ H ₁₂ O ₂	83.00	104.15	0.010					0.106
Ester	Methyl-acetate	linear	C ₃ H ₆ O ₂	44.00	74.08				0.004	0.068	0.512
Ester	Methyl-butanoate	linear	C ₅ H ₁₀ O ₂	104.20	102.13						0.008
Ester	Methyl-formate	linear	C ₂ H ₄ O ₂	26.00	60.05						0.012
Ester	Methyl-propanoate	linear	C ₄ H ₈ O ₂	67.90	88.11						0.029
Furan	1-(2-furanyl)-ethanone	cyclic	C ₆ H ₆ O ₂	183.40	110.11	0.001	0.002			0.024	
Furan	2,3-dihydro-benzofuran	cyclic	C ₈ H ₈ O	188.20	120.15	0.006	0.138	0.006	0.006	0.233	0.018
Furan	2,5-dimethyl-furan	cyclic	C ₆ H ₈ O	93.10	96.13	0.001		0.001			0.035
Furan	2-ethyl-5-methyl-furan	cyclic	C ₇ H ₁₀ O	119.10	110.15	0.002					0.015
Furan	2-ethyl-furan	cyclic	C ₆ H ₈ O	94.50	96.13						0.016
Furan	2-furanmethanol	cyclic	C ₅ H ₆ O ₂	170.00	98.10	0.000	0.001		0.003	0.014	0.048
Furan	2-methyl-furan	cyclic	C ₅ H ₆ O	64.50	82.10			0.003			0.196
Furan	Benzofuran	cyclic	C ₈ H ₆ O	174.00	118.13	0.010	0.002	0.006	0.010		0.024
Furan	Furan	cyclic	C ₄ H ₄ O	31.40	68.07						0.031
Furan	Furfural	cyclic	C ₅ H ₄ O ₂	161.80	96.08	0.005	0.001	0.001	0.005	0.003	0.062
Furan	Methyl-benzofuran	cyclic	C ₉ H ₈ O	190.00	132.16	0.006			0.006		0.025
Furan	Tetrahydrofuran (thf)	cyclic	C ₄ H ₈ O	68.30	72.11					0.001	0.018
Heterocyclic	1h-pyrrole	cyclic	C ₄ H ₅ N	129.80	67.09	0.001	0.000				0.031
Heterocyclic	Acetonitrile	cyclic	C ₂ H ₃ N	63.50	41.05	0.001	0.005	0.005	0.001	0.003	0.003
Heterocyclic	Dimethyl-pyridine	cyclic	C ₇ H ₉ N	142.50	107.15	0.006	0.001	0.002	0.006		0.013
Heterocyclic	Methyl-pyridine	cyclic	C ₆ H ₇ N	128.00	93.13	0.004	0.003	0.001	0.004	0.001	0.022
Heterocyclic	Pyridine	cyclic	C ₅ H ₅ N	115.30	79.10						0.017
Ketone	1-(acetyloxy)-2-propanone	linear	C ₅ H ₈ O ₃	153.70	116.12	0.014	0.025			0.004	0.004
Ketone	1-hydroxy-2-butanone	linear	C ₄ H ₈ O ₂	160.00	88.11	0.003	0.005			0.004	0.010
Ketone	1-hydroxy-2-propanone	linear	C ₃ H ₆ O ₂	145.50	74.08	0.025	0.005			0.040	0.034
Ketone	2,3-butanedione	linear	C ₄ H ₆ O ₂	88.00	86.09						0.017
Ketone	2,3-dimethyl-2-cyclopenten-1-one	cyclic	C ₇ H ₁₀ O	172.40	110.15	0.003	0.003	0.015	0.003	0.006	0.047
Ketone	2-cyclopenten-1-one	cyclic	C ₅ H ₆ O	136.00	82.10	0.001				0.003	0.011

Ketone	2-hexanone	linear	C ₆ H ₁₂ O	127.80	100.16	0.003	0.001	0.026
Ketone	2-methyl-2-cyclopent-2-enone	cyclic	C ₆ H ₁₀ O	139.00	98.14	0.005		0.043
Ketone	2-methyl-cyclopentanone	cyclic	C ₆ H ₁₀ O	141.60	98.14	0.003		0.019
Ketone	2-pentanone	linear	C ₅ H ₁₀ O	102.70	86.13	0.005	0.009	0.055
Ketone	3-hydroxy-2-butanone	linear	C ₄ H ₈ O ₂	145.40	88.11		0.007	0.011
Ketone	3-methyl-2-butanone	linear	C ₅ H ₁₀ O	78.30	86.13	0.003		0.008
Ketone	3-methyl-cyclopent-2-enone	linear	C ₆ H ₈ O	157.50	96.13	0.003	0.003	0.026
Ketone	3-penten-2-one	linear	C ₅ H ₈ O	122.00	84.12	0.002	0.004	0.015
Ketone	Acetone	linear	C ₃ H ₆ O	46.50	58.08	0.368	0.341	0.476
Ketone	Mek (methyl ethyl ketone)	linear	C ₄ H ₈ O	75.60	72.11	0.000	0.002	0.119
Ketone	Milbk	linear	C ₆ H ₁₂ O	116.50	100.16			0.008
PAH	9h-fluorene	cyclic	C ₁₃ H ₁₀	293.60	166.22	0.030	0.018	0.020
PAH	Antracene	cyclic	C ₁₄ H ₁₀	337.40	178.23	0.025	0.013	0.034
PAH	Fluoranthene	cyclic	C ₁₆ H ₁₀	375.00	202.25	0.010		0.013
PAH	Methyl-naphthalene	cyclic	C ₁₁ H ₁₀	244.42	142.20	0.150	0.058	0.093
PAH	Naphthalene	cyclic	C ₁₀ H ₈	221.50	128.17	1.280	0.044	1.119
PAH	Phenanthrene	cyclic	C ₁₄ H ₁₀	337.40	178.23	0.002	0.010	0.004
Phenolics	2,3-xylene	cyclic	C ₈ H ₁₀ O	216.90	122.16	0.020	0.017	0.030
Phenolics	2,4-xylene	cyclic	C ₈ H ₁₀ O	210.90	122.16	0.234	0.064	0.125
Phenolics	2,5-xylene	cyclic	C ₈ H ₁₀ O	211.10	122.16	0.104	0.032	0.070
Phenolics	2,6-dimethoxy-phenol (syringol)	cyclic	C ₈ H ₁₀ O ₃	264.50	154.16		0.045	
Phenolics	2,6-xylene	cyclic	C ₈ H ₁₀ O	201.10	122.16	0.028	0.019	0.048
Phenolics	2-methoxy-4-methyl-phenol (creosol)	cyclic	C ₈ H ₁₀ O ₂	220.00	138.16		0.006	
Phenolics	2-methoxy-phenol (guaiacol)	cyclic	C ₇ H ₈ O ₂	205.00	124.14		0.001	
Phenolics	3,5-xylene	cyclic	C ₈ H ₁₀ O	221.70	122.16	0.001		0.112
Phenolics	4-ethyl-2-methoxy-phenol (guaiacol)	cyclic	C ₉ H ₁₂ O ₂	246.50	152.19	0.014	0.003	0.122
Phenolics	4-vinyl-2-methoxy-phenol(guaiacol)	cyclic	C ₉ H ₁₀ O ₂	266.10	150.17		0.031	0.243
Phenolics	Ethyl-methyl-phenol (cresol)	cyclic	C ₉ H ₁₂ O	228.00	136.19	0.071	0.013	0.172
Phenolics	M-cresol	cyclic	C ₇ H ₈ O	202.30	108.14	0.195	0.139	0.184
Phenolics	M-ethyl-phenol	cyclic	C ₈ H ₁₀ O	211.70	122.16	0.471	0.025	0.447
Phenolics	O-cresol	cyclic	C ₇ H ₈ O	191.00	108.14	0.242	0.143	0.334

Phenolics	O-ethyl-phenol	cyclic	$C_8H_{10}O$	204.50	122.16	0.028	0.014	0.010	0.007	0.028	0.014	0.049	0.067
Phenolics	P-cresol	cyclic	C_7H_8O	202.00	108.14		0.153	0.247			0.091	0.231	
Phenolics	P-ethyl-phenol	cyclic	$C_8H_{10}O$	219.00	122.16	0.117	0.172	0.248	0.064	0.117	0.111	0.479	0.626
Phenolics	Phenol	cyclic	C_6H_6O	181.80	94.11	0.494	0.506	0.686	0.281	0.494	0.301	0.811	0.849

Appendix B – ASPEN model input file

```

DYNAMICS
  DYNAMICS RESULTS=ON
IN-UNITS SI MASS-FLOW='kg/hr' MOLE-FLOW='kmol/hr' &
  VOLUME-FLOW='cum/hr' PRESSURE=bar TEMPERATURE=C DELTA-T=C &
  PDROP-PER-HT='mbar/m' PDROP=bar
DEF-STREAMS MIXCINC ALL
SIM-OPTIONS
  IN-UNITS ENG
  SIM-OPTIONS ATM-PRES=14.69595 OLD-DATABANK=NO
DESCRIPTION "
  Solids Simulation with English Units :
  F, psi, lb/hr, lbmol/hr, Btu/hr, cuft/hr.
  Property Method: None
  Flow basis for input: Mass
  "DATABANKS 'APV71 PURE22' / 'APV71 AQUEOUS' / 'APV71 SOLIDS' / &
  'APV71 INORGANIC' / NOASPENPCD
PROP-SOURCES 'APV71 PURE22' / 'APV71 AQUEOUS' / 'APV71 SOLIDS' &
  / 'APV71 INORGANIC'
COMPONENTS
  C C /
  H2O H2O /
  H2 H2 /
  O2 O2 /
  N2 N2 /
  CL2 CL2 /
  S S /
  CO CO /
  CO2 CO2 /
  CH4 CH4 /
  H2S H2S /
  NH3 H3N /
  TAR C21H42 /
  NAPHTHA C11H10-2 /
  PHENOL C6H6O /
  OIL C6H6 /
  C3H8 C3H8 /
  COAL /
  BIOMASS /
  CHAR /
  ASH /
  COS COS /
  C2H6 C2H6

```

FLOWSHEET

BLOCK DECOMP-C IN=CHARS-C OUT=TOCOMB-C
 BLOCK GASIF IN=TOGASIF OUT=PROD-GAS
 BLOCK PRODMIX IN=PROD-GAS VOL-C VOL-B OUT=SYNGAS
 BLOCK ASHSEP IN=GAS2 OUT=TOGASIF ASH
 BLOCK COMB1 IN=TOCOMB OUT=GAS1
 BLOCK DECOMP-B IN=CHAR-B OUT=TOCOMB-B
 BLOCK COMBMIX IN=TOCOMB-B TOCOMB-C OXYGEN STEAM OUT= &
 TOCOMB
 BLOCK COMB2 IN=GAS1 OUT=GAS2
 BLOCK DEVOL-C IN=FEED-C OUT=PYPROD-C
 BLOCK VOLSEP-C IN=PYPROD-C OUT=CHARS-C VOL-C
 BLOCK VOLSEP-B IN=PYPROD-B OUT=CHAR-B VOL-B
 BLOCK DEVOL-B IN=FEED-B OUT=PYPROD-B

PROPERTIES IDEAL

PROPERTIES PENG-ROB / RK-SOAVE

NC-COMPS COAL PROXANAL ULTANAL SULFANAL
 NC-PROPS COAL ENTHALPY HCOALGEN / DENSITY DCOALIGT
 NC-COMPS BIOMASS PROXANAL ULTANAL SULFANAL
 NC-PROPS BIOMASS ENTHALPY HCOALGEN / DENSITY DCOALIGT
 NC-COMPS CHAR PROXANAL ULTANAL SULFANAL
 NC-PROPS CHAR ENTHALPY HCOALGEN / DENSITY DCOALIGT
 NC-COMPS ASH PROXANAL ULTANAL SULFANAL
 NC-PROPS ASH ENTHALPY HCOALGEN / DENSITY DCOALIGT

1340.329993

PROP-SET ALL-SUBS

IN-UNITS ENG

PROPNAME-LIS VOLFLMX MASSVFRA MASSSFRA RHOMX MASSFLOW TEMP &
 PRES UNITS='lb/cuft' SUBSTREAM=ALL

; "Entire Stream Flows, Density, Phase Frac, T, P"

STREAM FEED-B

IN-UNITS ENG

SUBSTREAM NC TEMP=77. PRES=14.7

MASS-FLOW BIOMASS 1E-008 <tonne/hr>

COMP-ATTR BIOMASS PROXANAL (0. 100. 0. 0.)

COMP-ATTR BIOMASS ULTANAL (0. 100. 0. 0. 0. 0.)

COMP-ATTR BIOMASS SULFANAL (0. 0. 0.)

STREAM FEED-C

IN-UNITS ENG

SUBSTREAM NC TEMP=77. PRES=14.7

MASS-FLOW COAL 44.384 <tonne/hr>

COMP-ATTR COAL PROXANAL (1.1851 86.04643632 10.74129509 &
 3.204678647)

COMP-ATTR COAL ULTANAL (3.204678647 73.39 1.39 0.78 0. &
 0.08 21.16)

COMP-ATTR COAL SULFANAL (0.08 0. 0.)


```

STREAM OXYGEN
  IN-UNITS ENG
  SUBSTREAM MIXED TEMP=275. PRES=500. &
  MASS-FLOW=10.81217229 <tonne/hr>
  MASS-FRAC O2 0.98 / N2 0.02
STREAM STEAM
  IN-UNITS ENG
  SUBSTREAM MIXED TEMP=620. PRES=415. &
  MASS-FLOW=43.53666471 <tonne/hr>
  MASS-FRAC H2O 1.
BLOCK COMBMIX MIXER
  IN-UNITS ENG
BLOCK PRODMIX MIXER
  IN-UNITS ENG
BLOCK ASHSEP SEP
  IN-UNITS ENG
  PARAM
  FRAC STREAM=TOGASIF SUBSTREAM=MIXED COMPS=C H2O H2 O2 &
  N2 CL2 S CO CO2 CH4 H2S NH3 TAR NAPHTHA PHENOL OIL &
  C3H8 COS FRACS=0. 1. 1. 1. 1. 1. 1. 1. 1. 1. &
  1. 1. 1. 1. 1. 1. 1.
  FRAC STREAM=TOGASIF SUBSTREAM=CISOLID COMPS=C FRACS=0.
  FRAC STREAM=TOGASIF SUBSTREAM=NC COMPS=COAL BIOMASS CHAR &
  ASH FRACS=0. 0. 0. 0.
BLOCK VOLSEP-B SEP
  IN-UNITS ENG
  PARAM
  FRAC STREAM=CHAR-B SUBSTREAM=MIXED COMPS=C H2O H2 O2 N2 &
  CL2 S CO CO2 CH4 H2S NH3 TAR NAPHTHA PHENOL OIL &
  C3H8 COS C2H6 FRACS=1. 0. 0. 0. 0. 0. 0. 0. 0. 0. &
  0. 0. 0. 0. 0. 0. 0. 0. 0. 0.
  FRAC STREAM=CHAR-B SUBSTREAM=CISOLID COMPS=C FRACS=1.
  FRAC STREAM=CHAR-B SUBSTREAM=NC COMPS=COAL BIOMASS CHAR &
  ASH FRACS=1. 1. 1. 1.
BLOCK VOLSEP-C SEP
  IN-UNITS ENG
  PARAM
  FRAC STREAM=CHARS-C SUBSTREAM=MIXED COMPS=C H2O H2 O2 &
  N2 CL2 S CO CO2 CH4 H2S NH3 TAR NAPHTHA PHENOL OIL &
  C3H8 COS C2H6 FRACS=1. 0. 0. 0. 0. 0. 0. 0. 0. 0. &
  0. 0. 0. 0. 0. 0. 0. 0. 0. 0.
  FRAC STREAM=CHARS-C SUBSTREAM=CISOLID COMPS=C FRACS=1.
  FRAC STREAM=CHARS-C SUBSTREAM=NC COMPS=COAL BIOMASS CHAR &
  ASH FRACS=1. 1. 1. 1.
BLOCK COMB1 RSTOIC
  IN-UNITS ENG
  PARAM PRES=465. DUTY=0.

```

```

STOIC 1 CISOLID C -1.013 / MIXED O2 -1. / CO 0.026 / &
  CO2 0.987
CONV 1 MIXED O2 1.
BLOCK COMB2 RSTOIC
IN-UNITS ENG
PARAM PRES=465. DUTY=0.
STOIC 2 CISOLID C -1. / MIXED H2O -1. / CO 1. / H2 &
  1.
CONV 2 CISOLID C 1.
BLOCK DECOMP-B RYIELD
IN-UNITS ENG
PARAM TEMP=1000. PRES=465.
MASS-YIELD NC ASH 0.050303255 / CISOLID C 0.719775574 / &
  MIXED H2 0.013632485 / N2 0.007682575 / S &
  0.000742078 / O2 0.207864033
COMP-ATTR NC ASH PROXANAL ( 0. 0. 0. 100. )
COMP-ATTR NC ASH ULTANAL ( 100. 0. 0. 0. 0. 0. 0. )
COMP-ATTR NC ASH SULFANAL ( 0. 0. 0. )
BLOCK DECOMP-C RYIELD
IN-UNITS ENG
PARAM TEMP=1000. PRES=465.
MASS-YIELD MIXED H2O 0. / NC ASH 0.440532095 / CISOLID &
  C 0.461790136 / MIXED H2 0.010712058 / N2 &
  0.013557449 / S 0.005415962 / O2 0.0679923
COMP-ATTR NC ASH PROXANAL ( 0. 0. 0. 100. )
COMP-ATTR NC ASH ULTANAL ( 100. 0. 0. 0. 0. 0. 0. )
COMP-ATTR NC ASH SULFANAL ( 0. 0. 0. )
BLOCK DEVOL-B RYIELD
IN-UNITS ENG
PARAM TEMP=1000. PRES=465.
MASS-YIELD MIXED H2 0.001721933 / CH4 0.075666637 / CO &
  0.028646123 / C2H6 0. / CO2 0.227772099 / PHENOL &
  0.083207272 / NAPHTHA 0.049538997 / H2O 0.239173738 / &
  NC CHAR 0.294273201
COMP-ATTR NC COAL PROXANAL ( 0. 100. 0. 0. )
COMP-ATTR NC COAL ULTANAL ( 0. 100. 0. 0. 0. 0. 0. )
COMP-ATTR NC COAL SULFANAL ( 0. 0. 0. )
COMP-ATTR NC BIOMASS PROXANAL ( 0. 100. 0. 0. )
COMP-ATTR NC BIOMASS ULTANAL ( 0. 100. 0. 0. 0. 0. 0. &
  )
COMP-ATTR NC BIOMASS SULFANAL ( 0. 0. 0. )
COMP-ATTR NC CHAR PROXANAL ( 0. 100. 0. 0. )
COMP-ATTR NC CHAR ULTANAL ( 0. 100. 0. 0. 0. 0. 0. )
COMP-ATTR NC CHAR SULFANAL ( 0. 0. 0. )
BLOCK DEVOL-C RYIELD
IN-UNITS ENG
PARAM TEMP=1000. PRES=465.

```

MASS-YIELD MIXED H2 0.000374384 / CH4 0.024843946 / CO &
0.004063939 / C2H6 0. / CO2 0.033283136 / PHENOL &
0.005126037 / NAPHTHA 0.019534911 / H2O 0.07138898 / &
NC CHAR 0.841384667
COMP-ATTR NC COAL PROXANAL (0. 100. 0. 0.)
COMP-ATTR NC COAL ULTANAL (0. 100. 0. 0. 0. 0. 0.)
COMP-ATTR NC COAL SULFANAL (0. 0. 0.)
COMP-ATTR NC CHAR PROXANAL (0. 100. 0. 0.)
COMP-ATTR NC CHAR ULTANAL (0. 100. 0. 0. 0. 0. 0.)
COMP-ATTR NC CHAR SULFANAL (0. 0. 0.)
BLOCK GASIF RGIBBS
IN-UNITS ENG
PARAM PRES=465. DUTY=0. <MW>
PROD C / H2 / CO / CO2 / CH4 / H2S / H2O / C2H6 / &
N2

EO-CONV-OPTI
STREAM-REPOR MOLEFLOW MASSFLOW STDVOLFLOW MOLEFRAC &
PROPERTIES=ALL-SUBS